The development of functionalized electrospun nanofibers for the control of pathogenic microorganisms in water

A thesis submitted to Rhodes University in fulfilment of the requirements for the degree of

Doctor of Philosophy (Science)

by

Phumelele Eldridge Kleyi

RHODES UNIVERSITY

Where leaders learn

Supervisor: Prof. Nelson Torto

Co-supervisor: Dr Zenixole Tshentu

February 2013

DEDICATION

I dedicate the thesis to my late father Lungile J. Kleyi:

"Father, let me dedicate, all this year to Thee,

In whatever worldly state Thou wilt have me be:

Not from sorrow, pain or care, freedom dare I claim;

This alone shall be my prayer, glorify Thy Name"

George A. McFarren

ACKNOWLEDGEMENTS

It is not so simple a task to acknowledge everyone that contributed, either directly or indirectly, towards the achievement of one's goals. However, it is my wish to ensure that I do my utmost best to extend my appreciation to everyone that was involved in my successes during the past three years of studies.

First and foremost, I would like to thank my supervisor Prof. Nelson Torto for accepting and allowing me to do my PhD degree in his research group. Your patience with me when things seemed not to be headed in the right direction, ensured that I remained focussed at all times. You kept your calmness and provided me with invaluable support, proper guidance and excellent advices. Believe me when I say "*You are one of the best mentors I have ever worked with*." I really appreciate everything.

I would also like to extend my gratitude to my co-supervisor Dr Zenixole Tshentu for inviting me to come and do my PhD degree at Rhodes University. You were not only my co-supervisor but my greatest friend as well. Through all the ups and downs, you were always there to offer me your unwavering support. Thank you for all the chemistry research lectures in your office; they ensured that I remained grounded but on my toes at the same time. I will always be indebted to you for everything you have done for me.

I would also like thank Prof. Carminita Frost (NMMU) and Dr Valencia Jacobs (CSIR) for performing the cytotoxicity studies and characterization (SEM-EDAX) of my samples, respectively.

I also extend my gratitude to Dr Manuel Fernandes (Wits University) for collecting the crystallographic data as well as solving the crystal structures for the silver(I) complexes.

To the Chemistry department staff, particularly the secretariat Mrs Benita Tarr and Ms. Barbara Ah Yiu, as well as the technical personnel (too many to mention names): The studies would not be possible without your involvement. From ordering of chemicals to repairing broken instruments you all were hands-on. I am grateful to you for doing your best everytime I needed your assistance.

I am also extending my appreciation to Dr Sam Chigome ('*Mnr*'), Dr Ryan Walmsley, Dr Shima Batlokwa ('*Morwa*'), Dr Janes Mokgadi ('*Ms J*') and Dr Godfred Darko ('*General*'). I

learnt so many things from you guys. I used to panic too much when I first came, especially when things were not going well. However, you always managed to calm me down and encouraged me to persevere. Thank you so much.

To my fellow colleagues (former and current F2/F3 and F12 members): I will not single out any particular individual because I feel everyone in the two labs was influential in my research, although each one in their own unique manner. I would like to thank you for making my life in the groups as simple as it could possibly be. The questions during group meetings were exceptionally beneficial to my project, and the laughs in the lab were definitely appreciated. I did thank you before, but I feel the need to reiterate it; I was really humbled by the support you offered during the toughest time of my life yet, the loss of my father. It enabled me to easily gather the strength and recover quickly from the setback. Thank you very much.

To my family, my Grandmother, Mother, Aunts, Uncles, Brothers as well as nieces and nephews, thank you for the support and encouragement you have given me. I could not have asked for a better family than you. To my son Zukhanye, thank you for allowing Daddy all the time to finish his studies. I promise to make it worth your while.

I am also grateful to the Andrew Mellon Foundation, Water Research Commission, Medical Research Council and National Research Foundation for financial assistance.

Lastly, to the Almighty God, thank you for granting me the time and strength as well as making sure that my dream becomes a reality.

ABSTRACT

The thesis presents the development of functionalized electrospun nylon 6 nanofibers for the eradication of pathogenic microorganisms in drinking water. Imidazole derivatives were synthesized as the antimicrobial agents and were characterized by means of NMR spectroscopy, IR spectroscopy, elemental analysis and X-ray crystallography. The first set of compounds (2-substituted *N*-alkylimidazoles) consisted of imidazole derivatives substituted with different alkyl groups (methyl, ethyl, propyl, butyl, heptyl, octyl, decyl and benzyl) at the 1-position and various functional groups [carboxaldehyde (CHO), alcohol (CH_2OH) and carboxylic acid (COOH)] at the 2-position. It was observed that the antimicrobial activity of the compounds increased with increasing alkyl chain length and decreasing pK_a of the 2-substituent. It was also observed that the antimicrobial activity was predominantly against a Gram-positive bacterial strains [*Staphylococcus aureus* (MIC = 5-160 μg/mL) and *Bacillus subtilis* subsp. *spizizenii* (MIC = 5-20 μg/mL)], with the latter being the more susceptible. However, the compounds displayed poor antimicrobial activity against Gram-negative bacterial strain, *E. coli* (MIC = 150- >2500 μg/mL) and did not show any activity against the yeast, *C. albicans*. The second set of compounds consisted of the silver(I) complexes containing 2-hydroxymethyl-*N*-alkylimidazoles. The complexes displayed a broad spectrum antimicrobial activity towards the microorganisms that were tested and their activity [*E. coli* (MIC = 5-40 μg/mL), *S. aureus* (MIC = 20-80 μg/mL), *Bacillus subtilis* subsp. *spizizenii* (MIC = 5-40 μg/mL) and *C. albicans* (MIC = 40-80 μg/mL)] increased with the alkyl chain length of the 2-hydroxymethyl-*N*-alkylimidazole. The third set of compounds consisted of the vinylimidazoles containing the vinyl group either at the 1-position or at the 4- or 5- position. The imidazoles with the vinyl group at the 4- or 5-position contained the alkyl group (decyl) at the 1-position. For the fabrication of the antimicrobial nanofibers, the first two sets of imidazole derivatives (2-substituted *N*-alkylimidazoles and silver(I) complexes) were incorporated into electrospun nylon 6 nanofibers while the third set (2-substituted vinylimidazoles) was immobilized onto electrospun nylon 6 nanofibers employing the graft polymerization method. The antimicrobial nylon nanofibers were characterized by IR spectroscopy and SEM-EDAX (EDS). The electrospun nylon 6 nanofibers incorporated with 2-substituted *N*-alkylimidazoles displayed moderate to excellent levels of growth reduction against *S. aureus* (73.2-99.8%). For the electrospun nylon 6 nanofibers incorporated with silver(I) complexes, the levels of growth reduction were >99.99%, after the antimicrobial

activity evaluation using the shake flask method. Furthermore, the grafted electrospun nylon 6 nanofibers showed excellent levels of growth reduction for *E. coli* (99.94-99.99%) and *S. aureus* (99.93-99.99%). The reusability results indicated that the grafted electrospun nylon 6 nanofibers maintained the antibacterial activity until the third cycle of useage. The cytotoxicity studies showed that grafted electrospun nylon 6 nanofibers possess lower cytotoxic effects on Chang liver cells with IC50 values in the range 23.48-26.81 μg/mL. The thesis demonstrated that the development of antimicrobial electrospun nanofibers, with potential for the eradication of pathogenic microoganisms in water, could be accomplished by incorporation as well as immobilization strategies.

TABLE OF CONTENTS

LIST OF ABBREVIATIONS

AATCC	American Association for Textile Chemists and Colorists
AgNPs	Silver nanoparticles
AIBN	Azobisisobutyronitrile
ASTM	American Society of Standards and Materials
ATR-FTIR	Attenuated total reflectance-Fourier transform infrared
BPO	Benzoyl peroxide
Da	Daltons
EDAX	Energy dispersive analysis spectroscopy
EDS	Energy dispersive spectroscopy
ESEM	Environmental scanning electron microscope
FBS	Foetal bovine serum
FRET	Fluorescence resonance energy transfer
HEPA	High efficiency particulate air filter
IR	Infrared
KET	Ketoconazole
LRV	Log reduction value
MSC	Mesenchymal stem cells
MET	Metronidazole
MIC	minimum inhibitory concentration
MTT	4,5-dimethylthiazol-2,5-diphenyltetrazolium bromide
NMR	Nuclear magnetic resonance
PA66	Poly(amide) 66

PAA	Poly(acrylic acid)
PAN	Poly(acrylonitrile)
PC	Polycarbonate
PCL	Poly(ε-caprolactone)
PEDOT	Poly(3,4-ethylenedioxythiophene)
PEI	Poly(ethylene imine)
PEO	Poly(ethylene oxide)
PES	Poly(ethersulfone)
PET	Poly(ethylene terephthalate)
PI	Poly(imide)
PLLA	Poly(L-lactic acid)
PP	Poly(propylene)
PPSU	Poly(phenyl sulfone)
PtNPs	Platinum nanoparticles
PU	Poly(urethane)
PVA	Poly(vinyl alcohol)
PVAc	Poly(vinyl acetate)
QCM	Quartz crystal microbalance
RPMI	Roswell Park Memorial Institute
Subsp.	Subspecies
TMACl	Tetramethylammonium chloride
TMAOH	Tetramethylammonium hydroxide
Tof-SIMS	Time of flight secondary ion mass spectrometry
UV	Ultraviolet

VIm	Vinylimidazole
XPS	X-ray photoelectron spectroscopy

LIST OF FIGURES

LIST OF TABLES

LIST OF SCHEMES

INTRODUCTION

CHAPTER 1 METHODS FOR THE ERADICATION OF PATHOGENS IN DRINKING WATER

CHAPTER 2 THE ELECTROSPINNING PROCESS

CHAPTER 1 METHODS FOR THE CONTROL OF PATHOGENS IN DRINKING WATER

1.1 Pathogenic microorganisms in water

The challenges associated with drinking water are compounded by prospects of pathogenic contamination. Pathogens are classified as the microorganisms that can lead to diseases, and these microorganisms include bacteria, viruses and protozoa. Table 1.1 illustrates some microorganisms found in water and their associated health effects to humans.[1] Some of the various pathways by which these pathogens end-up in drinking water are through human or animal wastes, sewage treatment systems, septic treatment discharges as well as storm water run-offs after heavy rains or floods.

In urban communities water is processed in water treatment plants to ensure the supply of safe and good quality drinking water. However, water supply systems from the treatment plants to households are susceptible to the growth of a layer of biological material (biofilm) from inside.[2-5] Generally, the biofilm cannot be detected or treated and could lead to the presence of total coliform cells in drinking water. Once the biofilm has grown inside the water supply systems, it becomes a breeding substrate for microorganisms. Moreover, in most rural communities, water is still obtained from rivers and is not treated; causing an increase in the probability of consumption of water contaminated with pathogens.

Table 1.1. Some waterborne pathogenic microorganism and associated health effects[1]

Microorganism	**Associated Health Effect**
<E6> Virus </E6>	
Coxsackie	Hemorrhagic conjunctivitis, fever, rash, pharyngitis (sore throat) rash, respiratory disease,myocarditis, pericaritis, aspetic meningitis, encephalitis, hand, foot and mouth disease, reactive insulin-dependn diabetes
Echo	Respiratory disease, aspetic meningitis, rash, fever
Norwalk	Gastroenteritis (fever, vomiting, diarrhoea)
Hepatitis A	Fever, nausea, jaundice, liver failure
Hepatitis E	Fever, nausea, jaundice, liver failure
Rota	Gastroenteritis (fever, vomiting, diarrhoea)
Enteric adeno	Respiratory disease, gastroenteritis, hemorrhagic conjunctivitis
Calici	Gastroenteritis (diarrhoea)
Astro	Gastroenteritis (diarrhoea)
<E6> Bacteria </E6>	
Escherichia coli	Gastroenteritis (diarrhoea)
Salmonella spp.	Enterocolitis (diarrhea, fever, vomiting), Guillain-barre syndrome
Yersinia spp.	Diarrhoea, reactive athritis
Legionella spp.	Legionnaires' disease, Pontiac fever, death
Vibrio cholera	Diarrhoea, vomiting, death
<E6> Protozoa </E6>	
Cryptosporidium parvum	Diarrhoea
Gardia Lamblia	Chronic diarrhoea

Drinking water that is contaminated with pathogens results in waterborne disease outbreaks such as diarrhea, tuberculosis, cholera, hepatitis and typhoid fever. It has been estimated that there are 34 million deaths per annum associated with waterborne diseases worldwide.[6] Of

the total deaths per annum, 2-3 million deaths are associated with diarrhoea and the majority are children.[6] Due to these adverse health effects of pathogens to humans, WHO has established international guidelines for the quality standards of drinking water.[7] Typically, the maximum contaminant levels (MCL) for bacteria must be zero total coliform colonies per 100 mL of drinking water.[7] There exists, therefore, a need for frequent monitoring, detection and treatment of pathogen levels to provide safe and good quality drinking water.

In 2008, UNICEF compiled and published a document in which it recommends household water treatment and safe storage.[8] The document also states that encouraging household water treatment and safe storage will enable vulnerable communities to be responsible for the quality of their drinking water. In turn, there would be an enormous reduction in reported cases of waterborne disease outbreaks.

1.2 Eradication of pathogens in water

Eradication of pathogens in drinking water can be achieved using two ways, namely: (i) physical removal (filtration) or (ii) inactivation (killing or disinfection). Conventional eradication methods that are currently being employed in water treatment plants have high efficiencies, but suffer some disadvantages. The conventional methods, their advantages and disadvantages are discussed in the following subsections.

1.2.1 Coagulation and flocculation

Coagulation and flocculation are used for the removal of suspended particles in water. The appropriate selection and application of coagulation and flocculation is dependent on the understanding of the interaction between factors such as the source, the surface charge, the size, the shape and the denstity of the particles.[9,10] Coagulation and flocculation are carried out in successive steps to overcome the stabilizing forces on suspended particles.

The suspended particles are first coagulated by the addition of a coagulant such as aluminium sulfate, ferric sulfate, ferric chloride, poly(aluminium chloride) and polymers to destabilize (and neutralize) the particle charges.[9-11] When mixed rapidly with water the coagulant forms hydroxide precipitates which trap the particles and microorganisms (Fig. 1.1). The

microorganism-trapping hydroxide precipitates, also known as flocs, which are capable of sticking together.

In the flocculation step, the flocs are allowed to grow by gently mixing and high molecular weight polymers (coagulant aids) may be added to enhance bridging binding and strengthening the flocs, as well as accelerating the settling rate. Heavy flocs are removed by sedimentation followed by direct filtration. The removal of very light flocs is achieved by first carrying them to the water surface using air flotation, and subsequently skimming them off.

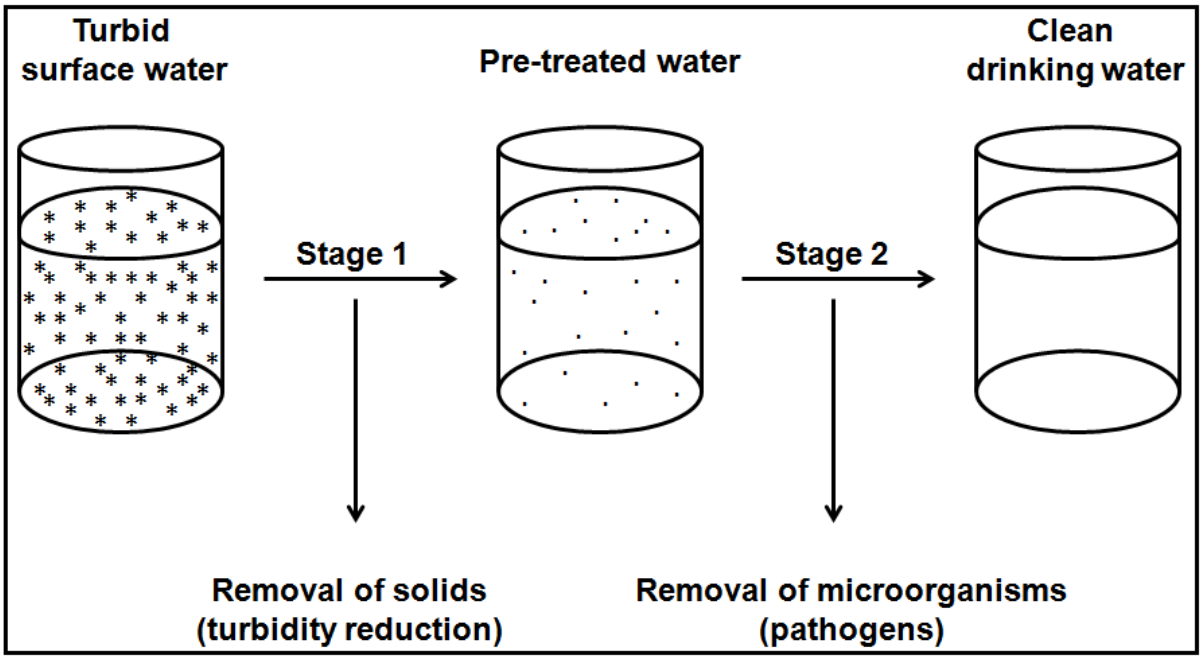

Figure 1.1. Schematic illustration of a coagulation process[12]

The utilization of toxic metals poses health hazards to humans since, for example, exposure to aluminium is known to cause Alzheimer's disease[13,14] although there are some contradictions.[15] Inorganic coagulant may either lower (e.g. aluminium sulfate and ferric sulfate)) or raise (e.g. sodium aluminate) the pH.[9] Very high alkalinity (pH 10-11) is required when removal of algae is performed using the coagulation method.[16] Polymers are more effective over a broader pH range but more expensive than inorganic coagulants. Coagulation can remove particles and dissolved matter, but may not completely remove pathogens.

1.2.2 Boiling

Water often becomes contaminated by pathogenic microorganisms after some emergency situations. A typical emergency could include natural disasters (floods, earthquakes, damage to electrical equipment due to lightning strikes), accidents (spillages in water dams) and damage to treatment plants and water supply systems.[7] In such cases of emergency, communities have always been advised to boil tap water for at least one minute before consumption. Although boiling water kills most of pathogenic microorganisms, it is time consuming and energy intensive. Boiled water can be susceptible to recontamination by microorganisms particularly in environments with low hygiene activities.[17,18] Boiling usually provides small quantities of water and thus cannot be considered a long-term option for disinfection of water supply. It is however the most common method for home-based disinfection of water and a benchmark against new point-of-use technologies for water treatment.[17,18]

1.2.3 Chlorination

For many years, chlorination has been the most commonly used method for disinfection of water worldwide. The method of disinfection is used in water treatment plants but could also be used in households, provided strict dosages are adhered to. Chlorine can be used as a secondary disinfectant since it maintains an adequate residual in water to prevent recontamination.[19] The chlorination agents used for disinfection of water are chlorine, hypochlorite, chloramine and chlorine dioxide.[19,20] Chlorination is highly effective against enteric bacteria, however, enteric viruses may be resistant. Moreover, microorganisms encapsulated in particles may be protected from the action of chlorination agents. Some carcinogenic organic (e.g. trihaloalkanes, trichloroacetic acids and haloacetonitriles) and inorganic (chlorite and chlorate ions) by-products may result from the chlorination method.[19-22] It could also result to unpleasant taste of water.

1.2.4 Ozonation

Ozonation is another method that has been used for the disinfection of water for many decades. It is very effective against Gram-negative *E. coli* but Gram-positive bacteria (*Staphylococci*, *Streptococci*, *Bacilli*) and mycobacteria are highly resistant to ozone.[23,24] Since ozone is a highly unstable gas, disinfection requires a continuous supply of ozone. For a continuous supply of ozone to be achieved, it must be generated on-site which is very costly and energy intensive. It can form bromates in water if bromide is present, and is less effective in cold water.[11]

1.2.5 Ultraviolet disinfection

Ultraviolet disinfection uses UV light to irradiate contaminated water which kills pathogenic microorganisms. Three types of UV lamps are used, namely, low-pressure mercury lamps, medium-pressure lamps and pulsed lasers. This method of disinfection has gained popularity over the years since it does not introduce chemical agents into water.[25,26] However, the efficiency of UV disinfection is dependent on the ability of water to transmit UV light.[26] Water with high turbidity does not transmit UV light efficiently resulting in survival of some microorganisms. Moreover, it has been observed that most bacteria have developed damage repair mechanisms against UV disinfection.[26] UV disinfection is also expensive and energy intensive.

However, the efficiency of disinfection methods (except for UV irradiation) is always dependent on the concentration (dose), temperature, contact time and pH.[25,27] Moreover, the disinfectant concentration and contact time play a crucial role in understanding the disinfection kinetics. Disinfection kinetics is defined as the product of the residual disinfectant concentration (mg/L) and the contact time (min) that the residual disinfectant is in contact with water.

1.2.6 Filtration

Filtration is a method in which microorganisms and particulate matter are physically removed from water by passing through a membrane. There are various filtration processes that are used for physical removal of microorganisms from water, namely, membrane filtration

(reverse osmosis, micro-, ultra- and nanofiltration) and granular filtration. The suitability of the type of filtration process to be used for removal of microorganisms is dependent on the size of the microorganism detected in water, as illustrated in Figure 1.2.

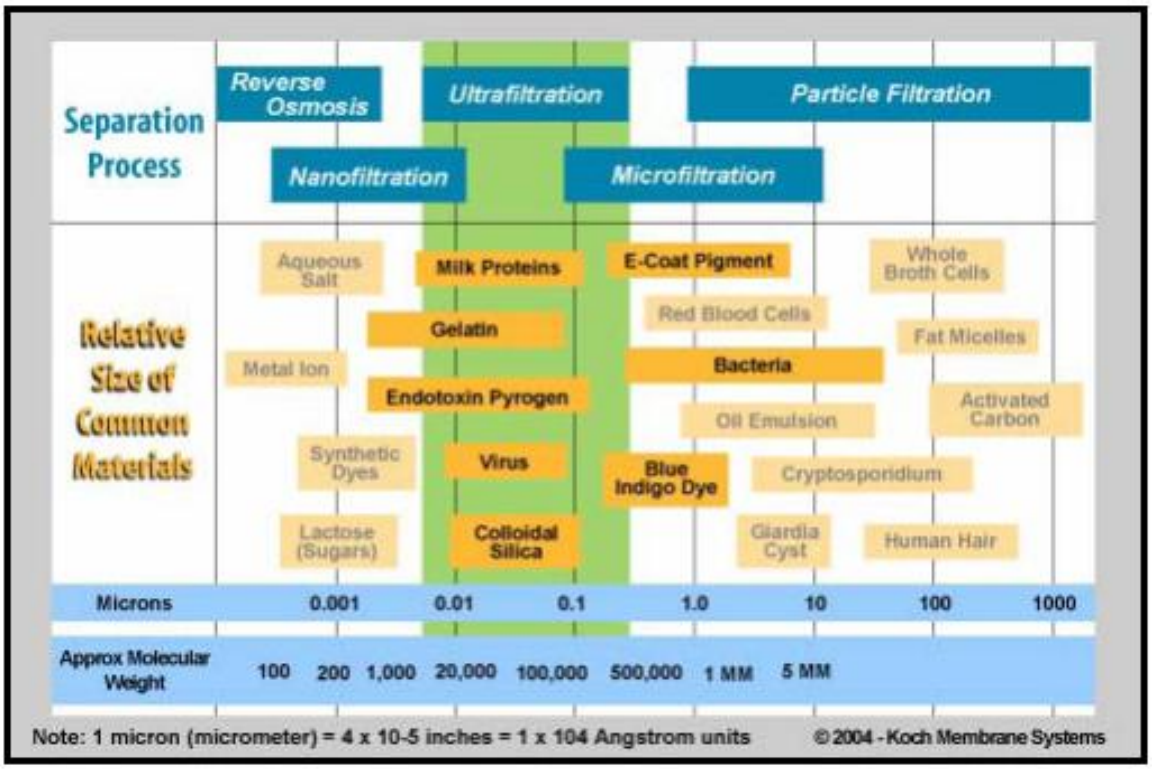

Figure 1.2. Pore sizes of microorganism and filtration medium. DE = diatomaceous earth, RO = reverse osmosis, MF = microfiltration, NF = nanofiltration, UF = ultrafiltration[28]

1.2.6.1 Granular filtration

Granular filtration is a process whereby water is passed through a packed bed of granular material (e.g., sand) and suspended solids (including microorganisms) are trapped. The suspended solids are then biochemically decomposed and the removal of pathogenic microorganisms is achieved by cleaning the filtration beds. The filtration beds are regularly cleaned to prevent the hydraulic resistance from becoming too high or the breakthrough of suspended solids. When the maximum hydraulic resistance is reached, due to clogging, the filtration bed must be cleaned by backwashing. The performance of a granular filter usually deteriorates, during a 'ripening period', before recovering to a stable level.[29] The adverse consequence is that during the 'ripening period' the number of microorganisms that pass

through can be very high. Filters for the granular filtration process can be constructed as monomedium (silica sand), dual media (sand and anthracite coal) and trimedia (sand, coal and garnet).[11]

Two types of granular filtration processes for water purification are slow and rapid sand filtration; with the latter being the most commonly used process.[30] Besides one process requiring a slow flow rate and the other a fast flow rate, there are other differences between them. For instance, for rapid sand filtration, chemical coagulation pre-treatment is required while slow granular filtration does not require coagulation. In slow sand filtration water is passed through the filtration bed under gravity and requires a large surface area. On the other hand, in rapid sand filtration, water is forced through under pressure and requires a small surface area. In slow sand filtration, the filtration bed is cleaned by scraping off the top layer of sand.[30]

1.2.6.2 Membrane filtration

Membrane filtration is a process where water is passed through a thin semi-permeable film for the removal of suspended particulate matter. In membrane filtration, removal of microorganisms is based upon size-exclusion; that is, microorganisms larger than the membrane pores are trapped. As a result of small pores, the membrane filtration process has the capability of removing almost any contaminant. The main challenge in the membrane filtration process is loss of performance due to fouling which results from accumulation of particulate matter on the membrane.[31,32] However, the challenge can be prevented by pre-treatment through coagulation, microstraining, addition of biocides or pH adjustment.[33,34] The most extensively used membrane filtration processes for the removal of microorganisms are reverse osmosis, microfiltration, ultrafiltation and nanofiltration.[31] The choice of a suitable membrane process depends on the type of available membrane material. The most important properties of a membrane include a high permeate flux, high contaminant rejection, great durability, good chemical resistance and low cost.

Microfiltration membranes (≥0.1 μm) can remove most of the microorganisms except viruses which have sizes smaller than the membrane pores (Figure 1.2). The performance of the microfiltration membrane can be affected by growth of bacteria in the membrane system. Ultrafiltration membranes (≥0.01 μm), with pore sizes smaller than microfiltration

membranes, have the capability of removing most microorganisms including some viruses. Both nanofiltration (≥0.001 μm) and reverse osmosis (≥0.0001 μm) have membranes pores smaller than microfiltration and ultrafiltrarion membranes, thus they can remove most microorganisms. However, nanofiltration and reverse osmosis membranes can be very expensive in comparison to both microfiltration and ultrafiltration membranes. Because of very small pores, reverse osmosis also removes essential nutrients which are needed in the human body. While all membrane filtration processes operate under pressure, nanofiltration and reverse osmosis require higher pressures than both micro- and ultrafiltration.[35] Moreover, separation in nanofiltration and reverse osmosis occurs mainly by diffusion through the membrane and not by the principle of filtration through pores.

The conventional methods for controlling pathogenic microorganisms in water have certainly yielded desirable results since they came into existence. However, each one of the methods has its own merits as well as limitations. For example, the filtration methods suffer largely from biofouling which subsequently results in replication of microorganisms. Therefore, the limitations necessitate more research to develop new technologies that are low cost, energy efficient and environmentally friendly for controlling pathogenic microorganisms in water. Table 1 summarises the strengths and limitations of the convetional methods for the removal of pathogens in water. Electrospun nanofibers have, over the years, emerged as possible alternatives to develop new technologies for contolling pathogenic in water due to their high permeate flux rate and low trans-membrane pressure.[36]

Table 1.2. Summary of convetional methods for the removal of pathogen in water

Method	Strength	Limitation
Coagulation	Removes most microorganisms	Uses toxic metal salts, may not completely remove pathogens
Boiling	Kills most microorganisms	Provides smaller volumes of water, time- and energy-intensive
Chlorination	Kills most microorganisms, maintains adequate residual to prvent recontamination	Formation of carcinogenic (in)organic species, unpleasant taste and odour
Ozonation	Effective against Gram-negative and gram-positive bacteria	Requires continuous supply, expensive and energy-intensive
Ultraviolet	Kills most microorganisms	Efficieny affected by turbidity, expensive and energy-intensive
Granular filtration	Removes most microorganisms	Requires chemical pre-treatment and regular cleaning
Membrane filtration	High permeate flux, high contaminant rejection, great durability, good chemical resistance and low cost	May not filter very small microorganisms, biofouling

1.3 Electrospun nanofibers with antimicrobial properties

It is well documented that some naturally occurring polymers (e.g., chitosan, cellulose, peptides) have inherent antimicrobial properties. The antimicrobial properties of natural polymers, together with their biodegradability and biocompatibility, make them excellent candidates for the control of pathogenic microorganisms in water. Although synthetic polymers may not have antimicrobial properties, it could be induced by functionalization (blending or immobilization) with biologically active molecules, metal ions or nanoparticles. Using the electrospinning process, the nanofibers obtained from the polymers (natural and synthetic) can be used for controlling pathogenic microorganisms in water. When used for the control of pathogenic microorganisms in water, antimicrobial electrospun nanofibers could eliminate the challenge of biofouling by killing the microorganisms instead of trapping them. The antibiofouling properties and high porosity of electrospun polymer nanofibers renders them as ideal alternatives to the conventional methods for the treatment of water.

1.3.1 Antimicrobial natural polymer nanofibers

Chitosan is obtained by alkaline deacetylation of chitin, the most abundant natural amino polysaccharide after cellulose. It is widely known to exhibit antibacterial and antifungal properties and its electrospun nanofibers were used for controlling pathogenic microorganisms either on its own or blended with other polymers.[37,38]

Desai *et al*.[38] fabricated electrospun polyethylene oxide (PEO):chitosan nanofiber filters and investigated their heavy metal binding, antimicrobial and physical filtration efficiencies. The efficiency of the nanofiber filters was correlated to the surface chemistry of the electrospun nanofibers. Electrospun polyacrylonitrile (PAN) nanofibers coated with a thin layer of chitosan have been evaluated as high flux ultrafiltration membranes for water treatment.[39] The ultrafiltration nanofiber composite system was made up of a three-tier composite structure, namely, non-porous hydrophilic coating that is water permeable (chitosan), an electrospun nanofibrous support (PAN) and a non-woven microfibrous substrate (polyethylene terephthalate (PET)). The role of the chitosan layer was to act as an antibiofouling agent because of its antimicrobial properties.

Ma *et al*.[40,41] demonstrated that electrospun cellulose and chitin nanofibers fabricated from electrospinning (2,2,6,6-tetramethylpiperidin-1-yl)oxidanyl (TEMPO)/NaBr/NaClO oxidized cellulose were 2-3 times better as high flux micro-and ultrafiltration membranes compared to commercial microfiltration membranes.

1.3.2 Antimicrobial synthetic polymer nanofibers

Most synthetic polymers (e.g., polystyrene, nylon 6, polysulfone) have no inherent antimicrobial properties, thus antimicrobial activity could be induced by functionalization of the polymers with biocides. Nylon 6 is among many other synthetic polymers that have been functionalized and evaluated for antimicrobial properties and other potential applications.[42-54] Nylon 6 was chosen as a solid support material because of its biocompatibility, biodegradability, mechanical stability, electrospinnability and insolubility in water.[55-57]

Some well known biocides that were used for functionalization of synthetic polymers include organic molecules (e.g., quaternary ammonium salts, imidazoles), metal oxides (e.g., TiO_2, ZnO, CuO) and metal nanoparticles (e.g, silver nanoparticles).[58-62] Synthetic co-polymers

functionalized with furanone derivatives have also been developed for inhibition of cell adhesion in water filtration systems.[63-65]

1.3.2.1 Organic and inorganic compounds with antimicrobial properties

The discovery of organic and inorganic compounds with antimicrobial properties dates back to many decades and some are still being discovered. Although a large number of biocides (compounds with antimicrobial properties) have been reported, the focus of the current thesis will mainly be on imidazoles (organic) and metallic silver (inorganic). The use of imidazole compounds is well established in the field of medicinal chemistry, finding applications as anticancer,[66] antibacterial,[67] antifungal,[68] antiparasitic[69] and antidiabetic[70] drugs, to name a few. The discovery of azole antibacterial and antifungal agents began with benzimidazole in 1944.[71] Since then there have been several reports noting the antifungal activity of imidazoles,[71-73] the action of which is suspected to be due to interference with ergosterol synthesis and membrane damage.[74]

Azoles inhibit lanosterol demethylase, a cytochrome P-450 dependent enzyme which is responsible for the synthesis of ergosterol. Ergosterol is a major sterol of the cytoplasmic membrane and is responsible for a variety of cellular functions. It is responsible for the [67]fluidity and integrity of the cytoplasmic membrane, as well as the proper functioning of chitin synthetase. Chitin synthetase is in turn responsible for cell growth and division.[74,75] The mechanism of antibacterial action of azoles is believed to be through the inhibition of enoyl acyl carrier protein reductase (FabI), a novel antibacterial target.[76]

Further development and modification of antimicrobial agents that possess broad spectrum antimicrobial properties remains very important.[77] Derivatizing the imidazole group, at the 1-position, with long alkyl chains has dramatically improved the antibacterial activity of simple imidazoles.[67] It was observed that the antimicrobial activity increased as the alkyl chain length was increased up to nine carbons and began to decrease thereafter. Several substituents at the 2-position of *N*-alkylimidazole derivatives such as the methyl group and the ether moiety have also been investigated for their effect on the antimicrobial activity.[67,69] It was observed *N*-alkyimidazoles with medium alkyl chain length at 1-position and a methyl substituent at the 2-position as well as methyl substituent at the 2-position and nitro group at the 4-position also exhibited an increase in antimicrobial activity.[67] Samant *et al.*[69]

demonstrated that *N*-methylimidazoles with various substituents at the 2-, 4- and 5-position exhibited enhanced activity against the human African trypanosomiasis.

Silver and its salts have been used as antimicrobial agents for many centuries.[78,79] Silver has the most superior properties among all metals with antimicrobial activity because of its higher toxicity to microorganisms and lower toxicity to mammalian cells.[80,81] The ancient Phoenicians used silver-coated containers to store water so as to prevent spoiling.[82] Storing water in silver-coated containers aided in the prevention of contamination by microorganisms. Aqueous silver nitrate was used as an eye drop to newly born babies for the prevention of *Neisseria gonorrhoeae* transmission from infected mothers.[83,84] Ionic silver is reportedly the active species while metallic silver is inert.[85]

There are several reported mechanisms by which silver acts on the microorganisms.[84,86] One proposed mechanism involves the reversible binding of silver to the nucleotide bases of the bacterial DNA. The reversible binding results in the denaturation by displacement of hydrogen bonds between adjacent purines and pyrimidines[84]. Davis *et al*.[87] proposed that the destruction of bacteria occurs through silver-catalyzed oxidation of sulfhydryl (S-H) moieties on the surface of the membrane. Atomic oxygen in the aqueous medium oxidizes Ag(0) to Ag(I) which readily reacts with adjacent S-H groups by replacing the hydrogens. Consequent coupling of the adjacent S-groups results in the formation of S-S bond, thereby blocking respiration and electron transfer.

Silver sulfadiazine was the first silver complex to be used as an antimicrobial agent.[88,89] It is currently clinically administered for the treatment of burn wounds. Due to the emergence of resistant microorganisms, new broad spectrum antimicrobial agents are necessary. Consequently, many silver complexes have been investigated for their antimicrobial activity.[90-95] The reported silver(I) complexes exhibited superior antibacterial activity against the Gram-positve than Gram-negative bacteria.[91-95] In contrast, the silver(I) complexes reported by Kazachenko *et al*.[90] displayed superior antibacterial activity against Gram-negative bacterial. Interestingly, silver complexes containing imidazole ligands have demonstrated remarkable broad spectrum antimicrobial activity.[96-102] The silver(I)-imidazole complexes displayed broader spectra of antibacterial and antibacterial properties. Thus imidazole derivatives, silver and its complexes as well as other biocidal compounds are ideal candidates for the functionalization of electrospun nanofibers to produce materials with antimicrobial (antibiofouling) properties.

1.3.2.2 Electrospun nanofibers functionalized with antimicrobial organic molecules

Tan and Obendorf[103] fabricated nylon 6 nanofibers incorporated with three structurally different *N*-halamines using the electrospinning technique. They observed that the electrospun nylon 6 nanofiber composites inhibited the growth of *E. coli* and *S. aureus* within a contact time of 40 min. A log 8 reduction for both bacteria was achieved. They also observed that the activity of the nylon 6 nanofiber composites increased with the addition of more chlorine. Sun *et al.*[104] conducted similar work where electrospun cellulose acetate nanofibers blended with *N*-halamines were investigated for antimicrobial activity.

Electrospun polyurethane cationomer (PUCs) containing quaternary ammonium functionalities were fabricated and investigated for their potential use as antimicrobial nanofilters.[58] The electrospun PUC nanofibers demonstrated very high antimicrobial activity against Gram-negative *E. coli* and Gram-positive *S. aureus*.

In a similar study Kim *et al.*[105] investigated the potential application of electrospun polycarbonate nanofibers containing a quaternary ammonium salt as ultrafiltration membranes. The electrospun nanofibers demonstrated a filtration efficiency of 99.97% at 0.3 μm particle size which is the requirement for HEPA (high efficiency particulate air) filters. The electrospun polycarbonate nanofibers were suitable to be used as HEPA filters.

Electrospun polyamide 6 (nylon 6) nanofibers were blended with various organic bactericides (thiocyanatomethylthiobenzothiazole (TCMBT), dibromocayanoacetamide (DBNPA), bronopol (BR), unspecified proprietary quaternary ammonium salt by Buckman (WSPC) and chlorhexidine (CH) and were investigated for water filtration and removal of microorganisns.[51] The nanofiber membranes were compared with polyamide 6 nanofibers incorporated with silver nanoparticles (AgNPs) as a reference. It was observed that the electrospun polyamide 6 nanofibers incorporated with the organic bactericides displayed better filtration efficiencies than other traditional microfiltration membranes.

Mei *et al.*[106] fabricated electrospun PAN nanofibrous membranes with high water flux, relative flux recovery and antifouling properties. Surface-modification of PAN nanofibers was achieved by immobilizing polyhexamethylene guanidine hydrochloride (PHGH) through hydrophilic flexible spacer groups. The spacers also demonstrated cell-resistant properties by removing attached dead cells. Polyhexamethylene guanidine hydrochloride imparted

antibacterial properties to the electrospun nanofibers. Therefore, they concluded that the electrospun nanofibers possessed both antibacterial and easy-cleaning properties.

Surface-modified electrospun polyethersulfone (PES) nanofibrous membranes with antifouling properties were prepared by photochemical graft polymerization of two different hydrophilic monomers, 2-acrylamido-2-methyl-1-propanesulfonic acid (AMPS) and quaternary 2-dimethylaminoethylmethacrylate (qDMAEMA).[107] The antifouling properties of the electrospun nanofibrous membrane were studied in the presence of *E. coli*, and the dDMAEMA-grafted membranes were found to have better efficiency compared to pristine PES nanofibrous membranes.

Graft polymerization is a post-functionalization technique used for the modification of polymeric material surfaces.[108,109] The grafting method has received much attention as a preferred surface-modification method of electrospun nanofibers for various applications including adsorption[110] and ion exchange membranes,[111] tissue engineering,[112] as well as antimicrobial activity.[113,114] Both natural and synthetic polymer surfaces could be modified using the graft polymerization technique to induce or enhance their antimicrobial properties.[113,115-117] Of the synthetic polymers that were modified to induce antimicrobial activity, nylon 6 is the most commonly chosen.[46,47]

Several vinyl monomers have been grafted on the surface of polymer nanofibers using the graft polymerization technique and the grafted polymer nanofibers evaluated for the antimicrobial properties. Azole monomers have received much attention for the surface modification of electrospun nanofibers *via* graft polymerization technique. For example, indole was grafted onto chitin and chitosan and the antimicrobial activity of the grafted polymer composites was evaluated.[115] Saad *et al*.[116] reported the antimicrobial activity of poly(3-hydroxybutyrate-co-3-hydroxyvalerate) copolymer grafted with *N*-vinylpyrrolidone. *N*-vinylimidazole is the most commonly explored azole monomer for fabrication of grafted electrospun nanofibers with antimicrobial activity because of the inherent antimicrobial properties of the imidazole moiety.[118-120]

1.3.2.3 Electrospun nanofibers blended with metal oxides and nanoparticles

Several metals, metal oxides, metal complexes and metal nanoparticles, such as Ag, Cu (CuO), Zn (ZnO) and Ti (TiO_2) are known to possess antimicrobial properties.[121-123] Of all

known antimicrobial metals, Ag is the most toxic element to microorganisms.[80,81] Electrospun nanofibers incorporated with metals, metal oxides, metal complexes or their nanoparticles were investigated for application as membrane filters in water purification.[54,60,62]

Electrospun nylon 6 nanofibers incorporated with ZnO nanoparticles were fabricated and investigated for antibacterial, air permeability and water vapour transmission properties.[54] It was observed that ZnO nanoparticles were evenly distributed but not necessarily encapsulated into the nanofibers. The electrospun nylon 6/ZnO nanoparticles displayed excellent antibacterial, air permeability and water vapour transmission properties. However, Franklin *et al*.[59] issued a caution about the application of ZnO nanoparticles for water treatment, due to their high solubility in aqueous media.

Titanium oxide (TiO_2) is known for its powerful photocatalytic inactivation of pathogenic microorganisms such as bacteria and viruses.[124,125] Alrousan *et al*.[60] demonstrated the photocatalytic disinfection ability of TiO_2 nanoparticle film immobilized onto borosilicate glass sheets against *E. coli* in surface and distilled water. It was observed that the addition of nitrate and sulfate anions resulted in the reduction of photocatalytic inactivation in distilled water. Even varying the pH was observed to have no effect on the photocatalytic inactivation. Interestingly, stand-alone TiO_2 electrospun nanofibers were developed for photocatalytic pre-treatment of synthetic hospital wastewater.[126]

Silver nanoparticles are the most extensively explored antimicrobial agents when embedded or immobilized on electrospun nanofibers. Lala *et al*.[61] performed a comparative study between three different electrospun polymer (cellulose acetate, polyacrylonitrile and poly vinyl chloride) nanofibers incorporated with AgNPs for the potential application in the disinfection of water. They observed that the electrospun PAN nanofibers containing AgNPs were the most effective of the prepared materials. Silver nanoparticles were found to have more inactivation power against Gram-negative bacteria (e.g. *E. coli*).[80] Gule *et al*.[64] reported the fabrication of antimicrobial electrospun poly(vinyl alcohol) incorporated with AquaQure (a reagent consisting predominantly Zn^{2+} and Cu^{2+} ions) for use as water filtration media. They observed up to a 5log reduction of the population of microorganisms that the electrospun nanofibers were evaluated against.

There have been instances where silver complexes were embedded into electrospun nanofibers and investigated for their antimicrobial efficacy. For example, silver(I)-imidazole

cyclophane gem-diol complexes have been incorporated into electrospun tecophilic nanofibers and were demonstrated to inhibit both bacterial and fungal growth.[98]

Most recently, Dasari *et al*.[62] demonstrated the antifouling properties of electrospun poly(L-lactic acid) (PLA) nanofiber membranes encapsulating Cu and Ag nanoparticles. The nanoparticles were capped in situ using sepiolite fibrillar nanoparticles. The membranes were biofouled within a cross-flow filtration device by pumping biofoulants (*Saccharomyces cerevisiae* (pH 4.5) and *Pseudomonas putida* as biofoulants (pH 7.5)) across the membranes for 24/48 h. They observed that nanofiber membranes containing AgNPs performed better than those containing CuNPs.

1.4 Scope and objectives of the thesis

The perception that some things which may seem obvious to one's eye may not necessarily be that obvious to someone else's eye can somehow be real. Although the antimicrobial properties of azoles are well documented, the compounds have not been extensively explored in the modern quest to develop new technologies for water purification, particularly for the eradication of pathogenic microorganisms. On the other hand, electrospun nanofibers have over the past decade received much attention in modern scientific research because of their versatility in many applications. Thus the two points provoked the idea for the development of electrospun nylon 6 nanofiber/imidazole composites as new materials to address the challenge of pathogenic microorganisms in drinking water. The focus will be to explore the possibility of developing functionalized electrospun nylon 6 nanofibers that have a potential to be used as filtration membranes with antibiofouling properties. The specific tasks of the thesis were:

(1) To synthesize *N*-alkylimidazole with various substituents (carboxaldehyde (CHO), alcohol (CH_2OH) and carboxylic acids (COOH)) at the 2-position and their silver(I) complexes, as well as screening them for antimicrobial properties.
(2) To investigate the possibility of using electrospun nylon 6 nanofibers as solid support materials to host antimicrobially active 2-substituted *N*-alkylimidazoles and silver(I) complexes for microbial growth inhibition in drinking water.
(3) To investigate the effect of the immobilization of 2-substituted *N*-alkylimidazoles onto electrospun nylon 6 nanofibers on the antimicrobial activity.

(4) To investigate the cytotoxic effects of the developed antimicrobial electrospun nylon 6 nanofibers on human cells.

The experimental pathway which the thesis will follow is outlined in Scheme 1.1.

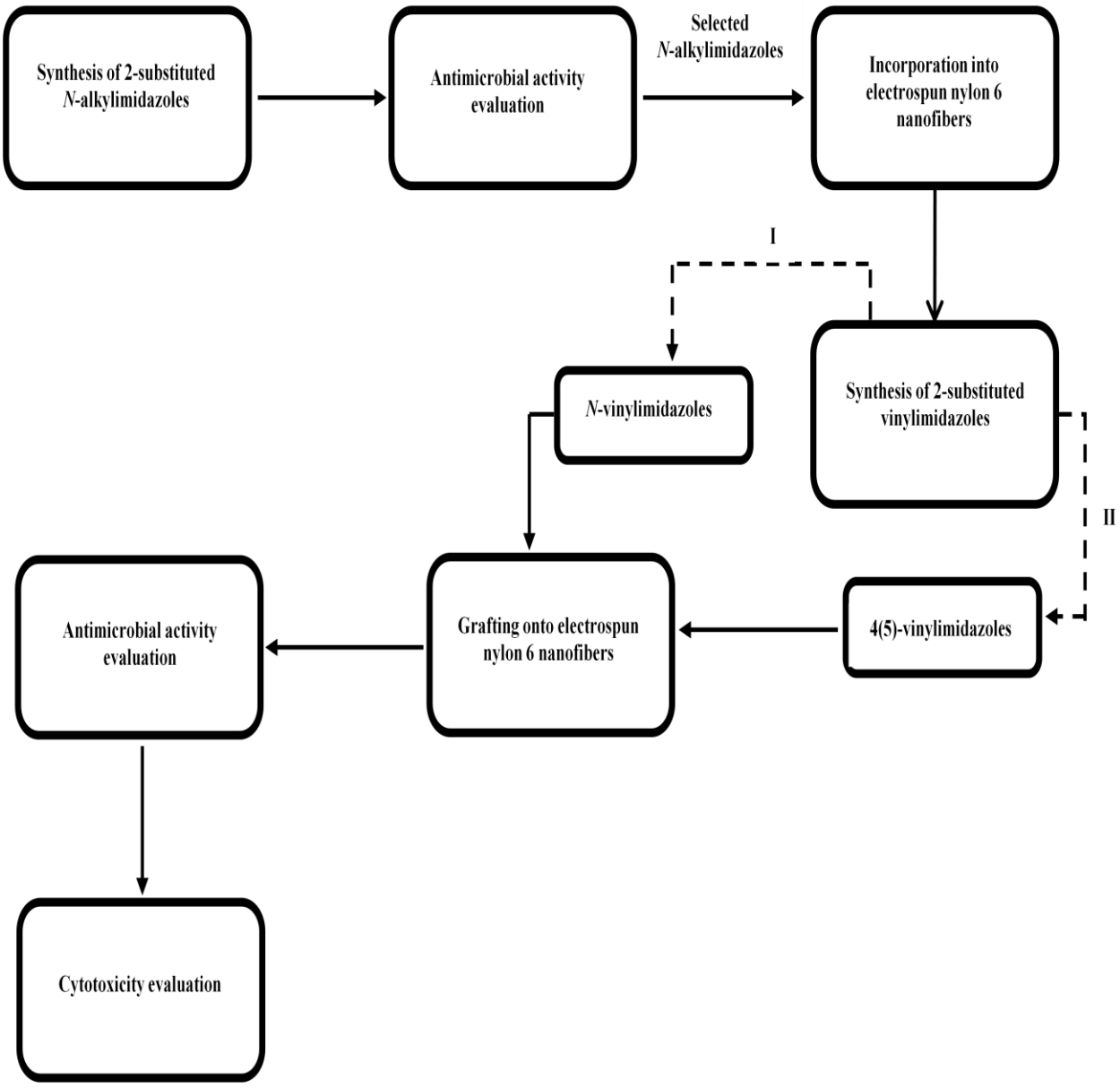

Scheme 1.1. The experimental outline of the thesis

CHAPTER 2 THE ELECTROSPINNING PROCESS

2.1 History of electrospinning

Electrospinning is a method of producing fibers, with diameters in the nanometer range, by applying electric charges to a polymer solution. The first documented account on electrospinning was carried out by Cooley and Morton in the early 1900s.[127-129] In 1914, Zeleny reported the effect of electric field on the behaviour of a fluid droplet and the study paved the way to mathematical modelling of the behaviour of the fluid droplet under the influence of electric field.[128] Between the years 1931 and 1944, Formhals filed a series of patents describing various experimental apparatus for electrospinning of polymer filaments.[127,128]

In 1969, Taylor reported the production of a nanofiber jet from a polymer solution. He found that a polymer jet was ejected from the cone-shaped droplet, later referred to as the Taylor cone, when the electric forces overcome the surface tension of the droplet. The findings contributed significantly towards the fundamental understanding of the behaviour of a polymer droplet under the influence of electric field and subsequently the electrospinning process. In 1987, Hayati explored the factors affecting the jet stability and the electrospinning process.[127] He reported that as the applied voltage increased, superconducting fluids produced very unstable jets that whipped around in different directions, while semiconducting and nonconducting fluids produced stable jets. Hohman *et al.*,[130,131] Yarin *et al*.[132] and Feng[133,134] would later contribute immensely to the in-depth understanding of the electrospinning process through experimental characterization and evaluation of jet instability.

The subsequent years saw an upsurge of research activity on electrospinning due to the potential application of electrospun nanofibers in various fields.[129] Figure 2.1 illustrates how the patent and publication growth on electrospinning has been increasing over the past decade.

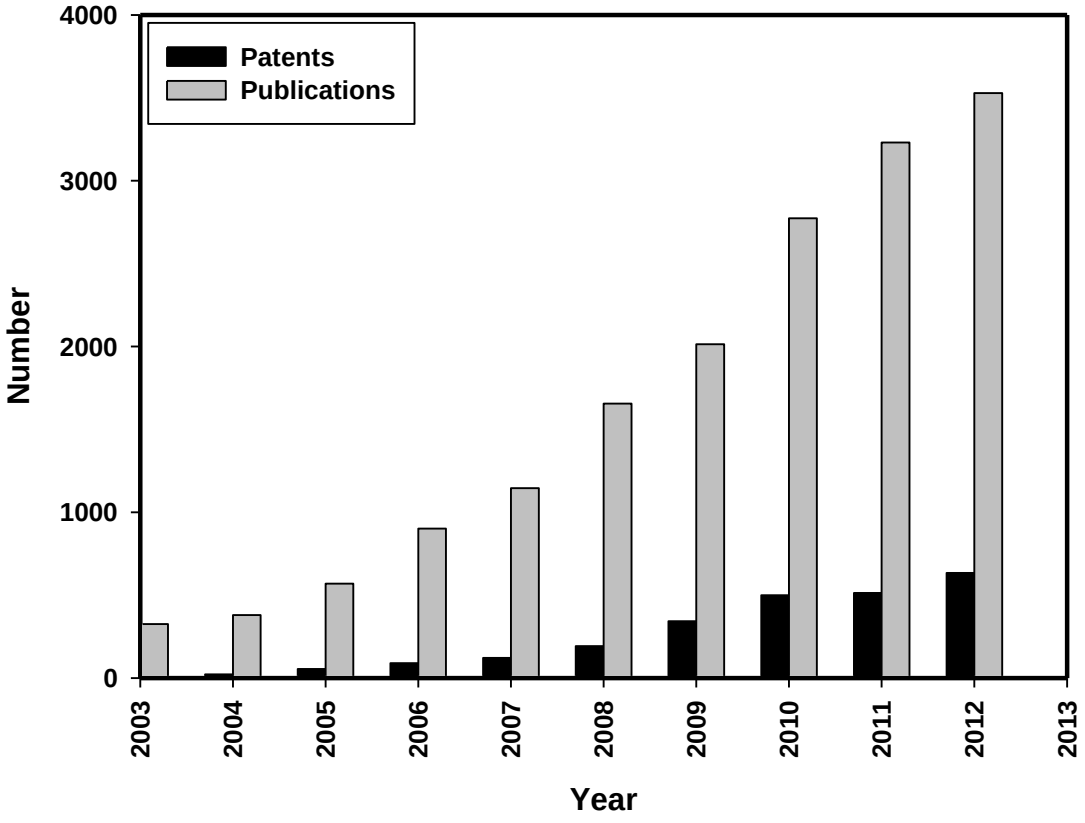

Figure 2.1. Electrospinning patents and publications in the past decade obtained from SciFinder Scholar search using the search terms "electrospinning and electrospun"

2.2 The electrospinning process

Electrospinning is a simple technique of producing nanofibers, from a polymer melt or solution under the influence of electric forces.[135] The electrospinning apparatus consists of three components, namely; the polymer reservoir (syringe) connected to a spinneret (needle), a high voltage power supply as well as a collector (usually a grounded metal sheet). In the electrospinning process a polymer droplet is suspended at the tip of a spinneret by its surface tension which is initially in equilibrium with the gravitational force.[136] When the applied voltage increases to a critical value the polymer droplet at the tip of the spinneret becomes cone-shaped (Taylor cone) due to repulsive forces between surface charges. When the applied voltage surpasses the critical value a jet emerges from the Taylor cone, which after a short distance experiences bending instability due to surface charge perturbation (Fig. 2.2).

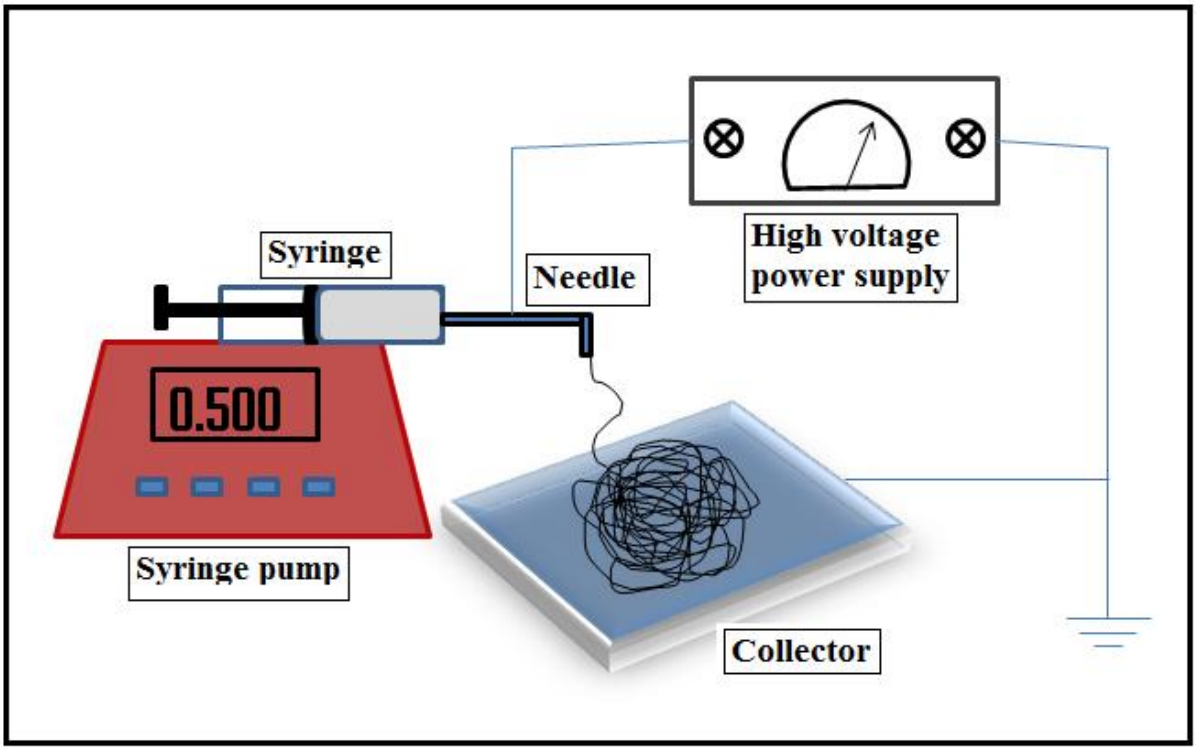

Figure 2.2. A schematic of an electrospinning apparatus for the fabrication of nanofibers

The helical loop formed by the Taylor cone as a result of bending instability increases the path of the jet allowing for its elongation and hence the formation of a continuous nanofiber. The parameters that affect the electrospinning process and morphology of nanofibers are classified as polymer solution (viscocity, conductivity, surface tension), process conditions (voltage, flow rate, needle diameter, temperature) and ambient conditions (humidity). However, the electrospinning process is most significantly affected by the polymer solution parameters.[135,137]

2.3 Factors affecting the electrospinning process

2.3.1 Solution parameters

The major solution properties of a polymer solution that significantly affect the electrospinning process include the viscocity, the conductivity and the surface tension. The manner in which the solution parameters affect the electrospinning process is discussed in the following subsections.

2.3.1.1 Viscosity

For the electrospinning process to take place a sufficiently high molecular weight polymer and viscosity are necessary.[135] However, the viscosity of the polymer solution is dependent on the molecular weight of polymer. The viscosity and the molecular weight are related by the Mark-Houwink-Sakurada equation (Eqn. 2.1);

$$[\eta] = KM^a \qquad (2.1)$$

where $[\eta]$ is the viscocity of the solution, M is the molecular weight, *K* and *a* are constants that depend on the polymer, solvent and temperature.[138,139] The solution of a polymer exhibiting higher molecular weight has a higher viscosity than that of a lower molecular weight polymer with the same concentration. The role played by the chain entanglements to the electrospinning process was explained by Shenoy *et al*.[140] They noted that at low concentration or volume fraction of the polymer, chain entanglements are non-existent (viscosity is low) leading to polymer solution break up (Fig. 2.3). However, above the critical concentration or volume fraction chain entanglements are present (higher viscosity), thus the charged jet stretches as it is ejected from the tip of the spinneret to the collector, and is prevented from breaking by the polymer entanglements resulting in a continuous polymer jet.[140,141] When the viscosity of the polymer solution is low, the polymer nanofibers that are formed become highly beaded.

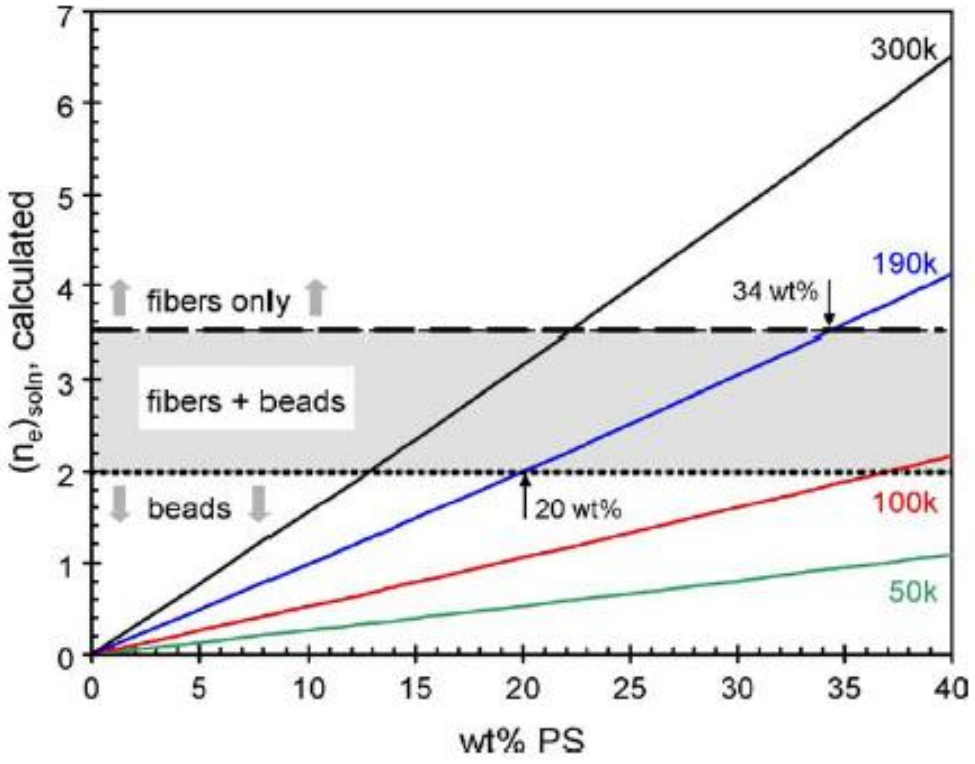

Figure 2.3. Plot of calculated number of entanglements (n_e) as a function of solution concentration[140]

The formation of beads along the nanofibers is attributed to the presence of fewer solvent molecules along the polymer chains and the dominance of surface tension.[135,138,139,142] However, at higher solution viscosity, smooth (beadless) nanofibers are obtained due to more polymer chain entanglements. An increase in the polymer concentration and molecular weight results in higher polymer chain entanglements and subsequently to higher solution viscosity. However, for any electrospinnable polymer solution there is an optimum viscosity beyond which the solution becomes difficult to electrospin. The difficulty to electrospin the polymer solution above the optimum viscosity is attributed to solidifying of the solution at the tip of the spinneret. A very high viscosity also leads to the formation of polymer nanofibers with larger diameters.

2.3.1.2 Surface tension

Electrospinning takes place when the electric charges (forces) on the surface of the polymer solution overcome the surface tension of the polymer solution. Surface tension could cause the formation of beads, along the jet's stretching path to the collector, due to the reduction of the surface area per unit mass.[135,137] At a lower concentration of the solvent molecules, aggregation of the molecules tends to occur with the formation of beads along the nanofiber jet due to surface tension (Fig. 2.4B). A higher viscosity prevents the aggregation of solvent molecules under the influence of surface tension, resulting in smooth (beadless) nanofibers (Fig. 2. 4A).

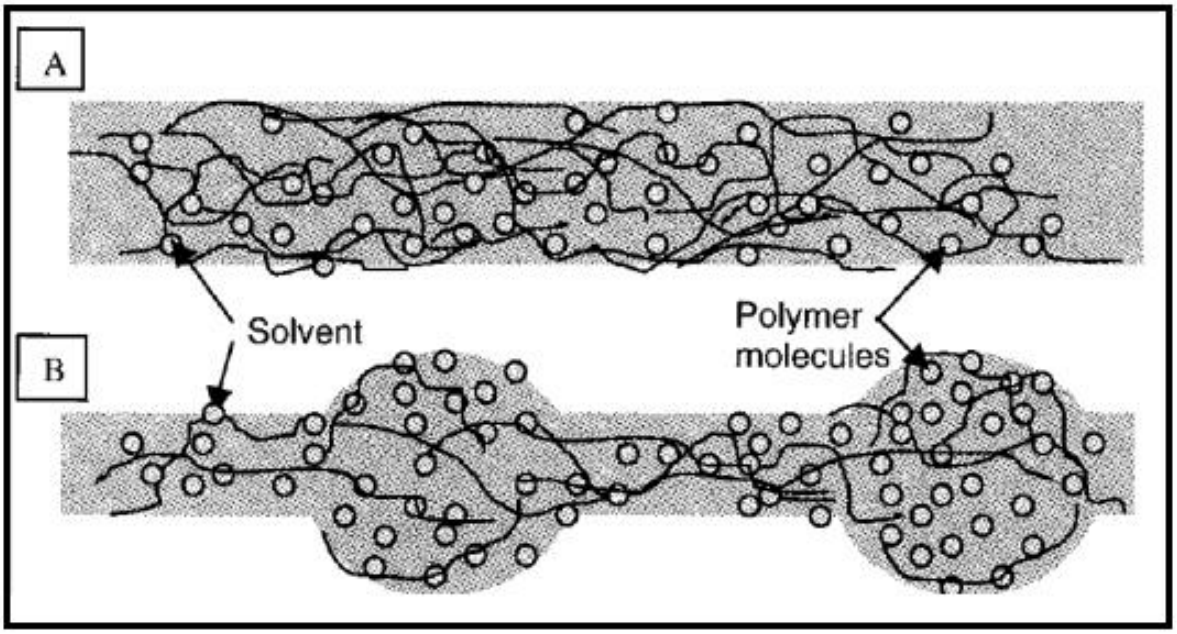

Figure 2.4. Interaction of solvent molecules with chain entanglements; (A) at high viscosity and (B) at low viscosity[135]

However, the formation of beads could be circumvented by the use of solvents with low surface tension or by the addition of a surfactant to the polymer solution. Fong *et al.*[143] observed that the addition of ethanol, a low surface tension solvent, in an aqueous polyethylene oxide (PEO) solution resulted in smooth nanofiber although they had larger diameters. Kriegel *et al.*[144] as well as Jia and Qin[145] investigated the influence of a surfactant on electrospinning and reported that the addition of a surfactant in the electrospinning

solution remarkably reduced the surface tension of the solution and the diameters of the nanofibers obtained.

2.3.1.3 Conductivity

The formation of nanofibers during the electrospinning process is a result of the stretching of the polymer solution due to the repulsive forces between electric charges on the surface. Thus increasing the conductivity of the polymer solution increases the electric charges on the jet and consequently the repulsive forces between them. Uyar and Besenbacher[146] investigated the effect of solution conductivity on the morphology of electrospun polystyrene (PS) nanofibers. Of all the solvents employed, dimethylformamide (DMF) (with the highest conductivity) gave smooth (beadless) polystyrene nanofibers (Fig. 2.5). An increase in the conductivity of the polymer solution was found to increase the Coulombic force (responsible for the stretching of the polymer jet) that overcomes the viscoelastic force which is accompanied by the formation of smooth nanofibers with smaller diameters.

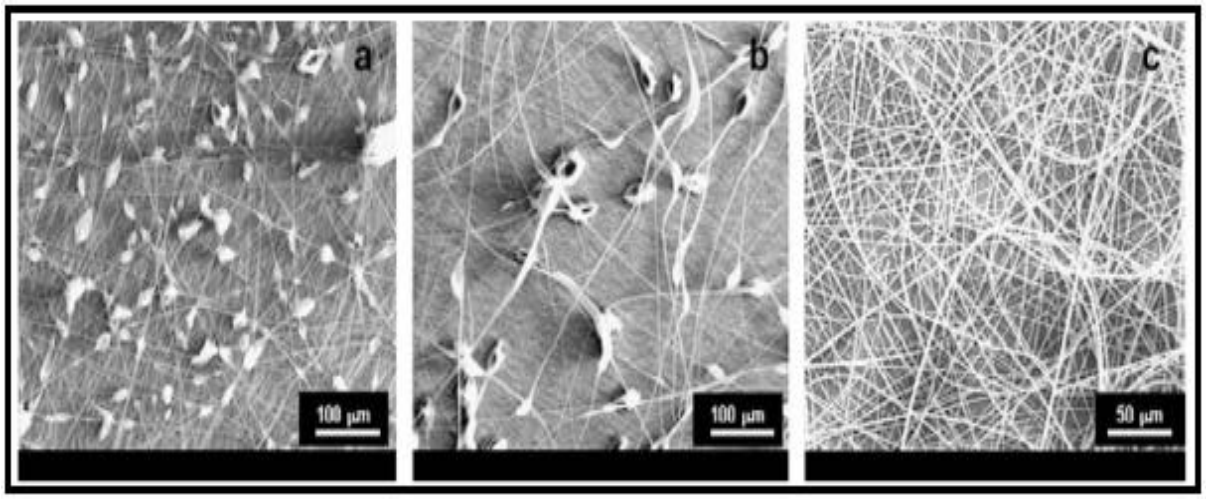

Figure 2.5. SEM images of electrospun PS nanofiber in (a) THF, (b) $CHCl_3$ and (c) DMF[146]

Moreover, an increase in conductivity reduces the critical applied voltage required for electrospinning as well as the increase in the bending instability of the jet. The greater bending instability, in turn, results in the larger deposition area of the nanofibers. It was also demonstrated that the conductivity could be increased by the addition of ionic salts,[142,143]

ionic surfactants,[147] changing the pH of the polymer solution[148,149] as well as the addition of solvents with high dielectric constants.[150]

2.3.2 Processing parameters

2.3.2.1 The applied voltage

For the electrospinning process to occur a high voltage must be applied to the polymer solution and the electric charges produced in the solution have to overcome the surface tension. The stability of the Taylor cone formed at the tip of the spinneret is ensured by finding the optimal flow rate of the solution and the applied voltage.[151] Low flow rates require lower applied voltages while high applied voltages are required when higher flow rates are used. It was observed by Zong and co-workers that when the voltage is higher and the flow rate is lower, the electric charges on the polymer jet causes the jet to accelerate faster.[152] The acceleration of the jet then results in the instability of the Taylor cone due to lack of the polymer solution at the tip of the spinneret.

The applied voltage would also have an influence on the morphology of the resultant nanofibers since it influences the stretching and acceleration of the polymer jet. The higher voltage causes a greater stretching of the polymer jet due to an increase in the Coulombic force and hence the formation of thinner nanofibers.[56,153,154] However, there were reported instances where the diameter of the nanofibers was found to increase with increasing applied voltage.[155-157] The observation was attributed to the drawing of a greater solution volume at higher applied voltages.[158] It was also observed that higher voltages could result in the formation of beaded nanofibers,[159] although in some cases beadless nanofibers were obtained.[160]

The electric charges on the jet are influenced by the external electric field which consequently affects the jet path. The effect inspired several attempts to control the electrospinning jet, by varying the electric field profile between the spinneret and the collector.[137] The formation of aligned and patterned nanofibers was achieved by the manipulation of the electric field using auxiliary electrodes[161,162] or by altering the speed, orientation or the shape of the collector.[163-167] Figure 2.6 illustrates aligned electrospun nanofibers collected using patterned gold electrodes.

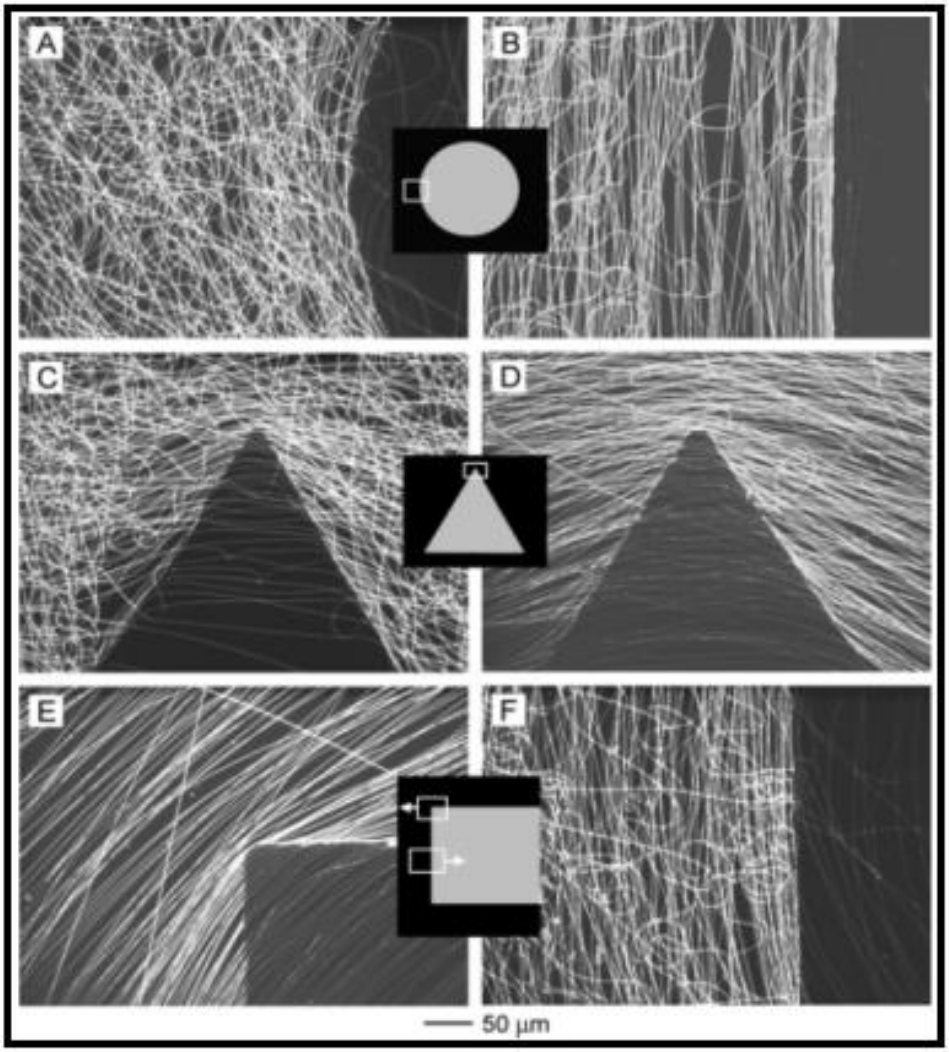

Figure 2.6. Aligned electrospun nanofibers collected using patterned gold electrodes[161]

2.3.2.2 The flow rate

The stability of the Taylor cone at the tip of the spinneret is dependent on the flow rate and the applied voltage. At a particular flow rate there exists an optimum (critical) applied voltage to maintain a stable Taylor cone. At a lower flow rate and a higher applied voltage the polymer jet recedes into the spinneret while at a higher flow rate and at lower applied voltage the solution has a tendency to electrospray. Electrospraying of the polymer jet is due to the imbalance between the viscoelastic force and the Coulombic force, i.e., the viscoelastic force overcomes the Coulombic force. There have been several studies that investigated the influence of solution flow rate on the magnitude and morphology of electrospun nanofibers.[152,168]

An increase in the flow rate also results in the fusion of the nanofibers on the collector due to slow evaporation of the solvent when the spinneret tip to collector distance is decreased. Higher flow rates result in thicker nanofibers while at lower flow rates nanofibers with thinner diameters are obtained.[168,169] Therefore, it is evident that lower flow rates are desirable since the solvents evaporate quicker and nanofibers with thinner diameters were usually obtained.[129]

2.3.2.3 The collector

A collector is mostly made up of a conducting material, usually an aluminium foil, which is grounded to maintain a constant potential difference between the spinneret and the collector. Sometimes a non-conducting material is used as a collector and in such cases the electric charges on the jet rapidly accumulate on the collector causing fewer nanofibers to be deposited.[135] Moreover, the nanofibers deposited on such materials have a lower packing density compared to when a conducting material is used. It is thought that the lower packing density could be due to the repulsive forces of the accumulated electric charges on the collector as electrospun nanofibers are being deposited.[166] However, the packing density of the deposited nanofibers increases when a conducting material is used since the charges would be dissipated. Deitzel *et al.*[158] also observed that the repulsion on the subsequent nanofibers resulted in the formation of honeycomb structures (Fig. 2.7) when there was sufficient density of electric charges on the initially collected nanofibers.

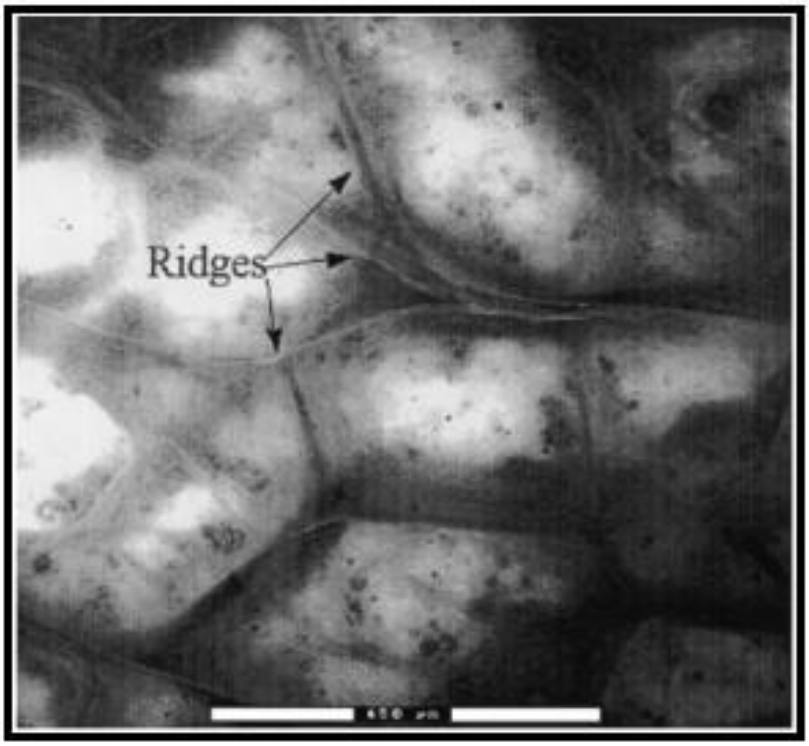

Figure 2.7. Honeycomb structures on nanofibers collected onto a non-conducting material[158]

The accumulation of electric charges causes the formation of dimples on the nanofiber mesh if the rate of deposition is higher and the nanofiber mesh is sufficiently thick, even when a conducting collector is used, since polymer nanofibers are generally non-conducting.[135] It has also been observed that porous collectors result in a lower packing density of nanofibers.[166] The lower packing density of nanofibers was attributed to the diffusion and faster evaporation rate of the residual solvent on the collected nanofibers. The motion of the collector also affects the electrospinning process. The formation of aligned or non-aligned electrospun nanofibers can be achieved by varying the speed of the rotating collector while a stationary collector results in a nanofiber mesh.[163-165] A rotating collector is also believed to increase the rate of evaporation of the residual solvent resulting in the collection of individual nanofibers.

2.3.2.4 The spinneret (needle) diameter

The internal diameter of the spinneret affects the electrospinning process. When a spinneret with a smaller internal diameter is used, it reduces clogging due to minimum exposure of the polymer solution to the external environment. A smaller internal diameter also reduces the

number of beads formed on electrospun nanofibers. The diameters of electrospun nanofibers were found to decrease when a spinneret with a smaller internal diameter was used.[170] In contrast, Macossay *et al.*[171] found that there was no correlation between the diameters of the electrospun nanofibers and the radii sizes of the three different spinnerets they used for the electrospinning of poly(methylmethacrylate) nanofibers. However, too small a diameter makes it difficult to pump the polymer solution from the tip of the spinneret.[158]

2.3.2.5 Spinneret tip-to-collector distance

The time of flight of the polymer jet and the strength of the electric field have a direct effect on the electrospinning process.[172] Both the time of flight and the electric field can be influenced by varying the distance between the spinneret tip and the collector. When the distance between the spinneret tip and the collector is decreased the distance that the jet travels to the collector is shortened resulting in insufficient time for the residual solvent to evaporate.[56,129,135] Moreover, the electric field strength increases as the distance between the spinneret tip and the collector is reduced resulting in a similar effect which causes the merging of the nanofibers. Whether or not varying the distance between the spinneret tip and the collector has an influence on the nanofiber morphology depends on the solution properties.[129,135] There have been reported cases where shorter distances between the spinneret tip and the collector were found to decrease the nanofiber diameter.[56,154,172] Other researchers have observed an increase in nanofiber diameter as the distance was increased.[56] However, if the distance between the spinneret tip and the collector results in an optimum electric field strength, the possibility of the formation of beads is significantly reduced since the electrostatic field provides sufficient stretching force to the polymer jet.[129]

2.3.2.6 Temperature

Increasing the temperature of the polymer solution increases the evaporation rate[142,173] of the solvent and the reduction in the viscosity[173] and the surface tension[174] of the solution. A lower viscosity, as already mentioned previously, results in the viscoelastic force being overcome by the Coulombic force thereby forming nanofibers with smaller diameters.

2.3.3 Ambient parameters

2.3.3.1 Humidity

The humidity of the electrospinning environment has an influence on the polymer solution during the electrospinning process. It was observed that at higher humidity there is a tendency for the nanofibers to have circular pores.[175] This effect has been attributed to the condensation of water molecules on the surface of the nanofibers. De Vrieze *et al*.[173] reported that the relative humidity could result in either smaller or larger diameter nanofibers, depending on the chemical nature of the polymer. It was also observed that the pore sizes increased with increasing humidity to a point where they coalesced to form large, non-uniformly shaped structures. Casper *et al*.[176] reported that the depth of the pores, the diameter size and the number of pores begin to saturate above a certain humidity.

The humidity of the electrospinning environment also affects the evaporation of the residual solvent. Volatile solvents evaporate very rapidly at very low humidity and the effect could lead to clogging of the spinneret. Li *et al*.[135,175] suggested the possibility of using humidity to discharge electrospun nanofibers.[161]

2.3.3.2 Type of atmosphere

The electrospinning process can also be influenced by the composition of air in the environment. It has been reported that in the presence of a gas with low breakdown voltage, such as helium, the electrospinning process was difficult.[135] Moreover, the diameter of nanofibers increases when a high breakdown gas, such as CO_2 and freons, is used.[177]

2.3.3.3 Pressure

It is generally understood that when the pressure is below atmospheric pressure, the polymer solution in the syringe has a tendency to extrude from the spinneret causing an unstable jet initiation.[135] At the same time, electrospinning is not possible at very low pressure due to the discharging of electric charges.

2.4 Functionalization of electrospun nanofibers

Most often the polymers used for the fabrication of electrospun nanofibers do not have the necessary functional groups required for various applications. For this reason, the introduction of functional groups in the polymer nanofibers, without altering the bulk properties, becomes inevitable. The functionalities can either be introduced before (pre-electrospinning functionalization method) or after (post-electrospinning method) electrospinning of the nanofibers. After functionalization the electrospun nanofibers possess a potential for application in a wide variety of fields such as filtration, sensing devices, drug delivery, tissue engineering, biomaterials, catalysis and electronics.[167,178]

2.4.1 Pre-electrospinning functionalization method

In the pre-electrospinning functionalization method (sometimes referred to as pre-functionalization method), the functionality is introduced first in the polymer and then the functionalized polymer is electrospun. In most cases the functional molecules are introduced into the electrospinning polymer solution before being electrospun and the method is referred to as 'blending'.

2.4.1.1 Blending

Pre-functionalization of nanofibers is carried out by blending of the molecules containing the target functionality in the electrospinning polymer solution (Fig. 2.8). Blending ensures that the functional molecules remain incorporated within the electrospun nanofibers.

However, blending of the functional molecules poses some challenges due to various factors including the leaching of the molecules from nanofibers, the uncertainty over the interaction of the blended molecules with the polymer and the availability of the molecules on the surface of the nanofiber. However, blending of functional molecules into electrospun nanofibers still remains the preferred method of functionalization in fields such as drug delivery systems.[135,179] The reason is that the nanofibers would have the ability to release the active molecules at the target site, preferably over prolonged periods.[179]

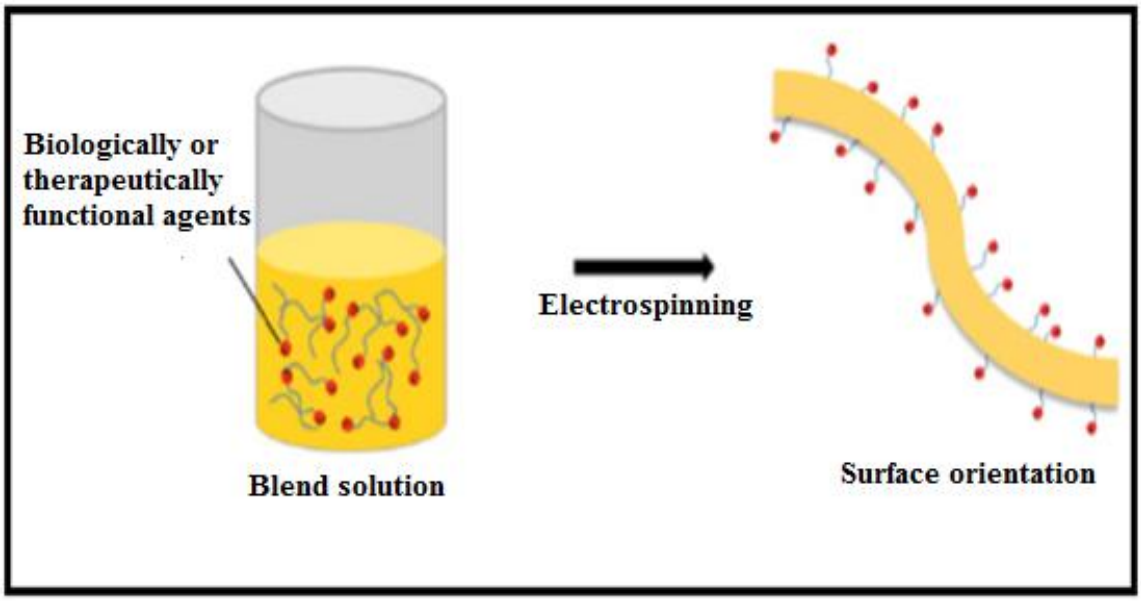

Figure 2.8. Blending technique for the surface functionalization of electrospun nanofibers[179]

Sometimes polymers could have the required functionalities for a particular application, but would prove very difficult to electrospin. In such a case, the polymers are usually blended with electrospinnable polymers to produce composite polymer nanofibers.[117,180]

To circumvent the challenges posed by blending functional molecules within the nanofibers, the method of covalently linking functional molecules onto the polymer could be used. A crucial requirement for this method of functionalization is the systematic choice of a polymer with appropriate reactive sites for successful attachment of functional molecules. For example, poly(vinylbenzyl chloride) (PVBC) has been extensively used for the immobilization of various functional groups.[181,182] PVBC has chloride groups that can easily be substituted by several functionalities. Another important requirement for immobilization of functional molecules in a covalent linkage technique is the solubility of the polymer before and after functionalization.[183] The polymer must be soluble before electrospinning for the reaction with the molecule being immobilized (covalently linked) to occur. Consequently, for the product to be fabricated into nanofibers, it has to be soluble. The major challenge with pre-functionalization is the uncertainty over the orientation of the functionalities on the surface of the electrospun polymer nanofibers. Recently, due to these challenges, the most commonly adopted method of functionalization of electrospun nanofiber is the post-electrospinning functionalization method.[184-187]

2.4.2 Post-electrospinning functionalization method

In the post-electrospinning functionalization method (also referred to as post-functionalization method) the polymer is electrospun first and then the functionality is subsequently introduced. It is worth noting that there are several techniques that could be used for the post-functionalization of the electrospun nanofibers. The techniques include, amongst others, physical adsorption, chemical vapour deposition, chemical treatment and graft polymerization. The major advantage of the post-functionalization method is that the functionalities are always exposed on the surface of the electrospun nanofibers resulting in performance enhancement of the nanofibers. Moreover, the functionalities remain immobilized on the surface of the electrospun nanofiber and hence there is no leaching (except in physical adsorption) of the functional molecules and thus the nanofibers can be used repeatedly without loss of performance.

2.4.2.1 Physical adsorption

Physical surface adsorption is the simplest post-functionalization technique commonly used for loading drugs onto electrospun nanofibers. The interaction of functional molecules (drugs) and the polymer nanofibers is generally through hydrogen bonding, Van der Waal's forces, hydrophobic and electrostatic interactions.[179]

As with the blending technique, physical adsorption has been extensively used for the functionalization of electrospun nanofibers for drug delivery purposes. Typically, laminin (a neurite promoting extracellular matrix protein) was physically adsorbed on poly(L-lactic acid) (PLLA) nanofiber scaffolds that were used for mimicking the extracellular matrix in the process of repairing and regeneration of damaged tissue.[188] Adsorption of nanoparticles on the surface of electrospun nanofibers, for application in various fields, has also been attempted.[189,190]

2.4.2.2 Chemical vapour deposition (CVD)

Chemical vapour deposition is a technique where a solid substrate is exposed to volatile gaseous precursors which react on contact with the surface of the substrate forming a thin film.[191] The process is usually promoted by heat (thermal CVD), ultraviolet (UV, photo-

assisted) or plasma (plasma-assisted CVD). The thickness of the deposited film is dependent on factors, such as the type of precursor, the carrier gas flow rate and the deposition time.

Ma *et al.*[192] produced superhydrophobic electrospun nanofiber fabrics using a chemical vapour deposition technique. They coated electrospun polycaprolactone (PCL) nanofibers with a thin layer of hydrophobic poly(perfluoroalkyl ethyl methacrylate) using *t*-butyl peroxide as an initiator.

2.4.2.3 Chemical Treatment

The functionalization of electrospun nanofibers by chemical treatment is similar to the previously described covalent linking of functional molecules (pre-functionaliztion), except that the immobilization of functional molecules is done onto already fabricated nanofibers. It is imperative, in this chemical immobilization technique, that the solvents used do not dissolve the nanofibers so as to maintain their integrity (nanofibrous structure). Functionalization using this technique results in non-leachable functional molecules, however, the immobilized molecules could partially lose their activity.[179] Moreover, functionalization is usually not complete even after long treatment periods.

Various functional molecules were immobilized on the surface of electrospun nanofibers for potential applications in many research fields. Proteins were immobilized on the surface of PCL nanofibers, after the plasma treatment, and were found to have a potential to be used as tissue engineering scaffolds to control cellular adhesion and differentiation.[193]

Another method for post-functionalization of electrospun nanofibers that recently received much attention is the graft (co)polymerization method. This post-functionalization method will be dealt with extensively in the following section.

2.5 Graft polymerization

Grafting is a process by which functionalized monomers are covalently attached on the surface of polymers. The graft polymerization process could be achieved by two approaches, namely; ‘grafting onto’ or ‘grafting from’ (Fig. 2.9). In the ‘grafting onto’ approach functionalized monomers react directly with the polymer backbone while in the ‘grafting

from' approach the initiator is first immobilized on the polymer, followed by polymerization of the functionalized monomers.[108] Graft polymerization can be achieved using several techniques such as chemical, plasma, enzymatic and radiation treatment.[194-197]

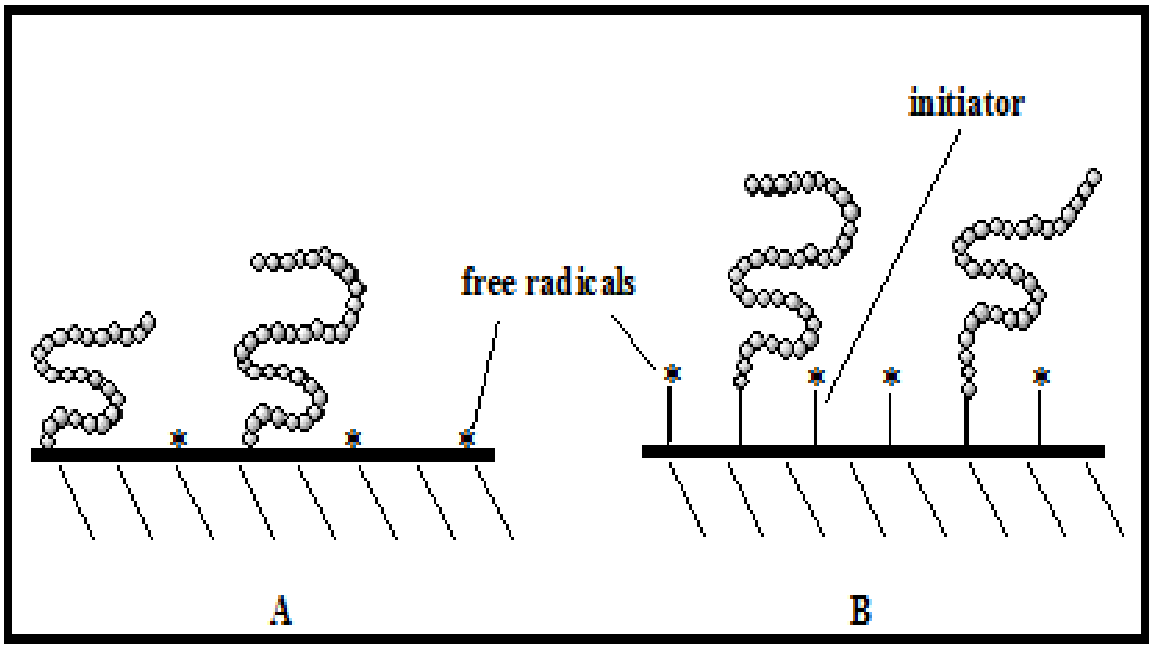

Figure 2.9. Schematic diagrams of grafting approaches; 'grafting onto' (A) and 'grafting from' (B)[109]

2.5.1 Grafting polymerization techniques

2.5.1.1 Grafting by chemical treatment

The chemical grafting technique can be accomplished either by a free radical or ionic pathway. In the free radical grafting pathway, free radicals are produced from the initiator and transferred to the substrate (polymer) followed by the reaction with the monomer. The formation of free radicals is induced by thermal decomposition (Scheme 2.1) of the initiator such as azobisisobutyronitrile (AIBN)[198] or benzoyl peroxide (BPO).[199] However, the two initiators are known to result in lower degrees of grafting, with BPO being more reactive than AIBN.[108] Azobisisobutyronitrile is less reactive than BPO due to resonance stabilization of its primary radical. The low degree of grafting is attributed to the fact that not all of the free radicals formed are involved in grafting.

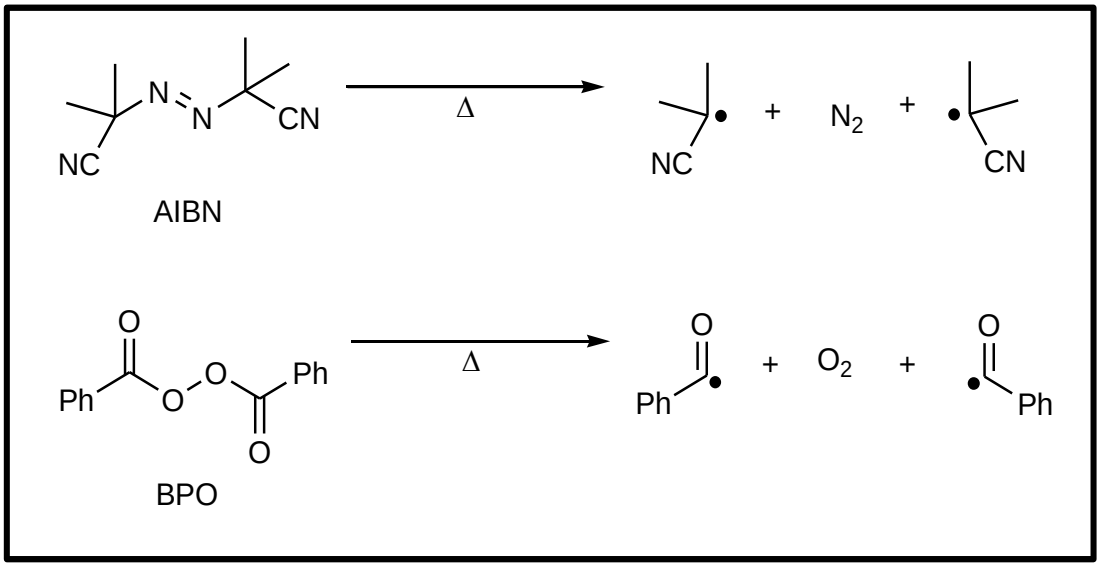

Scheme 2.1. Thermal decomposition of AIBN and BPO

The formation of free radicals could also be induced by redox initiators. Redox initiators consist of a mixture of metal ion and hydrogen peroxide, thiosulfate or persulfate ions (M^{n+}/H_2O_2, $S_2O_3^{2-}$ or $S_2O_8^{2-}$, M^{n+} = Cu^{2+}, Fe^{2+}).[46,197,200-202] The active species in the decomposition of H_2O_2 and $S_2O_8^{2-}$ induced by metal ions have been proposed to be $OH^{\bullet}$ and $SO_4^{-\bullet}$ respectively (Eqns 2.2 & 2.3).

$$M^{n+} + H_2O_2 \longrightarrow M^{(n-1)+} + OH^{\bullet} \qquad (2.2)$$

$$M^{n+} + S_2O_8^{2-} \longrightarrow M^{(n-1)+} + SO_4^{-\bullet} \qquad (2.3)$$

The $SO_4^{-\bullet}$ radical is thought to react in two different ways; either it reacts with H_2O to form $OH^{\bullet}$ which subsequently produces free radicals on the polymer backbone or the $SO_4^{-\bullet}$ radical reacts directly with the polymer backbone to produce radicals on the polymer backbone. There are many other redox initiator systems that have been employed for graft polymerization and all react in a similar manner.[108] Some transition metal ions have also been used for the oxidation of the polymeric backbone resulting in graft polymerization.[203-205] The important requirement is that the transition metal ion must have a low oxidation potential. Metal chelates with low oxidation potentials have also been reported to induce free radicals

on the polymer backbone.[206,207] It has also been reported that high redox potentials enhance the formation of the homopolymers.

Grafting has over the years been achieved by a 'living polymerization' method, and in the method graft polymerization occurs in a controlled manner such that polymer chains can be grown to a desired length. A 'living polymer' is described as the polymer that retains its ability to be propagated for a lengthy period and grows to a desired maximum chain size while the degree of termination or chain transfer remains insignificant.[208] Atom transfer radical polymerization (ATRP) has been the commonly used technique for grafting of living polymers with regulated molecular weights.[209-211] In the ATRP technique, the important reaction is the activation-deactivation dynamic equilibrium process (Eqn 2.4):

$$P_n\text{-X} + \text{Cu(I)/2L} \longrightarrow P_n^{\bullet} + \text{Cu(II)/2L} \qquad (2.4)$$

where P_n-X is a polymeric halide [e.g. polyvinylchloride (PVC)] and Cu(I) complex CuX/2L (X = Cl, Br and L = 2,2′-bipyridine or 4,4′-disubstituted bipyridine). The role of the Cu complex is to act as a reversible halogen transfer reagent between the active and dormant polymer chains. Other multidentate amine-based ligands such as tetraethylenediamine, *N*,*N*,*N*′,*N*′,*N*′-pentamethyltetraethylenediamine as well as (*tris*-2-aminoethyl)amine were also used in the Cu-mediated ATRP of monomers.[212,213]

2.5.2 Grafting by photochemical treatment

Some polymers contain chromophores (e.g. double bonds) that can absorb light and the electrons excited from a ground state into an excited state. While at the excited state, the chromophores then cleave into free radicals which could promote graft polymerization. In cases where absorption of light by the chromophores does not yield free radicals, photosensitizers are then used to mediate in bond cleavage and thus forming reactive free radicals. Several photosensitizers that were used in graft polymerization are the aromatic ketones (benzophenone and xanthones), dyes (sodium anthraquinone sulfonate or acrylated azo dyes), benzoin ethylether and metal ions such as UO_2^{2+}.[214-218] In the absence of a photosensitizer, free radicals are generated on the polymer backbone and subsequently react

with the monomer to produce a grafted polymer. On the other hand, in the presence of a photosensitizer the free radicals formed by the photosensitizer induce free radicals on the polymer backbone which then react with monomers yielding a grafted polymer.

2.5.3 Grafting with radiation treatment

Over the years, graft polymerization has been achieved using radiation-mediated techniques such as electron beam, plasma, γ-rays and UV irradiation. Irradiating macromolecules can cause homolytic fission (or cleavage) and therefore generate free radicals on the polymer backbone. The initiator need not be present when grafting is carried out under radiation conditions[108]. In the absence of the initiator, however, the grafting environment is important. For example, grafting in the presence of molecular oxygen or air generates peroxides on the polymer backbone. There are three different ways with which radiation-mediated graft polymerization can proceed, namely, (i) pre-irradiation, (ii) peroxidation and (iii) simultaneous irradiation.[108,219]

2.5.3.1 Pre-irradiation

In the pre-irradiation technique, the polymer is subjected to radiation in an inert gas or under reduced pressure (vacuum), followed by treatment with the monomer in the vapour or liquid state or in solution (Scheme 2.2).[108,219] Several polymers have been functionalized by pre-irradiation graft polymerization to afford functionality for different applications.[196,219-222]

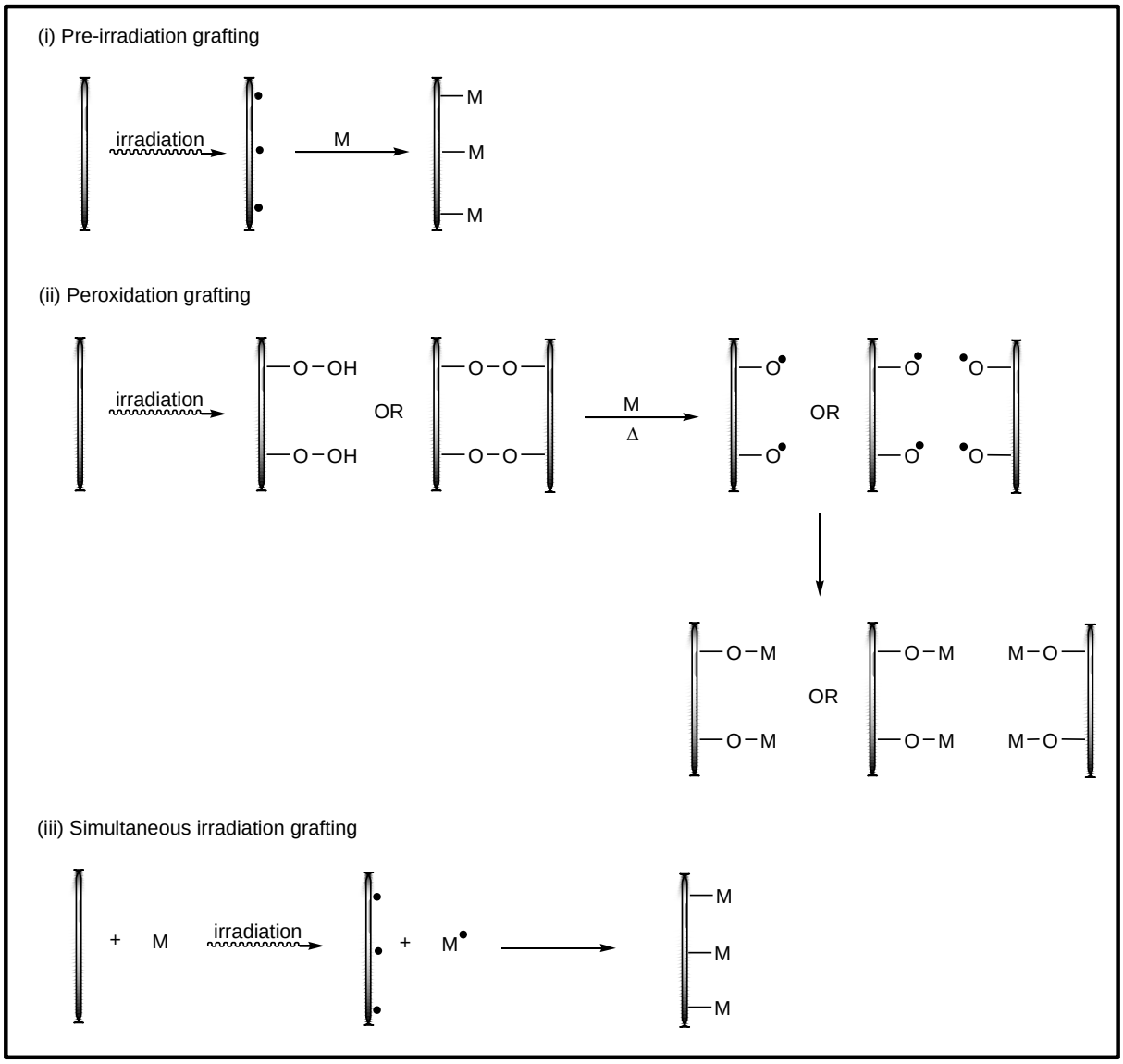

Scheme 2.2. Schematic representations of irradiation techniques for graft polymerization

2.5.3.2 Peroxidation

As with the pre-irradiation grafting technique, peroxidation is carried out in two steps (Scheme 2.2); the polymer is irradiated in an oxygen or air atmosphere which results in the generation of hydroperoxides or diperoxides, depending on the nature of the polymer backbone.[108,219] The second step involves the treatment of the irradiated polymer with the monomer at elevated temperatures. The peroxides then decompose to form free radicals with subsequent graft polymerization. The advantage with the peroxidation technique is that the peroxidated polymers obtained can be stored over long periods. The peroxidation technique

has been utilized by several groups for functionalization of different polymers.[223-226] However, the pre-irradiation and peroxidation methods could result in cleavage of the polymer chains.[108,219]

2.5.3.3 Simultaneous (mutual) irradiation

The simultaneous irradiation grafting technique involves the irradiation of the polymer and the monomer in a single step, with subsequent graft polymerization (Scheme 2.2). The major disadvantage of the simultaneous irradiation technique is the formation of a homopolymer. However, the simultaneous irradiation technique is faster than the peroxidation and pre-irradiation methods and also results in a lower level of polymer chain cleavage.[219]

2.6 Characterization of electrospun nanofibers

Although the electrospinning process dates back to the early 1900s, the resurgence of interest only began in the mid 1990s as qualitative and quantitative techniques that enabled characterization of nanomaterials became available. The surface roughness of two-dimensional polymers, porosity, pore size and distribution, the specific surface area for porous and non-woven polymer membranes, and the intra-fiber surface roughness can all be classified under geometric and topographic properties.[227] The surface chemical properties and chemical composition of electrospun nanofibers can be different from the bulk polymer, moreover, in some cases can be transformed by surface modification.[228] Therefore, the understanding of the topology, morphology and surface chemistry of electrospun nanofibers is very important for the determination of their suitability in a particular field of application.

2.6.1 Surface area and porosity

Electrospun nanofibers are highly porous materials, thus they have very large surface area-to-volume ratios (Fig. 2.10). The large surface area-to-volume ratio is the main property that is exploited for applications such as filtration and adsorption. Thus, it is always very important to accurately characterize the electrospun nanofibrous materials so as to optimize their use in different fields of application. There are several available techniques for more in-depth

characterization of electrospun nanofibers, including Brunauer-Emmet-Teller (BET) gas adsorption, capillary flow porometry and mercury flow porosimetry.

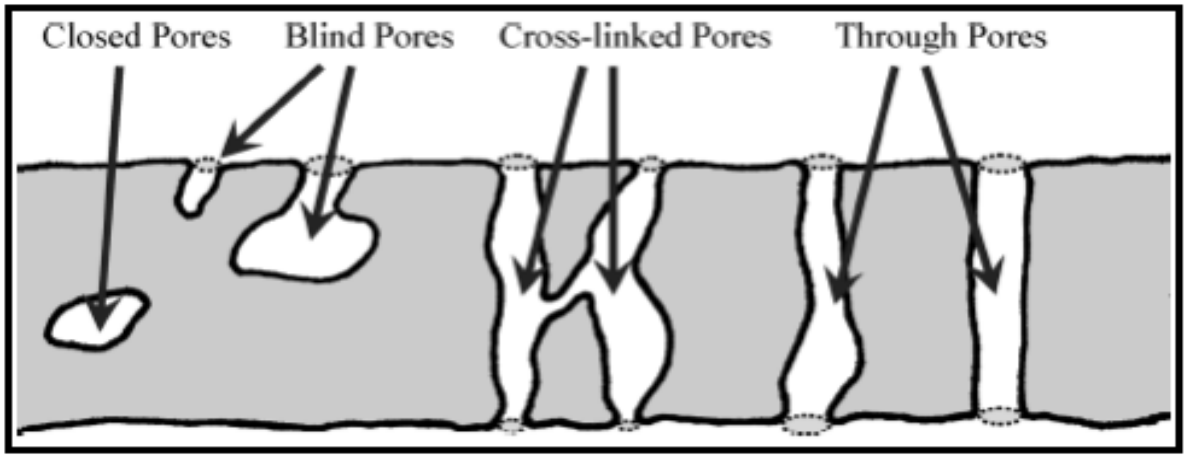

Figure 2.10. Schematic representation of pores[229]

2.6.1.1 Mercury porosimetry

Mercury porosimetry is a conventional technique used for the characterization of surface porosity, pore volume and pore size distribution.[229] It is a liquid intrusion method in which mercury is used for the determination of pore volume and pore size distribution. Mercury is a suitable liquid as it has a high surface tension and thus makes larger contact angles with many materials. The high surface tension results in mercury not being able to spontaneously penetrate pores by capillary action and therefore has to be forced into the pores by applying an external pressure.[227] Based on the assumption that the pores are cylindrically shaped, the diameter penetrated by mercury could be related to the applied external pressure (Eqn 2.5):

$$D = \frac{-4\gamma \cos\theta}{p} \qquad (2.5)$$

where D is the pore diameter, γ is the surface tension of mercury, θ is the contact angle between mercury and the material and p is the applied external pressure.[227] The pore volume is obtained from the measurement of the volume of mercury that penetrates the porous

material. The pore size distribution can be obtained from the relationship between log differential intrusion volume and log pore diameter, $dV/d(\log D)$.[227] Using the data obtained for the pore diameter and the mercury intrusion volume, the wall area of the pore can be calculated from Eqn 2.6;

$$A = \frac{4V}{D} \tag{2.6}$$

where A is the surface area of the pore, V is the intrusion volume and D is the pore diameter.[230] The major limitations of mercury porosimetry arise from the assumption that the pores are cylindrical since not all pores adopt the shape.[227] Moreover, due to the 'bottle neck' effect Eqn 2.6 may not provide accurate surface area results.[227,229]

2.6.1.2 Capillary flow porometry

Contrary to mercury porosimetry, capillary flow porometry is a liquid extrusion technique commonly used for pore size determination.[230] In capillary flow porometry, all the pores must first be completely filled with a wetting liquid. The liquid is then forced out of the pores using an inert gas. The hypothesis is that the work done to force the liquid out of the pores is equal to the surface free energy when the sample liquid interface is substituted by the sample-gas interface. The pore diameter can be determined from Eqn 2.7 below:

$$p = \frac{4\gamma_{l/g}\cos\theta}{D} \tag{2.7}$$

where $\gamma_{l/g}$ is the liquid gas interfacial tension or liquid surface tension; θ is the contact angle between mercury and the material and D is the diameter of the equivalent circular area of the pore cross-section.[230,231] Capillary flow porometry is only appropriate for the measurement of 'through pores', but cannot measure closed or blind pores and it also suffers from the 'bottle neck' effect.[227]

2.6.1.3 Brunauer-Emmet-Teller (BET) gas adsorption

Named after its inventors, Brunauer, Emmet and Teller, the BET gas adsorption technique, is the most commonly used technique for the measurement of surface areas of porous materials.[227,232] The technique is based on the principle of adsorption of gas molecules of the sample on the surface. By integration of the concept of multilayer adsorption of gas molecules as well as knowing the area covered by a single gas molecule to Langmuir's assumption of monolayer formation, the BET equation can be written as follows:

$$\frac{P}{V_a(P_0-P)} = \frac{1}{V_m C} + \frac{C-1}{V_m C}\left(\frac{P}{P_0}\right) \qquad (2.8)$$

where P is the gas pressure, P_o is the saturated (equilibrium) gas pressure at a given temperature, V_a is the volume of gas adsorbed at pressure P, V_m is the volume of gas required for the monolayer adsoption on the surface of the sample and C is the constant related to the monolayer adsorption.[227] V_m and C can be obtained from the intercept and slope of the curve of the plot of $P/V_a(P_o\text{-}P)$ versus (P/P_o).

The data obtained from the BET gas adsorption technique is usually more reliable in comparison to the mercury porosimetry and capillary flow techniques.[227] The reason is that in the BET gas adsorption technique, no assumption is made about the cylindrical shape of the pores. However, the BET gas adsorption technique cannot distinguish between pores within the nanofibers and spaces between the individual nanofibers. The major challenge associated with the BET technique is that there is no clear distinction between pores within electrospun nanofibers and the interstitial spaces between nanofiber strands. Thus, the surface area values and the pores volume sizes obtained for electrospun nanofibers may not be accurate.

2.6.2 Surface morphology

2.6.2.1 Scanning electron microscopy (SEM)

Scanning electron microscopy is a technique extensively used for imaging the surface of solid materials or samples.[227,233] A variety of information about electrospun nanofibers can be

obtained with SEM, including the nanofiber diameter, texture (smoothness (beadfree) or roughness (beaded)) and chemical composition. A high energy stream of electrons is bombarded on a selected region of the sample's surface under high vacuum conditions. On hitting the solid surface, the incident electron beam is reflected and backscattered. Secondary electrons (electrons ejected from the sample) that are reflected from the surface of the solid are detected and then converted into an image. Depending on the type of detector used, information about the surface morphology, chemical composition (energy dispersive spectroscopy (EDS)), crystalline structure and crystal orientation (electron backscattered diffraction spectroscopy (EBDS)) can be obtained. SEM micrographs of electrospun nanofibers with different morphologies are illustrate in Fig. 2.11.

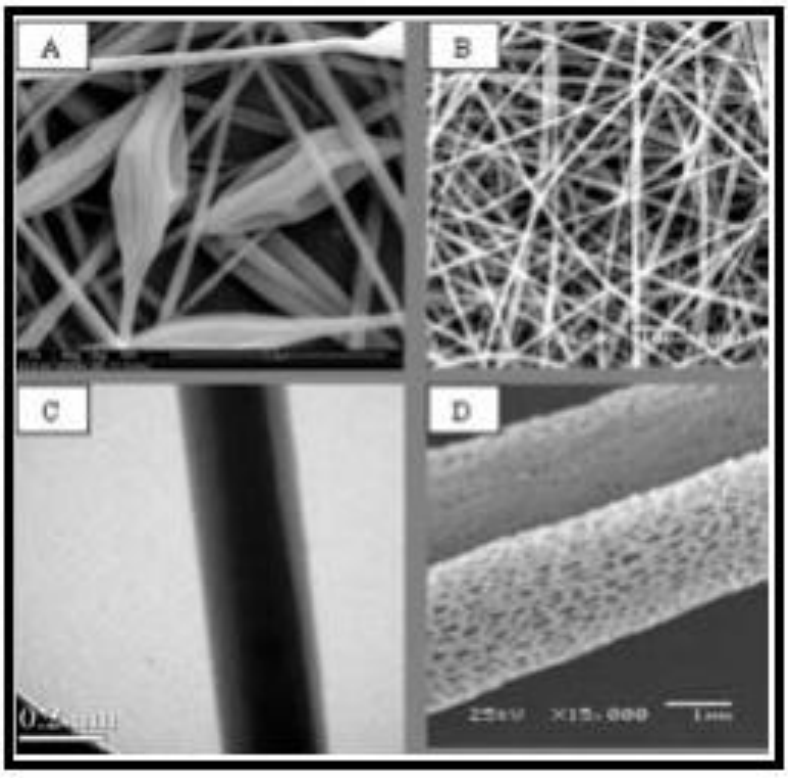

Figure 2.11. SEM micrographs showing different surface morphologies of electrospun nanofibers[178]

One major advantage of using SEM is that various types of detectors can be used to reveal characteristics of the sample. However, SEM is only limited to solid dry samples which must be stable under vacuum. The environmental scanning electron microscope (ESEM) was

developed to allow analysis of environmental and live biological samples.[234] Although non-conducting solid surfaces result in poor resolution, the challenge is curbed by coating the non-conducting surface with a conducting material (gold sputter coating).

2.6.2.2 Transmission electron microscopy (TEM)

Transmission electron microscopy is another technique widely used for imaging not only solid but liquid samples as well.[235,236] In the TEM technique a thin sample is irradiated with an electron beam of uniform energy. The incident beam of electrons interacts with atoms of the sample as it travels through before being emitted (transmitted) on the other side of the sample. The transmitted electrons, unlike in SEM technique which relies on deflected electrons, are then detected and converted into an image.

Transmission electron microscopy is mostly used for imaging of electrospun nanofiber/nanoparticle composites.[189,237] Because it relies on transmitted electrons, TEM has the capability of imaging the distribution of nanomaterials embedded within other materials (Fig. 2.12). However, the major limitation of TEM is that the sample has to be very thin and stable under high vacuum.

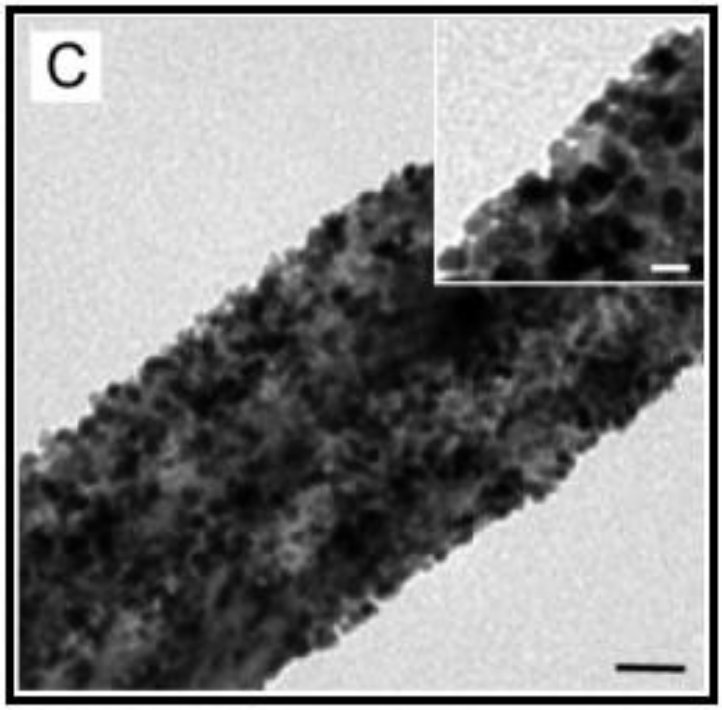

Figure 2.12. TEM micrographs of electrospun TiO_2/PtNPs nanofiber composites[189]

2.6.2.3 Atomic force microscopy (AFM)

Invented in 1985 by Binnig and Rohrer,[238] AFM uses a tip mounted in a cantilever to measure surface morphology (roughness and hardness) and other properties (such as the distribution of a chemical of interest in blended mixtures, distribution of crystalline and amorphous regions on a polymer surface, elasticity, adhesion and surface charge density) of solid materials.[227,239,240] There are various modes by which the tip interacts with the surface of the materials, namely, contact and non-contact modes. The contact mode is the simplest form of AFM imaging and is similar to feeling the surface texture by moving fingers over it. The contact mode has been employed to determine the adhesion force on electrospun nanofibers after plasma treatment.[241] However, the contact modes are usually considered inappropriate for electrospun nanofibers since even soft cantilevers cause damage to the sample. The damaging effect of the cantilevers has been attributed to the lateral friction forces.[227]

Non-contact modes use an oscillating AFM tip to examine the attractive forces near the surface of the materials and generally cause less structural damage. A non-contact mode most commonly used for imaging of electrospun nanofibers is the amplitude modulation (also referred to as intermittent contact or tapping mode).[227] In the tapping mode the tip is moved

at a constant frequency which permits simultaneous monitoring of the amplitude and phase changes. Fig. 2.13 illustrates AFM images of electrospun poly(vinyl acetate)/titanium oxide ($PVAc/TiO_2$) nanofiber composites using a tapping mode.

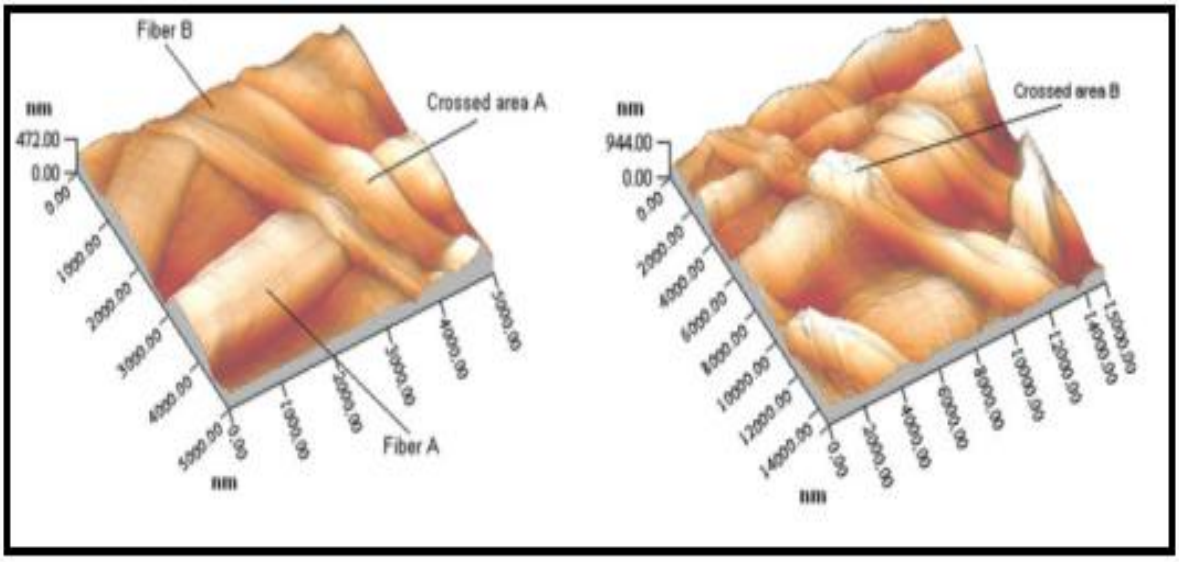

Figure 2.13. AFM images of electrospun $PVAc/TiO_2$ nanofiber composites[242]

Another non-contact mode called the phase imaging allows creation of the image by comparing the phase of the cantilever excitation with that of the response oscillation. Phase imaging allows many different surface properties to be examined. However, phase imaging does not permit direct investigation of the chemical composition of the sample and the drawback has been solved by combining AFM with spectroscopic techniques such as IR[243] and X-ray spectroscopy[244] which has allowed the investigation of physicochemical properties of nanomaterials. The major limitation of the AFM technique for the analysis of electrospun nanofibers is that there are always slight distortions in both the vertical and horizontal directions when a non-ideal tip interacts with the surface.[227]

2.6.3 Surface chemical composition

2.6.3.1 Attenuated total reflectance (ATR) Fourier transform infrared spectroscopy

Attenuated total reflectance (ATR) Fourier transform infrared spectroscopy (FTIR) is a technique in which the infrared radiation interacts with molecules by exciting their vibration modes, when it is reflected between the surface of the sample and the internal reflection element (or ATR crystals).[227,245] The most commonly used internal reflection elements are zinc selenide (ZnSe) or germanium (Ge). ATR-FTIR provides information about the presence or absence of specific functional groups (-OH, -NH_2, -CHO, -COOH, -CONHR).[227,245,246] Because of its simplicity, ATR-FTIR has been widely used for the characterization of functionalized electrospun nanofibers.[195,247-249]

Since the mean-free-path of infrared radiation is about 2 μm, it is usually not a very sensitive technique for surface characterization. For example ATR-FTIR is often not sensitive enough to detect the surface chemistry of grafted nanofibers/polymer in which the grafted layer is only several tens of nanometers.[245]

2.6.3.2 Energy dispersive spectroscopy (EDS)

Energy dispersive (X-ray) spectroscopy (EDS or EDX) is a technique that is commonly used in conjuction with scanning electron microscopy (SEM) and transmission electron microscopy (TEM), for the analysis of the surface composition of electrospun nanofibers. It uses the principle of the bombardment of solid surfaces with a beam of electrons. The emitted X-rays have unique energies that are characteristic to specific elements that are present on a solid sample. The emitted X-rays are detected, sorted based on their energies and then converted to signals that identify the elements present in a sample. EDS can also be used for the mapping of the elemental distribution on the surface of the solid sample. However, for the EDS analysis, samples should be perfectly flat so that surface roughness does not affect the results since the electron probe analyzes only to a shallow depth. Non-conducting samples should not be coated since the coating introduces unwanted element lines on the spectrum. Furthermore, the operators should have a clear understanding of what elements they are analyzing in the sample so as to eliminate unwanted elements. EDS is more accurate for heavy elements but less accurate for light elements.

2.6.3.3 X-ray photoelectron spectroscopy (XPS)

X-ray photoelectron spectroscopy is the most extensively used technique for the analysis of chemical composition of electrospun nanofibers.[227,233,245,246] The technique is based on the photoelectron effect where the photons (Mg Kα and Al Kα lines) are used to eject electrons from the surface when the photons strike the surface of the material. The binding energies of the electrons ejected from the surface of the material are measured and then converted into a spectrum with a sequence of photoelectron peaks. These peaks (binding energies) are characteristic of specific elements present on the surface (Fig. 2.14).[245,246] Figure 1.14 illustrates the XPS spectra depicting the binding energies of the elements (C1s, N1s and O1s) obtained for the surface chemistry characterization of electrospun collagen nanofibers, polyurethane (TPU) nanofibers and collagen/TPU nanofiber composite.

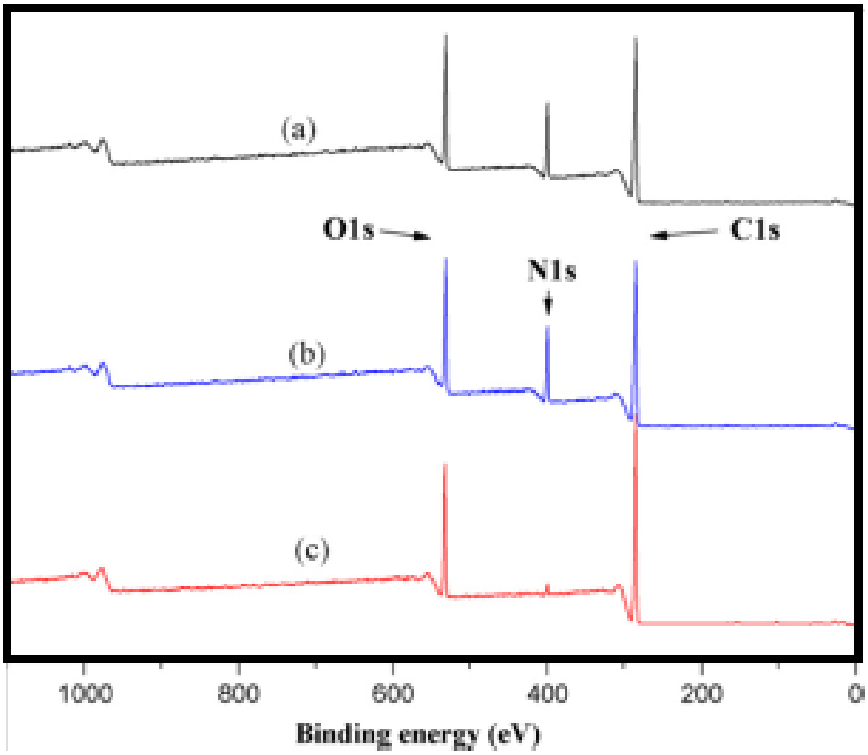

Figure 2.14. XPS spectra obtained for (a) collagen nanofibers, (b) collagen/TPU nanofiber composite and (c) TPU nanofibers[250]

The peak areas can be used to quantify the elemental composition on the surface provided appropriate sensitivity factors are taken into consideration. Depending on the chemical

environment of the emitting atom or element, the peak shape and binding energy can be slightly shifted, thus providing chemical bonding information. X-ray photoelectron spectroscopy (XPS) was used for surface characterization of functionalized electrospun nanofibers.[247,250-252] XPS is a highly sensitive technique for surface characterization since the mean-free-path of photoelectrons is small. Thus photoelectrons penetrate about 10 nm below the surface.[227] Moreover, broad poorly resolved binding energies (peaks) can be deconvoluted by curve fitting procedures. However, XPS is very expensive and requires ultra high vacuum conditions.

2.6.3.4 Time of flight secondary ion mass spectrometry (ToF-SIMS)

Secondary ion mass spectrometry is a technique used for molecular surface chemistry characterization and to develop a spatial distribution of the position of different chemical components.[227,246] In ToF-SIMS a high energy beam of primary ions is used to bombard the surface of a material, resulting in the removal of secondary ions or molecules in the vicinity of the impact site (Fig. 2.15). Some of the molecules are ionized and the ions are separated based on their mass per charge ratio (m/z) and analyzed. Uyar *et al*.[253] have used static ToF-SIMS to investigate the presence of cyclodextrin on the surface of electrospun polystyrene (PS) nanofibers after incorporation.

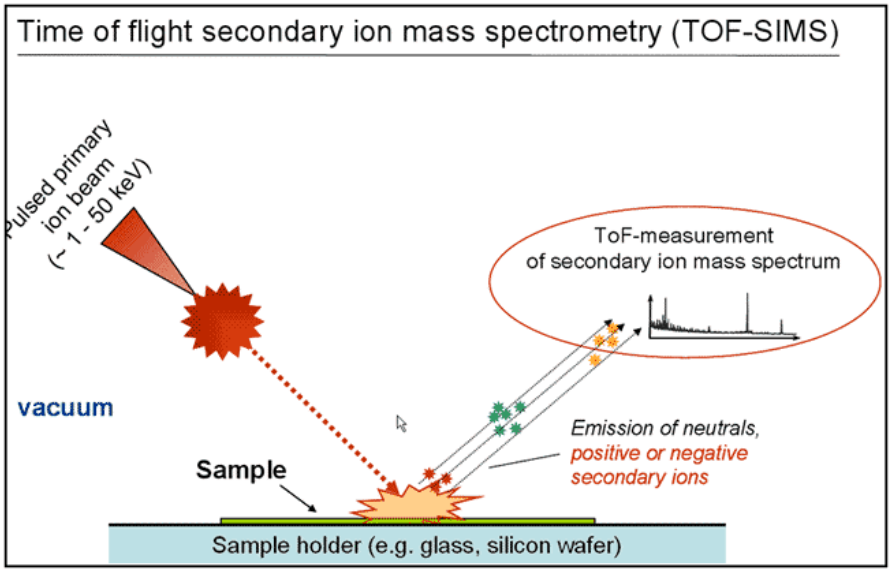

Figure 2.15. Schematic representation of time of flight secondary ion mass spectrometry (ToF-SIMS) technique[254]

There are two types of SIMS: static (low flux) and dynamic (high flux) SIMS. Dynamic SIMS has higher energy primary ion beam, thus results in greater damage of the surface than static SIMS.[227,246,255,256] As a result of etching of the surface due to the high energy ion beam in dynamic SIMS, it can be used for depth profiling of material surfaces. ToF-SIMS can also be used to determine covalent bonding of molecules to surfaces, as well as to predict wettability, adhesiveness and biological reactivity of surfaces.[246] Although it can be used for identification of all elements including hydrogen as well as atomic or molecular ions, it usually damages material surfaces. Moreover, quantification of mass spectra requires standards that must be obtained for the sample matrix.[227]

It is clear from the surface characterization techniques discussed that none can be used independently to provide full and accurate information about the surface of electrospun nanofibers. Thus, a combination of several of these techniques is often necessary for a complete and accurate characterization of the surface chemistry. There are also other surface characterization techniques (surface energy analysis and mechanical properties) that have not been discussed but they have been comprehensively reviewed elsewhere.[227,233,246]

2.7 Applications of electrospun nanofibers

Nanofibers obtained by the electrospinning process have attractive properties such as high porosity, high surface area-to-volume ratio and their surfaces are easily modified. Because of the properties of the electrospun nanofibers, they have gained popularity for application in various research fields. Exploitation of the nanofiber properties could make them better alternatives for specific applications compared to conventional methods. For example, the highly porous nature of electrospun nanofibers makes them suitable alternatives as drug delivery systems due to controlled release of incorporated drugs (pharmaceuticals) over time.[257] The surface of electrospun nanofibers can be modified with various functionalities to make them selective sorbents for specific analytes in sample clean-up.[258-260] Moreover, increased surface area of electrospun nanofibers enhances the surface interaction with targeted analytes, and improves the enrichment factors and therefore the sensitivity in trace analysis. In trace analysis, the selectivity and sensitivity of electrospun nanofibers can be tuned by a systematic choice of ligands that selectively bind to metal ions.[261] Some of the various application fields of electrospun nanofibers are illustrated in Fig. 2.16.

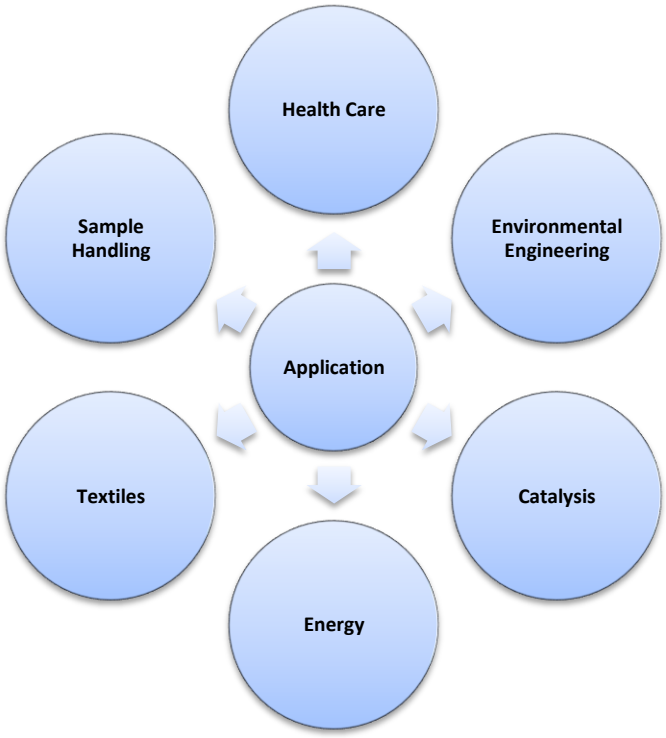

Figure 2.16. Some application fields of electrospun nanofibers

2.7.1 Textiles

Fire, chemical and biological threats pose huge challenges to firefighters, law enforcement, medical and military workforces. Therefore, a high level of protection is paramount in ensuring the safety of the personnel whenever they have to deal with such threats. The challenges of the present protective clothing which contains charcoal as absorbent include permeability to water and being too heavy.[167,262] In recent years, electrospun nanofibers have played an important role in the textile industry for the manufacture of thermal fabrics, protective clothing, waterproof materials and sportswear.

2.7.1.1 Protective clothing

Electrospun polyurethane (PU) nanofibers were fabricated and their properties as potential alternatives for breathable windproof protective clothing investigated.[262,263] It was found that air permeability decreased with increasing processing time (or nanofiber web density). It was also observed that the hydrostatic pressure increased and water vapour permeability remained constant.

Gallo *et al.*[264] prepared halogen-free fire retardant electrospun nanofibers by depositing nanofiber layers of polyacrylic acid (PAA) and polyimide (PI) onto polyamide 6,6 (PA66). They investigated the fire resistance behaviour of the nanofiber layer and concluded that PAA and PI coatings function by physical effects that alter the mass or heat transport between the pyrolysis and the flame zone. Moreover, both nanofiber coatings were sacrificial and protective layers due to advance thermal insulation.

Waterproof and breathable polyurethane materials suitable for sportwear design have been prepared via the electrospinning of layered fabric systems with varying composite nanostructures.[265] By varying the layer structure and substrates in the electrospun nanofiber layered system, different breathability and barrier performance levels were achieved.

2.7.2 Environmental systems

The porous structure, surface adhesion and high surface area-to-volume ratio of electrospun nanofibers make the nanofibers suitable alternatives for gas filter and sensor systems for

environmental pollution. Various types of materials including semiconductors, carbon graphites, (in)organic composites have been used as sensory devices to detect polluting gases in the environment; based on various sensing techniques and principles.[266] In recent years, electrospun nanofibers have also gained more popularity for application in gas filter systems since they were found to be more competitive compared to conventional techniques such as ion exchange, adsorption and sand filtration.[267]

2.7.2.1 Sensors

A gas sensor is a device that detects the presence of polluting or hazardous gases in an environment. The performance characteristics of a chemical gas sensor (selectivity, sensitivity, response time, stability, reversibility and reproducibility) are influenced by the type of sensing material used.[266] The most commonly used gas sensors are electrospun ceramic nanofibers which are produced by sol-gel and the electrospinning technique.[268]

Electrospun nanofibers of tungsten oxide (WO_3) and molybdenum oxide (MoO_3) were prepared and shown to possess the ability to detect ammonia (NH_3) and nitrogen dioxide (NO_2) in the atmosphere, respectively.[269,270] The sensors were found to be capable of detecting low concentrations of NH_3 (10 ppm) and NO_2 (50 ppm). It was also shown by Medrignac-Conanec *et al.*[271] that mixed MoO_3 and WO_3 nanofibers had a capability of simultaneous detection of several gases (NO, NO_2 and O_3).

Electrospun nanofibers of PAA and PVA were deposited on quartz crystal microbalances (QCM) and also used for the detection of NH_3 gas.[272] The nanofiber sensors were found to have a rapid response to NH_3 and they interacted with NH_3 through PAA, a weak polyelectrolyte. Another nanofiber sensor for hydrogen sulfide (H_2S) gas was also fabricated by deposition of polyethyleneimine (PEI)/polyvinyl alcohol (PVA) nanofibers on QCM.[273] The limit of detection of the nanofibrous sensor for H_2S was 500 ppb.

Electrospun nanofiber sensors were also used for the detection of water pollutants such as pharmaceuticals, cosmetics and hormones.[268,274,275] When encapsulated into electrospun nanofibers, molecularly imprinted nanoparticles were found to have the ability to detect trace concentrations of propanolol.[276] Electrospun nanofibers with a potential of being used as thermal,[277] biochemical[186] and fluorescence[278] sensors were also reported.

2.7.2.2 Filtration

The presence of chemical and biological contaminants in the environment (air and water) can be harmful to human and animal health. Thus, removal of contaminants from the environment is very critical in ensuring a clean and breathable environment. The use of electrospun nanofibers as filters has gained momentum in recent years. Mostly, the filtration membranes were produced by deposition of electrospun nanofibers on a substrate material whose pore size was often larger than the nanofibers being deposited.[262,279] It is worth noting that only the use of electrospun nanofibers as gas filters will be discussed in this section while their application in water filtration will be discussed in Chapter 2.

Han *et al*.[279] produced core-shell structured nanofiber membranes by co-axial electrospinning of polycarbonate (PC) (core) and polyurethane (PU) (shell) onto cotton. They observed that the core-shell nanofiber composite had good water vapour transmission performance in the removal of gaseous contaminants. Electrospun polyvinyl alcohol (PVA) nanofibers were deposited onto two differently prepared polypropylene (PP) sublayers (spun-bonded and melt-blown).[280] The filtration efficiencies of both nanofiber composites were compared. The filtration efficiency of the spun-bonded nanofiber composite was almost 100% after 2.9 g/m^2 of PVA nanofiber web was deposited, while that of melt-blown nanofiber composite required 2.4 g/m^2 of PVA nanofiber for the same result.

Electrospun nylon 6 nanofibers were also fabricated and their filtration efficiency and pressure drop investigated. Nylon 6 nanofibers were found to have better filtration efficiency (99.993%) than the commercially available high-efficiency particulate air filter (HEPA).[281] Patanaik *et al*.[282] fabricated electrospun polyethylene oxide (PEO) nanofibers and evaluated the effect of diameters on filtration efficiency and pressure drop. They observed that the filtration efficiency and the pressure drop decreased as the diameter of the nanofibers increased.

2.7.3 Energy

With the rapid depletion of fossil fuel reservoirs due to the ever-escalating global energy demands, there exists a need to find new technologies to generate renewable and clean energy resources. In addition, the storage of energy is another critical issue that requires attention as well. The highly attractive properties of electrospun nanofibers have received much attention

and are regarded as excellent alternatives to address the challenges. Scientists have studied electrospun nanofibers for potential use in fuel cells, Li-ion batteries, piezoelectric and thermoelectric materials, dye-sensitized solar cells and supercapacitors.[167,178,283]

2.7.3.1 Fuel cells

Electrospun Nafion/polyphenyl sulfone (PPSU) nanofiber composites were fabricated using two different approaches; (i) Nafion nanofibers were reinforced with PPSU nanofibers and (ii) Nafion nanofibers were embedded into PPSU nanofibers.[284] The two nanofiber composites were evaluated for their proton conductivity and other properties (including swelling and mechanical properties). Results showed that the proton conductivity of the two nanofiber composites increased linearly with Nafion volume ratio. Tamura and Kawakami prepared novel nanofiber composite membranes from uniaxially aligned sulfonated polyimide nanofibers as proton exchange membrane fuel cells.[285] The nanofiber composite membranes exhibited high proton conductivity, good chemical and thermal stability as well as low gas permeability. It was also concluded that the properties suggested that the composite nanofibers were promising polymer electrolyte membranes and have a potential to be used as fuel cells.

2.7.3.2 Lithium-ion batteries

Energy storage devices such as rechargeable lithium-ion batteries are regarded as an efficient solution to the increasing demand for high-energy electrochemical power sources. Recently, more focus has been directed towards the development of Li-ion batteries from electrospun nanofibers. Bonino *et al.*[286] fabricated electrospun carbon-tin oxide (C-SnO_2) nanofiber composites and evaluated them as anodes in Li-ion battery half-cells. They found that the incorporation of SnO_2 enhanced the performance of carbon nanofibers as anodes in Li-ion batteries.

Thermally-treated electrospun $LiFePO_4$-C nanofiber composite (using PAN as a precursor) were evaluated as cathodes in Li-ion battery half cells. It was observed that the electrospun $LiFePO_4$-C nanofiber composites displayed satisfactory capacity and good cycling stability as cathodes in Li-ion battery half cells. Li-ion battery separators have also been fabricated by

incorporating Perovskite-type lithiumlanthanum titanate $Li_{3x}La_{2/3-x}TiO_3$ (LLTO) into electrospun PAN naofibers.[287] These nanofiber composites were found to perform well as separators and also assisted in Li ion conduction, which could enhance battery kinetics.

2.7.3.3 Dye-sensitized solar cells

Much attention has been focused on dye-sensitized solar cells as potential low cost alternatives to silicon solar cells.[288,289] Other advantages include easy manufacturing process and simple large-scale production. Electrospun anatase TiO_2 nanofibers were deposited directly onto a thick nanoparticle electrode using a sol-gel method.[288] The nanofibers were evaluated as dye-sensitized solar cells and the results showed that the nanofibers exhibited an incident photon coversion efficieny (IPCE) of 85% at a wavelength of 540 nm. For areas of 0.25 and 0.052 cm^2, conversion efficiencies were 8.14 and 10.3%, respectively. From the results, it was deduced that the light harvesting nanofiber-modified TiO_2 nanoparticles had a potential to be used as dye-sensitized solar cells. Joshi *et al*.[289] demonstrated that electrospun carbon nanofibers could be an alternative low cost electrocatalyst to Pt for triiodide reduction in dye-sensitized solar cells.

2.7.3.4 Piezoelectric and thermoelectric materials

Recent technological innovations have moved towards miniaturization of portable and wireless electronic devices which are self-powered energy sources.[290,291] The materials have the capability of harvesting energy from the environment and converting it to a different form of energy. Such materials are said to have piezoelectricity; that is, the ability of some materials to convert electrical energy to mechanical energy. On the other hand, thermoelectric materials have the ability to convert waste heat energy into electricity in an effective, economical and environmentally benign manner.[292,293] Electrospun nanofibers are potential candidates for fabricating piezoelectric and thermoelectric materials since they are lightweight (for easy transportability) and mechanically flexible.

Electrospun lead zirconate titanate nanofibers were demonstrated as new piezoelectric nanogenerators (Fig. 2.17).[291] Some interesting properties of the electrospun piezoelectric

nanofibers include a peak output voltage of 1.63 V and the output power of 0.03 μW with a load resistance of 6 Ω.

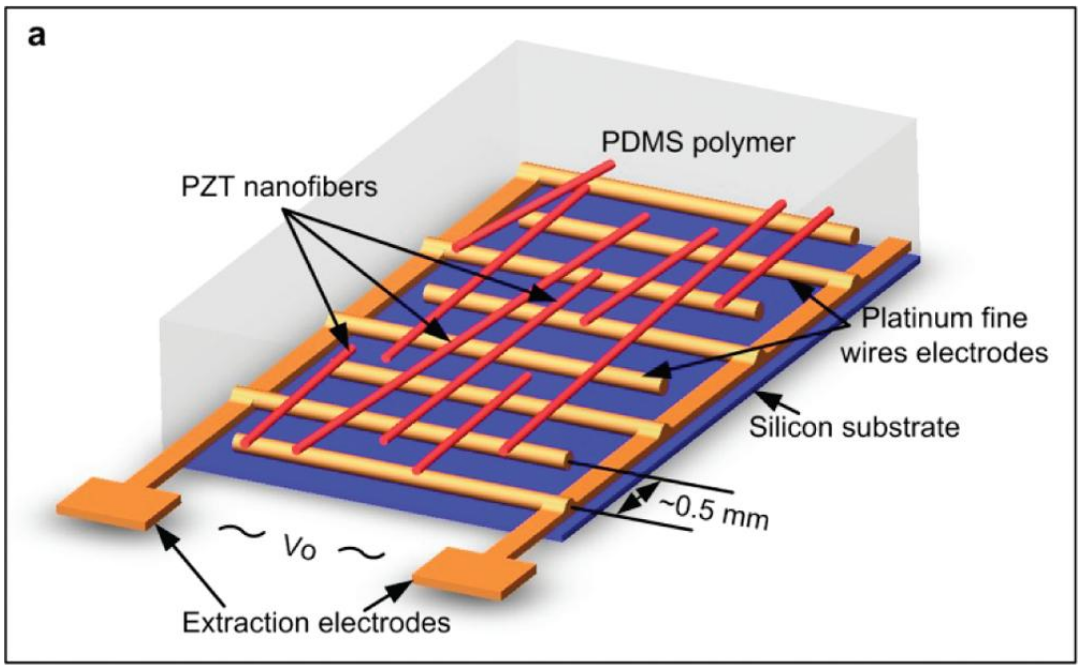

Figure2.17. Schematic view of the piezoelectric (PZT) nanogenerator[291]

Yin *et al.*[293] developed nanocrystalline thermoelectric $Ca_3Co_4O_9$ ceramics by sol-gel based electrospinning and spark plasma sintering. The nanofiber-sintered ceramic materials demonstrated simultaneous Seebeck coefficient, electric conductivity and thermal resistivity.

2.7.3.5 Supercapacitors

Electrospun nanofibers have also gained much popularity in developing another type of energy storage device known as the supercapacitor. Supercapacitors are considered as potential energy storage solutions since they possess higher power density and long cycle life compared to secondary batteries and traditional capacitors.[294] Electrospun V_2O_5 nanofibers were developed and demonstrated to have a potential for use as supercapacitors.[294] They were also shown to perform better in neutral electrolyte KCl, producing a capacitance of 190 F/g and an energy density of 5 Wh/kg. Laforgue *et al.*[295] demonstrated the capability of

electrospun poly(3,4-ethylenedioxythiophene) (PEDOT) nanofibers to be used as active materials of all-textile supercapacitors.[295] These electrospun nanofibers displayed very high flexibility and conductivity.

2.7.4 Biomedicine and biotechnology

The attractive properties including high porosity, large surface area-to-volume ratio, interconnectivity and microscale interstitial spaces render electrospun nanofibers as excellent materials for biomedicine and biotechnology applications. Biomacromolecules, enzymes or cells can be used to functionalize electrospun nanofibers for application in protein purification, enzymatic catalysis, diagnostics and chemical analysis.[178] Functionalized electrospun nanofibers have also found application in the areas of wound dressing, tissue engineering and drug delivery.[250,296,297]

2.7.4.1 Enzymatic catalysis

Enzymes are outstanding biocatalysts capable of catalyzing a broad spectrum of complex reactions with excellent selectivity. The immobilization of enzymes is desirable in the industry since it offers recyclability, reusability, simple purification and prevents leaching.[298] The excellent selectivity, recyclability and reusability, simple purification, as well as the large surface area-to-volume ratio of electrospun nanofibers make them ideal solid supports for immobilization of enzymes.

Co-axially electrospun nanofibers containing PEO (core) and diisopropylfluorophosphatase (DFPase) (sheath) have demonstrated very promising catalytic activity in the deactivation of chemical agents.[279] Electrospun polycaprolactone (PCL) nanofiber encapsulated lipase from *B. cepacia* displayed enhanced catalytic activity in the hydrolysis of *p*-nitrophenyl palmitate in an aqueous medium compared to the trans-esterification reaction in an organic medium.[299]

2.7.4.2 Protein purification

Biotherapeutic products (recombinant human immunoglobulins, fusion proteins, viruses and cell therapies) can be derived from genetically engineered bacteria, fungi, cells or

recombinant DNA technology.[187] The products are used to improve human and animal health, and therefore purification methods to separate them in large quantities are in great demand.

Schneiderman *et al*.[187] reported the development of electrospun carbon nanofibers for protein purification with high capacity and throughput. The selectivity of the nanofibers was enhanced by increasing the ligand concentration or by addition of a non-ionic surfactant to the adsorption environment. Electrospun polystyrene-poly(styrene-co-maleic anhydride) nanofibers were functionalized by immobilization of aptamers (Fig. 2.18).[300] The electrospun nanofibers were demonstrated to be successful in the purification of thrombin.

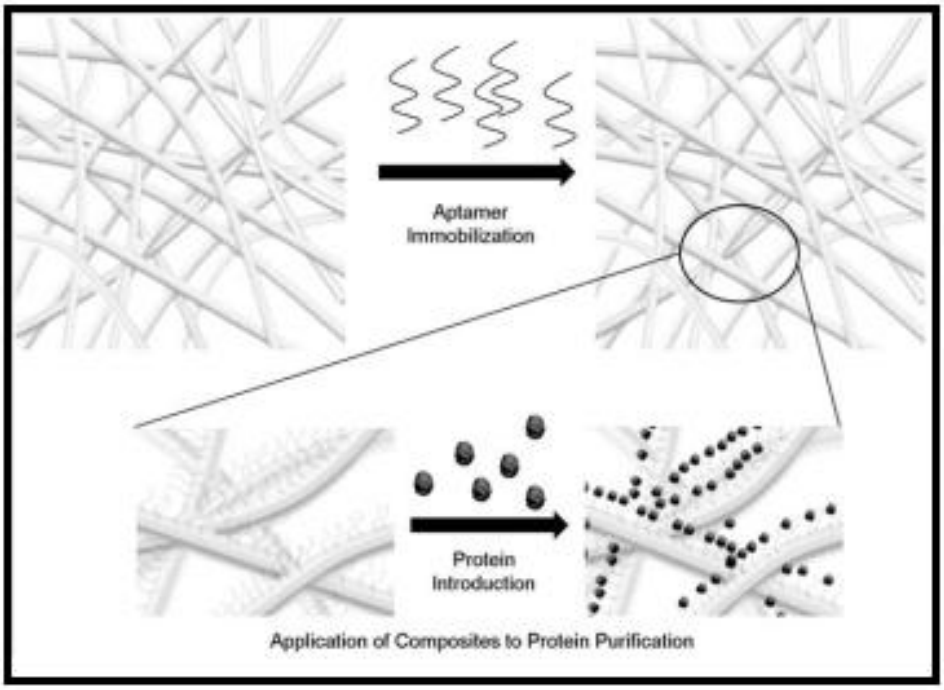

Figure 2.18. Schematic illustration of the protein purification process using nanofiber-aptamer composite[300]

2.7.4.3 Diagnostics

It is very important to detect diseases (acute or chronic) at an early stage in order to administer proper treatment and save human lives. The diagnostic probes are also needed for monitoring of health hazards present in the environment. Therefore, the development of rapid, sensitive, low cost and easy to use diagnostic probes has become the subject of

research activity. In recent years, electrospun nanofibers have received much attention as potential alternatives for application in medical diagnostics.[301]

Fluorescence resonance energy transfer (FRET) detection of proteins (haemoglobin, myoglobin cytochrome C, bovine serum albumin (BSA) and avidin) was demonstrated using an electrospun cellulose acetate nanofiber doped with dendritic fluorescent diphenylacetylenic systems.[302] The fluorescent-doped electrospun nanofibers displayed good reproducibility (RSD was ~5% between separate measurements on different days), reusability (<15% loss of fluorescence signal) and stability (no observable leaching). Recently, a CdSe quantum dot/polycaprolactone (PCL) composite nanofiber for the 'turn-on' fluorescent detection of lactase dehydrogenase was reported by He *et al*.[303]

2.7.4.4 Wound dressing

Growth of pathogenic microorganisms on wound surfaces causes inflammation and hence prolongs the healing process. Thus prevention of microbial growth on the wound surface is critical for the wound's healing process. Electrospun nanofibers could be utilized for biomedical applications as wound dressing materials for humans. For example, a hand-held electrospinning device was manufactured for directly electrospinning polymer nanofibers onto the affected skin area (Fig. 2.19).[167]

Figure 2.19. A hand-held electrospinning devices for wound dressing[167]

Khil *et al.*[304] reported electrospun PU nanofibrous membranes for the treatment of wounds. They observed that wounds that were treated with PU nanofibers were covered by a thinner scab and milder infiltration by inflammatory cells was observed compared to wounds treated with a control material. A recombinant human epidermal growth factor (rhEGF) was immobilized onto electrospun nanofibers prepared from a mixture of polycaprolactone and poly(ethyleneglycol)-polycaprolactone block polymer.[297] The resultant nanofiber-rhEGF composite was evaluated for the wound healing properties on diabetes ulcers. The nanofiber composite demonstrated better wound healing properties compared to control materials or rhEGF solutions.

2.7.4.5 Tissue engineering

To date, some of the most amazing applications of electrospun nanofibers have been for tissue engineering where they are used as biomimetic scaffolds for regeneration of human organs including, nerves, blood vessels, bones, and cartilage. Tissue engineering using

electrospun nanofibers scaffolds has gradually aided in minimization of dependence on donor organs.[305]

Tubular vessel-like electrospun poly(L-lactic acid-co-(ε-caprolactone)) (P(LLA-CL)) nanofibersgrafted with collagen after plasma treatment (Fig. 2.20), were reported.[306] The nanofiber scaffolds were demonstrated to be suitable for seeding of human endothelial cells with the possibility of application as blood vessels.

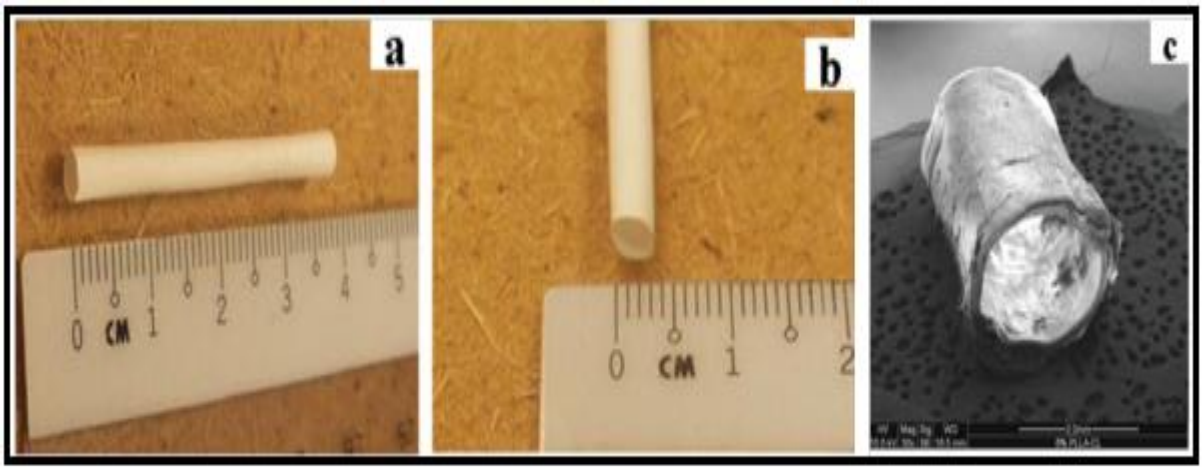

Figure 2.20. Dimensions and SEM micrograph of the P(LLA-CL) tubular nanofiber scaffold[306]

Zhang *et al.*[307] developed biomimetic electrospun hydroxyapatite/chitosan nanofiber composites using a two-step process; an *in situ* co-precipitation synthetic strategy and electrospinning process. Results obtained from cell proliferation, mineral deposition and morphology investigations suggested the feasibility of using the biomimetic nanofibers composites for bone tissue regeneration. Prabhakaran *et al.*[308] demonstrated the ability of electrospun poly(L-lactic acid)-co-poly(ε-caprolactone)/collagen nanofiber scaffolds to support neuronal differentiation of mesenchymal stem cells (MSCs). They concluded that differentiation of MSCs to neuronal cells could be very attractive on electrospun nanofiber scaffolds for transplantation after nerve repair to the location of the injury.

2.7.4.6 Drug delivery

The highly porous structure of nanofibrous materials presents them as highly attractive hosts for drugs or pharmaceuticals. The ability of electrospun nanofibers to sustain and control the release mechanism at the targeted site makes them potential alternatives as drug delivery systems.

Electrospun poly(ε-caprolactone) nanofibers incorporated with metronidazole benzoate were developed and investigated for their drug release properties.[309] Results obtained from *in vitro* drug release experiments carried out in phosphate buffer demonstrated that the kinetics of drug release were influenced by the solvent ratio and metronidazole benzoate concentration (Fig. 2.21). Moreover, metronidazole release was also sustained for at least 19 days.

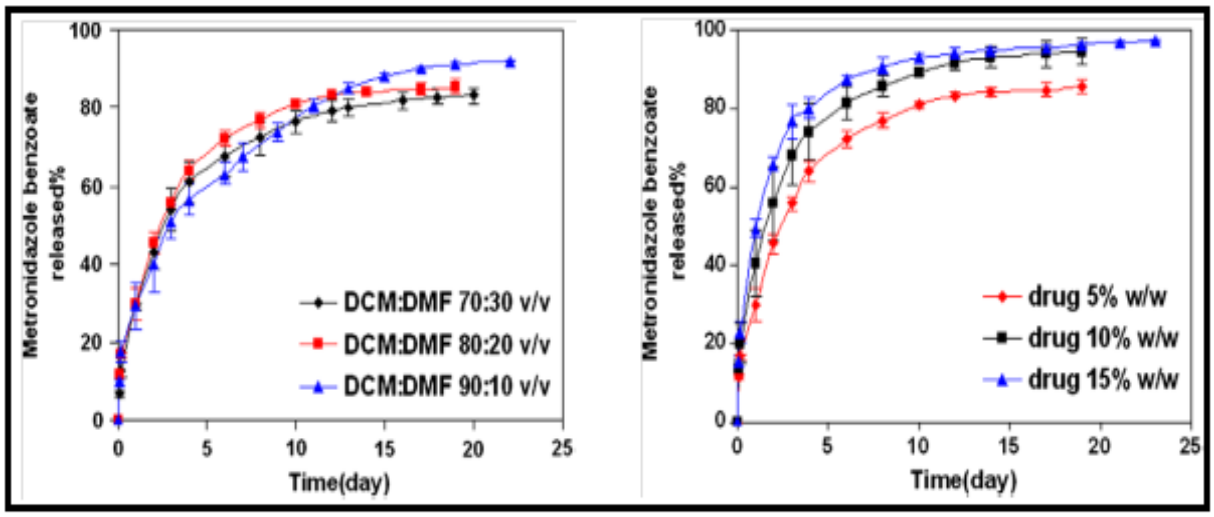

Figure 2.21. Effect of the solvent ratio and concentration on metronidazole release from electrospun nanofibers[309]

Biodegradable electrospun poly(L-lactic acid) nanofibers blended with a protein (cytochrome C) were fabricated and investigated for protein release properties.[310] Protein release studies in a phosphate buffer demonstrated that the hydrophilicity of the poly(L-lactic acid) nanofibers was highly influential.

Electrospun polypropylene membranes were fabricated by grafting 1-vinylimidazole onto polypropylene followed by treatment with an antimicrobial drug ciprofloxacin.[114] The

antimicrobial potency of the membranes was investigated against *E. coli* by the disk diffusion method. The polypropylene membranes displayed a gradual release of the antimicrobial drug over a period of 4-5 days.

The examples illustrated in the preceding sections clearly demonastrated how the electrospun nanofibers have been harnessed to systematically address a variety of real-life challenges. In the same vein, the thesis attempts to exploit electrospun nanofibers for the development of materials that can be potential alternatives for water purification application.

EXPERIMENTAL

CHAPTER 3 EXPERIMENTAL

3.1 Reagents and instrumentation

Alkylbromides, n-butyllithium (2.5 M in hexane), imidazole (99.5%), 1-vinylimidazole (99%), urocanic acid (99%), nylon 6 (Mw = 11200 Da) and acetone (laboratory reagent, >99.5%) were obtained from Sigma Aldrich (Milwaukee, USA). Hydrogen peroxide (30%), sodium borohydride, silver nitrate, benzophenone, hydrochloric acid (32%), potassium carbonate, sodium sulfate (anhydrous), potassium hydroxide, diethylether, dimethylformamide, formic acid (85%), acetic acid (95%) and chloroform were obtained from Merck Chemicals (Johannesburg, SA) and were used as received. *E. coli* (ATCC 8793), *S. aureus* (ATCC 6538), *B. subtilis*, subsp. *spizizenii* (ATCC 6633) and *C. albicans* (ATCC 2091) were obtained from Microbiologics Inc. (Minnesota, USA). Meuller-Hinton, Nutrient (agar/broth) and Potato dextrose agar (Merck, SA), metronidazole discs (50 μg) and blank discs (6.5 mm) were sourced from Davies Diagnostics (Johannesburg, SA). 2,5-Dimethylthiazol-2,5-diphenyltetrazolium bromide (MTT) was purchased at Sigma Aldrich (Milwaukee, USA). Metronidazole (for preparing 100 μg discs) was purchased from Changzhou Longcheng Medicine Raw Material Co., Ltd. (Changzhou City, Jiangsu, China), and ketoconazole was purchased from Oman Chemicals and Pharmaceuticals (Al Buraimi, Sultanate of Oman).

The NMR spectra were recorded on a Bruker Avance 400 NMR spectrometer. Infrared spectra were obtained with a Perkin Elmer Spectrum 400 FT-IR spectrometer. Microanalysis was carried out using a Vario Elementar Microtube ELIII. Potentiometric titrations were performed using a Metrohm 794 Titrino equipped with a Metrohm LL Ecotrode. The morphology of electrospun nanofibers was studied using the Tescan (TS5136ML) Scanning Electon Microscope (Brno, Czech Republic) operating at an accelerated voltage of 20 kV after gold sputter coating. The surface chemistry of grafted electrospun nanofibers was characterized using an Environmental Scanning Electron Microscopy (SEM/ESEM-EDAX) Quanta 200 operating at an accelerated voltage of 20 kV. The silver nanoparticle-adsorbed grafted electrospun nanofibers were characterized using an Oxford Instruments INCAPentaFET x3 Energy dispersive spectroscope fitted with INCA Analyzer software. The silver nanoparticles desorbed from the grafted electrospun nylon 6 nanofibers were characterized using a Zeiss Libra 120 Transmission electron microscope. The minimum

inhibitory concentrations were measured using a LEDETECT96 microplate reader, equipped with CAPTURE96 software. The voltage was applied using a Glassman EL40P01-22 High Voltage Power Supply (0-40 kV, 0-1 mA) (Eagle Appliances (Pty) Ltd, SA). The electrospun nanofibers were collected on a home-made rotating drum. The flow rate of the polymer solution was controlled using a NE-300 Just Infusion™ syringe pump (New York, USA). Viable bacterial colonies were enumerated using a Synbiosis aCOLade colony counter (Cambridge, UK). Grafting was initiated by UV radiation using a 400 W mercury vapour lamp (Osman, SA). For the cytotoxicity experiments, absorbance was measured using a Biotek Powerwave XS Spectrophotometer and the results were analyzed using Graphpad Prism 5 software.

3.2 Syntheses, protonation constants and antimicrobial activity of 2-substituted *N*-alkylimidazole derivatives

3.2.1 Synthesis of 2-substituted *N*-alkylimidazole derivatives

N-alkylimidazole-2-carboxaldehyde and *N*-alkylimidazole-2-methanol derivatives were prepared using literature methods.[311-313] Several new *N*-alkylimidazole-2-carboxylic acids were prepared from the corresponding *N*-alkylimidazole-2-carboxaldehydes, by hydrogen peroxide facilitated oxidation in aqueous conditions at room temperature. The only purification necessary was the removal of residual water *in vacuo*, at room temperature. This afforded the *N*-alkylimidazole-2-carboxylic acid derivatives in quantitative yields.

3.2.1.1 Synthesis of *N*-alkylimidazoles

Imidazole (0.088 mol) was dissolved in 50 mL acetone and powdered KOH (0.10 mol) was added and the mixture allowed to stir for 2 h. Thereafter, alkylbromide (0.090 mol) was added dropwise and the solution stirred overnight. The white precipitate was removed by filtration and the filtrate evaporated. The resulting brown oil was distilled under vacuum (150-200 °C, 4.7×10^{-2} mbar) to afford clear oil.

3.2.1.2 Synthesis of *N*-alkylimidazole-2-carboxaldehydes

To a suspension of *N*-alkylimidazole (0.020 mol) in dry diethyl ether (50 mL) was added 2.5

M butyllithium (0.021 mol) at -78 °C (dry ice/acetone slurry). After stirring for 1 h, DMF (0.030 mol) was added and the resulting solution was stirred overnight. After completion of the reaction, water (2 mL) was added followed by 15 mL of 4 N HCl. The aqueous layer was made basic by the addition of potassium carbonate, subsequently; the product was extracted into chloroform. The organic layer was concentrated and the product was distilled at $3.0x10^{-1}$ mbar and 80 °C to yield brown oil and in other cases the oil crystallized after cooling.

N-Methylimidazole-2-carboxaldehyde (***1a***)

N-Methylimidazole-2-carboxaldehyde was synthesized using the general method in **3.2.1.2**. *N*-Methylimidazole (0.025 mol), n-butyllithium (0.026 mol) and DMF (0.038 mol). The product was obtained as a brown solid (76.1%). ^{1}H NMR (400 MHz, $CDCl_3$, δ) 4.03 (3H, s, NC**H$_3$**), 7.16,7.27 (2H, s, Im-**H**), 9.81 (1H, s, C**H**O); ^{13}C NMR (400 MHz, $CDCl_3$, δ) 35.20, 127.69, 131.74, 144.00, 182.37. IR (cm^{-1}, KBr disk) 1686 ν(C=O). *Anal.* Calcd (found) for $C_5H_6N_2O$: C, 54.54 (54.25); H, 5.49 (5.65); N, 25.44 (25.19).

N-Ethylimidazole-2-carboxaldehyde (***1b***)

N-Ethylimidazole-2-carboxaldehyde was synthesized using the general method in **3.2.1.2**. *N*-Ethylimidazole (0.031 mol), n-butyllithium (0.033 mol) and DMF (0.047 mol). The product was obtained as a brown solid (46.1%). ^{1}H NMR (400 MHz, $CDCl_3$, δ) 1.44 (3H, t, *J* 8.0, NCH_2C**H$_3$**), 4.46 (2H, q, *J* 8.0, NC**H$_2$**CH_3), 7.25, 7.28 (2H s, Im-**H**), 9.81 (1H, s, C**H**O); ^{13}C NMR (400 MHz, $CDCl_3$, δ) 16.08, 42.60, 125.54, 131.37, 142.93, 181.60. IR (cm^{-1}, KBr disk) 1684 ν(C=O). *Anal.* Calcd (found) for $C_6H_8N_2O$: C, 58.05 (57.90); H, 6.50 (6.74); N, 22.57 (22.46).

N-Propylimidazole-2-carboxaldehyde.H_2O (***1c***)

N-Propylimidazole-2-carboxaldehyde was synthesized using the general method in **3.2.1.2**. *N*-Propylimidazole (0.027 mol), n-butyllithium (0.028 mol) and DMF (0.041 mol). The product was obtained as a brown oil (77.4%). ^{1}H NMR (400 MHz, $CDCl_3$, δ) 0.93 (3H, t, *J* 8.0, $N(CH_2)_2C$**H$_3$**), 1.81 (2H, m, NCH_2C**H$_2$**), 4.37 (2H, t, *J* 8.0, NC**H$_2$**), 7.21, 7.28 (2H, s, Im-**H**), 9.81 (1H, s, C**H**O); ^{13}C NMR (400 MHz, $CDCl_3$, δ) 11.30, 24.77, 49.71, 126.92, 131.96, 143.83, 182.38. IR (cm^{-1}, KBr disk): 1686 ν(C=O). *Anal.* Calcd (found) for $C_7H_{12}N_2O_2$: C, 58.83 (58.50); H, 7.74 (7.66); N, 17.94 (18.04).

N-Butylimidazole-2-carboxaldehyde.H_2O (***1d***)

N-Butylimidazole-2-carboxaldehyde was synthesized using the general method in **3.2.1.2**. *N*-Butylimidazole (0.033 mol), n-butyllithium (0.035 mol) and DMF (0.049 mol). The product was obtained as a brown oil (82.8%). ^{1}H NMR (400 MHz, $CDCl_3$, δ) 0.94 (3H, t, *J* 8.0, $N(CH_2)_3C\mathbf{H_3}$), 1.33 (2H, m, $CH_2CH_2C\mathbf{H_2}$), 1.77 (2H, m, N $CH_2C\mathbf{H_2}$), 4.40 (2H, t, *J* 8.0, $NC\mathbf{H_2}$) 7.20, 7.28 (2H, s, Im-**H**), 9.81 (1H, s, C**H**O); ^{13}C NMR (400 MHz, $CDCl_3$, δ) 13.81, 19.85, 33.30, 47.77, 126.61, 131.78, 143.61, 182.19. IR (cm^{-1}, KBr disk) 1686 ν(C=O). *Anal.* Calcd (found) for $C_8H_{14}N_2O_2$: C, 56.45 (56.96); H, 8.29 (7.99); N, 16.46 (16.95).

N-Heptylimidazole-2-carboxaldehyde.H_2O (***1e***)

N-Heptylimidazole-2-carboxaldehyde was synthesized using the general method in **3.2.1.2**. *N*-Heptylimidazole (0.030 mol), n-butyllithium (0.031 mol) and DMF (0.045 mol). The product was obtained as a brown oil (74.2%). ^{1}H NMR (400 MHz, $CDCl_3$, δ) 0.88 (3H, t, *J* 8.0, $N(CH_2)_6C\mathbf{H_3}$), 1.28 (8H, m, $NCH_2CH_2(C\mathbf{H_2})_4$), 1.78 (2H, m, $NCH_2C\mathbf{H_2}$), 4.38 (2H, t, *J* 8.0, $NC\mathbf{H_2}$) 7.15, 7.27 (2H, s, Im-**H**), 9.81 (1H, s, C**H**O); ^{13}C NMR (400 MHz, $CDCl_3$, δ) 14.36, 22.88, 26.73, 29.11, 31.41, 31.99, 48.18, 126.55, 131.91, 143.70, 182.28. IR (cm^{-1}, KBr disk): 1685 ν(C=O). *Anal.* Calcd (found) for $C_{11}H_{20}N_2O_2$: C, 62.23 (62.01); H, 9.50 (9.56); N, 13.20 (13.29).

N-Octylimidazole-2-carboxaldehyde (***1f***)

N-Octylimidazole-2-carboxaldehyde was synthesized using the general method in **3.2.1.2**. *N*-Octylimidazole (0.029 mol), n-butyllithium (0.030 mol) and DMF (0.043 mol). The product was obtained as a brown oil (53.3%). ^{1}H NMR (400 MHz, $CDCl_3$, δ) 0.90 (3H, t, *J* 8.0, $N(CH_2)_7C\mathbf{H_3}$), 1.30 (10H, m, N $CH_2CH_2(C\mathbf{H_2})_5$), 1.79 (2H, m, $NCH_2C\mathbf{H_2}$), 4.40 (2H, t, *J* 8.0, $NC\mathbf{H_2}$) 7.16, 7.29 (2H, s, Im-**H**), 9.83 (1H, s, C**H**O); ^{13}C NMR (400 MHz, $CDCl_3$, δ) 14.39, 22.96, 26.78, 29.41, 29.45, 48.19, 126.55, 131.91, 143.82, 182.39. IR (cm^{-1}, KBr disk): 1687, ν(C=O). *Anal.* Calcd (found) for $C_{12}H_{20}N_2O$: C, 69.19 (69.12); H, 9.68 (9.87); N, 13.45 (13.25).

N-Decylimidazole-2-carboxaldehyde (***1g***)

N-Decylimidazole-2-carboxaldehyde was synthesized using the general method in **3.2.1.2**. *N*-Decylimidazole (0.028 mol), n-butyllithium (0.029 mol) and DMF (0.042 mol). The product

was obtained as a brown oil (54.2%). ^{1}H NMR (400 MHz, $CDCl_3$ δ) 0.85 (3H, t, *J* 8.0, $N(CH_2)_9C\mathbf{H_3}$), 1.24 (14H, m, $NCH_2CH_2\mathbf{(}C\mathbf{H_2)_7}$), 1.76 (2H, m, $NCH_2C\mathbf{H_2}$), 4.46 (2H, t, *J* 8.0, $NC\mathbf{H_2}$) 7.14, 7.25 (2H, s, Im-**H**), 9.78 (1H, s, C**H**O); ^{13}C NMR (400 MHz, $CDCl_3$, δ) 14.50, 23.05, 26.78, 29.48, 29.65, 29.86, 31.42, 32.24, 48.22, 126.67, 131.90, 143.71, 182.38. IR (cm^{-1}, KBr disk) 1687, ν(C=O). *Anal.* Calcd (found) for $C_{14}H_{24}N_2O$: C, 71.14 (71.24); H, 10.23 (10.26); N, 11.85 (11.90).

N-Benzylimidazole-2-carboxaldehyde (***1h***)

N-Benzylimidazole-2-carboxaldehyde was synthesized using the general method in **3.2.1.2**. *N*-Benzylimidazole (0.038 mol), n-butyllithium (0.040 mol) and DMF (0.057 mol). The product was obtained as a brown crystalline solid (75.1%). M.p. 88-90°C, ^{1}H NMR (400 MHz, $CDCl_3$, δ) 5.61 (2H, s, $NC\mathbf{H_2}$-Ph), 7.30-7.33 (4H, m, Ar-**H**), 7.21, 7.19 (2H, s, Im-**H**), 7.14 (1H, s, Ar-**H**), 9.84 (1H, s, C**H**O); ^{13}C NMR (400 MHz, $CDCl_3$, δ) 51.00, 126.41, 127.85, 128.48, 129.10, 132.02, 135.89, 143.39, 182.31. IR (cm^{-1}, KBr disk) 1685 ν(C=O). *Anal.* Calcd (found) for $C_{11}H_{10}N_2O$: C, 70.95 (70.91); H, 5.41 (5.44); N, 15.04 (14.96).

3.2.1.3 Synthesis of 2-hydroxymethyl-*N*-alkylimidazoles

To a stirred solution of the *N*-alkylimidazole-2-carboxaldehyde (3.4 mmol) in methanol (10 mL) at 0°C was added $NaBH_4$ (3.4 mmol). After stirring at 0 °C for 2.5 h the solution was concentrated. The residue was taken up in Et_2O and extracted three times with H_2O. The ethereal solution was dried with anhydrous Na_2SO_4, filtered and Et_2O removed *in vacuo* to obtain a pure product without further purification.

2-Hydroxymethyl-N-methylimidazole (***2a***)

2-Hydroxymethyl-*N*-methylimidazole was synthesized using the general method in **3.2.1.3**. *N*-Methylimidazole-2-carboxaldehyde (3.1 mmol) and $NaBH_4$ (3.1 mmol). The product was obtained as a white crystalline solid (56.1%). M.p. 107-110 °C, ^{1}H NMR (400 MHz, $CDCl_3$, δ) 3.75 (3H, s, $NC\mathbf{H_3}$), 4.66 (2H, s, $C\mathbf{H_2}OH$), 6.84, 6.89 (2H, s, Im-**H**); ^{13}C NMR (400 MHz, $CDCl_3$, δ) 32.97, 55.60, 121.58, 126.65, 148.28. IR (cm^{-1}, KBr disk) 3417 ν(O-H); 1637 ν(C=N); 1499. *Anal.* Calcd (found) for $C_5H_8N_2O$: C, 53.56 (53.19); H, 7.19 (7.10); N, 24.98 (24.52).

2-Hydroxymethyl-N-ethylimidazole (***2b***)

2-Hydroxymethyl-*N*-ethylimidazole was synthesized using the general method in **3.2.1.3**. *N*-Ethylimidazole-2-carboxaldehyde (3.3 mmol) and $NaBH_4$ (3.3 mmol). The product was obtained as a white crystalline solid (57.3%). M.p. 83-86 °C, ^{1}H NMR (400 MHz, $CDCl_3$, δ) 1.44 (3H, t, *J* 8.0, $NCH_2C\mathbf{H_3}$), 4.05 (2H, q, *J* 8.0, $NC\mathbf{H_2}CH_3$), 4.66 (2H, s, $C\mathbf{H_2}OH$), 6.16 (1H, s, $CH_2\mathbf{OH}$), 6.87, 6.91 (2H, s, Im-**H**); ^{13}C NMR (400 MHz, $CDCl_3$, δ) 16.54, 41.08, 55.62, 119.40, 126.81, 147.77. IR (cm^{-1}, KBr disk): 3429 ν(O-H); 1639 ν(C=N); 1497. *Anal.* Calcd (found) for $C_6H_{10}N_2O$: C, 57.12 (56.95); H, 7.99 (8.08); N, 22.21 (21.98).

2-Hydroxymethyl-N-propylimidazole (***2c***)

2-Hydroxymethyl-*N*-propylimidazole was synthesized using the general method in **3.2.1.3**. *N*-Propylimidazole-2-carboxaldehyde (3.4 mmol) and $NaBH_4$ (3.4 mmol). The product was obtained as clear oil (62.7%). ^{1}H NMR (400 MHz, $CDCl_3$, δ) 0.93 (3H, t, *J* 8.0, $N(CH_2)_2\mathbf{CH_3}$), 1.79 (2H, q, *J* 8.0, $NCH_2\mathbf{CH_2}$), 3.96 (2H, t, *J* 8.0, $N\mathbf{CH_2}$), 4.61 (2H, s, $\mathbf{CH_2}OH$), 6.82, 6.93 (2H, s, Im-**H**); ^{13}C NMR (400 MHz, $CDCl_3$, δ) 11.04, 23.68, 49.71, 53.69, 119.04, 121.61, 146.34. IR (cm^{-1}, KBr disk) 3417 ν(O-H); 1635 ν(C=N); 1497. *Anal.* Calcd (found) for $C_7H_{12}N_2O$: C, 59.98 (59.55); H, 8.63 (8.97); N, 19.98 (19.37).

2-Hydroxymethyl-N-butylimidazole (***2d***)

2-Hydroxymethyl-*N*-butylimidazole was synthesized using the general method in **3.2.1.3**. *N*-Butylimidazole-2-carboxaldehyde (3.1 mmol) and $NaBH_4$ (3.1 mmol). The product was obtained as clear oil (52.6%). ^{1}H NMR (400 MHz, $CDCl_3$, δ) 0.94 (3H, t, *J* 8.0, $N(CH_2)_3C\mathbf{H_3}$), 1.36 (2H, m, $NCH_2CH_2C\mathbf{H_2}$), 1.76 (2H, m, $NCH_2\mathbf{CH_2}$), 3.99 (2H, t, *J* 8.0, $NC\mathbf{H_2}$), 4.62 (2H, s, $C\mathbf{H_2}OH$), 6.85, 6.83 (2H, s, Im-**H**); ^{13}C NMR (400 MHz, $CDCl_3$, δ) 13.97, 20.22, 33.42, 46.25, 55.96, 120.24, 126.96, 148.05. IR (cm^{-1}, KBr disk) 3485 ν(O-H); 1638 ν(C=N); 1495. *Anal.* Calcd (found) for $C_8H_{14}N_2O$: C, 62.31 (62.11); H, 9.15 (9.45); N, 18.17 (17.91).

2-Hydroxymethyl-N-heptylimidazole.H_2O (***2e***)

2-Hydroxymethyl-*N*-heptylimidazole was synthesized using the general method in **3.2.1.3**. *N*-Heptylimidazole-2-carboxaldehyde (3.1 mmol) and $NaBH_4$ (3.1 mmol). The product was obtained as clear oil (61.7%). ^{1}H NMR (400 MHz, $CDCl_3$, δ) 0.88 (3H, t, *J* 8.0,

$N(CH_2)_6C\mathbf{H_3}$), 1.29 (8H, m, $NCH_2CH_2(C\mathbf{H_2})_4$), 1.78 (2H, m, N $CH_2C\mathbf{H_2}$), 3.99 (2H, t, *J* 8.0, $NC\mathbf{H_2}$), 4.62 (2H, s, $C\mathbf{H_2}OH$), 6.84, 6.82 (2H, s, Im-**H**); ^{13}C NMR (400 MHz, $CDCl_3$, δ) 14.10, 22.63, 26.73, 28.93, 31.14, 31.76, 46.25, 55.68, 119.93, 126.67, 147.86. IR (cm^{-1}, KBr disk) 3486 ν(O-H); 1638 ν(C=N); 1494. *Anal.* Calcd (found) for $C_{11}H_{22}N_2O_2$: C, 61.65 (61.53); H, 10.35 (10.30); N, 13.07 (13.12).

2-Hydroxymethyl-N-octylimidazole.2H₂O (***2f***)

2-Hydroxymethyl-*N*-octylimidazole was synthesized using the general method in **3.2.1.3**. *N*-Octylimidazole-2-carboxaldehyde (3.6 mmol) and $NaBH_4$ (3.6 mmol). The product was obtained as clear oil (68.6%). ^1H NMR (400 MHz, $CDCl_3$, δ) 0.88 (3H, t, *J* 8.0, $N(CH_2)_7C\mathbf{H_3}$), 1.29 (10H, m, $NCH_2CH_2(C\mathbf{H_2})_5$), 1.78 (2H, m, $NCH_2C\mathbf{H_2}$), 3.99 (2H, t, *J* 8.0, $NC\mathbf{H_2}$), 4.62 (2H, s, $C\mathbf{H_2}OH$), 6.85, 6.82 (2H, s, Im-**H**); ^{13}C NMR (400 MHz, $CDCl_3$, δ) 14.17, 22.74, 26.83, 29.26, 29.29, 31.88, 46.29, 55.74, 119.95, 126.77, 147.97. IR (cm^{-1}, KBr disk) 3602 ν(O-H); 1638 ν(C=N); 1494. *Anal.* Calcd (found) for $C_{12}H_{26}N_2O_3$: C, 58.51 (58.55); H, 10.64 (10.63); N, 11.37 (11.59).

2-Hydroxymethyl-N-decylimidazole (***2g***)

2-Hydroxymethyl-*N*-decylimidazole was synthesized using the general method in **3.2.1.3**. *N*-Decylimidazole-2-carboxaldehyde (3.0 mmol) and $NaBH_4$ (3.0 mmol). The product was obtained as clear oil (79.2%). ^1H NMR (400 MHz, $CDCl_3$, δ) 0.88 (3H, t, *J* 8.0, $N(CH_2)_9C\mathbf{H_3}$), 1.22 (14H, m, $NCH_2CH_2(C\mathbf{H_2})_7$), 1.78 (2H, m, $NCH_2C\mathbf{H_2}$), 3.99 (2H, t, *J* 8.0, $NC\mathbf{H_2}$), 4.63 (2H, s, $C\mathbf{H_2}OH$), 6.83, 6.86 (2H, s, Im-**H**); ^{13}C NMR (400 MHz, $CDCl_3$, δ) 14.30, 22.86, 26.86, 29.37, 29.46, 29.66, 46.32, 55.17, 120.05, 126.80, 147.88. IR (cm^{-1}, KBr disk) 3636 ν(O-H); 1637 ν(C=N); 1494. *Anal.* Calcd (found) for $C_{14}H_{26}N_2O$: C, 70.54 (69.96); H, 10.99 (10.43); N, 11.75 (11.48).

2-Hydroxymethyl-N-benzylimidazole (***2h***)

2-Hydroxymethyl-*N*-benzylimidazole was synthesized using the general method in **3.2.1.3**. *N*-Benzylimidazole-2-carboxaldehyde (3.1 mmol) and $NaBH_4$ (3.1 mmol). The product was obtained as a white powder (93.1%). M.p. 85-88°C, ^1H NMR (400 MHz, $CDCl_3$. δ) 4.62 (2H, s, $C\mathbf{H_2}OH$), 5.22 (2H, s, Ph-$C\mathbf{H_2}$), 6.80, 6.88 (2H, s, Im-**H**), 7.14-7.34 (5H, m, Ar-**H**); ^{13}C NMR (400 MHz, $CDCl_3$, δ) 50.07, 56.26, 120.98, 127.37, 127.62, 128.45, 129.31, 136.78, 148.55. IR (cm^{-1}, KBr disk) 3485 ν(O-H); 1638 ν(C=N); 1495. *Anal.* Calcd (found) for

$C_{11}H_{12}N_2O$: C, 70.19 (70.07); H, 6.43 (6.16); N, 14.88 (14.14).

3.2.1.4 Synthesis of *N*-alkylimidazole-2-carboxylic acids

N-Alkylimidazole-2-aldehyde (3.0 mmol) was dissolved in water (1 mL). To the solution was added 30% H_2O_2 (1 mL). The solution mixture was allowed to stir overnight, followed by the removal of water using a high vacuum pump to produce (without further purification) a pure white crystalline product, white paste or colourless oil.

N-Methylimidazole-2-carboxylic acid.H_2O (***3a***)

N-Methylimidazole-2-carboxylic acid was synthesized using the general method in **3.2.1.4**. *N*-Methylimidazole-2-carboxaldehyde (3.0 mmol) and 30% H_2O_2 (1 mL). The product was obtained as a white crystalline solid (99.9%). M.p. 105-108°C, ^{1}H NMR (400 MHz, D_2O, δ) 4.01 (3H, s, NC**H$_3$**), 7.46, 7.41 (2H, s, Im-**H**); ^{13}C NMR (400 MHz, D_2O, δ) 36.73, 118.45, 125.83, 139.68, 158.67. IR (cm^{-1}, KBr disk) 3189 ν(OH); 1655 ν(C=O); 1517 ν(C=C); 1464. *Anal.* Calcd (found) for $C_5H_8N_2O_3$: C, 41.67 (41.58); H, 5.59 (5.53); N, 19.44 (19.42).

N-Ethylimidazole-2-carboxylic acid.2H_2O (***3b***)

N-Ethylimidazole-2-carboxylic acid was synthesized using the general method in **3.2.1.4**. *N*-Methylimidazole-2-carboxaldehyde (3.3 mmol) and 30% H_2O_2 (1 mL). The product was obtained as a white fatty solid. Yield 99.9%. M.p. 68-70°C, ^{1}H NMR (400 MHz, D_2O) δ 1.45 (3H, t, *J* 8.0, NCH$_2$C**H$_3$**), 4.56 (2H, q, *J* 8.0, NC**H$_2$**), 7.40, 7.51 (2H, s, Im-**H**); ^{13}C NMR (400 MHz, D_2O) δ 15.62, 45.05, 118.84, 124.05, 139.19, 158.59. IR (cm^{-1}, KBr disk) 3186 ν(OH); 1657 ν(C=O); 1508 ν(C=C); 1465. *Anal.* Calcd (found) for $C_6H_{12}N_2O_4$: C, 40.91 (40.82); H, 6.87 (6.82); N, 15.90 (15.89).

N-Propylimidazole-2-carboxylic acid.2H_2O (***3c***)

N-Propylimidazole-2-carboxylic acid was synthesized using the general method in **3.2.1.4**. *N*-Propylimidazole-2-carboxaldehyde (3.0 mmol) and 30% H_2O_2 (1 mL). The product was obtained as clear oil (99.9%). ^{1}H NMR (400 MHz, D_2O, δ) 0.84 (3H, t, *J* 8.0, NCH$_2$CH$_2$C**H$_3$**), 1.80 (2H, m, NCH$_2$C**H$_2$**), 4.47 (2H, t, *J* 8.0, NC**H$_2$**), 7.38, 7.47 (2H, s, Im-**H**); ^{13}C NMR (400 MHz, D_2O, δ) 10.33, 23.95, 50.95, 118.75, 124.56, 139.39, 158.56. IR

(cm^{-1}, KBr disk) 3143 ν(OH), 1658 ν(C=O), 1509 ν(C=C); 1465. *Anal.* Calcd (found) for $C_7H_{14}N_2O_4$: C, 44.20 (44.18); H, 7.42 (7.57); N, 14.73 (14.94).

N-Butylimidazole-2-carboxylic acid.3H_2O (***3d***)

N-Butylimidazole-2-carboxylic acid was synthesized using the general method in **3.2.1.4**. *N*-Butylimidazole-2-carboxaldehyde (3.0 mmol) and 30% H_2O_2 (1 mL). The product was obtained as a white paste (99.9%). ^{1}H NMR (400 MHz, D_2O, δ) 0.86 (3H, t, *J* 8.0 $NCH_2CH_2CH_2C\mathbf{H_3}$), 1.25 (2H, m, $NCH_2CH_2C\mathbf{H_2}$), 1.78 (2H, m, $NCH_2C\mathbf{H_2}$), 4.51 (2H, t, *J* 8.0, $NC\mathbf{H_2}$), 7.38, 7.47 (2H, s, Im-**H**), 14.53 (1H, s, COO**H**); ^{13}C NMR (400 MHz, D_2O, δ) 13.16, 19.34, 32.51, 49.27, 118.82, 124.53, 139.44, 158.63. IR (cm^{-1}, KBr disk): 3177 ν(OH); 1660 ν(C=O); 1506 ν(C=C); 1462. *Anal.* Calcd (found) for $C_8H_{18}N_2O_5$: C, 43.24 (43.34); H, 8.16 (7.94); N, 12.61 (12.62).

N-Heptylimidazole-2-carboxylic acid.H_2O (***3e***)

N-Heptylimidazole-2-carboxylic acid was synthesized using the general method in **3.2.1.4**. *N*-Heptylimidazole-2-carboxaldehyde (3.1 mmol) and 30% H_2O_2 (1 mL). The product was obtained as clear oil (99.9%). ^{1}H NMR (400 MHz, D_2O, δ) 0.87 (3H, t, *J* 8.0, $N(CH_2)_6C\mathbf{H_3}$), 1.27 (8H, m, $NCH_2CH_2(C\mathbf{H_2})_4$), 1.87 (2H, m, $NCH_2C\mathbf{H_2}$), 4.66 (2H, t, *J* 8.0, $N\mathbf{CH_2}$), 7.10, 7.47 (2H, s, Im-**H**), 9.87 (1H, s, COO**H**); ^{13}C NMR (400 MHz, D_2O, δ) 14.36, 22.87, 26.71, 29.09, 31.21, 31.95, 49.77, 119.89, 122.83, 140.76, 156.98. IR (cm^{-1}, KBr disk) 3148 ν(OH); 1663 ν(C=O); 1507 ν(C=C); 1464. *Anal.* Calcd (found) for $C_{11}H_{20}N_2O_3$: C, 57.87 (57.93); H, 8.83 (8.99); N, 12.27 (12.29).

N-Octylimidazole-2-carboxylic acid.H_2O (***3f***)

N-Octylimidazole-2-carboxylic acid was synthesized using the general method in **3.2.1.4**. *N*-Octylimidazole-2-carboxaldehyde (3.1 mmol) and 30% H_2O_2 (1 mL). The product was obtained as a white fatty solid (99.9%). M.p. <40°C, ^{1}H NMR (400 MHz, D_2O) δ 0.85 (3H, t, *J* 8.0, $N(CH_2)_7C\mathbf{H_3}$), 1.25 (10H, m, $NCH_2CH_2(C\mathbf{H_2})_5$), 1.82 (2H, m, $NCH_2C\mathbf{H_2}$), 4.60 (2H, t, *J* 8.0,$NC\mathbf{H_2}$), 7.18, 7.49 (2H, s, Im-**H**), 8.29 (1H, s, COO**H**); ^{13}C NMR (400 MHz, D_2O) δ 14.39, 22.95, 26.78, 29.43, 29.45, 31.13, 32.10, 49.77, 119.93, 123.36, 140.23, 157.59. IR (cm^{-1}, KBr disk) 3140 ν(OH); 1639 ν(C=O); 1508 ν(C=C); 1464. *Anal.* Calcd (found) for $C_{12}H_{22}N_2O_3$: C, 59.48 (59.71); H, 9.15 (9.51); N, 11.56 (11.51).

N-Decylimidazole-2-carboxylic acid.H_2O (***3g***)

N-Decylimidazole-2-carboxylic acid was synthesized using the general method in **3.2.1.4**. *N*-Decylimidazole-2-carboxaldehyde (3.0 mmol) and 30% H_2O_2 (1 mL). The product was obtained as a white paste. Yield 99.9%. ^{1}H NMR (400 MHz, $CDCl_3$) δ 0.88 (3H, t, *J* 8.0, $N(CH_2)_9C\mathbf{H_3}$), 1.25-1.33 (14H, m, $NCH_2CH_2(C\mathbf{H_2})_7$), 1.88 (2H, m, $NCH_2C\mathbf{H_2}$), 4.71 (2H, t, *J* 8.0, $N\mathbf{CH_2}$), 7.06, 7.41 (2H, s, Im-**H**), 9.34 (1H, s, COO**H**); ^{13}C NMR (400 MHz, $CDCl_3$) δ 14.26, 22.83, 26.55, 29.27, 29.58, 29.79, 29.85, 31.07, 32.01, 49.44, 119.37, 122.23, 141.07, 156.05. IR (cm^{-1}, KBr disk) 3137 ν(OH); 1672 ν(C=O); 1508 ν(C=C); 1464. *Anal.* Calcd (found) for $C_{14}H_{26}N_2O_3$: C, 62.19 (62.15); H, 9.69 (9.64); N, 10.36 (10.33).

N-Benzylimidazole-2-carboxylic acid (***3h***)

N-Methylimidazole-2-carboxylic acid was synthesized using the general method in **3.2.1.4**. *N*-Methylimidazole-2-carboxaldehyde (3.0 mmol) and 30% H_2O_2 (1 mL). The product was obtained as a white powder (99.9%). M.p. 72-73°C, ^{1}H NMR (400 MHz, $CDCl_3$, δ) 5.89 (2H, s, Ph-C$\mathbf{H_2}$), 7.34-7.51 (7H, m, Ar-**H**); ^{13}C NMR (400 MHz, $CDCl_3$, δ) 36.73, 118.45, 125.83, 139.68, 158.67. IR (cm^{-1}, KBr disk) 3137 ν(OH); 1656, ν(C=O); 1498, ν(C=C); 1460. *Anal.* Calcd (found) for $C_{11}H_{10}N_2O_2$: C, 65.34 (65.10); H, 4.98 (5.05); N, 13.85 (13.64).

3.2.2 Potentiometric studies

The protonation constants for the imidazole compounds were determined by potentiometric titration (mV) of approximately 25 ml samples at 25(±0.1) °C. All solutions were prepared using freshly boiled and degassed deionized milli-Q water to ensure the removal of dissolved oxygen and carbon dioxide. Titrations were performed over the pH range of 2–11 under a continuous flow of purified nitrogen using HCl and tetramethylammonium hydroxide (TMAOH). The ligand solution was acidified by the addition of 0.1 M HCl (1 mL) followed by titration with 0.1 M TMAOH. The ionic strength of the titration solutions was kept constant at 0.10 M tetramethylammonium chloride (TMACl). Titrations were controlled using Tiamo software. The glass electrode was calibrated for a strong acid–base reaction by the Gran-method[314] using the program GLEE,[315] to determine the standard potential E^o. The ionic product of water (pK_w) of 13.83(1) at 25.0(± 0.1) °C in 0.10 M TMACl was used in all calculations.[316] The titration data were resolved using the computer program

HYPERQUAD.[317] The final values of the constants were obtained from an average of six independent titrations using an average of 400 data points in total for each refinement.

3.2.3 Antimicrobial activity evaluation

3.2.3.1 Disk diffusion and minimum inhibitory concentration (MIC) methods

The antimicrobial activity of the compounds was investigated against a Gram-negative (*E. coli* ATCC 8793), Gram-positive (*S. aureus* ATCC 6538 and *B. subtilis* subsp. *spizizenii* ATCC 6633) bacteria and yeast (*C. albicans* ATCC 2091) using the disk diffusion and the broth microdilution methods. To determine the zones of inhibition, blank disks (6.5 mm) were impregnated with 20 μL of a methanolic solution containing the various compounds (including ketoconazole and ampicillin) such that 50 μg and 100 μg of the pure compound remained on the disk. Disks containing 100 μg of metronidazole were prepared in a similar manner as the disks for the 100 μg of test compounds. The disks were left overnight at room temperature to allow the methanol to evaporate, and then placed onto Mueller-Hinton agar plates streaked with the various bacteria. The plates were incubated at 37 °C for 18 h after which the zones of clearance were measured. For *C. albicans*, potato dextrose agar plates were streaked and incubated at 30 °C for 48 h. A 0.5 McFarland standard (OD_{625} = 0.08-0.13, 1.5 x 10^8 CFU/ml) was used to match the turbidity of the culture suspensions.

The minimum inhibitory concentrations were determined using the broth microdilution method. Single colonies were suspended in the Mueller-Hinton or Nutrient broth and incubated over a period of 2-6 h until an appropriate optical density (OD = 0.6-0.8) at 625 nm was achieved. Methanolic solutions of test compounds (2.5 mg/mL) were serially diluted in 96 well microplates using the broth. The bacterial suspension (5 μL) was added and the plates incubated at 37 °C for 18 h. Metronidazole was used as a negative control for antibacterial activity, and Ampicillin[318] and ketoconazole[319] were used as positive controls for bacteria and yeast, respectively.

3.3 The fabrication and antimicrobial activity evaluation of electrospun nylon 6 nanofibers incorporated with 2-substituted *N*-alkylimidazoles

3.3.1 Incorporation of 2-substituted *N*-alkylimidazoles into electrospun nylon 6 nanofibers

The polymer solution for electrospinning was prepared by dissolving nylon 6 (1.6 g, 16% (w/v)) and the selected compounds (0.08 g, 5% (w/w)) in 10 mL of HCOOH/CH_3COOH mixture (1:1). The electrospinning parameters were optimized at ambient conditions as follows: flow rate (0.75 mL/h), applied voltage (+22.5 kV, -5 kV), tip-to-collector distance (8 cm). The flow rate of the polymer solution was controlled using a digital pump. The nanofibers were collected on a rotating drum covered with an aluminium foil.

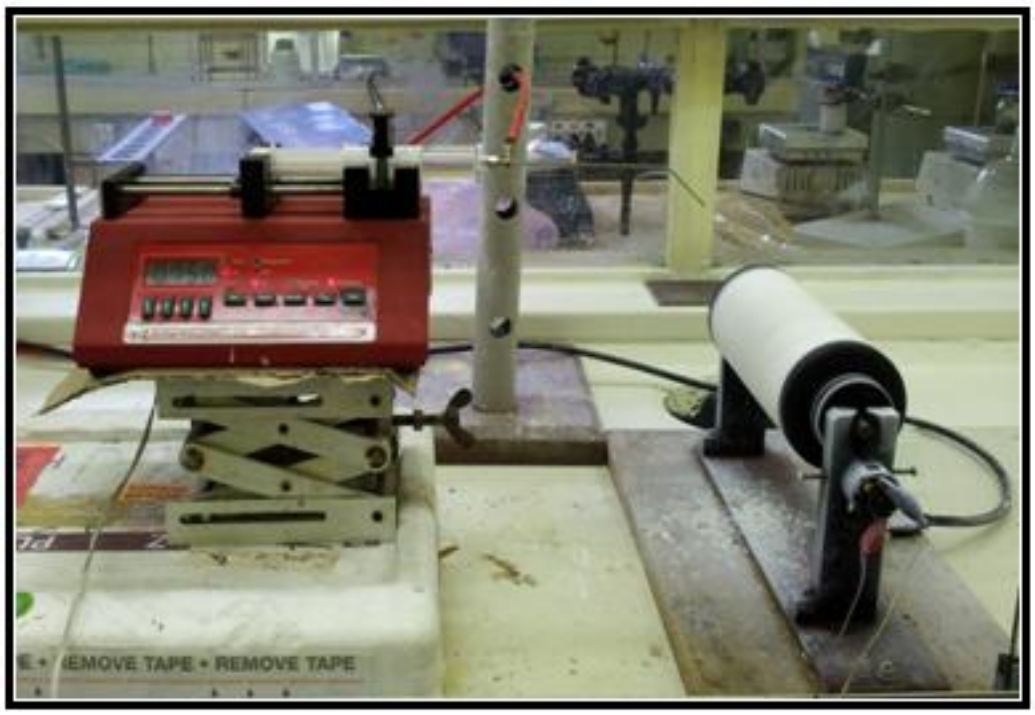

Figure 3.1. Electrospinning set-up for fabrication of nylon 6 composite nanofibers

3.3.2 Antimicrobial activity evaluation

3.3.2.1 Disk diffusion method

The disk diffusion method, for the antimicrobial activity evaluation of electrospun nylon 6/imidazoles nanofiber composites (diameter of disk = 7.0 ± 0.1 mm), was carried out as already described in **3.2.3.1**.

3.3.2.2 AATCC Test Method 100

The antimicrobial activity of electrospun nylon 6/imidazoles nanofibers was investigated using a modified version of the American Association of Textile Chemists and Colorists (AATCC) Test Method 100-2004.[320] *E. coli* and *S. aureus* were used as model challenge microorganisms. A diluted bacterial suspension with about 1×10^8 CFU/mL concentration was used, and (500 µL) of this suspension was loaded onto the electrospun nylon 6 nanofiber swatches (diameter = ~4.8 cm) surface in the presence of a nonionic wetting agent (Triton X-100). The inoculum on the surface was then carefully covered with another identical nylon 6 nanofiber in a sterialized glass jar. After incubation for 24 h contact time, 0.02 N sodium thiosulfate was added in excess to quench the biological growth. The mixture was then vortexed vigorously for 2 min. An aliquot of the solution was serially diluted plated onto nutrient agar plates. Electrospun nylon 6 nanofibers with no additives were used as a negative control and were evaluated using same procedure. Viable bacterial colonies on the agar plates were counted after incubation at 37 °C for 48 h. The reduction rate in the number of bacteria was calculated using Eqn 3.1:

$$R\ (\%) = \frac{N_0 - N_t}{N_0}\ x\ 100 \qquad (3.1)$$

where R is the reduction rate, N_t the number of bacteria recovered from the inoculated electrospun nylon 6 nanofibers over 24 h of contact time, and N_o is the number of bacteria recovered from the inoculated electrospun nylon 6 nanofibers at zero contact time.

3.4 Syntheses and antimicrobial activity evaluation of silver(I) complexes containing 2-hydroxymethyl-*N*-alkylimidazole ligands

3.4.1 Synthesis of silver(I) complexes containing 2-hydroxymethyl-*N*-alkylimidazoles

To a solution of $AgNO_3$ (1 mol equivalent) in ethanol (15 ml) was added 2-hydroxymethyl-*N*-alkylimidazole (2 mol equivalents). The reaction mixture was stirred at room temperature for 24 h. The reaction mixture was filtered, ethyl acetate (15 ml) was added to the mother liquor and the solvent evaporated slowly at atmospheric pressure to obtain a pure product in good yield.

$[Ag_2$(2-hydroxymethyl-N-methylimidazole)$_4](NO_3)_2$ ***(C1)***

The complex **C1** was synthesized using the general method in **3.4.1** and was obtained as a white crystalline solid (82.3%). M.p. 134-138°C. Anal. Calc. (found) for $C_{20}H_{32}Ag_2N_{10}O_{10}$ (%): C, 30.47 (30.50); H, 4.09 (4.19); N, 17.77 (17.75). IR (cm^{-1}) 3330, 3124, 2951, 1545, 1505, 1455, 1367, 1310, 1286, 1233, 1188, 1158, 1070, 1024(vs), 977, 827, 767, 702(w), 664.

$[Ag_3$(2-hydroxymethyl-N-ethylimidazole)$_6](NO_3)_3$ ***(C2)***

The complex **C2** was synthesized using the general method in **3.4.1** and was obtained as a white crystalline solid (78.6%). M.p. 94-96°C. Anal. Calc. (found) for $C_{36}H_{60}Ag_3N_{15}O_{15}$ (%): C, 34.14 (34.08); H, 4.77; N (4.84), 16.59 (16.59). IR (cm^{-1}) 3306, 3126, 2980, 2934, 1498, 1441, 1351, 1319, 1292, 1261, 1222, 1180 1157, 1029, 1007, 928, 823, 768, 755, 692.

$[Ag_2$(2-hydroxymethyl-N-propylimidazole)$_4](NO_3)_2$ ***(C3)***

The complex **C3** was synthesized using the general method in **3.4.1** and was obtained as a white crystalline solid (58.2). Anal. Calc. (found) for $C_{28}H_{48}Ag_2N_{10}O_{10}$ (%): C, 37.35 (37.12); H, 5.37 (5.23); N, 15.55 (15.48). IR (cm^{-1}) 3331, 3134, 2960, 2932, 2873, 1498, 1456, 1368, 1307, 1277, 1168, 1157, 1079, 1033, 976, 826, 751, 662.

*[Ag_2(2-hydroxymethyl-N-butylimidazole)$_4$](NO_3)$_2$ (**C4**)*

The complex **C4** was synthesized using the general method in **3.4.1** and was obtained as yellow oil (64.1%). Anal. Calc. (found) for $C_{32}H_{56}Ag_2N_{10}O_{10}$ (%): C, 40.18 (40.18); H, 5.90 (5.82); N, 14.64 (14.44). IR (cm^{-1}) 3358, 3124, 2960, 2934, 2874, 1520, 1454, 1366, 1323, 1236, 1173, 1153, 1115, 1092, 1033, 948, 826, 747, 656.

*[Ag_2(2-hydroxymethyl-N-heptylimidazole)$_4$](NO_3)$_2$ (**C5**)*

The complex **C5** was synthesized using the general method in **3.4.1** and was obtained as light yellow oil (87.7%). Anal. Calc. (found) for $C_{44}H_{80}Ag_2N_{10}O_{10}$ (%): C, 46.98 (47.05); H, 7.17 (7.22); N, 12.45 (12.83). IR (cm^{-1}) 3382, 3118, 2957, 2927, 2857, 1517, 1457, 1335, 1235, 1111, 1088, 1038, 828, 748, 660.

*[Ag_2(2-hydroxymethyl-N-octylimidazole)$_4$](NO_3)$_2$ (**C6**)*

The complex **C6** was synthesized using the general method in **3.4.1** and was obtained as colourless oil (89.3%). Anal. Calc. (found) for $C_{48}H_{88}Ag_2N_{10}O_{10}$ (%): C, 48.82 48.32); H, 7.51 (6.88); N, 11.86 (11.73). IR (cm^{-1}) 3485, 3123, 2925, 2855, 1520, 1454, 1331, 1287, 1237, 1113, 1091, 1030, 948, 819, 738, 655.

*[Ag_2(2-hydroxymethyl-N-decylimidazole)$_4$](NO_3)$_2$ (**C7**)*

The complex **C7** was synthesized using the general method in **3.4.1** and was obtained as a grey needle-like solid (84.4%). M.p. 75-77°C. Anal. Calc. (found) for $C_{56}H_{104}Ag_2N_{10}O_{10}$ (%): C, 52.01 (52.19); H, 8.11 (7.85); N, 10.83 (10.51). IR (cm^{-1}) 3384, 3122, 2919, 2851, 1498, 1466, 1351, 1318, 1284, 1153, 1115, 1039, 975, 827, 772, 743, 689, 657.

*[Ag_2(2-hydroxymethyl-N-benzylimidazole)$_4$](NO_3)$_2$ (**C8**)*

The complex **C8** was synthesized using the general method in **3.4.1** and was obtained as a white crystalline solid (72.8%). M.p. 142-145°C. Anal. Calc. (found) for $C_{44}H_{40}N_{10}Ag_2O_{10}$ (%): C, 48.73 (48.19); H, 3.72 (4.00); N, 12.91 (12.80). IR (cm^{-1}) 3367, 3199, 3126, 1495, 1454, 1399, 1324, 1294, 1268, 1156, 1127, 1081, 1026, 976, 824, 751, 706, 657.

3.4.2 X-ray crystal structure determination

Intensity data was collected on a Bruker APEX II CCD area detector diffractometer with graphite monochromated Mo K_α radiation (50kV, 30mA) using the APEX 2[321] data collection software. The collection method involved ω-scans of width 0.5° and 512x512 bit data frames. Data reduction was carried out employing the program *SAINT+*[322] and face indexed absorption corrections were made using *XPREP*.[322] The crystal structure was elucidated by direct methods using *SHELXTL*.[323] Non-hydrogen atoms were first refined isotropically followed by anisotropic refinement employing full matrix least-squares calculations based on F^2 using *SHELXTL*. For complex **C2**, the oxygen atom O2 was found to be disordered and was refined over two positions with final occupancies of 0.888(3) and 0.112(3) for O2 and O2B respectively. Hydrogen atoms were first located in the difference map, then positioned geometrically and allowed to ride on their respective parent atoms. Diagrams and publication material were generated using SHELXTL, PLATON.[324]

3.4.3 Antimicrobial activity evaluation

The antimicrobial activity of silver(I) complexes containing 2-hydroxymethyl-*N*-alkylimidazoles was evaluated using the disk diffusion and minimum inhibitory concentration methods. The procedures for both methods were the same as those in **3.2.3.1**.

3.5 The fabrication and antimicrobial activity evaluation of electrospun nylon 6 nanofibers incorporated with silver(I) complexes and silver nanoparticles

3.5.1 Incorporation of Ag(I) complexes containing 2-hydroxymethyl-*N*-alkylimidazoles into electrospun nylon 6 nanofibers

The incorporation of selected silver(I) complexes (**C6** and **C7**) into electrospun nylon 6 nanofibers was performed as already described in **3.3.1** with slight adjustments in the applied voltage, to maintain a stable jet. The applied voltage was increased by +0.5 to +1 kV from (+22.5 kV, -5 kV) while the negative voltage was kept constant.

3.5.2 Incorporation of silver nanoparticles (AgNPs) onto electrospun nylon 6 nanofibers

The AgNPs were prepared by in situ reduction of $AgNO_3$ in the presence of formic acid without the addition of any reducing agent.[50] The polymer solution for electrospinning was prepared by dissolving nylon 6 (16% (w/v)) and $AgNO_3$ (5% (w/w)) in 10 mL of $HCOOH/CH_3COOH$ mixture (1:1). The electrospinning conditions were the same as those used in **3.3.1** with slight adjustments to the applied voltage as already mentioned.

3.5.3 Antimicrobial activity evaluation

3.5.3.1 Disk diffusion method

The disk diffusion method, for the antimicrobial activity evaluation of electrospun nylon 6/silver(I) complexes nanofiber composites (disk diameter = 7.0 ± 0.1 mm) , was carried out as already described in **3.2.3.1**.

3.5.3.2 AATCC test method 100

The AATCC test method 100, for antimicrobial evaluation of electrospun nylon 6/silver complexes nanofiber composites, was performed as already described in **3.3.2.2**.

3.5.3.3 Dynamic shake flask test method (ASTM E2149-10)

The antimicrobial activity of electrospun nylon 6 nanofiber grafted with vinylimidazole derivatives was evaluated using the dynamic shake flask test method (American Society for Testing and Materials (ASTM) E2149).[325] A working suspension was prepared by diluting, with a sterile 3 mM phosphate buffer (pH 7.2 ±0.1), a 24 h culture to an optical density of 0.28 at 475 nm (1.5-30 x 10^8 CFU/mL). Further appropriate dilution using a sterile phosphate buffer gave a final concentration of 1.5-30 x 10^5 CFU/mL. Electrospun nylon 6 nanofiber composites (0.2-0.3 g) were placed into flasks containing 20 mL of the working dilution. The flasks were incubated with continuous shaking at 37 °C for 1 h. After serial dilutions using the phosphate buffer, the bacterial suspensions (0.1 mL) were plated in nutrient agar. The inoculated plates were incubated at 37 °C for 24 h and surviving bacterial cells counted using

a colony counter. The percentage reduction of the microorganisms after contact with the test specimen (nanofiber composites) was compared to the number of bacterial cells surviving after contact with the control. Equation 3.2 in paragraph 3.6.2 was used to calculate the percentage reduction of microbial growth.

3.6 The fabrication and antimicrobial activity evaluation of electrospun nanofibers by immobilization of *N*-vinylimidazoles using graft polymerization

3.6.1 Synthesis of vinylimidazole derivatives

4(5)-Vinylimidazole

4(5)-Vinylimidazole was synthesised by decarboxylation of urocanic acid, a method obtained from literature.[326] Urocanic acid (5.0 g, 0.053 mol) was placed into a short distillation apparatus and then heated *in vacuo* at 230°C. The resulting 4(5)-vinylimidazole which solidified in the condenser was washed off with THF. After removal of the solvent, the crude 4(5)-vinylimidazole syrup was placed in a refrigerator overnight to induce crystallization. The purification of crude 4(5)-vinylimidazole was done by sublimation in a 70°C oil bath under a vacuum of (~1.5 x 10^{-2} mbar). 4(5)-vinylimidazole was obtained as colourless crystals. Yield 45.6%. White crystalline powder, ^{1}H NMR (400 MHz, D_2O) δ 7.66 (s, Im-**H**), 7.07 (s, Im-**H**), 6.66-6.59 (m, vinyl-C**H**), 5.63 (d, *J* 16, vinyl-C**H$_2$**), 5.14 (d, *J* 8.0, vinyl-C**H$_2$**); ^{13}C NMR (400 MHz, D_2O) δ 137.19 (Im-N=**C**H), 136.73 (Im-**C**H), 127.34 (vinyl-**C**H), 118.42 (Im-**C**H), 112.37 (vinyl-**C**H_2). IR (cm^{-1}) 3088, 3033, 2942, 2815, 2679, 2610, 1807, 1644, 1540, 1524, 1505, 1469, 1464, 1352, 1286, 1249, 1166, 1108, 1024, 985, 940, 899, 833, 788, 723.

N-Decyl-4(5)-vinylimidazole

N-Decyl-4(5)-vinylimidazole was synthesized using 4(5)-vinylimidazole, by employing the same procedure as in **3.2.1.1** and was obtained a white crystalline powder (88.3%). ^{1}H NMR (400 MHz, $CDCl_3$) δ 7.37 (s, Im-**H**), 6.83 (s, Im-**H**), 6.59-6.54 (m, vinyl-C**H**), 5.77 (d, vinyl-C**H$_2$**), 5.07 (d, vinyl-C**H$_2$**), 3.84 (t, C**H$_2$**), 2.06 (s, C**H$_2$**), 2.15 (s, C**H$_2$**), 1.75-1.68 (m, C**H$_2$**), 1.27-1.23 (m, C**H$_2$**), 0.86 (t, C**H$_3$**); ^{13}C NMR (400 MHz, $CDCl_3$) δ 140.81 (Im-N=**C**H), 137.18 (Im-**C**H), 128.68 (vinyl-**C**H), 116.54 (Im-**C**H), 111.64 (vinyl-**C**H_2), 53.87, 47.62, 31.81, 30.96, 29.34, 29.21, 21.03, 26.47, 22.63, 14.07. IR (cm^{-1}) 3089, 3028, 2942, 2820,

2775, 2673, 2610, 1810, 1644, 1537, 1523, 1507, 1464, 1352, 1286, 1252, 1163, 1109, 1024, 985, 940, 899, 833, 788, 723, 650.

N-Vinylimidazole-2-carboxaldehyde

N-vinylimidazole-2-carboxaldehyde was synthesized using the same procedure as in **3.2.1.2** and was obtained as colourless crystals (73.4%). ^{1}H NMR (400 MHz, $CDCl_3$) δ 9.88 (C**H**O), 7.99-7.93 (m, vinyl-C**H**), 7.56 (s, Im-**H**), 7.35 (s, Im-**H**), 5.43 (d, *J* 16, vinyl-C**H$_2$**), 5.13 (d, *J* 8.0, vinyl-**C**H$_2$); ^{13}C NMR (400 MHz, $CDCl_3$ δ 182.76 (**C**HO), 142.83 (Im-N=**C**H), 132.73 (Im-**C**H), 130.25 (vinyl-**C**H), 121.30 (Im-**C**H), 105.84 (vinyl-**C**H$_2$). IR (cm^{-1}) 3122, 3092, 1800, 1674, 1640, 1500, 1474, 1412, 1378, 1342, 1320, 1285, 1152, 1099, 1050, 969, 956, 893, 780, 685, 671.

2-Hydroxymethyl-N-vinylimidazole

2-hydroxymethyl-*N*-vinylimidazole was synthesized using the same procedure as in **3.2.1.3** and was obtained as a white hygroscopic solid (97.1%). ^{1}H NMR (400 MHz, D_2O) δ 7.45 (s, Im-**H**), 7.17-7.11 (m, vinyl-C**H**), 6.98 (s, Im-**H**), 5.43 (d, *J* 16, vinyl-C**H**), 5.03 (d, *J* 8.0, vinyl-C**H$_2$**), 4.69 (s, CH$_2$O**H**); ^{13}C NMR (400 MHz, D_2O) δ 146.46 (Im-N=**C**H), 128.81 (vinyl-**C**H), 127.77 (Im-**C**H), 118.07 (Im-**C**H), 104.56 (vinyl-**C**H$_2$), 55.28 (**C**H$_2$OH). IR (cm^{-1}) 3347, 3112, 2922, 2854, 2236, 1646, 1528, 1493, 1434, 1342, 1276, 1161, 1060, 1037, 954, 879, 731, 689, 662.

N-Vinylimidazole-2-carboxylic acid

N-Vinylimidazole-2-carboxylic acid was synthesized using the same procedure as in **3.2.1.4** and was obtained as white hygroscopic (98.6%). ^{1}H NMR (400 MHz, D_2O) δ 7.85-7.79 (m, vinyl-C**H**), 7.74 (s, Im-**H**), 7.40 (s, Im-**H**), 5.69 (d, *J* 16, vinyl-C**H$_2$**), 5.36 (d, *J* 8.0, vinyl-C**H$_2$**). ^{13}C NMR (400 MHz, D_2O) δ 215.82 (**C**OOH), 158.64 (Im-N=**C**H), 139.20 (Im-**C**H), 129.66 (vinyl-**C**H), 120.34 (Im-**C**H), 110.12 (vinyl-**C**H$_2$). IR (cm^{-1}) 3112, 2804, 1644, 1605, 1578, 1496, 1457, 1424, 1379, 1340, 1313, 1295, 1274, 1125, 1022, 966, 906, 805, 760, 668.

N-Decyl-4(5)-vinylimidazole-2-carboxaldehyde

N-Decyl-4(5)-vinylimidazole-2-carboxaldehyde was synthesized using the same procedure as in **3.2.1.2** and was obtained as brown oil (94.2%). ^{1}H NMR (400 MHz, $CDCl_3$) δ 8.01 (s, C**H**O); 7.37 (s, Im-**H**), 7.26 (s, Im-**H**), 6.59-6.52 (m, vinyl-C**H**), 5.81 (d, vinyl-C$\mathbf{H_2}$), 5.08 (d, vinyl-C$\mathbf{H_2}$), 3.85 (t, C$\mathbf{H_2}$), 2.93 (s, C$\mathbf{H_2}$), 2.85 (s, C$\mathbf{H_2}$), 1.27-1.23 (m, C$\mathbf{H_2}$), 1.73 (m, C$\mathbf{H_2}$), 0.85 (t, C$\mathbf{H_3}$); ^{13}C NMR (400 MHz, $CDCl_3$) δ 182.91 (**C**HO) 140.71 (Im-N=**C**H), 137.15 (Im-**C**H), 128.56 (vinyl-**C**H), 116.52 (Im-**C**H), 111.81 (vinyl-**C**H_2), 47.11, 35.51, 30.94, 29.44, 29.38, 29.22, 29.02, 26.48, 22.62, 14.08. IR (cm^{-1}) 2924, 2854, 1673, 1537, 1493, 1457, 1406, 1386, 1348, 1256, 1228, 1163, 1149, 1090, 1062, 1047, 1024, 986, 971, 897, 822, 771, 722.

N-Decyl-2-hydroxymethyl-4(5)-vinylimidazole

N-Decyl-2-hydroxymethy-4(5)-vinylimidazole was synthesized using the same procedure as in **3.2.1.3** and was obtained as yellow oil (86.7%). ^{1}H NMR (400 MHz, $CDCl_3$) δ 7.37 (s, Im-**H**), 6.84 (s, Im-**H**), 6.60-6.53 (m, vinyl-C**H**), 5.82 (d, vinyl-C$\mathbf{H_2}$), 5.29 (s, C$\mathbf{H_2}$OH), 5.10 (d, vinyl-C$\mathbf{H_2}$), 3.85 (t, C$\mathbf{H_2}$), 1.73 (m, C$\mathbf{H_2}$), 1.24 (m, C$\mathbf{H_2}$), 0.87 (t, C$\mathbf{H_3}$); ^{13}C NMR (400 MHz, $CDCl_3$) δ 140.77 (Im-N=**C**H), 137.9 (Im-**C**H), 128.60 (vinyl-**C**H), 116.51 (Im-**C**H), 111.78 (vinyl-**C**H_2), 53.44 (C$\mathbf{H_2}$OH), 47.71, 31.82, 30.96, 29.46, 29.39, 29.23, 29.04, 26.49, 22.64, 14.09. IR (cm^{-1}); 3099, 2924, 2854, 1712, 1676, 1641, 1539, 1496, 1465, 1404, 1371, 1224, 1450, 1119, 1048, 1027, 985, 898, 821, 753, 722.

N-Decyl-4(5)-vinylimidazole-2-carboxylic acid

N-Decyl-4(5)-vinylimidazole-2-carboxylic acid was synthesized using the same procedure as in **3.2.1.4**. and was obtained as yellow oil (94.9%). ^{1}H NMR (400 MHz, $CDCl_3$) δ 7.60 (s, Im-**H**), 6.94 (s, Im-**H**), 6.62-6.55 (m, vinyl-C**H**), 5.83 (d, vinyl-C$\mathbf{H_2}$), 5.31 (s, COO**H**), 5.14 (d, vinyl-C$\mathbf{H_2}$), 3.90 (t, C$\mathbf{H_2}$), 1.76 (m, C$\mathbf{H_2}$), 1.31-1.25 (m, C$\mathbf{H_2}$), 0.87 (t, C$\mathbf{H_3}$); ^{13}C NMR (400 MHz, $CDCl_3$) δ 174.36 (**C**OOH), 137.21 (Im-**C**H), 128.29 (vinyl-**C**H), 116.52 (Im-**C**H), 112.19 (vinyl-**C**H_2), 47.23, 31.84, 30.93, 26.47, 29.40, 29.24, 29.05, 26.50, 22.65, 14.10. IR (cm^{-1}) 3369, 3124, 2923, 2854, 1751, 1669, 1542, 1501, 1465, 1411, 1377, 1257, 1223, 1166, 1118, 1090, 1047, 986, 931, 888, 817, 761, 722.

3.6.2 Grafting of vinylimidazole derivatives onto electrospun nylon 6 nanofibers

Electrospun nanofibers with dimensions 5 cm x 5 cm were immersed in test tubes containing vinylimidazoles (1 g) and benzophenone (0.015 g) in H_2O/MeOH mixture (80/20). The test tubes were purged with N_2 gas and placed in the oven preheated to 70°C. The test tubes were allowed to equilibrate at the set oven temperature for about 30 min. A 400 W mercury vapour UV lamp was used to irradiate the solution and the radiation distance was 10 cm. At the end of the experiment, the grafted nanofibers were washed with hot water, Soxhlet extracted with methanol overnight and then dried at 60 °C. The percentage grafting was calculated using Eqn 3.2.

$$Grafting\ (\%) = \frac{B-A}{A}\ x\ 100 \qquad (3.2)$$

where *A* is the initial mass of electrospun nylon 6 nanofiber and *B* is mass of the grafted nylon 6 nanofiber.

3.6.3 Adsorption of silver nanoparticles (AgNPs) onto grafted nylon 6 nanofibers

Grafted nylon 6 nanofibers were placed in a solution of $AgNO_3$ (0.1 g) in methanol (20 mL) and shaken at room temperature for 48 h. Methanol acted as both a solvent and a reducing agent. The nanofibers were then washed with methanol and subsequently dried at room temperature in the dark.

3.6.4 Antimicrobial activity evaluation

3.6.4.1 Shake flask method (ASTM E2149-10)

The dynamic shake flask method, for antimicrobial activity evaluation of grafted electrospun nylon 6 nanofibers was carried out as already described in **3.5.3.3**.

3.6.5 Cytotoxicity studies

Chang liver cells were seeded in 10 cm diameter culture dishes, maintained in Roswell Park Memorial Institute (RPMI) medium supplemented with 10% foetal bovine serum (FBS). Cells were incubated in a humidified atmosphere containing 5% CO_2 at 37 °C. Chang liver cells were seeded at a density of 6000 cells/200 µL in 96 well microplates. After 24 h, medium was removed from the cells and replaced with RPMI medium containing each test compound ranging from a concentration of 100 µg/mL to 0.098 µg/ml. Viable cells were determined using the 4,5-dimethylthiazol-2,5-diphenyltetrazolium bromide (MTT) assay.[327] The assay is based on a metabolic reduction of tetrazolium salt by a mitochondrial reductase in living cells. The yellow MTT was reduced to dark purple formazan. The formazan product was extracted from the cells by addition of dimethyl sulfoxide (DMSO). After the various treatments, the medium in all the wells was aspirated, replaced with 100 µl of 0.5 mg/mL MTT, and incubated at 37°C for 1 h, after which the MTT was removed through aspiration. The formazan crystals were solubilized by the addition of 100 µL DMSO and the absorbance measured at 570 nm. All results were analysed using the Graphpad Prism 5 data analysis program.

RESULTS & DISCUSSION

CHAPTER 4 THE DEVELOPMENT OF ANTIMICROBIAL ELECTROSPUN NYLON 6/BIOCIDE NANOFIBER COMPOSITES

4.1 Overview

The chapter will summarize the data for the synthesis and antimicrobial activity studies of 2-substituted *N*-alkylimidazoles and their silver(I) complexes. It will discuss the incorporation of the 2-substitued *N*-alkylimidazoles and the silver(I) complexes into electrospun nylon 6 nanofibers as solid support materials. Furthermore, the evaluation of the antimicrobial properties of the electrosspun nylon 6 nanofibers incorporated with 2-substituted *N*-alkylimidazoles and silver(I) complexes will be discussed. It will conclude by discussing the fabrication of antimicrobial electrospun nylon 6 nanofiber composites, by immobilization (using the graft polymerization technique) of selected 2-substituted vinylimidazoles, and the evaluation of their antimicrobial activity, together with the cytotoxicity experiments.

4.1.1 Synthesis and characterization of 2-substituted *N*-alkylimidazoles

The synthesis of *N*-alkylimidazole-2-carboxaldehydes (**1a-h**) and *N*-alkylimidazole-2-methanols (**2a-h**) was carried out according to previously reported methods.[311-313] Scheme 4.1 illustrates the synthesis steps of the 2-substituted *N*-alkylimidazole derivatives. The first step was the synthesis of *N*-alkylimidazole which was carried out by the reaction of imidazole and alkylbromides in the presence of potassium hydroxide. The second step involved the synthesis of *N*-alkylimidazole-2-carboxaldehydes (**1a-h**) by the acylation of *N*-alkylimidazole. Subsequently, *N*-alkylimidazole-2-methanols (**2a-h**) and *N*-alkylimidazole-2-carboxylic acids (**3a-h**) were obtained by the reduction and oxidation of *N*-alkylimidazole-2-carboxaldehydes (**1a-h**), respectively.

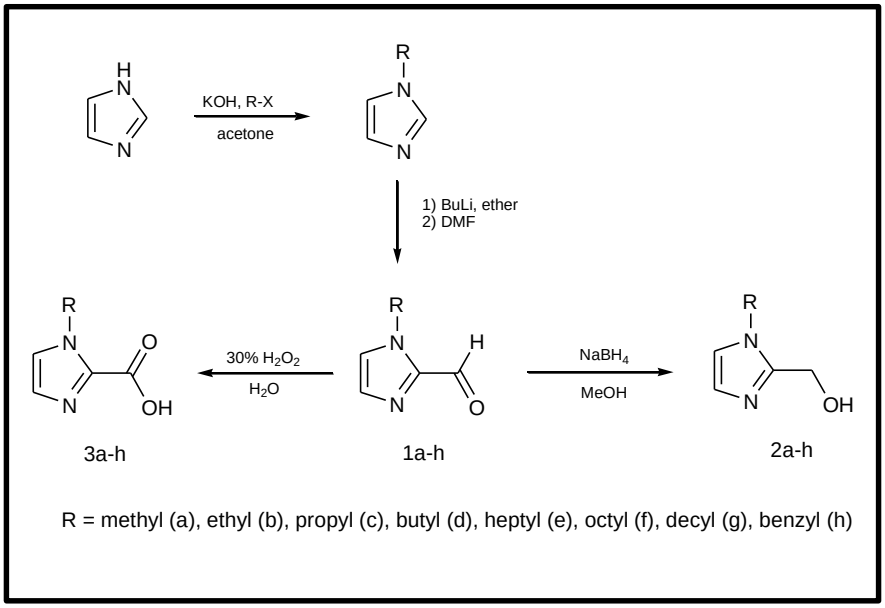

Scheme 4.1. Synthesis of 2-substituted *N*-alkylimidazole derivatives

The characterization of the 2-subtituted *N*-alkylimidazole derivatives was carried out using ^{1}H and ^{13}C NMR, IR and elemental analysis. ^{1}H NMR spectra of **1a-h** showed the appearance of a singlet in the region 9.7-9.9 ppm for one proton indicative of an aldehydic proton (C**H**O). Furthermore, the disappearance of the singlet in the region 7.5-8.0 ppm indicated to the substitution of the imidazole proton at the 2-position (Figure 4.1).^{13}C NMR spectra of **1a-h** showed the appearance of a signal in the region 180-185 ppm indicating the presence of the carbonyl carbon (**C**HO). For **2a-h**, the ^{1}H NMR spectra showed the disappearance of the aldehydic proton singlet, in **1a-h**, and the appearance of a new singlet in the region 4.5-4.7 ppm, indicative of the two methylene protons (C**H**$_2$OH). ^{13}C NMR of **2a-h** exhibited the disappearance of the carbonyl carbon signal and the appearance of a new signal in the region 146-149 ppm for the methylene carbon (**C**H$_2$OH). ^{13}C NMR showed a marked upfield shift of the carbonyl carbon to the region 156-159 ppm for the carboxylic carbon (**C**OOH) compared with the aldehydic carbons in the range 180-185 ppm. The signals for the alkyl group (octyl) were observed in the region 0-2 ppm. Figure 4.2 illustrates the ^{13}C NMR spectra of 2-substituted *N*-decylimidazoles.

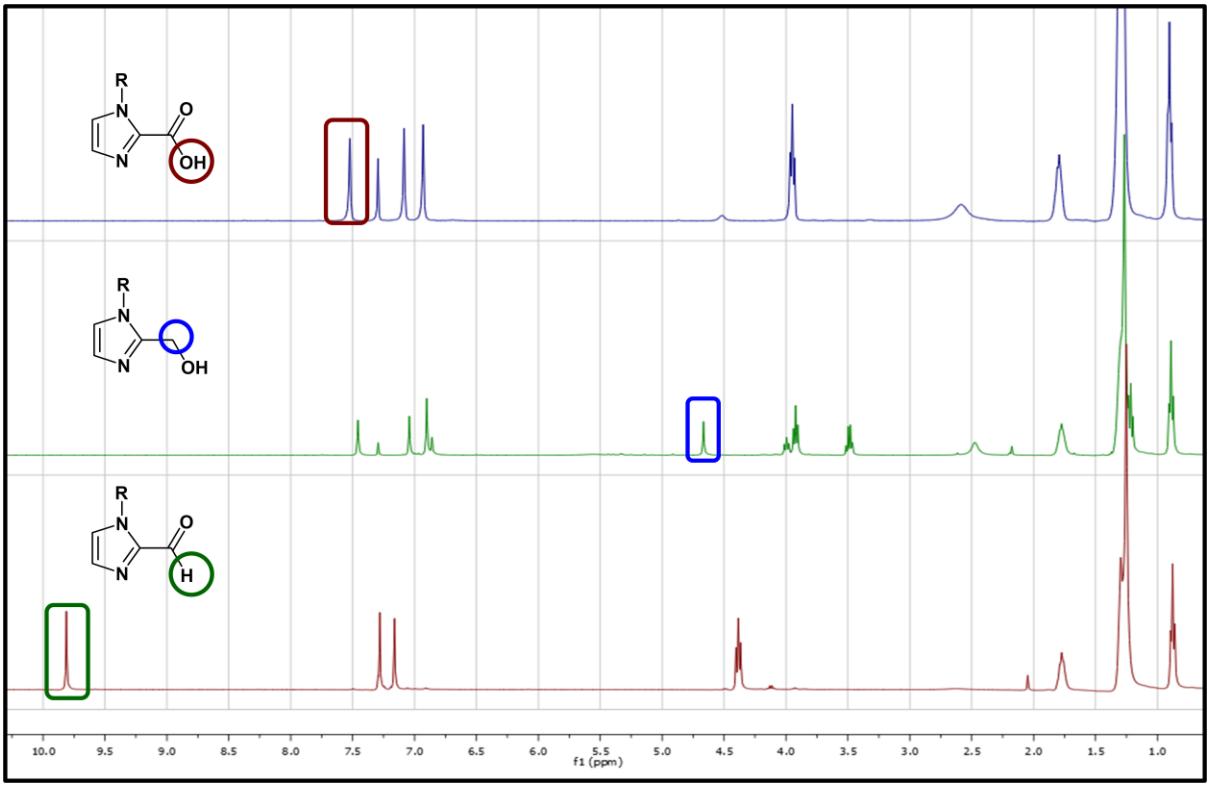

Figure 4.1. ^{1}H NMR spectra of 2-substituted *N*-alkylimidazoles (R = octyl)

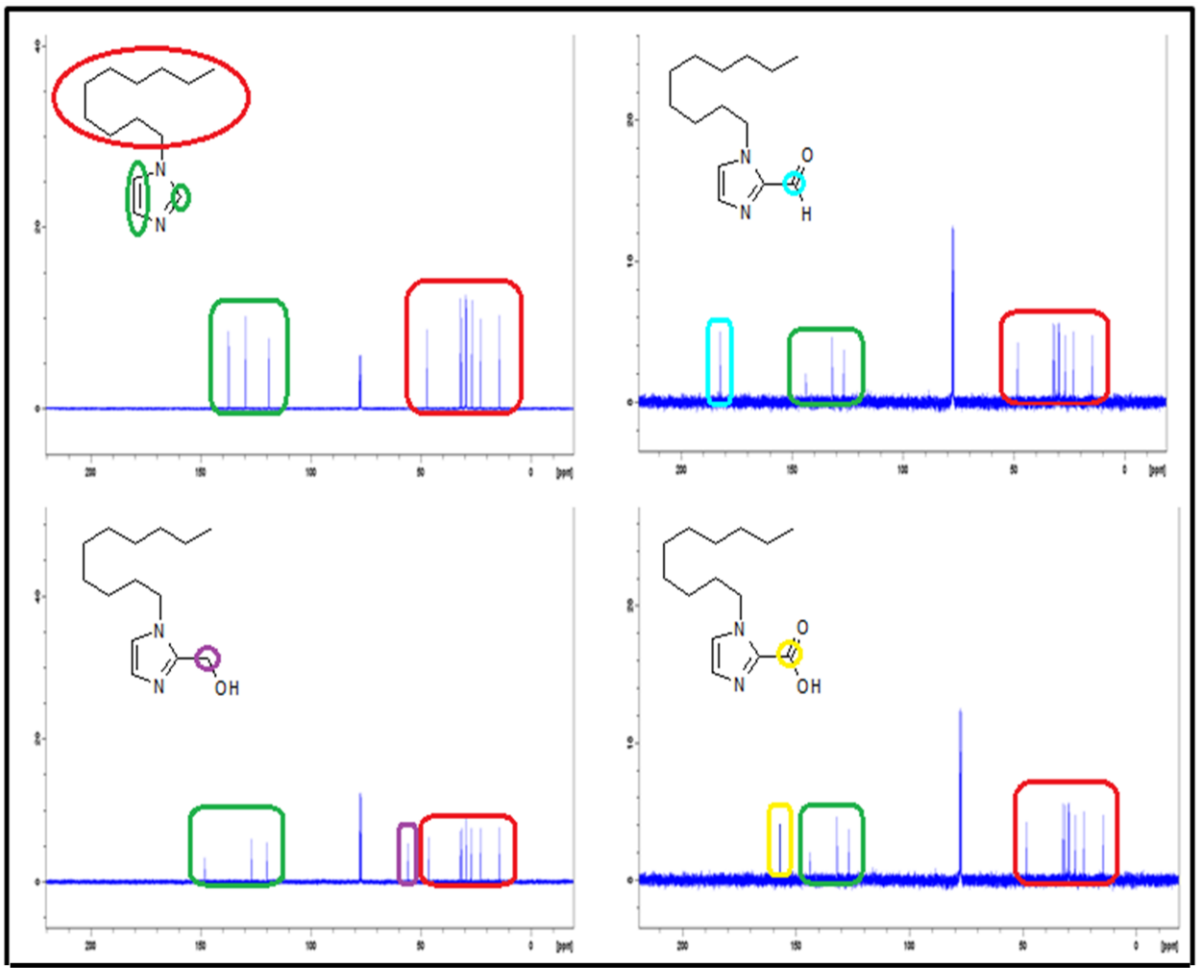

Figure 4.2. The ^{13}C NMR spectra of 2-substituted *N*-decylimidazole

IR spectra showed absorption bands as follows: 1680-1690 cm^{-1} (C=O) confirming the formation of *N*-alkylimidazole-2-aldehydes **1a-h**, 3650-3480 cm^{-1} (OH) which confirmed the formation of *N*-alkylimidazole-2-methanols **2a-h**, and 1639-1673 cm^{-1} (C=O) and 3137-3190 cm^{-1} (OH) which the confirmed the formation *N*-alkylimidazole-2-carboxylic acids **3a-h**. In view of the study, the compounds were a representation of a simple synthetic strategy through which the antimicrobial compounds based on azoles can be prepared. The approach was based on simply tuning the lipophilicity (alkyl chain)/hydrophilicity (2-substituent) balance, compared with current imidazole-based antimicrobial agents which require specific configurations for the substituents.[328] Tuning the lipophilicity of imidazole by increase the alkyl chain length at the 1-position ensures easy diffusion through the membrane of the microorganism while tuning the hydrophilicity by substituting an ionizable group at the 2-position enhances the ionazability in the cytoplasm. In turn, the two parameters enhance the

interaction of the molecule with the cells of the microorganism and subsequently the antimicrobial activity.

4.1.2 Potentiometric studies (protonation constants)

The pK_a values, which may relate to drug solubility, permeability and protein binding,[329] were determined for all the synthesized imidazole compounds. Scheme 4.2 depicts the protonation reaction equilibria for the 2-substituted *N*-alkylimidazole derivatives. The imidazole-nitrogen showed pK_a values of 6.72-7.9 for the *N*-alkylimidazole-2-carboxylic acid derivatives, and similar values of 6.20-6.96 for the *N*-alkylimidazole-2-methanol derivatives (Table 4.1). For the *N*-alkylimidazole-2-carboxaldehyde derivatives, however, the constant shifted to significantly lower values (pK_a = 5.19-5.37) due to the electron withdrawing effect of the aldehyde group. Similarly, the electron withdrawing benzyl substituent decreased the pK_a values for the carboxylic acids, aldehydes and alcohols. The pK_a values for the carboxylic acid group were in the range 1.25-3.38, while for the alcohol group the values fell in the range 9.50-11.49. The pK_a values of compounds **3a** and **2d** were in accordance with literature values.[330] In the current study, compound **3a** displayed pK_a value of 6.75 while the literature pK_a value was 6.88 for the same compound.

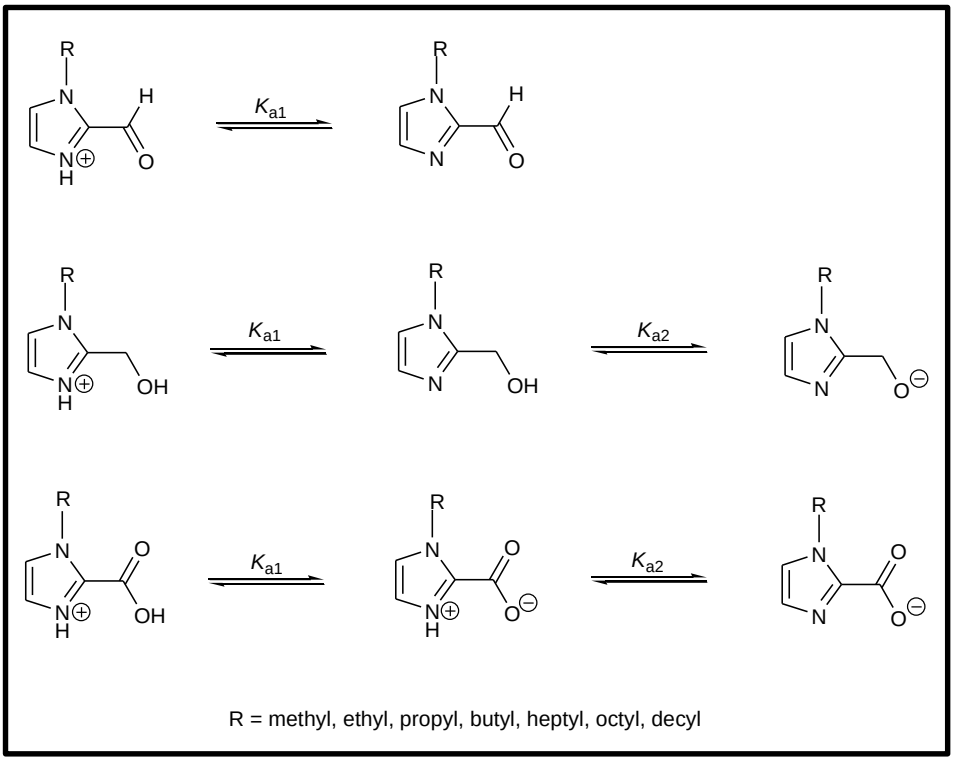

Scheme 4.2. The protonation reaction equilibria for the *N*-alkylimidazole derivatives. The protons are omitted for simplicity

Table 4.1. Protonation constants (pK_a) for 2-substituted *N*-alkylimidazole derivatives determined at 25±0.1°C and I = 0.10 M (TMACl)

Compound	R	pK_{a1}	pK_{a2}
1a	Methyl	5.12(2)	-
1b	Ethyl	5.11(3)	-
1c	Propyl	5.37(4)	-
1d	Butyl	5.32(4)	-
1e	Heptyl	5.36(8)	-
1f	Octyl	5.39(7)	-
1g	Decyl	5.50(3)	-
1h	Benzyl	5.06(9)	-
2a	Methyl	6.61(1)	10.91(3)
2b	Ethyl	6.94(9)	10.49(9)
2c	Propyl	6.92(9)	10.15(8)
2d	Butyl	6.95(6)	10.40(2)
2e	Heptyl	6.96(7)	10.22(7)
2f	Octyl	6.87(7)	11.32(6)
2g	Decyl	6.75(9)	11.49(8)
2h	Benzyl	6.20(5)	9.50(3)
3a	Methyl	1.25(6)	6.75(4)
3b	Ethyl	3.03 (6)	7.08(5)
3c	Propyl	3.00(5)	7.50(5)
3d	Butyl	2.90(1)	7.90(1)
3e	Heptyl	3.10(1)	7.50(1)
3f	Octyl	2.82(6)	7.77(6)
3g	Decyl	3.38(5)	7.68(9)
3h	Benzyl	2.37(6)	6.72(9)

4.1.3 Antimicrobial evaluation

The antimicrobial activity of 2-substituted *N*-alkylimidazoles was evaluated using the disk diffusion and microdilution methods. The disk diffusion method is a qualitative antimicrobial test, that is, it gives an indication about the activity (diameter of the zone of clearance), or lack thereof, of biocides towards a particular microorganism. The diameter of the zone of clearance is linked to the susceptibility of the microorganism and to the diffusion rate of the biocide through the agar medium.[331] The microdilution method is a quantitative method

which gives the minimum inhibitory concentration (MIC), that is, the lowest concentration of the antimicrobial agent required to inhibit the growth of microorganisms.

4.1.3.1 Disk diffusion method

The antimicrobial activity of 2-substituted *N*-alkylimidazole derivatives was tested against *Escherichia coli*, *Bacillus subtilis* subsp. *spizizenii*, *Staphylococcus aureus* and *Candida albicans* using the disk diffusion and microdilution methods. A summary of the antimicrobial activity data appears in Table 4.2. The *N*-alkylimidazole-2-carboxaldehydes (**1e-g**), 2-hydroxymethyl-*N*-alkylimidazoles (**2e-g**) and *N*-alkylimidazole-2-carboxylic acids (**3e-g**) derivatives showed excellent concentration dependent antibacterial activity against the Gram-positive bacteria, as evidenced by the zones of clearance. The activity was also highly dependent on the length of the alkyl chain, a trait previously observed.[67,72] Figure 4.3 illustrates the effect of the alkyl chain length on the antimicrobial activity of the imidazole derivatives.

It could clearly be seen that the activity increased, irrespective of the substituent at the 2-position, as the alkyl chain length increased. The trend can be observed for all the bacterial strains (*S. aureus* and *B. subtilis* subsp. *spizizenii*) that the test compounds were active against. The antimicrobial activity also increased as the pK_a of the 2-substituent decreased because the test compounds were fully ionized at the pH (~7.3) of the culture medium. However, it was also observed that, for *B. subtilis* subsp. *spizizenii*, compounds with the aldehyde substituent exhibited similar activities as those of the compounds with carboxylic acid substituent (Figure 4.3 B). This anomaly could probably be due to the oxidative environment in the *B. subtilis* subsp. *spizizenii* cell; resulting to the oxidation of the carboxaldehyde to carboxylic acid.

At both concentrations (50 and 100 μg), the compounds showed excellent activity against *B. subtilis* subsp. *spizizenii*, with the exception of **3e** which showed little activity (Table 4.2). Substitution of the alkyl chain with a benzyl group (**1h**, **2h**, **3h**) eliminated antibacterial activity completely.

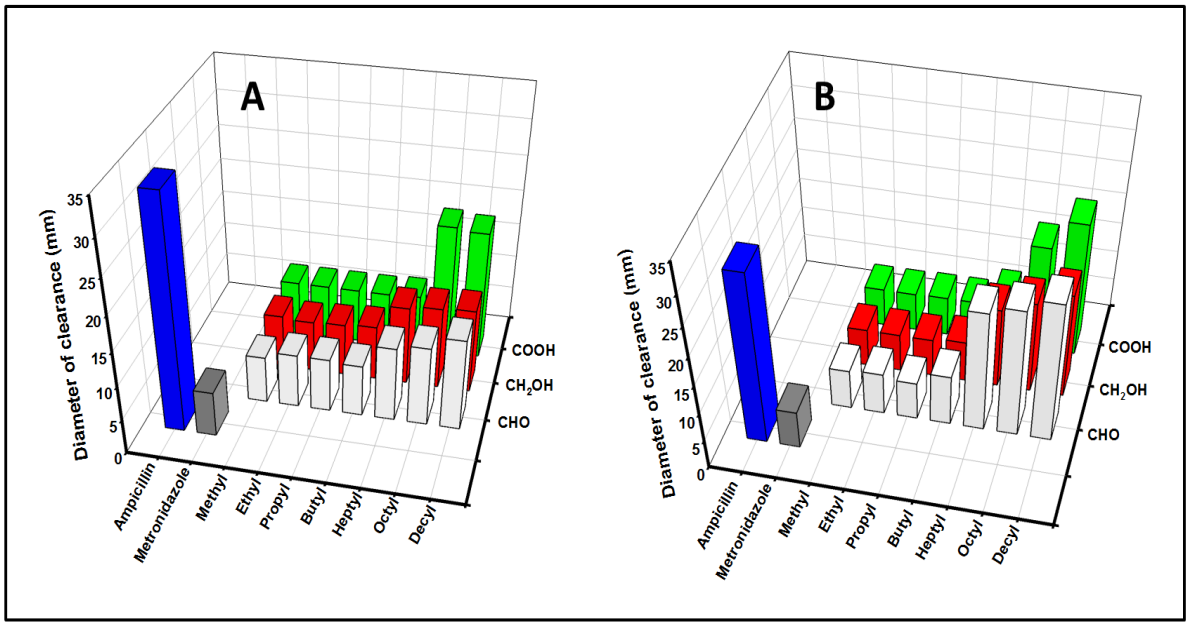

Figure 4.3. The effect of the alkyl chain length on the antimicrobial activity of 2-substituted *N*-alkylimidazole derivatives at 50 µg against *S. aureus* (A) and *B. subtilis*, subsp. *spizizenii* (B), CHO = *N*-alkylimidazole carboxaldehydes, CH_2OH = 2-hydroxymethyl-*N*-alkylimidazole and COOH = *N*-alkylimidazole-2-carboxylic acids.

Generally, imidazole compounds are more active against Gram-positive bacteria,[72] as was the case in the study. The Gram-negative bacteria, *E. coli* proved to be the most resistant of all the bacteria tested. The resistance of *E. coli* has been attributed to it having an outer cell membrane which regulates the contents that enter or leave the cell.[332] Only compound **3g** showed slight activity at 50 µg against *E. coli*, while all the other compounds showed slight activity only at 100 µg. *C. albicans* was also highly resistant towards the compounds tested, with only compounds **1g** and **3g** showing a slight activity at 100 µg.

Table 4.2. Zones of inhibition (mm) of *N*-alkylimidazole derivatives using 50 and 100 µg of compounds, and MIC values

Compound			***E. coli***			***S. aureus***			***B. subtilis* subsp. *Spizizenii***			***C. albicans***	
2-substituent	R	No.	50	100	MIC (µg/mL)	50	100	MIC (µg/mL)	50	100	MIC (µg/mL)	50	100
-CHO	Heptyl	**1e**	6.5(±0)	7.3(±0.3)	>2500	8.7(±0.6)	10.8(±0.3)	40	20.7(±1.2)	23.7(±0.6)	20	6.5(±0)	6.7(±0)
	Octyl	**1f**	6.5(±0)	7.2(±0.3)	>2500	9.7(±0.6)	11.5(±0.5)	10	22.0(±0)	25.7(±0.6)	5	6.5(±0)	8.7(±0.6)
	Decyl	**1g**	6.5(±0)	7.8(±0.3)	>2500	11.7(±0.6)	13.3(±0.6)	5	24.0(±0)	28.0(±0)	5	8.2(±0.3)	10.3(±0.6)
	Benzyl	**1h**	6.5(±0)	6.5(±0)	nd	6.7(±0.6)	8.5(±0.6)	nd	9.3(±0.6)	11.3(±0.6)	nd	6.5(±0)	6.5(±0)
-CH_2OH	Heptyl	**2e**	6.5(±0)	8.7(±0.3)	500	9.3(±0.6)	11.5(±0)	160	13.7(±0.6)	17.3(±1.2)	20	6.5(±0)	6.5(±0)
	Octyl	**2f**	6.5(±0)	9.0(±0)	400	8.7(±0.6)	12.0(±0)	80	15.7(±0.6)	17.7(±0.6)	10	8.3(±0.6)	8.7(±0.6)
	Decyl	**2g**	6.5(±0)	8.3(±0.3)	200	12.7(±0.6)	12.3(±0.6)	10	18.0(±0)	17.3(±0.6)	5	8.3(±0.3)	8.0(±0)
	Benzyl	**2h**	6.5(±0)	6.8(±0.3)	nd	6.7(±0.6)	8.5(±0)	nd	6.5(±0)	6.5(±0)	nd	6.5(±0)	6.5(±0)
-COOH	Heptyl	**3e**	7.3(±0.3)	7.0(±0)	300	8.2(±0.3)	9.0(±0.3)	30	9.0(±0)	8.8(±0.3)	20	6.5(±0)	6.5(±2.6)
	Octyl	**3f**	8.2(±0.3)	8.5(±0.5)	150	11.7(±0.6)	19.2(±0.3)	20	18.0(±0)	23.7(±0.6)	5	6.5(±0)	8.0(±0)
	Decyl	**3g**	9.7(±0.3)	8.0(±0)	400	18.8(±1.2)	22.7(±0.3)	10	22.7(±0)	21.8(±0.3)	5	9.7(±0.6)	10.8(±0.3)
	Benzyl	**3h**	7.8(±0.3)	7.2(±0.3)	nd	8.3(±0)	8.0(±0)	nd	6.8(±0.3)	7.3(±0.6)	nd	6.5(±0)	6.5(±0)
Metronidazole			6.5(±0)	7.3(±0.6)	650	6.5(±0)	8.0(±0.)	300	6.5(±0)	11.3(±1.2)	300		
Ampicillin			29.7(±1.5)	40.0(±2.0)	40	33.3(±1.2)	38.7(±1.2)	>2500	29.3(±1.2)	32.7(±2.3)	5		
Ketoconazole												16.3(±0.6)	17.7(±0.6)

MIC means minimum inhibitory concentration; nd means not determined; 50 and 100 refer to the mass (µg) of compound used

Generally, the active 2-substituted *N*-alkylimidazole derivatives exhibited excellent antibacterial activity compared to metronidazole, a commercial imidazole-containing antibacterial agent, which was used as a negative control in this study. It is well known that metronidazole possesses no activity against the chosen microorganisms but has been used for treatment of protozoan infections such as *Entamoeba hystolica*, *Giardia lamblia* and *Trichomonas vaginalis*.[333] Metronidazole, in this case, was chosen to illustrate how the effects of derivatization of imidazole could impact a wide spectrum antimicrobial activity. Ampicillin, a commercial antimicrobial agent used as a positive control, however showed superior antibacterial activity compared to the 2-substituted *N*-alkylimidazole derivatives.

4.1.3.2 Microdilution method (minimum inhibitory concentration)

The microdilution method displayed a similar trend (alkyl chain dependence and susceptibility of bacteria) to that observed in the disc diffusion method (Figure 4.4). Very low concentrations of **1e-g**, **2e-g** and **3e-g** (5-20 μg/mL) were required for the inhibition of the growth of Gram-positive *B.subtilis* subsp. *spizizenii*. The concentration ranges were better than those reported by Sharma *et al*.[77] for their imidazole derivatives. For example the concentration range for the inhibition of the growth of *B.subtilis* subsp. *spizizenii* was 2-702 μg/mL. As expected, the minimum inhibitory concentrations decreased as the alkyl chain length on imidazole was increased. Higher concentrations of *N*-alkylimidazole-2-carboxaldehydes **1e-g** (>2500 μg/mL) were required to inhibit the growth of *E. coli* (Table 4.2). The 2-hydroxymethyl-*N*-alkylimidazoles **2e-g** (200-500 μg/mL) and *N*-alkylimidazole-2-carboxylic acids **3e-g** (40-300 μg/mL) showed lower minimum inhibitory concentrations against *E. coli*, compared to *N*-alkylimidazole-2-carboxaldehydes **1e-g** (>2500 μg/mL). Since only compounds **1g** and **3g** showed a slight activity (at 100 μg) against *C. albicans*, in the disc diffusion method, the MICs were not determined.

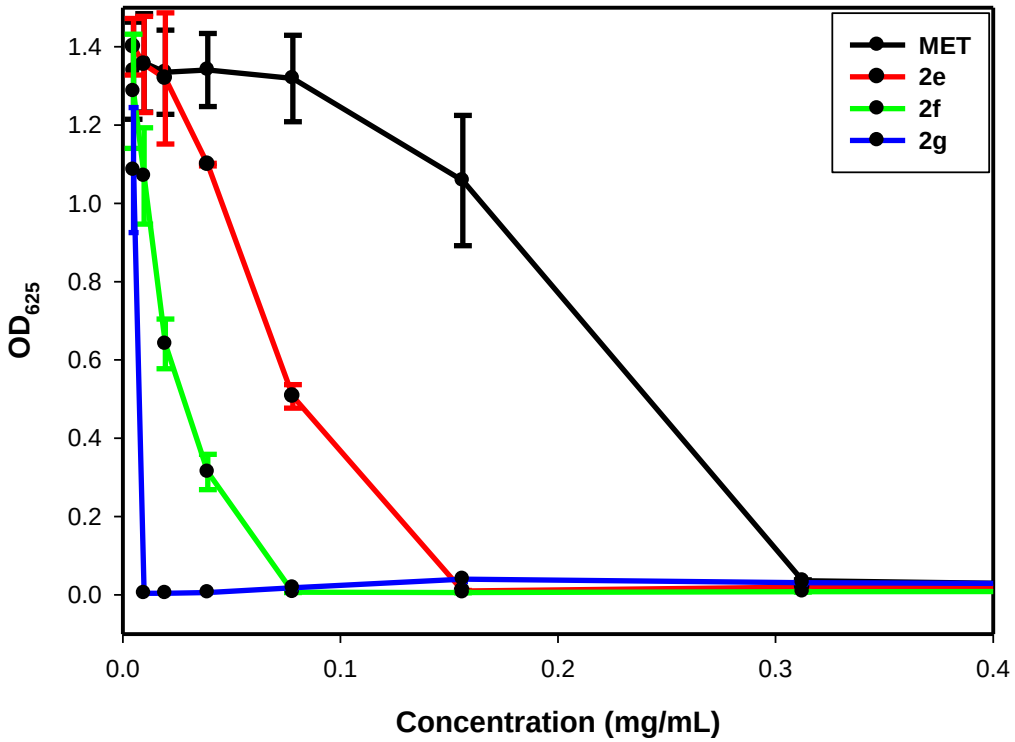

Figure 4.4. MIC profile of 2-hydroxymethyl-*N*-alkylimidazoles for *S. aureus* (alcohols **2e-g**)

In an attempt to establish the effect of the substituents at the 2-position of imidazole on the antimicrobial activity, *N*-alkylimidazole derivatives with the same alkyl chain but different substituent at the 2-position, were grouped together and their MICs compared (Figure 4.5). It was observed that the carboxylic acid derivatives **3e-g** (with lowest pK_{a1} values in the range 1.25-3.38) generally had the greatest activity at least for the octyl and decyl derivatives (Figure 4.5) which was in agreement with the disc diffusion method. The superior activity of the carboxylic acids could be because at the pH (~7.3) conditions of the culture medium the carboxylic acids were fully ionized, which probably allowed for interaction with reactive residues on the surface of the cell membrane. Compounds with longer alkyl chain length and the carboxylic acid substituent exhibited enhanced antimicrobial activity compared to compounds with the same alkyl chain length and the other substituents (carboxaldehydes and alcohols). Compounds with shorter chain length exhibited poor antimicrobial activity, even with the carboxylic acid at the 2-position. It was postulated that increasing the alkyl chain length increased the lipophilicity of the compounds, allowing for easy diffusion through the membrane.

The low pK_a of the carboxylic acid substituent allowed for easy ionizability which enhanced binding to the proteins in the cell membrane. The pK_a dependence of the activity of antimicrobial agents is well documented and, in general, a reduction in the pK_a of the antimicrobial agent enhances its penetration of the microorganism membrane which results in increased activity.[328,334-336] On the other hand, the antimicrobial activities of the aldehyde and alcohol derivatives were comparable to each other and under the pH conditions employed the two derivatives would remain non-ionized.

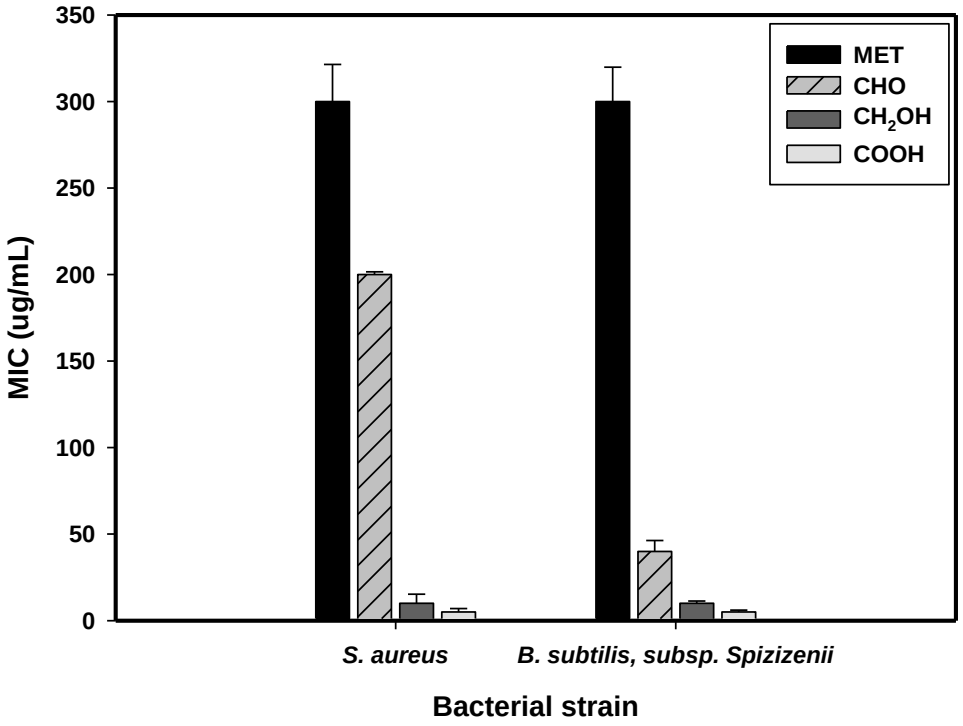

Figure 4.5. The effect of the 2-substituent (pK_a effect) on antimicrobial activity of *N*-alkylimidazole derivatives [*N*-decylimidazole-2-carboxaldehyde (**1g**), *N*-decylimidazole-2-methanol (**2g**) and *N*-decylimidazole-2-carboxylic acid (**3g**)]

In summary, the results clearly showed that a simple *N*-alkylation of imidazoles with long alkyl chains at the 1-position, coupled with derivatization at the 2-position with low pK_a subtituents resulted in an enhanced antimicrobial activity. Therefore, the imidazole derivatives with long alkyl chain length (octyl and decyl) were selected for use in the fabrication of antimicrobial electrospun nylon 6 nanofibers composites.

4.2 The fabrication and antimicrobial activity evaluation of electrospun nylon 6 nanofibers containing 2-substituted *N*-alkylimidazoles

4.2.1 Incorporation of 2-substituted *N*-alkylimidazoles into electrospun nylon 6 nanofibers

The polymer solution for electrospinning was prepared by dissolving nylon 6 and the 2-substituted *N*-alkylimidazole (alkyl = octyl and decyl) in a $HCOOH/CH_3COOH$ (1:1) mixture. Nylon 6 was the polymer of choice because of its biocompatibility, biodegradability, mechanical stability, electrospinnability and insolubility in water.[55-57] The characterization of the electrospun nylon 6 nanofibers was performed using known techniques.

The morphology of the electrospun nylon 6 nanofiber composites was characterized using scanning electron microscopy. SEM micrographs (Figure 4.6) showed that smooth or beadless nanofibers with uniform diameters were obtained under the electrospinning conditions. The diameters ranges of the electrospun nanofibers incorporated with 2-substituted *N*-alkylimidazoles were *N*-octylimidazole-2-carboxaldehyde (39-155 nm), 2-hydroxymethyl-*N*-octylimidazole (59-150 nm) and *N*-octylimidazole-2-carboxylic acid (72-146 nm) using the ImageJ software.

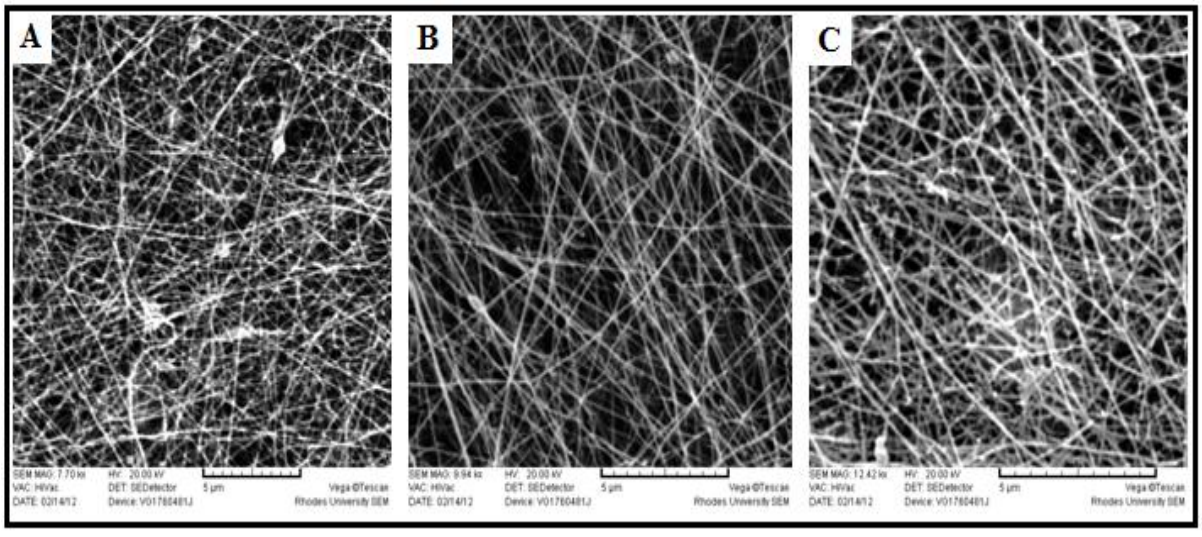

Figure 4.6. Electrospun nanofibers incorporated with, (A): *N*-octylimidazole-2-carboxalehyde (**1g**), (B): 2-hydroxymethyl-*N*-octylimidazole (**2g**) and (C): *N*-octylimidazole-2-carboxylic acid (**3g**)

The electrospun nanofiber composites were also characterized using ATR-FTIR to ascertain the presence of the compounds within the electrospun nanofiber matrix (Figure 4.7). Incorporation of 2-substituted *N*-alkylimidazoles could have easily been done, by idendification of the C=O band for *N*-alkylimidazole-2-carboxaldehydes (~1700 cm^{-1}), the OH band for 2-hydroxymethyl-*N*-alkylimidazoles (3500-3000 cm^{-1}) and C=O and/or OH for the *N*-alkylimidazole-2-carboxylic acids (~1700 and 3500-3000 cm^{-1}, respectively). However, the bands could not be identified; instead, two bands were observed in the region 1200-1000 cm^{-1} and one band in the region 800-650 cm^{-1} in the electrospun nylon 6 nanofiber composite which coincided with bands observed in 2-hydroxymethyl-*N*-octylimidazole (**2f**). The bands were a confirmation that the compound was successfully incorporated into the electrospun nylon 6 nanofibers. The intensities of the bands were however very low; this effect was expected considering the mass of the compounds (5% w/w) used with respect to the mass of polymer (nylon 6). The band intensities associated with incorporated compounds were believed to have been suppressed by those of the polymer. Once incorporation of the 2-substituted *N*-alkylimidazoles had been ascertained, the antimicrobial activity of the electrospun nanofiber composites was evaluated.

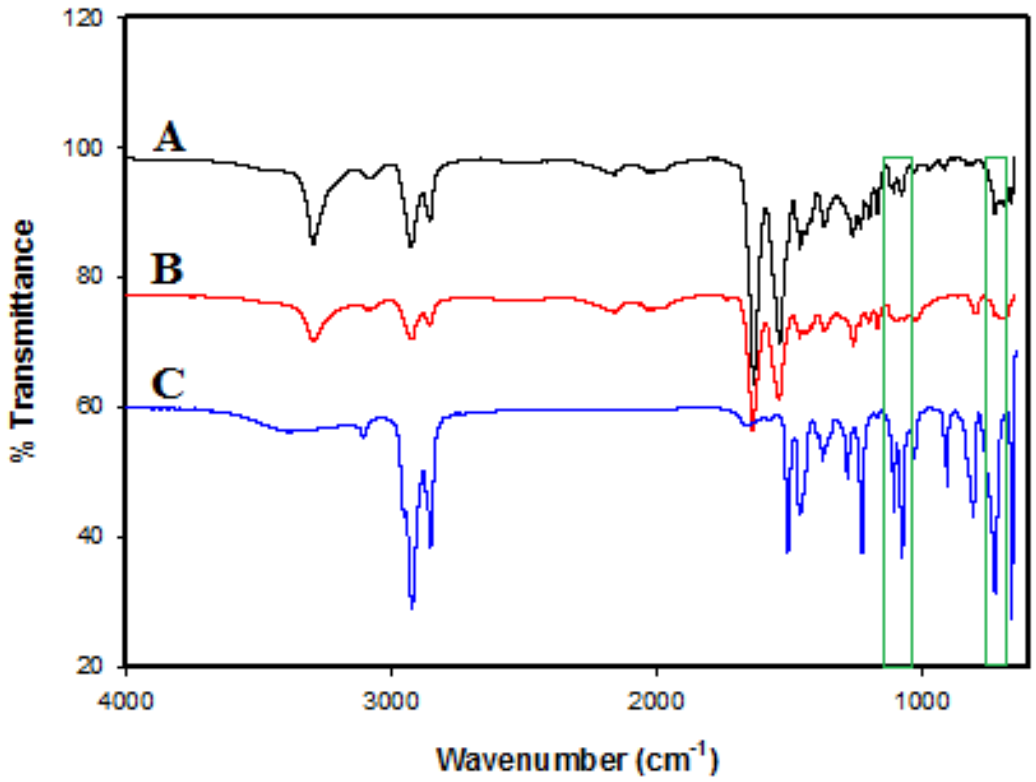

Figure 4.7. ATR-FTIR spectra of (A): nylon 6 nanofiber composite, (B): nylon 6 and (C) 2-hydroxymethyl-*N*-octylimidazole (**2f**)

4.2.2 Antimicrobial activity studies

The antimicrobial activity of electrospun nylon 6 nanofibers incorporated with selected 2-substituted *N*-alkylimidazoles was investigated using the disk diffusion and AATCC Test 100-2004 methods. The AATCC test method 100-2004, like the microdilution method, is quantitative as it illustrates the extent of reduction of microbial growth by a biocide towards a particular microorganism. It is also a method suitable for testing the antimicrobial activity of fabrics containing leachable biocides.[320]

4.2.2.1 Disk diffusion method

Disks (diameter = 7.0 ±0.1 mm) were cut from the electrospun nylon 6 nanofiber composites and used for antimicrobial testing. Disk diffusion results showed that the 2-substituted *N*-alkylimidazoles maintained the antimicrobial properties even when incorporated into polymer

nanofibers as solid support. It was also observed that the antimicrobial activity remained predominantly against Gram-positive bacteria (*S. aureus* and *B. subtilis* subsp. *spizizenii*) with the latter being the most susceptible (Fig. 4.8, Table 4.3).

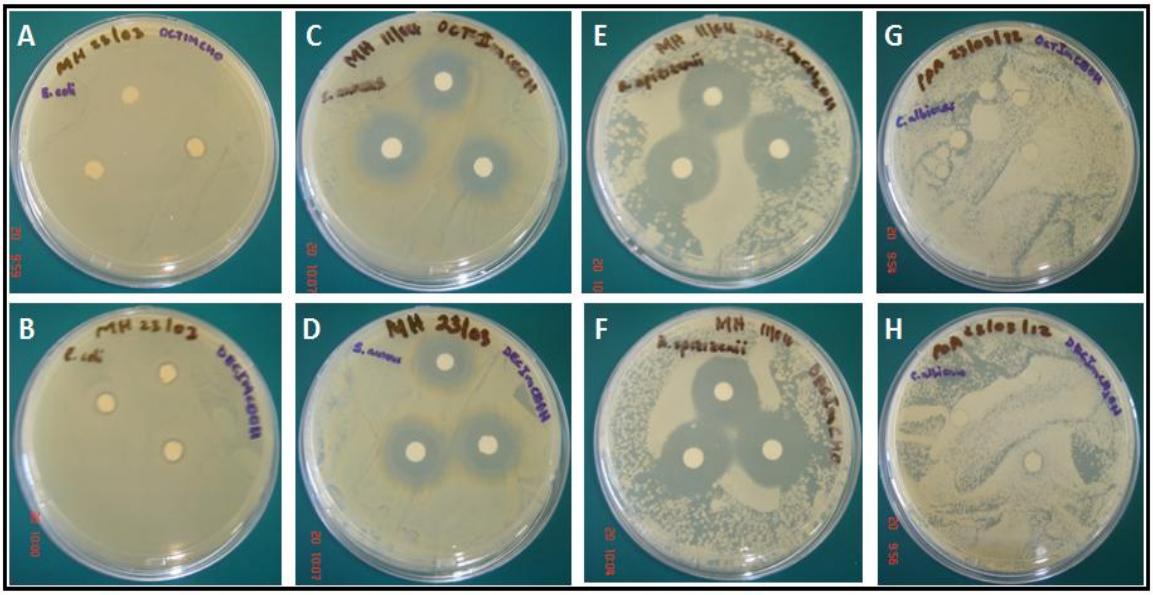

Figure 4.8. Zones of inhibition illustrating antimicrobial activity for electrospun nylon 6 nanofiber composites containing 2-substituted *N*-alkylimidazoles towards *E. coli* (A & B), *S. aureus* (C & D), *B. subtilis subsp, spizizenii* (E & F) and *C. albicans* (G & H)

Table 4.3. Diameters of zones of clearance for the electrospun nylon 6 nanofiber containing 2-substituted *N*-alkylimidazoles

Nanofibers composite	***E. coli***	***S. aureus***	***B. subtilis subsp. spizizenii***	***C. albicans***
	Diameter (mm)	Diameter (mm)	Diameter (mm)	Diameter (mm)
nylon 6 + **1f**	7.2 (±0.3)	12.7 (±0.3)	29.7 (±0.6)	7.0 (±1.0)
nylon 6 + **1g**	7.0 (±0.1)	11.8 (±1.0)	22.7 (±0.6)	7.2 (±0.2)
nylon 6 + **2f**	8.3 (±0.6)	12.8 (±1.2)	22.0 (±1.7)	7.0 (±0.2)
nylon 6 + **2g**	7.7 (±0.6)	12.2 (±1.0)	24.0 (±1.7)	7.1 (±0.1)
nylon 6 + **3f**	7.3 (±0.6)	16.7 (±0.6)	23.3 (±2.3)	7.1 (±0.1)
nylon 6 + **3g**	8.0 (±0.1)	15.7 (±0.8)	28.7 (±0.6)	7.2 (±0.1)

In addition, the electrospun nylon 6 nanofiber composites showed poor antimicrobial activity towards *E. coli* and *C. albicans* as was the case with free 2-substituted *N*-alkylimidazoles. The advantage of using electrospun nanofibers incorporated with biocides was attributed to the interesting capability of controlled release of biocides due to their highly porous nature.[114,257,337,338] Once the antimicrobial activity of the electrospun nylon 6 nanofiber composites was established, the AATCC test method 100, a method suitable for evaluating the antimicrobial properties of treated fabrics, was used to investigate the reduction of microbial growth by the electrospun nanofiber composites.

4.2.2.2 AATCC test method 100

The American Association of Textile Chemists and Colorists (AATCC) Test Method 100-2004[320] was used to investigate the antimicrobial activity of the electrospun nylon 6 nanofibers incorporated with 2-substituted *N*-alkylimidazoles. In the AATCC test method, the antimicrobial activity of electrospun nanofibers was depicted by the percentage reduction of the microbial growth. The percentage reduction of microbial growth was calculated using Eqn 3.2.

The electrospun nanofiber composites were first cut into swatches (diameter = 4.8 ±0.1 cm) and the swatches were used for conducting the experiments. Since disk diffusion results showed that the electrospun nylon 6 nanofiber composites were active against Gram-positive bacteria (*S. aureus* and *B. subtilis* subsp. *spizizenii*), only one strain was chosen for AATCC

experiments. *Staphylococcus aureus* was the easier of the two Gram-positive strains to work with and hence chosen to perform the experiments. The results showed that the percentage reduction of bacterial growth against *S. aureus* ranged between 73.2-99.8% for the 2-substituted *N*-alkylimidazoles, with electrospun nylon 6 nanofibers containing the carboxylic acid derivatives demonstrating the largest growth reduction. Figure 4.9 illustrates the reduction of bacterial growth due to electrospun nylon 6 nanofiber composites in comparison to pristine nylon 6 nanofibers.

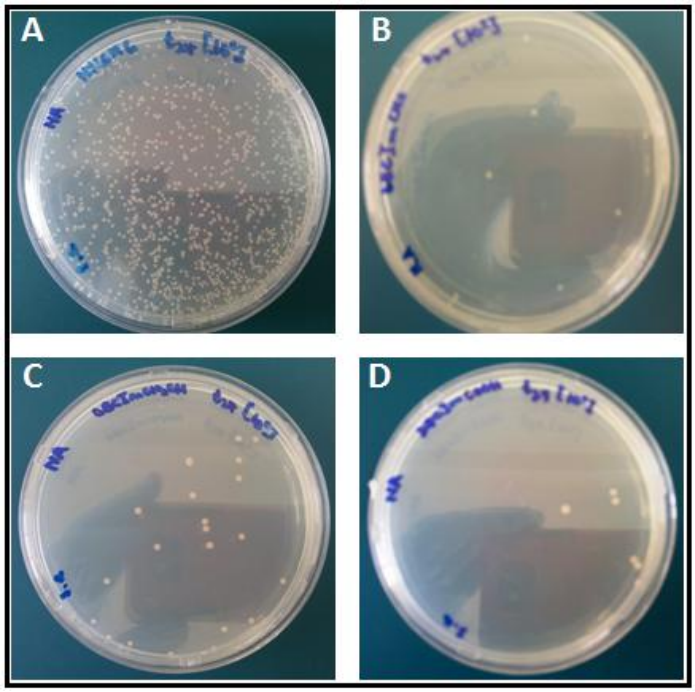

Figure 4.9. Bacterial growth after 24 h contact time with antimicrobial nanofibers. (A) nylon 6 nanofibers; (B) nylon 6 nanofibers incorporated with **1g**; (C) nylon 6 nanofibers incorporated with **2g** and (D) nylon 6 nanofibers incorporated with **3g**

It was demonstrated that incorporating 2-substituted *N*-alkylimidazoles into electrospun nylon 6 nanofibers did not affect their antimicrobial activity. The carboxylic acid derivatives still demonstrated the highest antimicrobial activity. The 2-substituted *N*-alkylimidazoles were then used to synthesize silver(I) complexes, in an attempt to effect broad spectrum antimicrobial properties.

4.3 The fabrication and antimicrobial activity evaluation of nylon 6/silver(I)-(2-hydroxymethyl-*N*-alkylimidazoles) nanofiber composites

4.3.1 Synthesis of silver(I) complexes containing 2-hydroxymethyl-*N*-alkylimidazoles

The initial idea was to synthesize silver(I) complexes using imidazoles containing all the various substituents (-CHO, -CH_2OH and COOH) at the 2-position. However, due to the well known reduction of Ag(I)-Ag(0) by the carbonyl compounds, only the imidazoles with the alcohol substituent could be used for the synthesis. Thus, only silver(I) complexes containing 2-hydroxymethyl-*N*-alkylimidazoles were synthesized and evaluated for their antimicrobial properties.

The silver(I) complexes containing 2-hydroxymethyl-*N*-alkylimidazole ligands were prepared by the reaction of 1 mole equivalent of silver nitrate and 2 mole equivalents of the ligands (Scheme 4.3). IR spectra of the silver(I) complexes showed bands in the 3500-3100 cm^{-1} region depicting the presence of –OH functional groups. This also indicated that the –OH groups were not participating in the coordination to the metal centre. The vibrational bands of imidazole at 1450-1300 cm^{-1} appeared slightly shifted to lower frequencies in the complexes compared to the free ligands and also appeared to exhibit a marked broadening. The two phenomena indicated to coordination of the ligands through the C=N nitrogen atoms of imidazoles.[339]

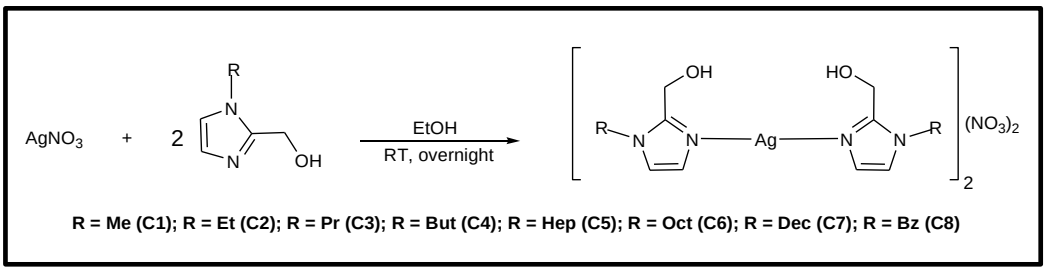

Scheme 4.3. Synthesis scheme of silver(I) complexes containing 2-hydromethyl-*N*-alkylimidazole ligands

4.3.2 X-ray crystallography

X-ray crystal structures of complexes **C2** and **C8** were obtained from single crystals which were grown by the addition of ethyl acetate to their mother liquors, followed by slow evaporation of the solvent mixture. Table 4.4 shows the crystallographic and structure

refinement data for complexes **C2** and **C8**. The crystal structure of **C2** (Figure 4.10) revealed a dimeric complex $[Ag_2(L)_4](NO_3)_2$ where an Ag-Ag bond was formed, as well as a monomeric $[Ag(L)_2]NO_3$ complex (L = 2-hydroxymethyl-*N*-ethylimidazole), while C**8** (Figure 4.11) showed only a dimeric $[Ag_2(L)_4](NO_3)_2$ complex (L = 2-hydroxymethyl-*N*-benzylimidazole). The Ag(1)-Ag(1) bond distances for the dimeric complexes **C2** and **C8** were 3.1749(3) and 3.2009(3) Å, respectively (Table 4.5). The metal-metal interactions were due to the presence of π-π interactions between the imidazoles,[97] and the distances between the imidazole rings were ~3.6 and ~3.4 Å for complexes **C2** and **C8** respectively. The Ag-Ag bond distances were similar to those previously reported by others.[92,97,340,341] The dimeric unit of complex **C2** had N(1)-Ag(1)-N(3) bond angle of 170.27(6)° and the monomeric unit had N(5)-Ag(2)-N(5) bond angle of 161.17(9)°. Complex **C8** had N(5)-Ag(2)-N(5) bond angle of 173.91(6)°. The bond angles indicated that in both complexes, Ag(I) was linearly coordinated to the C=N nitrogens of imidazoles.[340] The bond angles were slightly distorted probably due to the imidazoles being slightly out of plane.[341] The dihedral angles between the imidazoles in the monomeric and the dimeric unit of **C2** were 76.64 and 8.54°, respectively. For **C8** the interplanar angle between the imidazoles was 8.21°. The Ag-N bond distances (~2.1 Å) for both complexes were similar to those previously reported in the literature.[97,102,340] There appeared to be some long range interaction between the nitrate ions and the metal centre in the dimeric units. The Ag-O bond distances were 2.884 and 2.720 Å for **C2** and **C8**, respectively. The other two oxygen atoms of the nitrate ions were involved in H-bonding with the hydroxyl groups in both complexes (Figure 4.11).

Table 4.4. Crystallographic data and structure refinement for **C2** and **C8**

Compound	**C2**	**C8**
Empirical formula	$C_{36}H_{60}Ag_3N_{15}O_{15}$	$C_{22}H_{24}AgN_5O_5$
Formula weight	1266.60	546.33
Temperature (K)	173(2)	173(2)
Wavelength (Å)	0.71073	0.71073
Crystal system	Monoclinic	Triclinic
Space group	*C2/c*	*P*-1
a (Å)	36.6084(6)	9.9792(2)
b (Å)	8.95010(10)	10.0353(2)
c (Å)	16.2218(2)	13.1525(2)
α (°)	90	70.2900(10)
β (°)	114.7500(10)	86.8700(10)
γ (°)	90	62.9010(10)
Volume ($Å^3$)	4826.83(11)	1096.12(4)
Z	4	2
Density (Mg/cm^3)	1.743	1.655
Absorption coefficient (mm^{-1})	1.286	0.965
F(000)	2568	556
Crystal size (mm^3)	0.30 x 0.16 x 0.14	0.40 x 0.27 x 0.11
Theta range data for collection (°)	2.36-28.00	1.66-28.00
Reflections collected	45274	36626
Independent reflections	5830 [R(int) = 0.0449]	5288 [R(int) = 0.0501]
Completeness of theta = 28.00°	99.9%	100%
Max. and min. transmission	0.8604 and 0.7312	0.9058 and 0.7491
Data / restraints / parameters	5830 / 0 / 319	5288 / 1 / 305
Goodness-of-fit on F^2	1.058	1.105
R1, wR2 [I>2σ(I)]	0.0251, 0.0602	0.0279, 0.0673
R1, wR2 (all data)	0.0318, 0.0626	0.0323, 0.0692

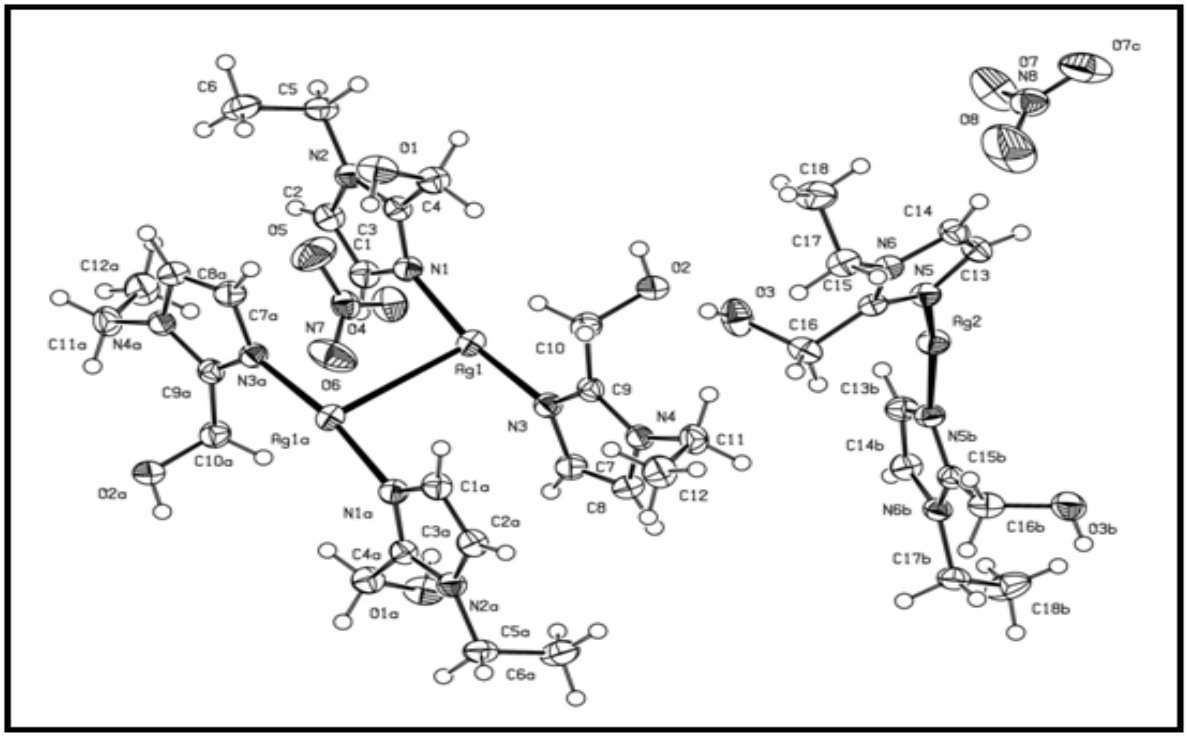

Figure 4.10. ORTEP diagram of C2 showing the atom labelling scheme. Displacement ellipsoids are drawn at the 50% probability level

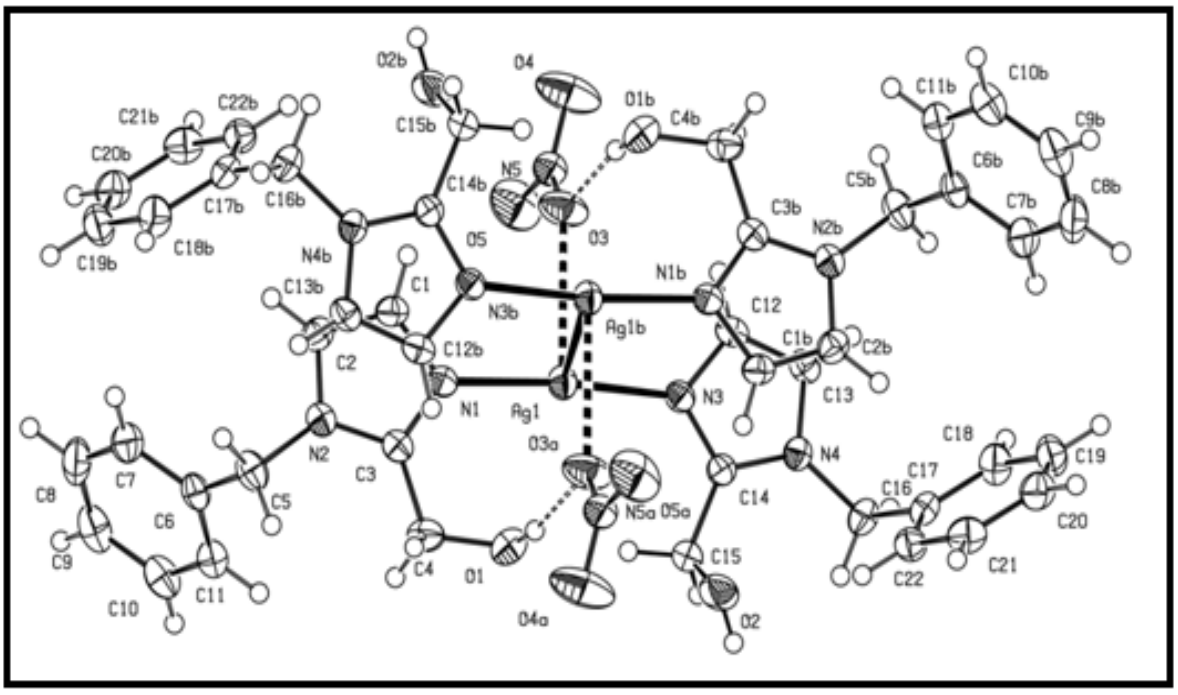

Figure 4.11. ORTEP diagram of C8 showing the atom labelling scheme, long range interaction of the nitrates with the metal centers, as well as hydrogen bonding of the ligand hydroxyl groups with the nitrates. Displacement ellipsoids are drawn at the 50% probability level

Table 4.5. Selected bond lengths (Å) and angles (°) for **C2** and **C8**

C2		**C8**	
Bond lengths			
Ag(1)-Ag(1)#2	3.1749(3)	Ag(1)-Ag(1)#1	3.2009(3)
N(1)-Ag(1)	2.0973(17)	N(1)-Ag(1)	2.1145(16)
N(3)-Ag(1)	2.1063(16)	N(3)-Ag(1)	2.1108(16)
N(5)-Ag(2)	2.1238(15)	C(3)-N(1)	1.328(2)
C(3)-N(1)	1.330(2)	C(3)-N(2)	1.352(3)
C(3)-N(2)	1.349(2)	C(14)-N(3)	1.334(3)
C(9)-N(3)	1.328(2)	C(14)-N(4)	1.347(3)
C(9)-N(4)	1.343(2)		
C(15)-N(5)	1.328(2)		
C(15)-N(6)	1.348(2)		
Bond angles			
N(1)-Ag(1)-N(3)	170.27(6)	N(1)-Ag(1)-N(3)	173.91(6)
N(5)-Ag(2)-N(5)	161.17(9)		

Symmetry transformations used to generate equivalent atoms: **C2**: #1 -x+1,y,-z+1/2 #2 -x+1/2,-y+3/2,-z+1 #3 -x+1,y,-z+3/2; **C8**: #1 -x+1,-y,-z+2

4.3.3 Antimicrobial activity evaluation

4.3.3.1 Disk diffusion method

The antimicrobial activity of the silver(I) complexes was investigated against *E. coli*, *S. aureus*, *B. subtilis* subsp. s*pizizenii* and *C. albicans*. A summary of the results for the *in vitro* antimicrobial activity experiments is presented in Table 4.6. The Ag(I) complexes containing 2-hydroxymethyl-*N*-alkylimidazole ligands displayed antimicrobial activity against a broad spectrum of microorganisms (Fig. 4.12, Table 4.6). The antimicrobial activity against *E. coli* and *C. albicans* was entirely due to Ag(I) for all the complexes (**C1**-**C8**) since the free 2-substituted *N*-alkylimidazoles did not display any activity against the two microorganisms.

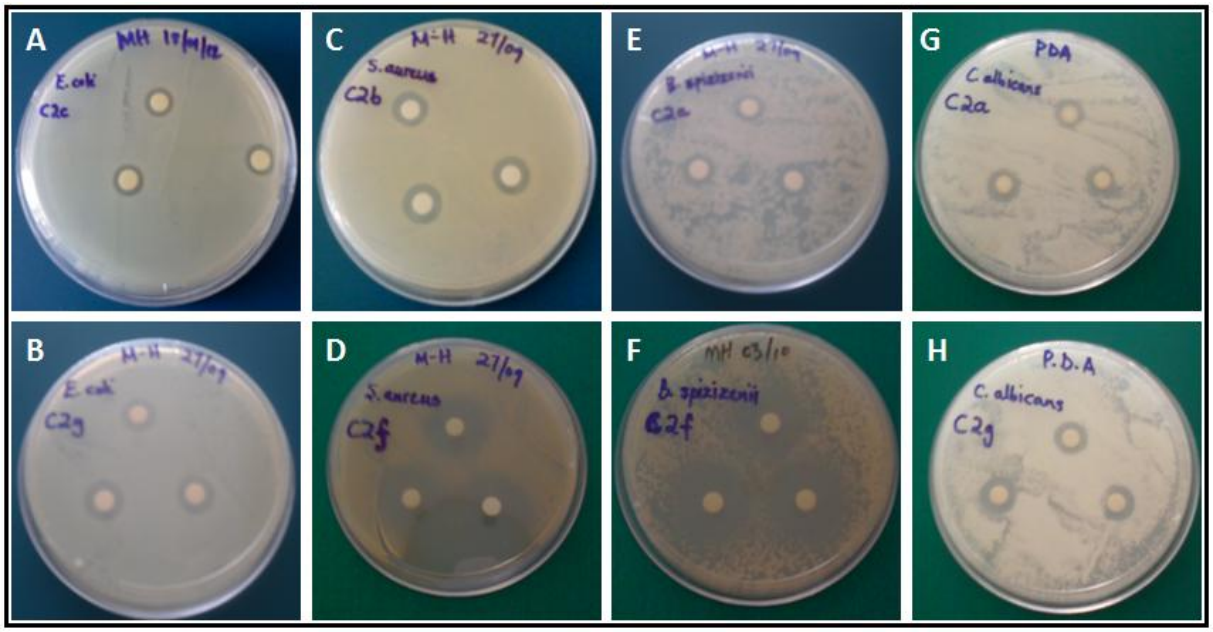

Figure 4.12. Zones of clearance for antimicrobial activity of silver(I) complexes against *E. coli* (A & B), *S.aureus* (C & D), *B. subtilis* subsp, *spizizenii* (E & F) and *C. albicans* (G & H)

It was shown, in **4.1.3**, that the metal-free 2-hydroxymethyl-*N*-alkylimidazoles exhibited poor activity against *E. coli* and *C. albicans*. It was also shown that only metal-free ligands with long alkyl chain length displayed excellent activity against *S. aureus* and *B.subtilis* subsp. *spizizenii*. Therefore, it was anticipated that the Ag(I) complexes containing 2-hydromethyl-*N*-alkylimidazole ligands (**C5**-**C8**) would display better activity than $AgNO_3$ (Table 4.6) because the antimicrobial activity of the complexes **C5**-**C8** should be impacted by both Ag(I) and the ligands. It was observed that against *E. coli* the antimicrobial activity of the silver(I) complexes was comparable with that of $AgNO_3$. However, silver(I) complexes displayed better antimicrobial activity against *S. aureus* and *B. subtilis* subsp. *spizizenii* compared $AgNO_3$.

There have been reports showing that the Ag(I) complexes were better antifungal than antibacterial agents.[92,340] Other reports have shown that the Ag(I) complexes possess antimicrobial activity predominantly against Gram-negative than Gram-positive bacteria[90] or vice versa.[95] In the current study, it was observed that the silver(I) complexes possessed better antibacterial than antifungal properties and the antibacterial activity was predominantly against Gram-positive bacteria. Furthermore, the predominance of activity towards a particular microorganism was dependent on the alkyl chain length of the ligand. The

minimum concentration (MIC) required for the silver(I) complexes to inhibit microbial growth was also determined using the microdilution method.

4.3.3.2 Microdilution method

The microdilution results (Table 4.6) showed that for complexes containing ligands with shorter alkyl chain length (**C1**-**C4**), the activity was in the order *E. coli* (MIC = 20 μg/mL), *B. subtilis* subsp. *spizizenii* (MIC = 40 μg/mL), *S. aureus* and *C. albicans* (MIC = 80 μg/mL). Since the antimicrobial activity of silver(I) complexes containing imidazoles with short alkyl chains was entirely due to the silver(I) ions; the result is consistent with literature that silver(I) ions were predominantly active against Gram-negative bacteria. For complexes containing longer alkyl chain length (**C5**-**C7**), the activity order was *B. subtilis* subsp. *spizizenii* (MIC =5 μg/mL), *E. coli* (MIC =10 μg/mL), *S. aureus* (MIC = 20 μg/mL) and *C. albicans* (MIC = 40 μg/mL).

In summary, it has been shown that the antimicrobial activity of silver(I) complexes containing imidazoles with long alkyl chain length was due to both the silver(I) ions and the 2-hydroxymethyl-*N*-alkylimidazoles. Therefore, the silver(I) complexes **C6** (L = 2-hydromethyl-*N*-octylimidazole)and **C7** (L = 2-hydroxymethyl-*N*-decylimidazole) were selected for the fabrication of antimicrobial electrospun nylon 6 nanofiber composites.

Table 4.6. Zones of clearance and MICs for the silver(I) complexes containing 2-hydroxymethyl-*N*-alkylimidazoles (**C1-C8**)

Complex	**R**	***E. coli***		***S. aureus***		***B. subtilis* subps. *spizizenii***		***C. albicans***	
		Diameter (mm)	MIC (μg/mL)	Diameter (mm)	MIC (μg/mL)	Diameter (mm)	MIC (μg/mL)	Diameter (mm)	MIC (μg/mL)
C1	Methyl	13.0(±0.1)	20	12.0(±0.3)	80	11.0(±0.2)	40	11.0(±0.1)	80
C2	Ethyl	12.3(±0.6)	20	12.0(±0.2)	80	11.3(±0.6)	40	11.3(±0.6)	80
C3	Propyl	10.0(±0,3)	20	11.0(±0.2)	80	10.5(±0.3)	40	10.7(±0.1)	80
C4	Butyl	10.2(±0.3)	20	11.5(±0.1)	80	11.3(±0.6)	40	11.5(±0.6)	80
C5	Heptyl	12.0(±0.1)	10	12.2(±0.3)	40	17.3(±0.6)	20	12.0(±0.2)	40
C6	Octyl	13.7(±0.6)	5	19.7(±0.6)	20	18.0(±0.2)	5	12.3(±0.6)	40
C7	Decyl	12.0(±0.1)	10	18.0(±0.2)	20	16.3(±0.3)	5	12.7(±0.6)	40
C8	Benzyl	11.0(±0.1)	40	12.0(±0.3)	80	11.0(±0.1)	80	10.3(±0.6)	40
$AgNO_3$		12.7(±0.6)	10	12.0(±0.2)	20	11.0(±0.1)	10	14.0(±0)	20

MIC means minimum inhibitory concentration

Disk diameter = 7.0 ± 0.1 mm

4.4 The fabrication of antimicrobial electrospun nylon 6 nanofibers incorporated with silver(I) complexes and silver nanoparticles

Electrospun nylon 6 nanofibers incorporated with Ag(I) complexes containing 2-hydroxymethyl-*N*-alkylimidazoles (**C6** and **C7**) were fabricated using the optimized conditions as described in **3.5.1**. The morphology of the electrospun nylon 6 nanofibers was characterized using scanning electron microscopy (Fig. 4.13) while the presence of the Ag(I) complexes after electrospinning was ascertained using ATR-FTIR spectroscopy (Fig. 4.14).

SEM micrographs revealed that the nanofibers obtained had uniform diameters with A (52-141 nm) and B (74-187 nm) using the ImageJ software. Ascertaining the incorporation of the silver(I) complexes into the electrospun nylon 6 nanofibers should have easily been done, from the ATR-FTIR spectra, by identifying two bands. One band was the vibrational frequency of the hydroxyl group (-OH) in the region 3500-3000 cm^{-1} and the other one was the broad imidazole band due coordination with the silver(I) ions (1450-1300 cm^{-1}).

However, it was very difficult to identify bands belonging to the silver(I) complexes used for the fabrication of the antimicrobial nylon 6 nanofibers. The challenge was attributed to the suppression of the bands belonging to the silver(I) complexes due to the relative mass (5% w/w) of the compounds that was incorporated into the nanofibers. Nonetheless, a low intensity band could be identified in the region 1000-1200 cm^{-1} which corresponded to a band from the spectrum of the compound used (Fig. 4.14). The band was taken as a confirmation that the silver(I) complexes were successfully incorporated into the electrospun nylon 6 nanofibers.

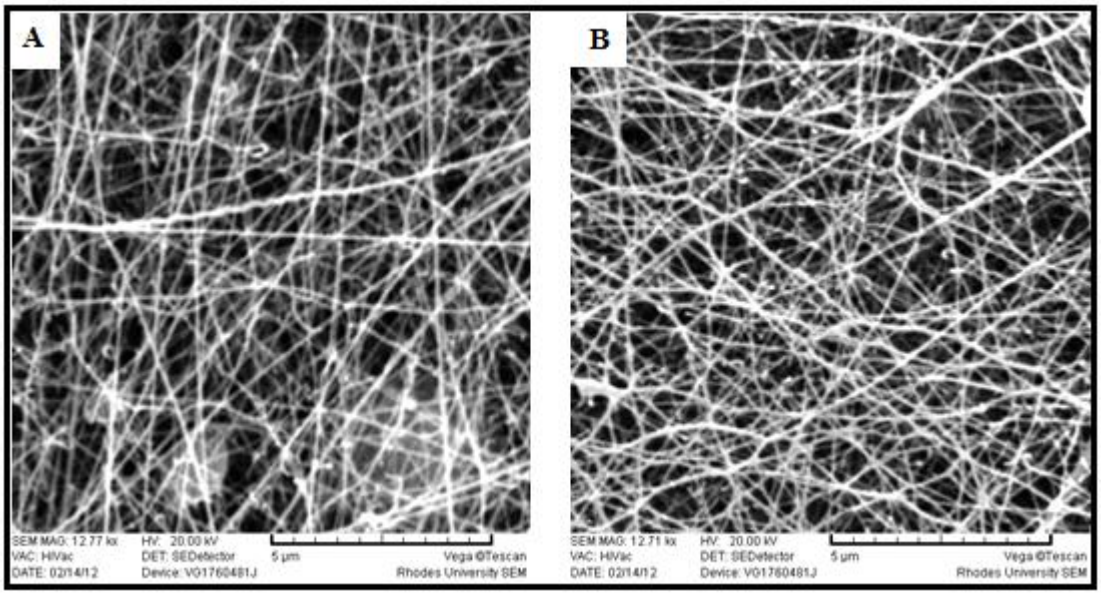

Figure 4.13. SEM micrographs of electrospun nylon 6 nanofibers incorporated with silver(I)-imidazole complex; (A) nylon 6/complex **C6** nanofiber and nylon 6/complex **C7** nanofiber

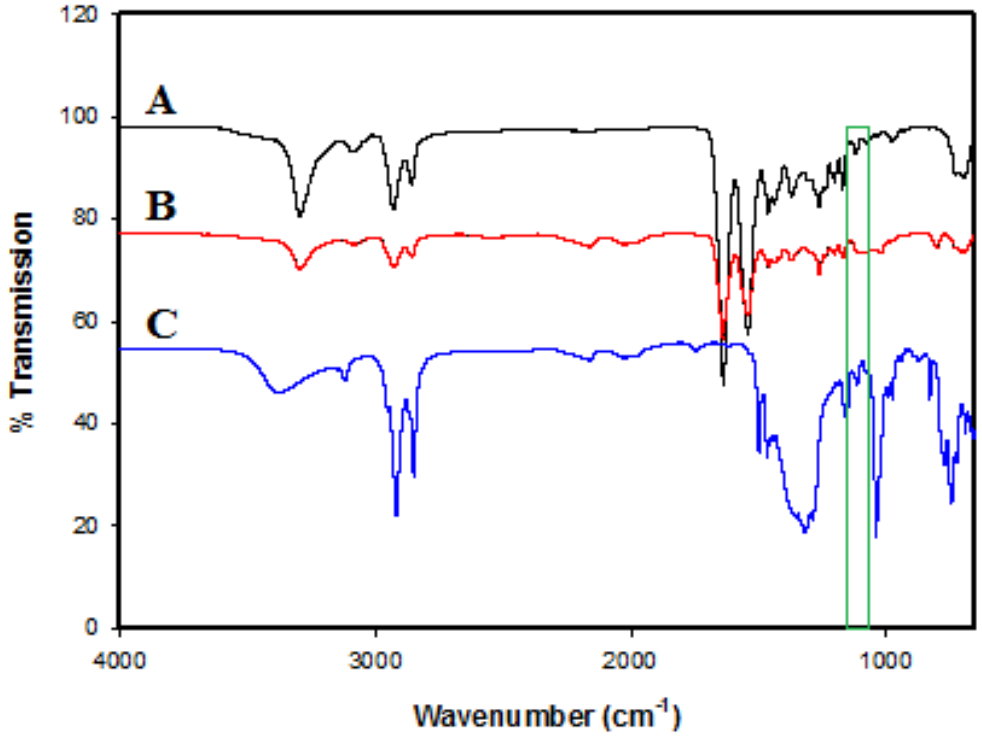

Figure 4.14. ATR-FTIR spectra of (A) nylon 6; (B) silver(I)-imidazole complex (**C7**) and (C) nanofiber composite

Electrospun nylon 6 nanofibers incorporated with AgNPs were also fabricated for comparison with antimicrobial activity of electrospun nanofibers incorporated with silver(I)

complexes. The silver nanoparticles were prepared by *in situ* reduction of $AgNO_3$ in nylon 6 solution without the addition of a reducing agent.[50] Formic acid, one of the solvents used for dissolution of nylon 6, is known to be capable of reducing Ag(I)-Ag(0). Figure 4.15 presents a UV spectrum of AgNPs in nylon 6 solution before electrospinning. The UV spectrum indicated that the AgNPs experienced a sharp surface plasmon resonance at 410 nm; indicative of spherically-shaped nanoparticles with a narrow size distribution.[342] Transmission electron microscopy could have been used to further confirm the presence of the AgNPs within the electrospun nylon 6 nanofibers as well as their shape and size distribution. However, due to sample preparation challenges pertaining to the lack of availability of a proper sample holder for electrospun nanofibers, TEM micrographs could not be obtained.

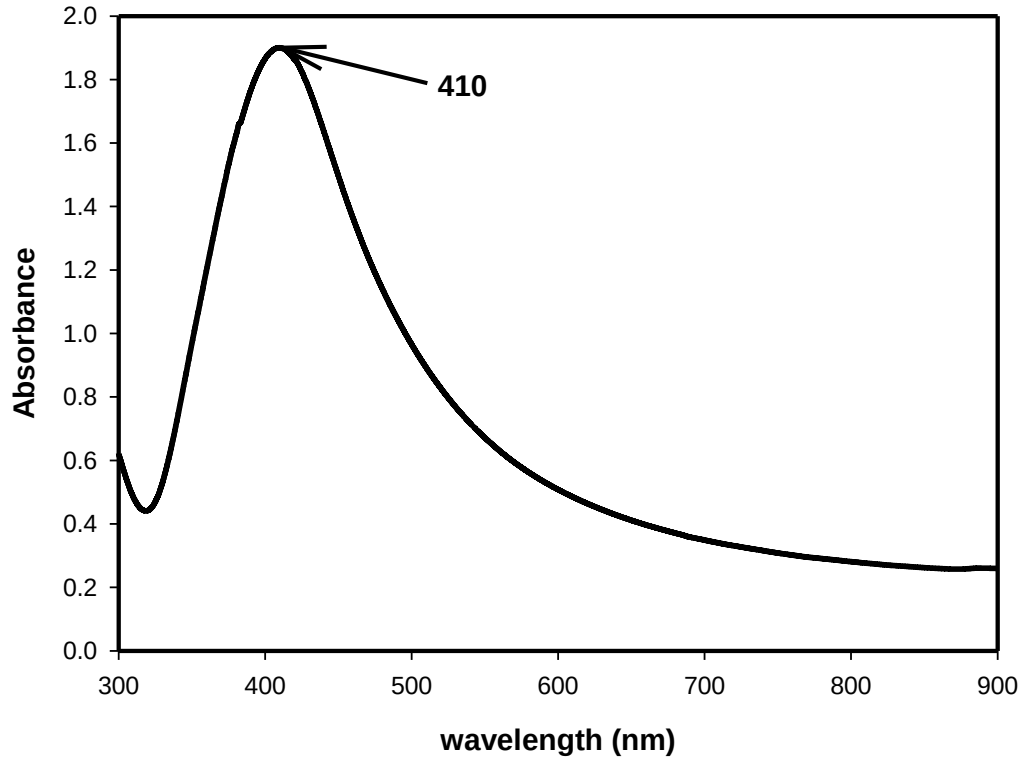

Figure 4.15. UV spectrum of AgNPs in nylon 6 solution

The incorporation of the AgNPs into electrospun nylon 6 nanofibers was also confirmed using SEM-EDS. Figure 4.16 depicts an SEM-EDS histogram which illustrated the presence of electrospun nylon 6 nanofibers. The relative intensities of the silver signals were lower

compared to the intensities of the elements for nylon 6 due to the mass of $AgNO_3$ (5% w/w) used for the fabrication of electrospun nanofiber composites.

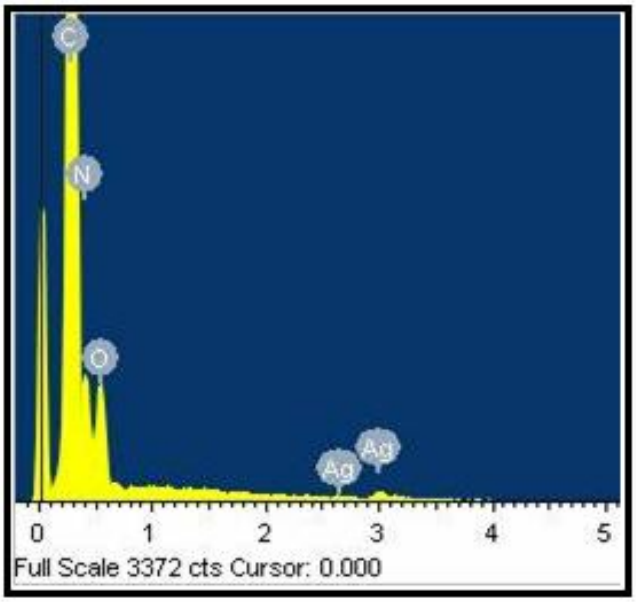

Figure 4.16. SEM-EDS histogram of electrospun nylon 6 nanofibers incorporated with AgNPs

4.4.1 Antimicrobial activity evaluation

The antimicrobial activity of electrospun nylon 6 nanofibers incorporated with selected Ag(I) complexes containing 2-hydroxymethyl-*N*-alkylimidazoles (**C6** and **C7**) with long chains was investigated using the disk diffusion and AATCC Test 100 methods. The AATCC Test method 100 is suitable for evaluating the antimicrobial activity of fabrics or textile materials with leachable antimicrobial agents.

4.4.1.1 Disk diffusion method

The disk diffusion method showed that the silver(I) complexes maintained their broad spectrum antimicrobial properties after being incorporated into electrospun nylon 6 nanofibers as solid support (Table 4.7). The electrospun nylon 6 nanofiber composites remained predominantly active against Gram-positive bacteria (*S. aureus* and *B. subtilis* subsp. *spizizenii*). The antimicrobial activity of the electrospun nylon 6 nanofibers incorporated with silver(I) complexes was compared with that of electrospun nylon 6 nanofibers incorporated with silver nanoparticles (AgNPs).

Table 4.7. Diameters of the zones of clearance for the electrospun nylon 6 nanofibers incorporated with Ag(I) complexes (**C6** & **C7**)

Nanofiber composite	***E. coli***	***S. aureus***	***B. subtilis subsp. spizizenii***	***C. albicans***
	Diameter (mm)	Diameter (mm)	Diameter (mm)	Diameter (mm)
Nylon 6 + **C6**	13.3 (±0.6)	22.3 (±0.6)	24.3 (±1.5)	13.3 (±0.6)
Nylon 6 + **C7**	10.7 (±0.6)	15.7 (±0.6)	16.7 (±0.6)	12.7 (±0.6)
Nylon 6 + AgNPs	9.7 (±0.6)	12.0 (±0)	11.0 (±0)	7.2 (±0.3)

The electrospun nylon 6 nanofibers incorporated with AgNPs exhibited poor antimicrobial activity in comparison to the electrospun nylon 6 nanofibers incorporated with silver(I) complexes (Table 4.7). The observation was, however, not surprising since silver(0) does not have antimicrobial activity unless it is oxidized to silver(I) by moisture.[85] The poor antimicrobial activity of the nanoparticles suggested that there was not sufficient moisture to oxidize Ag(0)-Ag(I) in the culture medium. Further evaluation of the antimicrobial activity of electrospun nylon 6 nanofibers was performed using the AATCC test method 100-2004.

4.4.1.2 AATCC test method 100-2004

The American Association of Textile Chemists and Colorist (AATCC) Test Method 100-2004 was also used to investigate the antimicrobial activity of the electrospun nylon 6 nanofibers incorporated with silver(I)-imidazole complexes.[320] The nanofiber composites were first cut into swatches (diameter ~4.8 cm) and the swatches were used for conducting the experiments. The antimicrobial activity of the nylon 6 nanofiber composites was tested against a Gram-negative bacterium (*E. coli*) and one Gram-positive bacterium (*S. aureus*). The results showed that the percentage reduction of bacterial growth against *E. coli* and *S. aureus* was significantly low (Fig. 4.17).

The low percentage reduction of bacterial growth for the nanofiber composites was attributed to poor contact of the bacteria with the Ag(I) complexes encapsulated within the electrospun nylon 6 nanofibers. The effect was probably due to lack of moisture on the nanofibers resulting to low diffusibility of the Ag(I) complexes. It was previously reported that moisture is necessary for the release of Ag(I) ions from the electrospun nanofibers.[98] Moreover, the

hydrophobicity of nylon 6 could have also contributed significantly to the observed effect. Even the presence of a surfactant (Triton X100), which was added to enhance the wettability of the polymer nanofibers, seemed not to have assisted probably due to lack of solubility of the Ag(I) complexes in it.

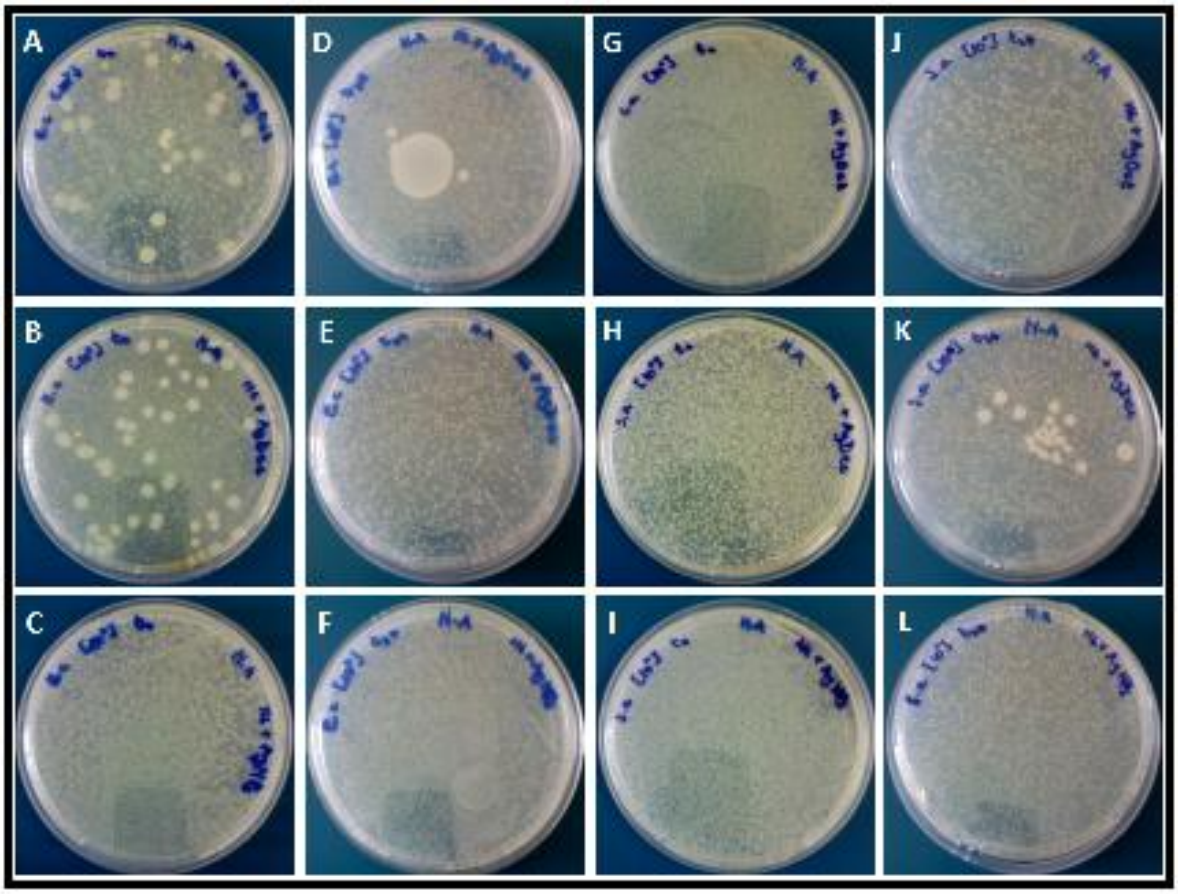

Figure 4.17. Bacterial growth after 0 and 24 h contact times with antimicrobial nanofibers. At time t = 0 h: *E. coli* (A-C), *S. aureus* (G-I) and time t = 24 h: *E. coli* (D-F), *S. aureus* (J-L)

It was concluded, based on the results obtained, that the AATCC test method 100 was not suitable for evaluating the antimicrobial activity of the electrospun nylon 6 nanofibers incorporated with both the silver(I) complexes and silver nanoparticles. A different method for evaluating the antimicrobial activity of electrospun nanofiber composites was therefore necessary, and the shake flask method was employed.

4.4.1.3 Dynamic shake flask testing method (ASTM E2149-10)

The dynamic shake flask testing method (American Society for Testing and Materials (ASTM) E2149-10) is an approved method for evaluation of the antimicrobial activity of immobilized antimicrobial agents.[325] The method is performed under dynamic conditions to allow efficient contact of the microorganisms with the treated antimicrobial materials. Moreover, the method has also been used to evaluate the antimicrobial activity of electrospun nanofibers incorporated with AgNPs.[50,53] The shake flask method, as with AATCC test method 100, expresses the antimicrobial activity as the percentage reduction of the growth of microorganisms.

The results showed that there was tremendous improvement in the antimicrobial activity of electrospun nylon 6 nanofibers (Fig. 4.18). All the electrospun nylon 6 nanofiber composites, incorporated with silver(I) complexes and AgNPs, that were evaluated, displayed a very high percentage reduction of microbial growth (>99.99%) for both *E. coli* and *S. aureus*.

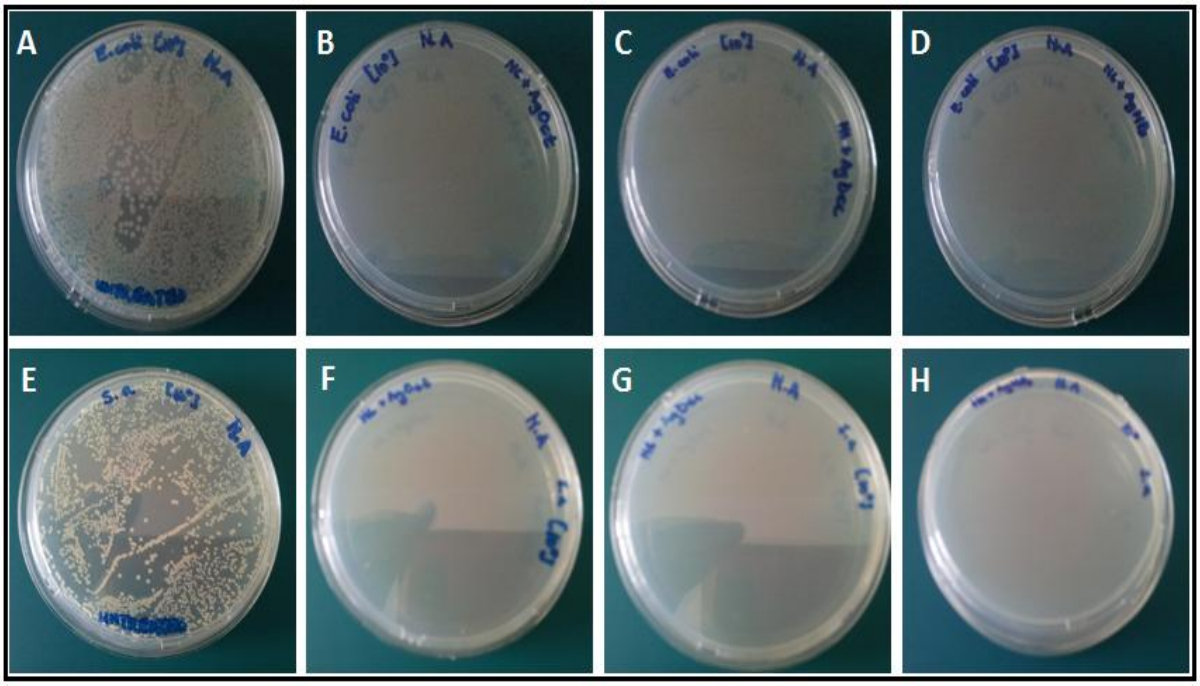

Figure 4.18. Bacterial growth after 1 h contact time with antimicrobial nanofibers. *E. coli* (A-D) and *S. aureus* (E-H). A and E represent the bacterial growth for the untreated suspensions

The results obtained from the shake flask test method showed that electrospun nylon 6 nanofibers incorporated with silver(I)-imidazole complexes retained the antimicrobial activity

after incorporation into electrospun nylon 6 nanofibers. However, it was observed in **4.1.3** and **4.4.1** that the antimicrobial compounds have to diffuse out of the electrospun nanofiber to exhibit the antimicrobial activity. The limitation is that diffusion exhausts the biocides in the polymeric material which could result in development of resistance by the microorganisms.[343] Moreover, for drinking water applications, the leaching of antimicrobial compounds from electrospun nanofibers could have adverse health effects to humans. The challenge could be averted by immobilization of the antimicrobial compounds onto the surface electrospun nanofibers.

4.5 The fabrication of antimicrobial electrospun nanofibers by immobilization of *N*-vinylimidazoles using graft polymerization

4.5.1 Synthesis of 2-substituted vinylimidazoles

It was demonstrated in the study that the antimicrobial activity of the 2-substituted *N*-alkylimidazoles increased with the increase in the length of the alkyl chain at the 1-position of imidazoles. The idea was then to immobilize the imidazoles with the longest alkyl chain length (decyl) and the different substituents (-CHO, -CH_2OH, COOH) at the 2-position onto electrospun nylon 6 nanofibers. There were 2 possibilities that could be explored: (1) to attach the vinyl group at the 1-position, and (2) to attach the vinyl group at the 4 or 5-position (Fig. 4.19). In the first possibility the role of the alkyl chain would be played by the polymer backbone while in the second possibility the alkyl chain would be attached at 1-position.

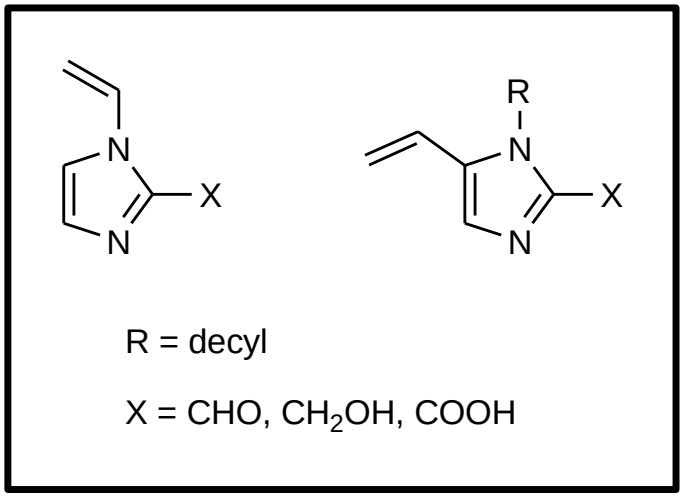

Figure 4.19. Two possibilties for the synthesis of 2-substituted vinylimidazoles

4.5.1.1 The 2-substituted 1-vinylimidazoles (*N*-vinylimidazoles)

The 2-substituted *N*-vinylimidazoles were synthesized using the synthetic route in Scheme 4.4. Briefly, the acylation of *N*-vinylimidazole (1-VIm) resulted in the production of *N*-vinylimidazole-2-carboxaldehyde (1-VImCHO). Furthermore, the reduction of 1-VImCHO resulted in the formation of 2-hydroxymethyl-*N*-vinylimidazole (1-VImCH_2OH) while the oxidation of 1-VImCHO gave *N*-vinylimidazole-2-carboxylic acid (1-VImCOOH).

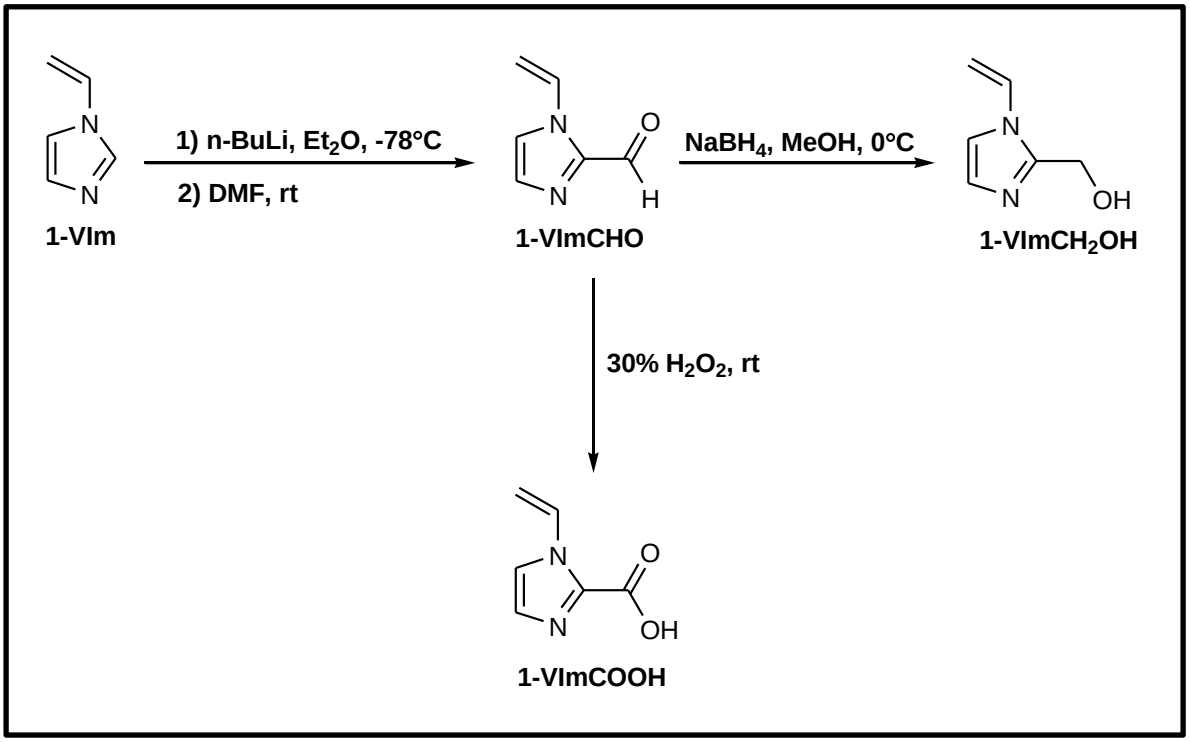

Scheme 4.4. Synthesis of 2-substituted *N*-vinylimidazoles

The synthesized 2-substituted *N*-vinylimidazoles were characterized using NMR (Fig. 4.20) and IR spectroscopic techniques. The ^{1}H NMR spectrum of 1-VImCHO displayed a singlet at 9.88 ppm which indicated the presence of the aldehydic C**H**O proton. The multiplet at 7.99-7.93 ppm (C**H**) and the two doublets at 5.43 and 5.13 ppm (C**H**$_2$) indicated the presence of the vinyl group. The ^{1}H NMR spectrum of 1-VImC**H**$_2$OH exhibited a multiplet at 7.17-7.11 ppm (C**H**) and two doublets at 5.43 and 5.03 ppm (C**H**$_2$) which indicated the presence of the vinyl group. The singlet at 4.69 ppm indicated the presence of methylene protons (C**H**$_2$OH). For 1-VImCOOH, the presence of the vinyl group was indicated by the multiplet at 7.85-7.79 ppm(C**H**) and the two doublets at 5.69 and 5.36 ppm (C**H**$_2$).

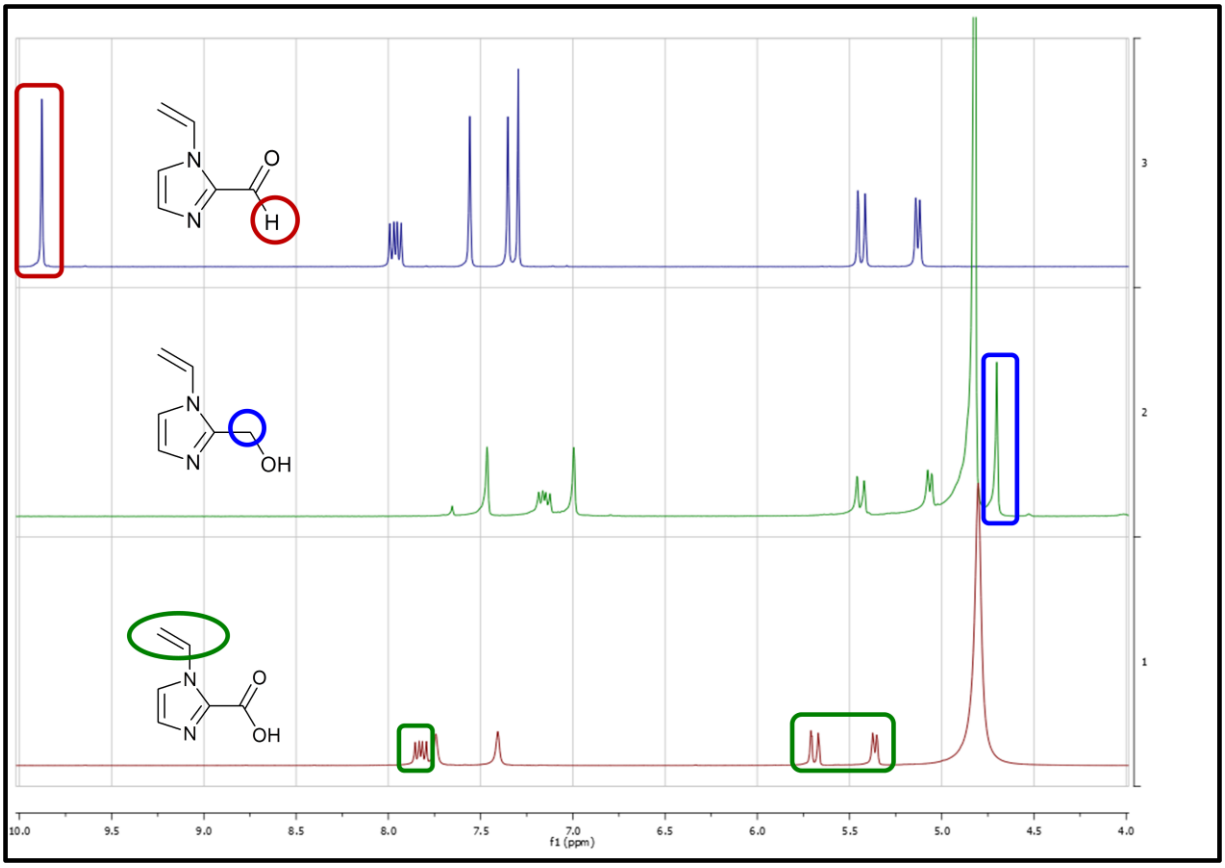

Figure 4.20. ^{1}H NMR spectra of 2-substituted *N*-vinylimidazoles

Figure 4.21 illustrates the ^{13}C NMR spectra of 2 the 2-substituted *N*-vinylimidazoles. The spectrum of 1-VImCHO showed a signal at 182.76 ppm indicating the presence of a carbonyl group (C=O). The signals at 130.25 and 105.84 ppm indicated the presence of the vinyl group carbons; CH and CH_2, respectively. For 1-VImCH_2OH, the signal at 128.81 (CH) and 104.56 ppm (CH_2) indicated the presence of the vinyl group. The signal at 55.28 ppm indicated the presence of the methylene carbon (**C**H_2OH). The ^{13}C NMR spectrum of 1-VImCOOH displayed a signal at 215.82 ppm indicating the presence of C=O, while the presence of the vinyl group was indicated by the signals at 129.66 (CH) and 110.12 (CH_2) ppm.

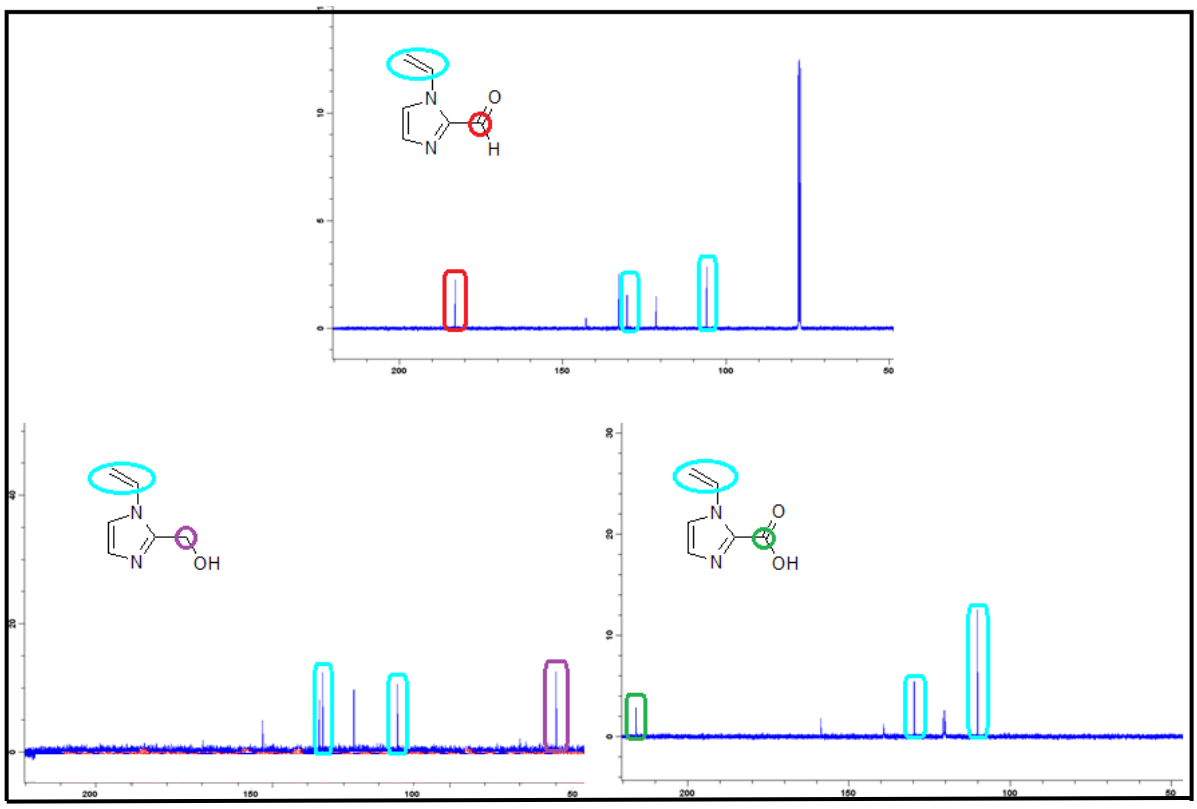

Figure 4.21 The ^{13}C NMR spectra of 2-substituted N-vinylimidazoles

The IR spectrum of 1-VImCHO exhibited a band at 1674 cm^{-1} confirming the C=O group, while the spectrum of 1-VImCH_2OH displayed two bands at 3347 and 3112 cm^{-1} which indicated the presence of the hydroxyl group (-OH). The bands at 3112 and 1644 cm^{-1}, in the spectrum of 1-VImCOOH, indicated the presence of the hydroxyl (-OH) and carbonyl (C=O) groups, respectively. The synthesis of 2-substituted *N*-alkylimidazoles was then followed by the synthesis of 2-substituted *N*-alkyl-4(5)-vinylimidazoles.

4.5.1.2 The 2-substituted *N*-alkyl-4(5)-vinylimidazoles

The synthesis of 2-substituted *N*-alkyl-4(5)-vinylimidazoles was achieved as outlined in Scheme 4.5. Briefly, 4(5)-vinylimidazole (4(5)-VIm) was synthesized by decarboxylation of urocanic acid.[326] The *N*-alkylation of 4(5)-VIm using bromodecane gave *N*-decyl-4(5)-vinylimidazole (1-dec-4(5)-VIm). In the following step, 1-dec-4(5)-VIm underwent acylation at the 2-position to produce *N*-decyl-4(5)-vinylimidazole-2-carboxaldehyde (1-dec-4(5)-VImCHO). The reduction and oxidation of 1-dec-4(5)-VImCHO gave 2-hydroxymethyl-*N*-

decyl-4(5)-vinylimidazole (1-dec-4(5)-VImCH_2OH) and *N*-decyl-4(5)-vinylimidazole-2-carboxylic acid (1-dec-4(5)-VImCOOH), respectively.

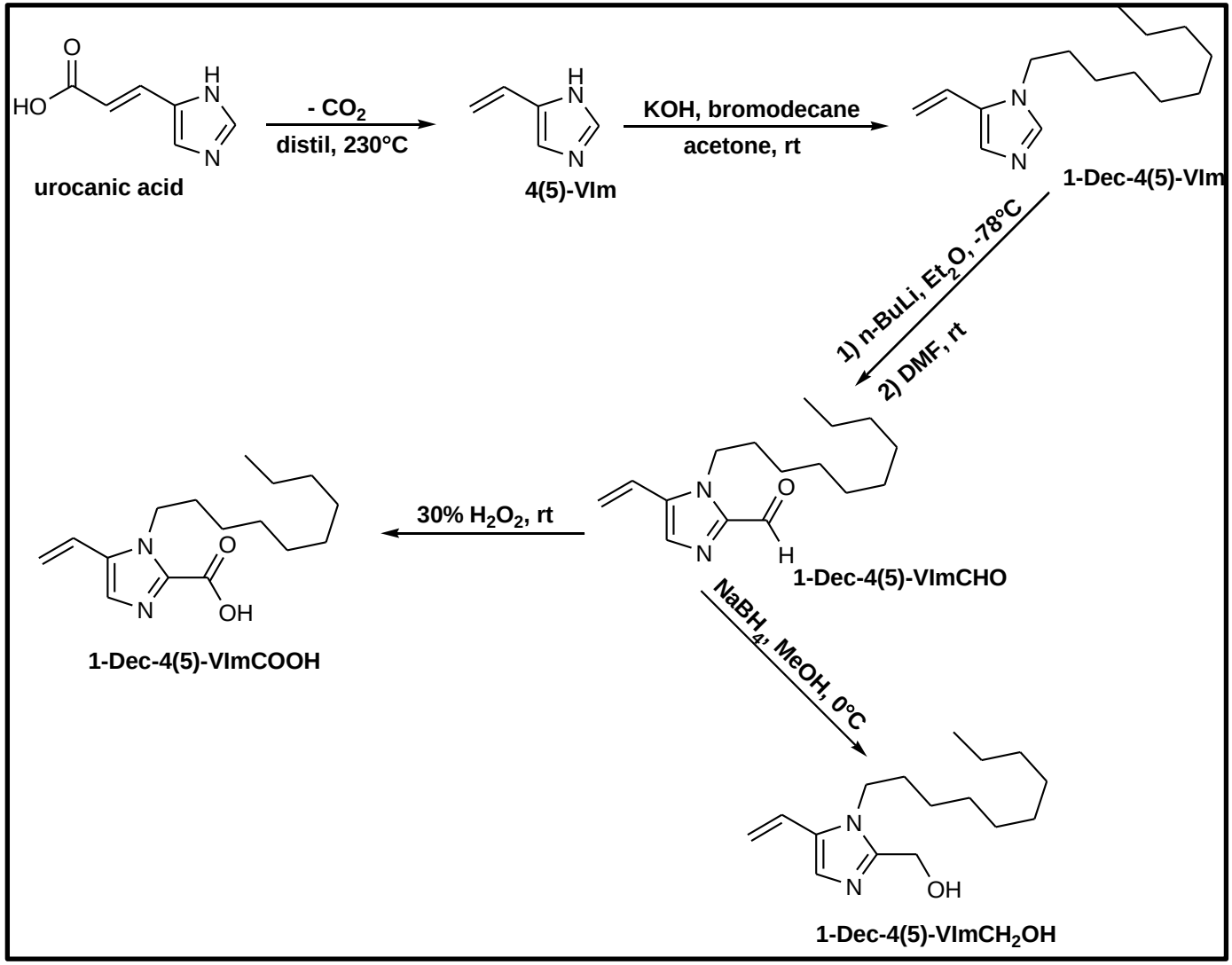

Scheme 4.5. Synthesis of 2-substituted *N*-alkyl-4(5)-vinylimidazoles

NMR and IR spectroscopic techniques were used for the characterization of the 2-substituted *N*-alkyl-4(5)-vinylimidazoles. The ^{1}H NMR spectrum of 4(5)-VIm showed two singlets at 7.66 and 7.07 ppm representing the imidazole protons at the 2- and 4(or 5)-positions, respectively. The presence of the vinyl group at the 4(5)-position was indicated by a multiplet at 6.66-6.59 ppm (CH) and two doublets at 5.63 and 5.14 ppm (CH_2). The ^{1}H NMR spectrum of 4(5)-VIm is illustrated in Fig. 4.22.

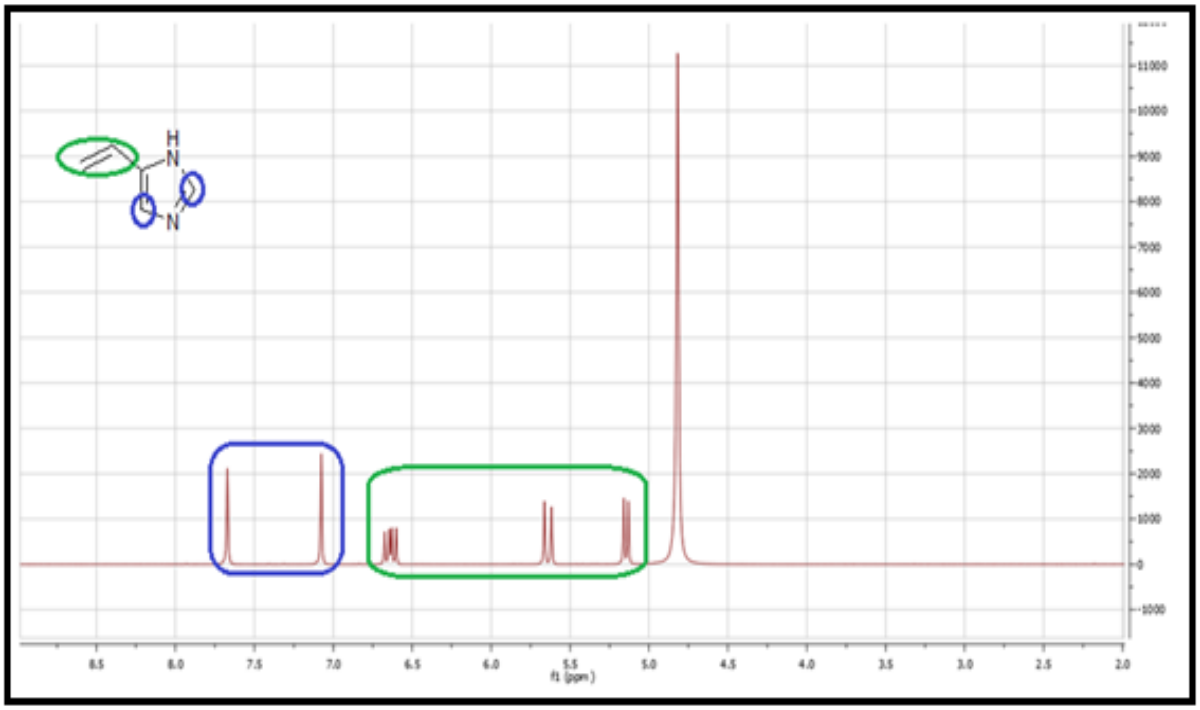

Figure 4.22. ^{1}H NMR spectrum of 4(5)-VIm

The alkylation of 4(5)-VIm using bromodecane resulted in the formation of 1-decyl-4(5)-vinylimidazole (1-dec-4(5)-VIm). The ^{1}H NMR spectrum displayed new signals between 4.0 and 0.5 ppm, in addition to the signals observed for 4(5)-VIm, indicating the presence of the alkyl (decyl) group. The ^{13}C NMR showed two signals at 137.18 and 116.54 ppm which represented the imidazole moiety (Fig. 4.23). Furthermore, the two signals that appeared at 128.68 (CH) and 111.64 ppm (CH_2) indicated the presence of the vinyl group.

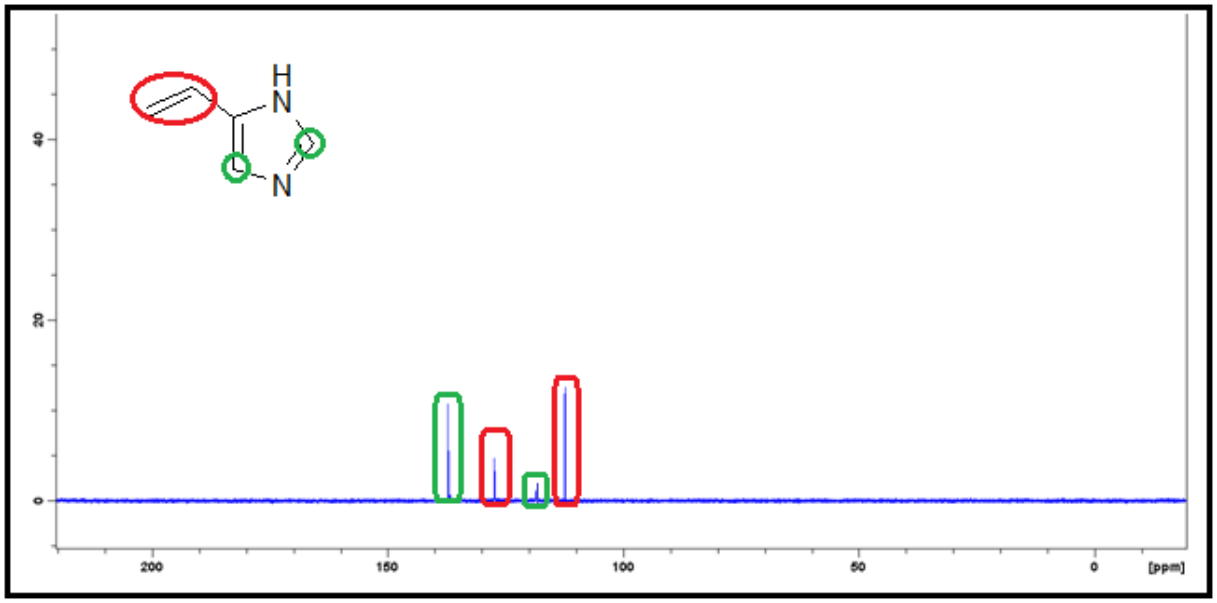

Figure 4.23. The ^{13}C NMR spectrum of 4(5)-VIm

1-Decyl-4(5)-vinylimidazole-2-carboxaldehyde (1-dec-VImCHO) was synthesized by the acylation of 1-dec-VIm. The ^{1}H NMR spectrum of 1-dec-4(5)-VImCHO exhibited the disappearance of the proton signal at the 2-position and the emergence of a new signal at 8.01 ppm. The new signal confirmed the presence of the aldehyde (CHO) group at the 2-position. 1-Decyl-4(5)-VImCH_2OH (1dec-VImCH_2OH) and 1-decyl-4(5)-VImCOOH (1-dec-4(5)-VImCOOH) were produced by the reduction and oxidation of 1-dec-4(5)-VImCHO, respectively. The ^{1}H NMR spectra of both 1-dec-4(5)-VImCH_2OH and 1-dec-4(5)-VImCOOH both showed the disappearance of the CHO signal. For 1-dec-4(5)-VImCH_2OH, a new signal was observed at 5.29 ppm indicating the methylene protons of the CH_2OH group. The hydroxyl (OH) groups for both 1-dec-4(5)-VImCH_2OH and 1-dec-4(5)-VImCOOH were not observed. The reason is that the –OH proton is easily exchangeable and is sometimes replaced by deuterium, which is not observable on the ^{1}H NMR spectrum.

The formation of 1-dec-4(5)-VIm, 1-dec-4(5)-VImCHO, 1dec-4(5)-VImCH_2OH and 1-dec-4(5)-VImCOOH were also confirmed by ^{13}C NMR spectroscopy. Figure 4.24 illustrates the ^{13}C NMR spectra for the 2-substituted 1-decyl-4(5)-VIm derivatives. The two substituents were identified by the carbon signals: 182.23 ppm (CHO) for 1-dec-4(5)-VImCHO, 53.44 ppm (CH_2OH) for 1-dec-4(5)-VImCH_2OH and 174.36 (COOH) for 1-dec-4(5)-VImCOOH. The vinyl group signals were 128.68 ppm (CH)

and 111.64 ppm (CH_2) for -1-dec-4(5)-VIm; 128.56 ppm (CH) and 111.81 ppm (CH_2) for 1-dec-4(5)-VImCHO; 128.60 ppm (CH) and 111.78 ppm (CH_2) for 1-dec-4(5)-VImCH_2OH, and 128.29 ppm (CH) and 112.19 ppm (CH_2) for 1-dec-4(5)-VImCOOH. The alkyl group signals appeared in the normal region (50-10 ppm) for all the compounds.

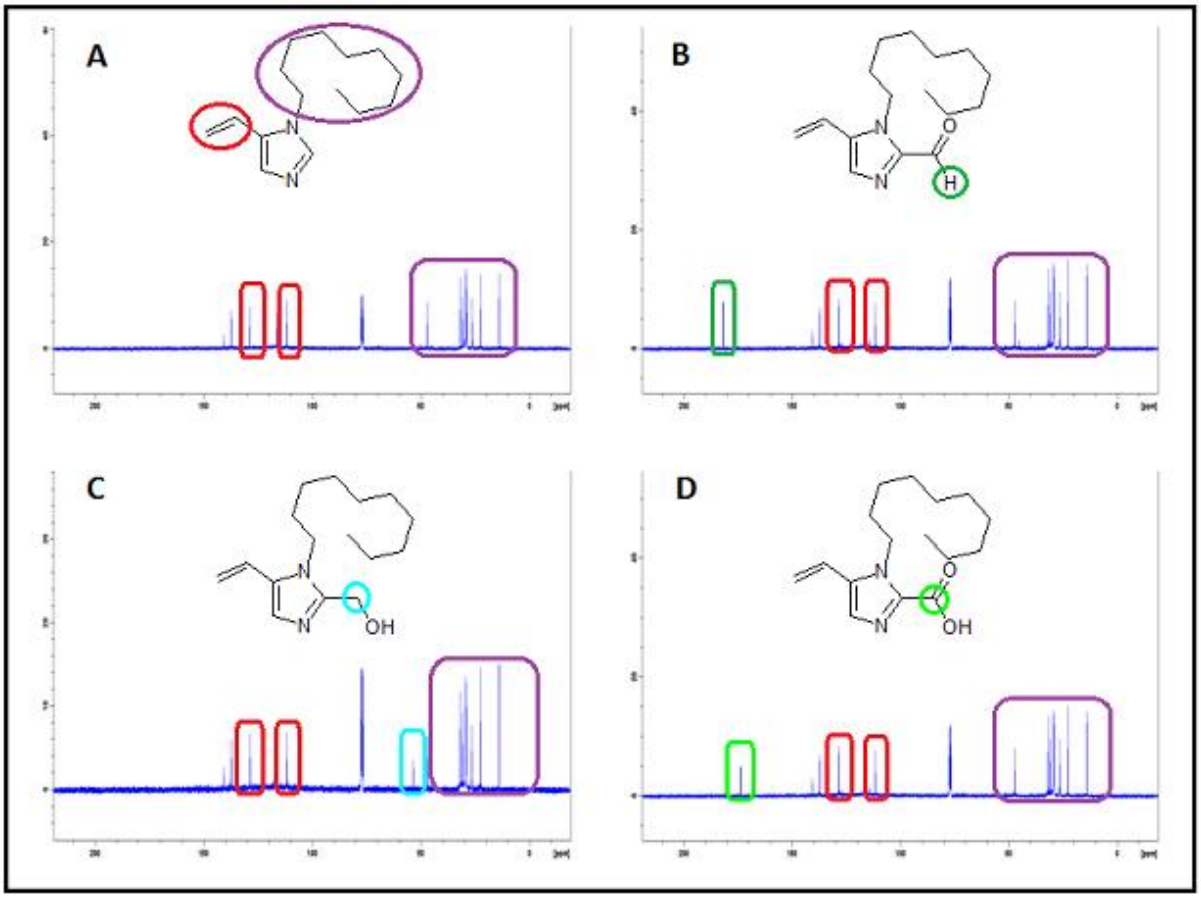

Figure 4.24. ^{13}C NMR spectra of 2-substituted *N*-vinylimidazoles (1-vinylimidazoles)

After the successful synthesis and characterization of the 2-substituted *N*-vinylimidazoles, the compounds were grafted onto electrospun nylon 6 nanofibers.

4.5.2 Grafting of 2-substituted vinylimidazoles onto electrospun nylon 6 nanofibers

4.5.2.1 Grafting of 2-substituted *N*-vinylimidazoles

Grafting of the 2-substituted *N*-vinylimidazoles onto electrospun nylon 6 nanofibers was performed using a simultaneous UV-initiated graft polymerization technique (Scheme 4.6). Graft polymerization onto nylon 6 is known to occur on the N of the amide moiety, *via* the abstraction of the hydrogen radical.[344] All the 2-substituted *N*-vinylimidazoles were grafted successfully except for *N*-vinylimidazole-2-carboxaldehyde (1-VImCHO). The failure to perform grafting of 1-VImCHO onto electrospun nylon 6 nanofibers was attributed to the stability of the aldehyde (CHO) functional group under UV radiation. When exposed to UV radiation, the aldehyde group undergoes photo-decomposition *via* a homolytic cleavage (Norrish Type 1) of the α-C-C bond.[345] Grafting percentage ranges for the successfully grafted 2-substituted vinylimidazoles were 1-VIm (39.9-44.7%), 1-VImCH_2OH (25.4-33.6%) and 1-VImCOOH (4.5-12.3%). The relatively low grafting percentages were attributed to the observed degree of homopolymerization. Another reason for the low grafting percentages could probably be due to the reduced reactivity of the vinyl group when attached at the 1-position. However, the grafting percentages that were obtained were much higher than those obtained for grafting 4-vinylpyridine (2.34%) onto electrospun nylon 6 nanofibers, using the free radical grafting method.[346]

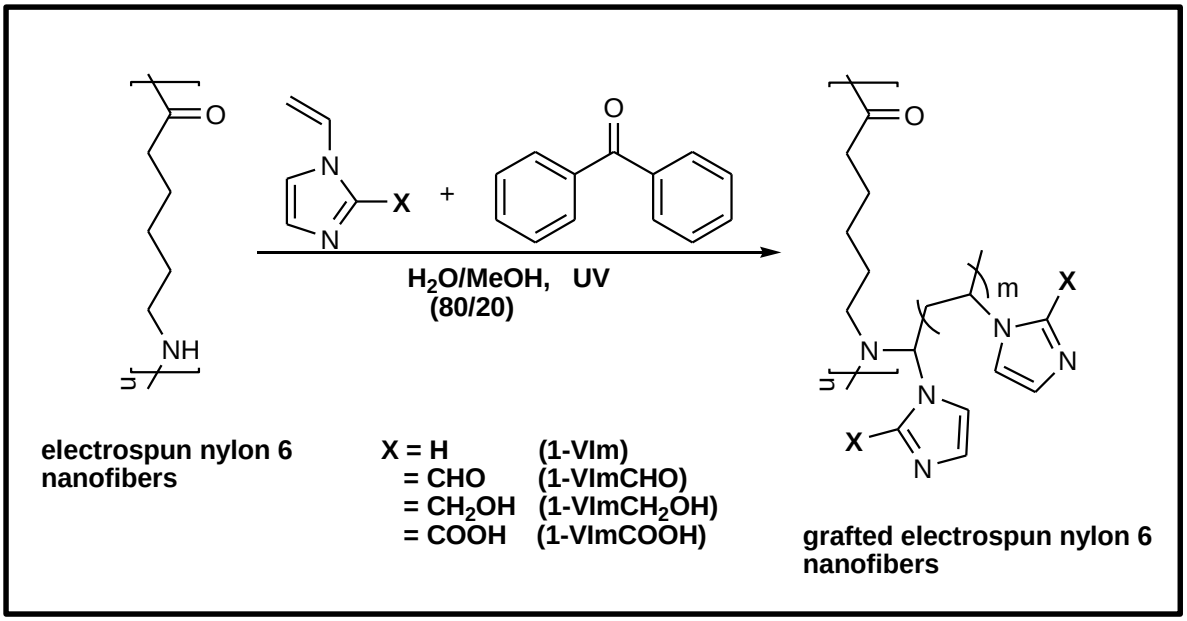

Scheme 4.6. Grafting of 2-substituted *N*-vinylimidazoles onto electrospu nylon 6 nanofibers

Successfully grafted 2-substituted *N*-vinylimidazoles were characterized using ATR-FTIR and energy dispersive analysis x-ray spectroscopy (EDAX). ATR-FTIR spectra revealed very low intensity bands for all grafted electrospun nylon 6 nanofibers which made it slightly difficult to confirm the presence of the 2-substituted *N*-vinylimidazoles (Fig. 4.25).

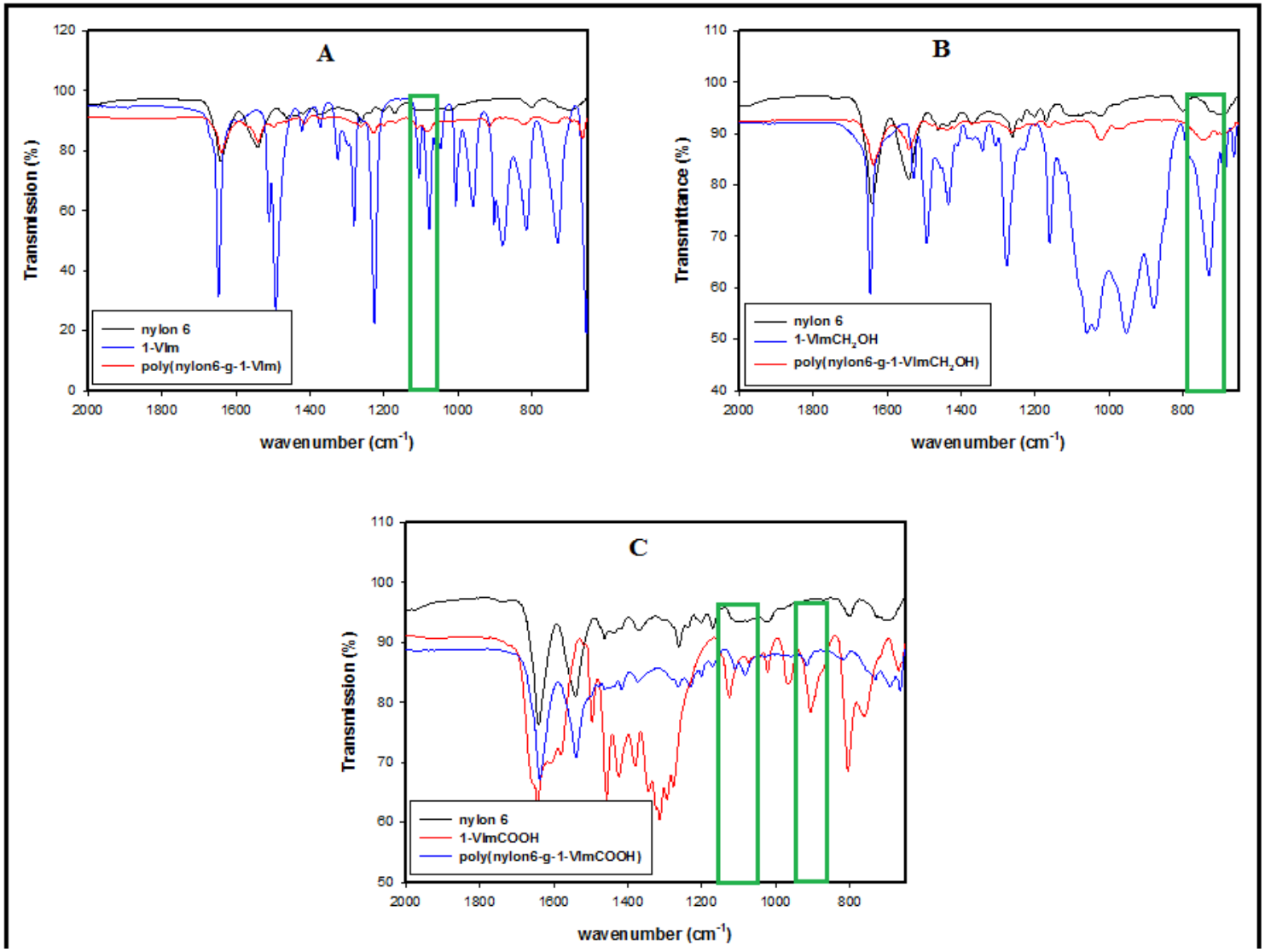

Figure 4.25. ATR-IR spectra of electrospun nylon 6 nanofibers grafted with 2-substituted *N*-vinylimidazoles

Recently, Sabaa *et al.*[119] reported that the intensities of the C=C, C=N and C-H vibration bands of imidazole increase as the grafting percentage increases. Moreover, since the grafting layer is only several tens of nanometers thick, ATR-FTIR is usually not a sensitive technique for surface characterization of grafted nanofibers since the mean free path of infrared radiation is 2 μm.[245]

Nevertheless, the ATR-FTIR spectrum showed two bands in the region 1200-1000 cm^{-1} which coincided with bands in the spectrum of the corresponding vinylimidazole derivative, a confirmation that 1-VIm was successfully grafted onto electrospun nylon 6 nanofibers (Fig. 4.25A). Grafting of 1-VImCH_2OH onto electrospun nylon 6 nanofibers was confirmed by a band between 800-600 cm^{-1} (Fig. 4.25B) while grafting of 1-VImCOOH was ascertained by bands between 1200-1000 cm^{-1} and 900-800 cm^{-1} (Fig. 4.25C). Further characterization of the grafted electrospun nylon 6 nanofibers was perfomed using energy dispersive analysis x-ray (EDAX) spectroscopy.

Energy dispersive analysis x-ray spectroscopy was used to evaluate the elemental composition of the surface of grafted electrospun nylon 6 nanofibers. The specific element of interest was N since the imidazole moiety contains two N atoms. Therefore, an increase in the N content of grafted electrospun nylon 6 nanofibers would confirm successful grafting of 2-substituted *N*-vinylimidazoles.

The EDAX spectra for the grafted electrospun nylon 6 nanofibers displayed an increase in the N content which indicated that the 2-substituted *N*-vinylimidazoles were successfully grafted (Fig. 4.26). It was observed that, in comparison to ungrafted electrospun nylon 6 nanofibers, the N content of the electrospun nylon 6 nanofibers grafted with 1-VIm (poly(nylon6-g-1-VIm) and 1-VImCH_2OH (poly(nylon6-g-1-VImCH_2OH) increased as the O content decreased and N was uniformly distributed on the grafted nanofibers.

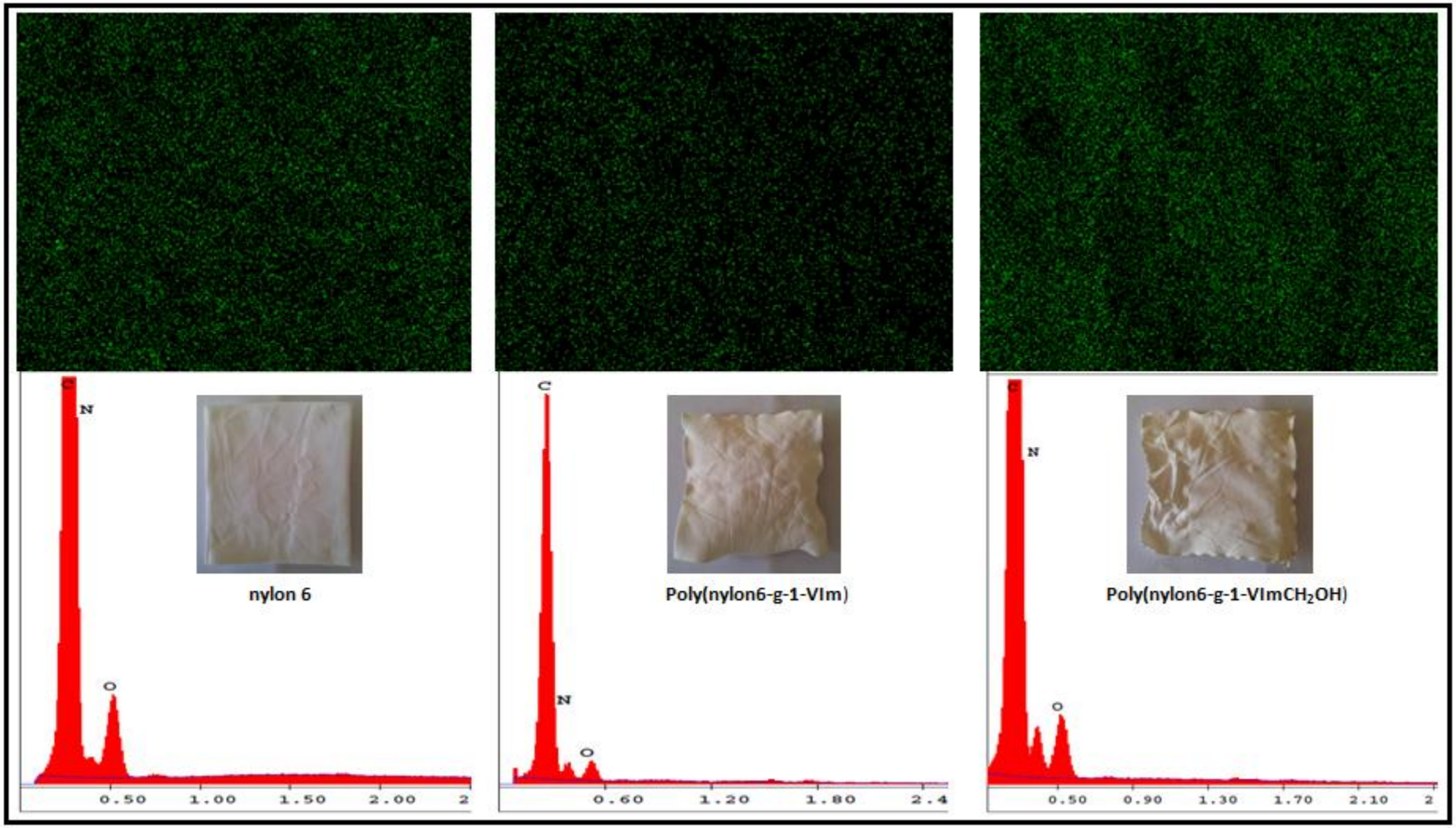

Figure 4.26. EDAX spectra and the N distribution mappings for electrospun nylon 6 nanofibers grafted with 2-substituted *N*-vinylimidazoles

Energy dispersive spectroscopy (EDS) also demonstrated that the N content of grafted electrospun nylon 6 nanofibers [poly(nylon 6-g-1-VImCOOH)] increased in comparison with ungrafted electrospun nylon 6 nanofibers (Fig. 4.27). The information obtained from ATR-FTIR and EDAX (EDS) confirmed that grafting of 2-substituted *N*-vinylimidazoles onto electrospun nylon 6 nanofibers was successful.

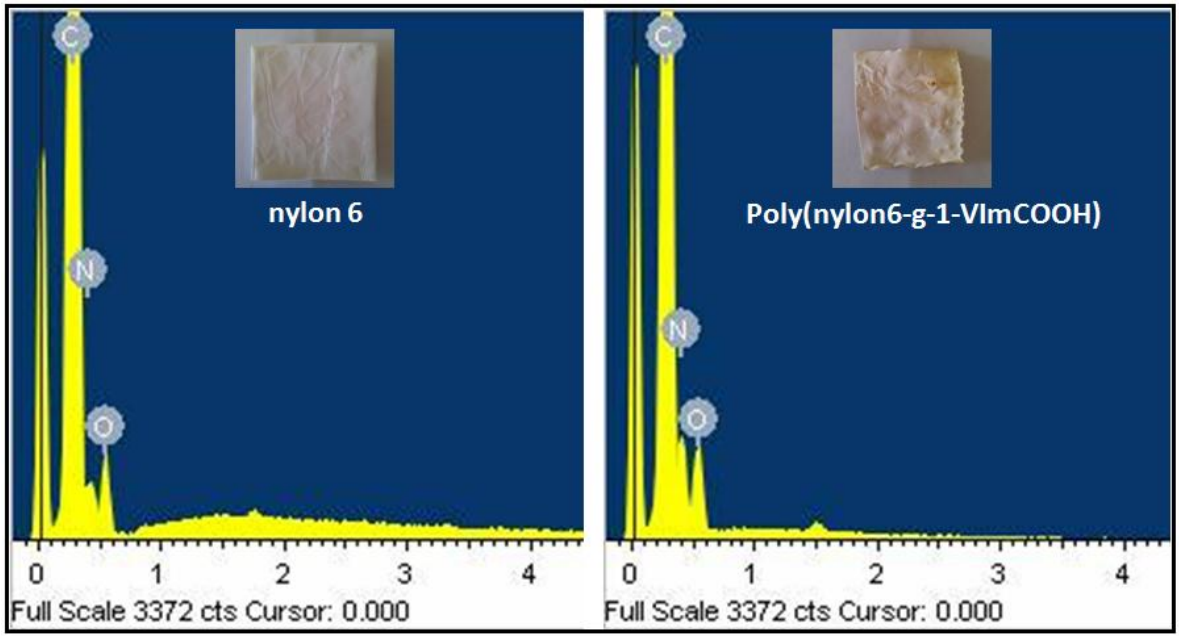

Figure 4.27. EDS spectra for ungrafted nylon 6 nanofibers and 1-VImCOOH grafted nylon 6 nanofibers

4.5.2.2 Grafting 2-substituted *N*-decyl-4(5)-vinylimidazoles

Grafting of the 2-substituted *N*-decyl-4(5)-vinylimidazoles onto electrospun nylon 6 nanofibers was also performed by the simultaneous UV-assisted graft polymerization technique (Scheme. 4.7). However, only the unsubstituted vinylimidazole (4(5)-VIm) could be successfully grafted onto electrospun nylon 6 nanofibers. Figure 4.28 illustrates the EDAX spectrum and the N distribution mapping on the surface of grafted nylon 6 nanofibers. It could be seen that the N content increased while the O content decreased indicating that grafting was successful. Moreover, the elemental distribution mapping showed that N was uniformly distributed on the surface of electrospun nylon 6 nanofibers.

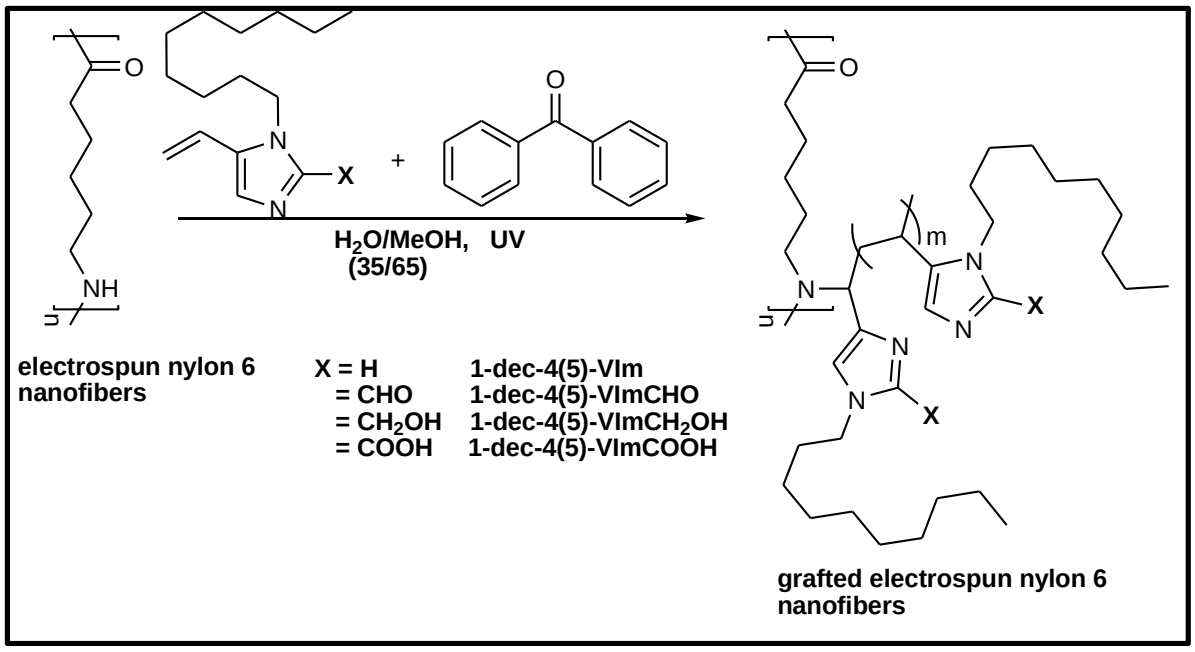

Scheme 4.7. Grafting of 2-substituted 1-decyl-4(5)-Vinylimidazoles onto electrospun nylon 6 nanofibers

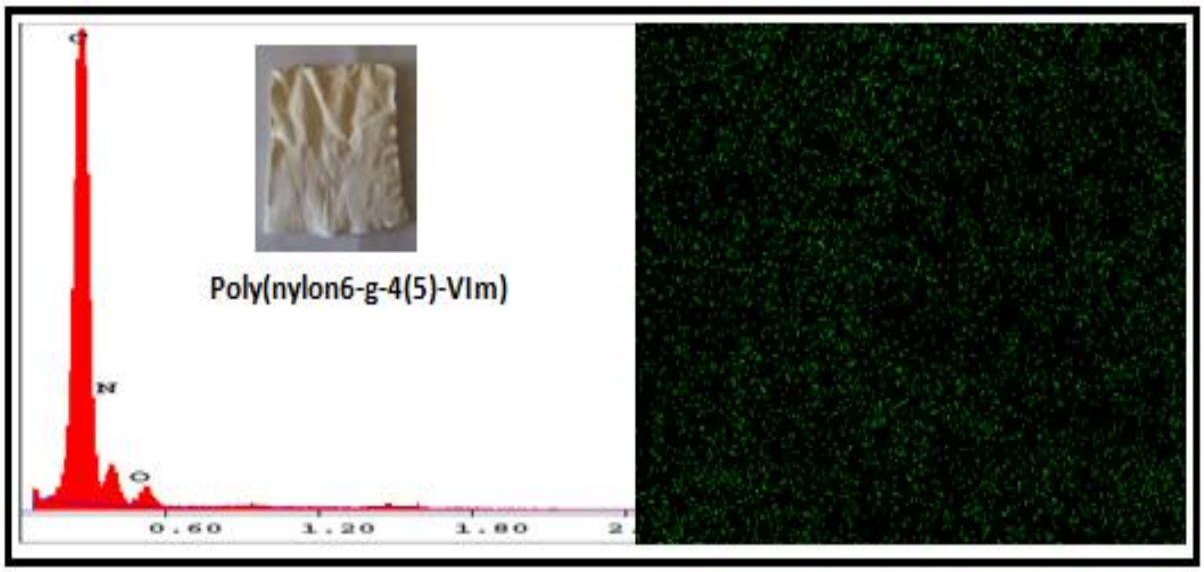

Figure 4.28. EDAX spectrum and the N distribution mapping of electrospun nylon 6 nanofibers grafted with 4(5)-VIm

The first challenge encountered during graft polymerization experiments of 1-dec-4(5)-vinylimidazoles was that the MeOH/H_2O (20/80) solvent system did not work. It was observed that the compounds became insoluble hence grafting was not taking place. However, Athawale and Rathi[347] disputed that solubility of vinyl monomers could have an

influence on graft polymerization. Nonetheless, it was decided to vary the ratio of the solvent system, MeOH/H_2O, so as to ensure the solubility of the vinylimidazoles. Unfortunately, even 100% MeOH did not give any positive results since no grafting was observed. Therefore, another approach to address the challenge was to use a different solvent that would dissolve both the vinyl monomer and the initiator to perform the grafting experiments. It was reported that Unal *et al*.[198] were able to graft *N*-vinylimidazoles using dimethyl formamide (DMF) as the solvent. However, attempts to graft the 2-substituted 1-decyl-4(5)-vinylimidazoles were unsuccessful.

In another study, it was reported that the addition of a metal salt/acid mixture in the grafting solution aided in stabilizing the free radicals (accelerated graft polymerization) and reduced homopolymerization.[348,349] For example, $FeSO_4.7H_2O$ and H_2SO_4 were used as grafting accelerator and homopolymer inhibitor, respectively, in the photografting of acrylic acid onto polypropylene.[349] Once again, attempts to effect grafting of 2-substituted 1-decyl-4(5)-vinylimidazoles by the addition of $FeSO_4.7H_2O/H_2SO_4$ mixture did not yield positive results.

It was later realized that the major factor that inhibited the grafting of the 2-substituted 1-decyl-4(5)-vinylimidazoles could be the alkyl chain (decyl). It was reported previously that the grafting efficiency decreased as the alky chain length was increasd.[347] The reduction in the grafting efficiency was attributed to steric hindrance by longer alkyl chains. With all the challenges that were encountered, it was not possible to graft the 2-substituted 1-decyl-4(5)-vinylimidazoles onto electrospun nylon 6 nanofibers, and further experiments were performed using poly(nylon 6-g-4(5)-VIm).

4.5.2.3 Adsorption of silver nanoparticles on electrospun nylon 6 nanofibers grafted with unsubstituted vinylimidazoles

Antimicrobial electrospun nylon 6 nanofibers were fabricated by adsorption of AgNPs on the surface of nylon 6 nanofibers grafted with vinylimidazoles (1-VIm and 4(5)-VIm). Figure 4.29 depicts the fabrication of AgNPs-adsorbed grafted nanofibers. Methanol acted as both the solvent and the reducing agent, hence there was no reducing agent added. The reduction of silver(I) to metallic silver ions using methanol is a well-documented phenomenon.[350-354] During the reduction of silver(I) ions methanol is oxidized to formaldehyde and the polymer acts as the capping agent.[352,354] The nanofibers were characterized using energy dispersive spectroscopy. The EDS spectra showed that the AgNPs were successfully adsorbed on the surface of the grafted nanofibers (Fig. 4.30).

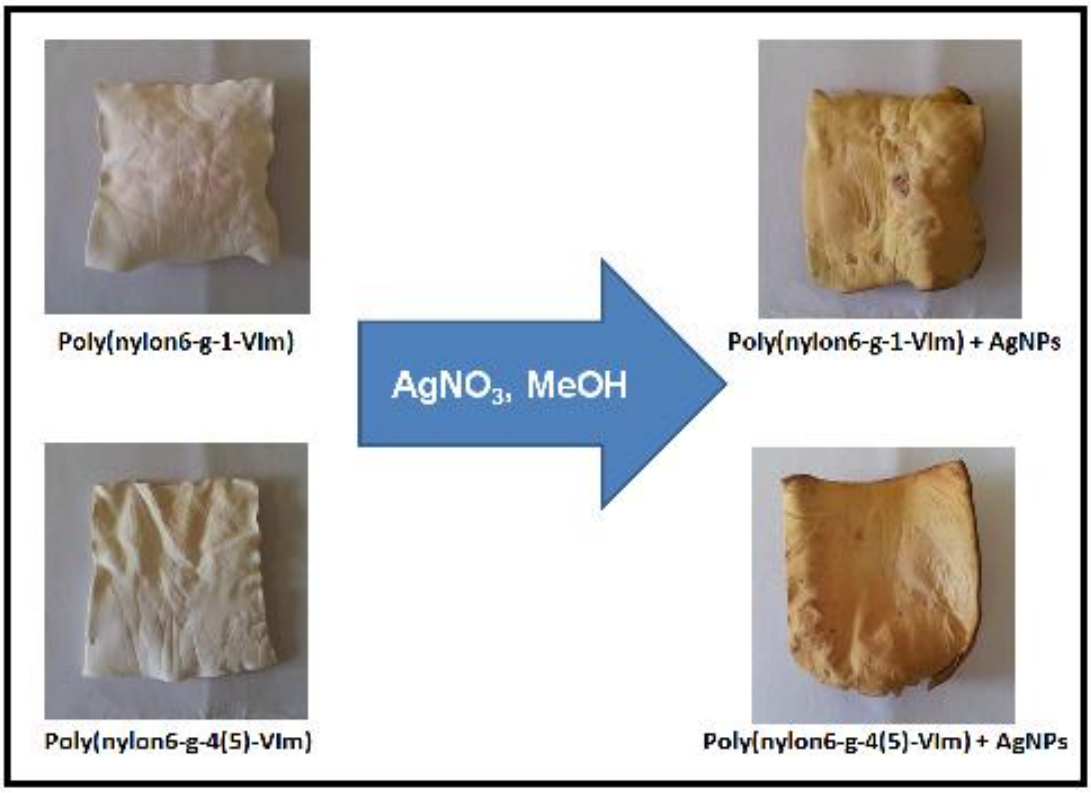

Figure 4.29. Adsorption of AgNPs onto nylon 6 nanofibers grafted with vinylimidazoles

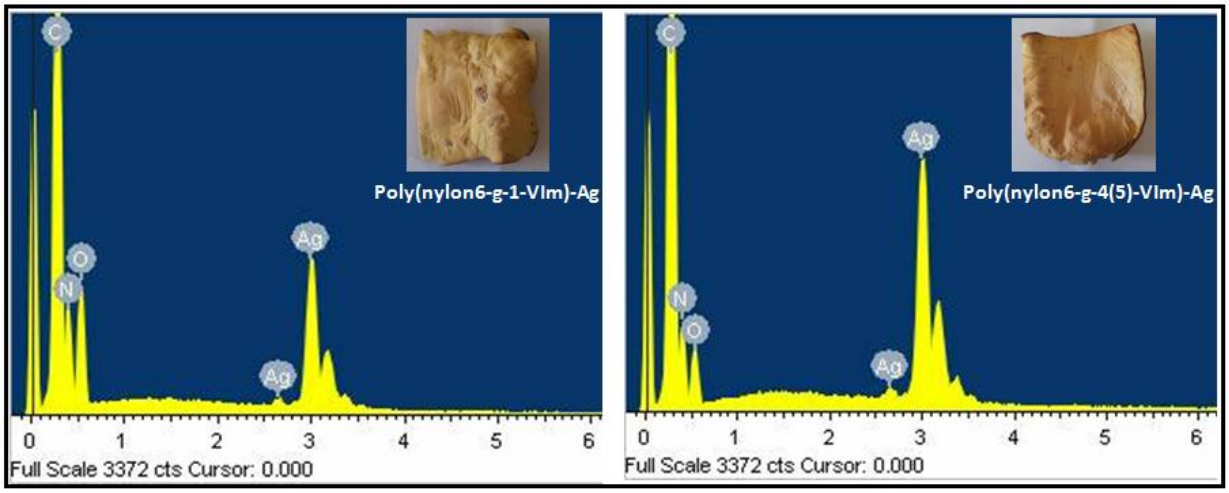

Figure 4.30. EDS spectra of AgNPs-adsorbed grafted nanofibers

Transmission electron microscopy (TEM) was employed to confirm that it was AgNPs that were adsorbed onto the grafted electrospun nylon 6 nanofibers and not complexation of the silver(I) ion with electrospun nylon 6 nanofibers. The AgNPs were desorbed from the grafted electrospun nylon 6 nanofibers by soaking in ethanol and the solution was used to obtain TEM micrographs. The micrographs showed the presence of dispersed AgNPs with the size

distribution between 4-11 nm (Fig. 4.31) which indicated that AgNPs particles were present on the surface of grafted electrospun nylon 6 nanofibers. When all the materials were fabricated and characterized, they were evaluated for antimicrobial activity.

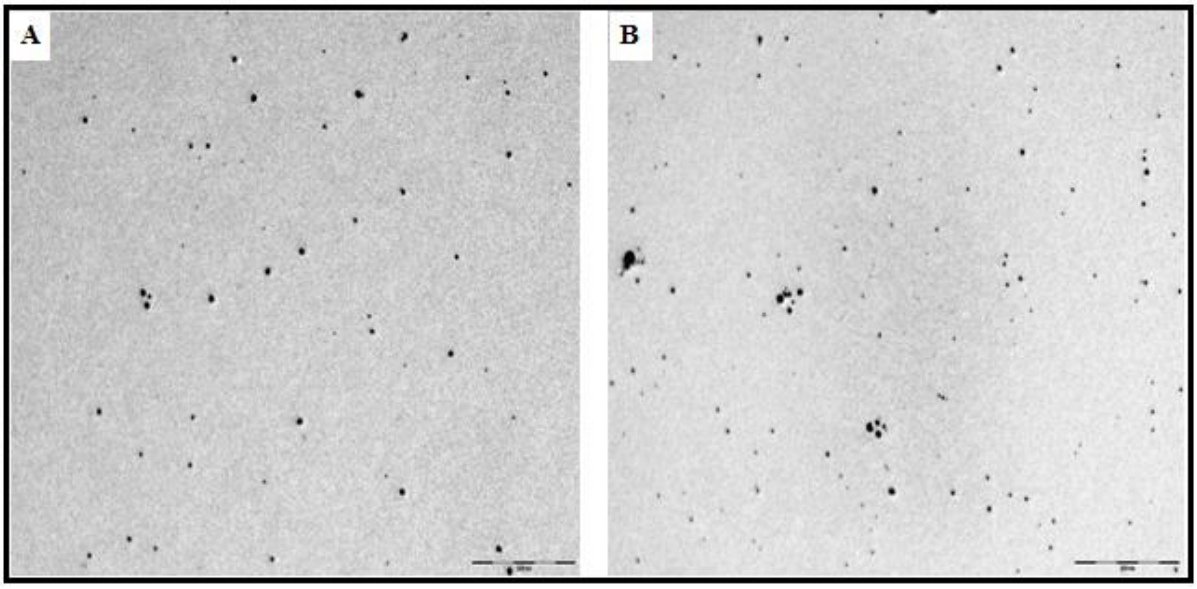

Figure 4.31. TEM micrographs of AgNPs desorbed from (A) poly(nylon6-g-1-VIm)-AgNPs and (B) poly(nylon6-g-4(5)-VIm)-AgNPs

4.5.3 Antimicrobial activity evaluation

The antimicrobial activity of the grafted electrospun nylon 6 nanofibers was evaluated using the dynamic shake flask test method (ASTM E2149-10). The antimicrobial activity of the grafted electrospun nanofibers was evaluated against one Gram-negative bacterial strain (*E. coli*) and one Gram-positive bacterial strain (*S. aureus*). Table 4.8 presents the data of the percentage reduction of the growth of *E. coli* and *S. aureus* after treatment with grafted electrospun nanofibers.

Table 4.8. Percentage reduction data for grafted electrospun nylon 6 nanofibers

Materials tested	**Reduction (%)**	
	E. coli	*S.aureus*
Poly(nylon 6-g-1-VIm)	99.98(±0.02)	99.93(±0.04)
Poly(nylon 6-g-1-VImCH_2OH)	99.97(±0.01)	99.55(±0.24)
Poly(nylon 6-g-1-VImCOOH)	99.94(±0.09)	99.98(±0.19)
Poly(nylon 6-g-4(5)-VIm)	99.99(±0.01)	99.94(±0.08)
Poly(nylon 6-g-1-VIm)-AgNPs	99.99(±0.00)	99.99(±0.02)
Poly(nylon 6-g-4(5)-VIm)-AgNPs	99.99(±0.00)	99.99(±0.03)

From the results that were obtained, it was observed that all the grafted electrospun nanofibers demonstrated excellent antimicrobial activity (Table 4.8). The percentage reduction of the growth of *E. coli* and *S. aureus* in water was in the range 99.93-99.99% and 99.94-99.99%, respectively. However, it was surprising to see that the electrospun nylon 6 nanofibers that were grafted with 1-VImCOOH and 1-VImCH_2OH displayed relatively low percentage reduction for *E. coli* and *S. aureus*, respectively. The discrepancy could be attributed to some experimental errors. The fact that the electrospun nylon 6 nanofibers grafted with 1-VIm and 4(5)-VIm displayed reduction in the growth of both *E. coli* and *S. aureus* was not surprising. For instance, the antimicrobial activity of *N*-vinylimidazole grafted polymers was reported by other researchers.[118-120] The AgNPs-adsorbed grafted electrospun nylon nanofibers displayed the highest percentage reduction of the bacterial growth for both strains. The result was infact expected because the activity was due to both the grafted nanofibers and the AgNPs that were adsorbed on the surface. Figure 4.32 illustrates growth reduction of *E. coli* and *S. aureus* after contact with antimicrobial electrospun nanofibers.

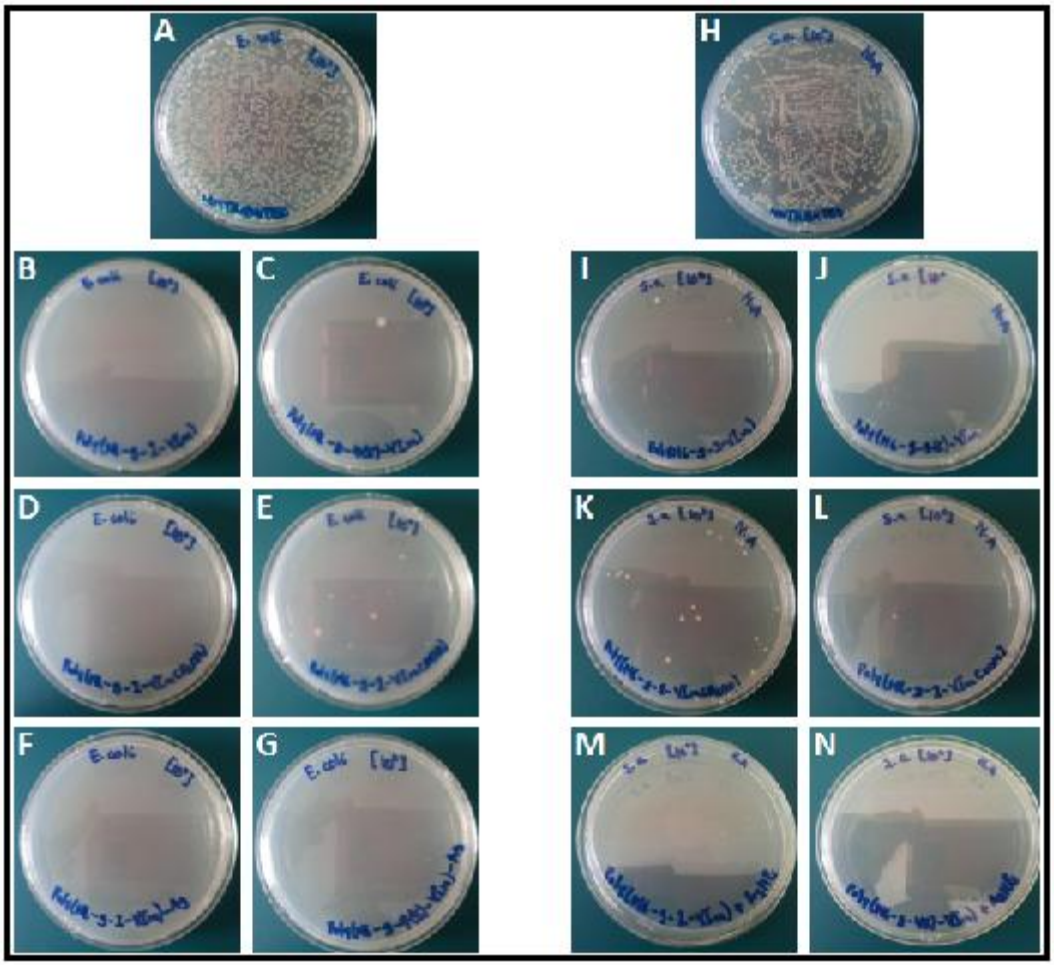

Figure 4.32. Growth of bacteria after contact with grafted electrospun nylon 6 nanofibers; *E. coli*: (A) Untreated, (B-G) contact time = 1 h and *S. aureus*: (H) Untreated, (I-N) contact time = 1 h

According to the WHO guidelines for the quality of drinking water, there should be no more than zero bacteria per 100 milliliter of water.[7] These quality standards could be achieved in water treatment plants, by various traditional methods through the reduction of microbial growth. The maximum log reduction values (LRV) achieved by the membrane filtration method were $\log_{10}(>6.5)$ [>99.9%] for viruses and $\log_{10}(>7)$ [>99.9%]for bacteria and protozoa.[7] These data clearly indicated that the performance of electrospun nylon 6 nanofibers grafted with the vinylimidazole derivatives was equivalent to that required for membrane filtration.

It could be concluded from the obtained results that immobilization of the 2-substituted vinylimidazoles, using the graft polymerization technique, did not negatively affect their antimicrobial activity. Moreover, the grafted electrospun nanofibers have a potential to be used repeatedly since the antimicrobial active moieties are immobilized on the surface. Therefore, the possibility of leaching during water application was eliminated completely.

However, the toxicity of the nanofibers was another factor that needed to be investigated to assess their impact on humans when the nanofiber strands are dislodged into water during treatment, and when they are disposed in the environment.

4.5.4 Cytotoxicty studies

The cytotoxic effects of free 2-substituted *N*-alkylimidazoles, electrospun nylon 6 nanofibers incorporated with 2-substituted *N*-alkylimidazoles and electrospun nylon 6 nanofibers grafted with 2-substituted vinylimidazoles were evaluated on the Chang liver cells. The liver cells were chosen since the liver is the organ where the effects of cytotoxic molecules that enter the human body are manifested. Table 4.9 presents the IC_{50} values obtained from the cytotoxicity experiments.

Table 4.9. IC_{50} values for the tested compounds and nanofibers

Test compound or material	Concentration (µg/mL & μ M)
N-Decylimidazole-2-carboxaldehyde (**1g**)	13.80 (5.84 x 10^{-5})
Complex **C7**	10.91 (1.87 x 10^{-5})
Poly(nylon6-g-1-VIm)	25.12*
Poly(nylon6-g-1-VImCH_2OH)	26.81*
Poly(nylon6-g-4(5)-VIm)	23.48*
Nylon 6	33.20*

(*) represents the mass of nanofiber per mL of cell culture medium

The cytotoxicity effect of a compound is indicated by the IC_{50} values, the concentration required to inhibit the growth of cells by 50%. A smaller IC_{50} value indicates that the test compound has a stronger affinity for the cell receptors and thus possesses more cytotoxicity.[355] *N*-Decylimidazole-2-carboxaldehyde (**1g**) and the silver(I) complex **C7** exhibited the lowest IC_{50} values (Table 6.2) indicating that they could have more cytotoxic effects to humans cells. The grafted electrospun nylon 6 nanofibers [poly(nylon6-g-1-VIm), poly(nylon6-g-1-VImCH_2OH) and poly(nylon6-g-4(5)-VIm)] exhibited higher IC_{50} values which indicated that they could be less toxic than the free imidazoles and silver(I) complexes.

Electrospun nylon 6 nanofibers displayed the least IC_{50} values which implied the lowest cytotoxic effect.

Many studies have reported the cytotoxic effects of imidazole derivatives against various human cell lines.[356-360] Assadieskandar *et al*.[360] considered their imidazole derivatives to be highly cytotoxic against various human cell lines with the following IC_{50} values; HT-29 (0.18- >50 μM); MCF-7 (0.40-22.90 μM); NIH-3T3 (0.02- >50 μM) and AGS (0.04-48.43 μM). The IC_{50} values for imidazole derivatives against K562 (140-220 μM) and CEM cells (210-245 μM) were considered to be moderate.[356] In comparison, the IC_{50} values displayed by decImCHO (5.84×10^{-5} μM) and Ag-decImCH_2OH (1.87×10^{-5} μM) were significantly lower and could be considered to be potentially cytotoxic to the humans.

The cytotoxicity results implied that application of biocides incorporated electrospun nanofibers in drinking water could have adverse effects to human health because of leaching. On the other hand grafted electrospun nanofibers would have less adverse effects to human health. Thus, immobilization of biocides for antimicrobial applications in drinking water should be the method of choice for the functionalization of nanofibers. Another added advantage is the possibility of re-usability of the electrospun nanofibers.

4.6 Reusability evaluation

To evaluate the reusability of the electrospun nylon 6 nanofibers grafted with vinylimidazoles, the nanofibers were recovered, after being used, by washing with ethanol and sterilization in an autoclave. The results showed that the grafted nanofibers could be used twice without any significant loss of the antibacterial activity (Fig. 33).

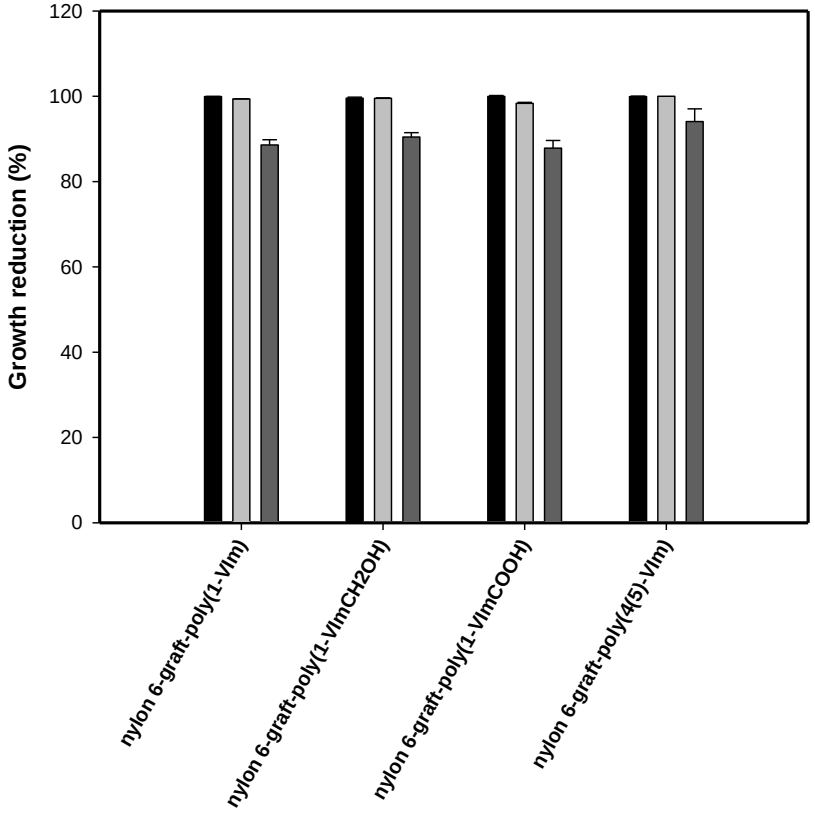

Figure 4.33. Evaluation of the reusability of the grafted electrospun nylon 6 nanofibers

However, after using for the third time, there was a significant loss of antibacterial activity (5-11%) observed for all the materials. Further investigations need to be performed to establish the reasons for the loss of activity of the grafted nylon 6 nanofibers. A possible reason could be biofouling as a result the bacteria trapped on the nanofibers.

CONCLUSIONS

AND

FUTURE WORK

CHAPTER 5 CONCLUSIONS AND FUTURE WORK

5.1 Conclusions

The thesis presented the development of antimicrobial electrospun nylon 6 nanofibers, functionalized with 2-substituted *N*-alkylimidazole derivatives and their silver(I) complexes, for the control of pathogenic microorganisms in drinking water. The 2-substituted *N*-alkylimidazole derivatives were synthesized by varying the alkyl chain length at the 1-position and the substituents at the 2-position. The effect of the alkyl chain length and the pK_a of the substituent at the 2-position on the antimicrobial activity was evaluated. It was observed that the antimicrobial activity increased with the increasing alkyl chain length as well as the decreasing pK_a of the substituent at the 2-position of the imidazole moiety. The carboxylic acid (COOH) substituent (with the lowest pK_a value) displayed the best antimicrobial properties of all the substituents. It was also observed that the antimicrobial activity was predominantly against Gram-positive bacterial strains (*S. aureus* and *B. subtilis* subsp. *spizizenii*), with *B. subtilis* subsp. *spizizenii* being the more susceptible to the biocides.

The silver(I) complexes containing 2-hydroxymethyl-*N*-alkylimidazoles exhibited a broad spectrum antimicrobial activity against all the microorganisms used (*E. coli*, *S. aureus*, *B. subtilis* subsp. *spizizenii* and *C. albicans*). Furthermore, it was observed that against *E. coli* and *C. albicans*, the antimicrobial activity of silver(I) complexes containing 2-hydroxymethyl-*N*-alkylimidazoles was solely due to silver(I) ions. On the other hand, the antimicrobial activity of silver(I) complexes containing 2-hydroxymethyl-*N*-alkylimidazoles with longer alkyl chains was due to both the silver(I) ions and the imidazole derivatives against *S. aureus* and *B. subtilis* subsp. *spizizenii*.

The study also demonstrated that the antimicrobial activity of the 2-substituted *N*-alkylimidazoles was not affected when they were incorporated into electrospun nylon 6 nanofibers as solid support materials. It was observed that the antimicrobial activity of the electrospun nylon 6 nanofibers followed the same trends as those observed when evaluating the antimicrobial activity of the free 2-substituted *N*-alkylimidazoles. The carboxylic acid derivatives still displayed the best antimicrobial properties and the antimicrobial activity remained predominantly against Gram-positive bacterial strains. *Bacillus subtilis* subsp. *spizizenii* remained the most susceptible bacterium.

The study demonstrated that the antimicrobial activity of the silver(I) complexes was affected when they were incorporated into electrospun nylon 6 nanofibers. It was observed that the method for evaluating the antimicrobial activity of the electrospun nylon 6 nanofibers incorporated with silver(I) complexes was very critical. For instance, the AATCC Test Method 100-2004 displayed a remarkable decrease in the antimicrobial activity of the silver complexes. The decrease was attributable to a lack of diffusibility of the siver(I) complexes. However, changing to the dynamic shake flask method (ASTM E2149-10) showed a huge improvement in the antimicrobial activity. The improvement in the antimicrobial activity was attributed to the increased diffusibility of the silver complexes.

The thesis demonstrated that immobilization of the 2-substituted *N*-vinylimidazoles onto the surface of electrospun nylon 6 nanofibers using graft polymerization also did not affect the antimicrobial activity. The grafted electrospun nylon 6 nanofibers displayed excellent percentage growth reduction of *E. coli* and *S. aureus*. The grafted electrospun nylon 6 nanofibers also displayed lower cytotoxicity effect compared to the free 2-substituted *N*-alkylimidazoles and the silver(I) complexes. Thus, the development of functionalized electrospun nanofibers was achieved by the incorporation and the immobilization strategies. The functionalized electrospun nylon 6 nanofibers displayed a potential to be used to control pathogenic microorganisms in drinking water.

5.2 Future work

It would make an interesting study to revisit the graft polymerization of 1-alkyl-4(5)-vinylimidazoles using stronger radical initiating techniques such as gamma irradiation, electron beam or plasma treatment. It could be that the reason for the difficulty to graft the 1-alkyl-4(5)-vinylimidazoles was the lower energy of ultraviolet rays. Immobilization of biocides onto the surface of electrospun nylon 6 nanofibers opens up the prospect of reusability of the nanofibers. Hence, it could also be very interesting to perform reusability experiments for the antimicrobial activity of the grafted electrospun nylon 6 nanofibers that were developed. Investigation of how the surface morphology (porosity) of the electrospun nylon 6 nanofibers could be affected by immobilization of 2-substituted vinylimidazoles would be very important in deciding on the mode of application (e.g. filtration or immersion) of the grafted electroslpun nylon 6 nanofibers in drinking water.

REFERENCES

(1) Macler, B. A.; Merkle, J. C.: Current knowledge on groundwater microbial pathogens and their control. *Hydrogeology Journal* **2000**, *8*, 29-40.

(2) Keevil, C. W.; Mackerness, C. W.; Colbourne, J. S.: Biocide treatment of biofilms. *International Biodeterioration* **1990**, *26*, 169-179.

(3) O'Toole, G.; Kaplan, H. B.; Kolter, R.: Biofilm formation as microbial development. *Annual Review of Microbiology* **2000**, *54*, 49-79.

(4) Parsek, M. R.; Singh, P. K.: Bacterial Biofilms: An emerging link to disease pathogenesis. *Annual Review of Microbiology* **2003**, *57*, 677-701.

(5) Simões, M.; Simões, L. C.; Vieira, M. J.: Species association increases biofilm resistance to chemical and mechanical treatments. *Water Research* **2009**, *43*, 229-237.

(6) Souter, P. F., Cruickshank, G. D., Tankerville, M. Z., Keswick, B. H., Ellis, B. D., Langworthy, D. E., Metz, K. A., Appleby, M. R., Hamilton, N., Jones, J. D. Perry, J. D.: Evaluation of a new water treatment for point-of-use household applications to remove microorganisms and arsenic from drinking water. *Journal of Water and Health* **2003**, *1*, 73-84.

(7) "Guidelines for drinking-water quality," World Health Organization: Recommendations, 2006.

(8) " Promotion of Household water treatment and safe storage in UNICEF wash programmes," 2008.

(9) http://www.mrwa.com/OP-coagulation.pdf; Vol. 2012. Date accessed: 22 November 2012.

(10) http:/www.iwawaterwiki.org/xwiki/bin/export/Articles/CoagulationandFlocculationinwaterandwastewater; Vol. 2012. Date accessed: 23 December 2012.

(11) Betancourt, W. Q.; Rose, J. B.: Drinking water treatment processes for removal of *Cryptosporidium* and *Giardia*. *Veterinary Parasitology* **2004**, *126*, 219-234.

(12) http://www.nzdl.org; Vol. 2012. Date accessed: 23 December 2012.

(13) Foster, H. D.: How aluminum causes Alzheimer's disease: The implications for prevention and treatment of Foster's multiple antagonist hypothesis. *Journal of Orthomolecular Medicine* **2000**, *15*, 21-51.

(14) Doll, R.: Review: Alzheimer's disease and environmental aluminium. *Age and Ageing* **1993**, *22*, 138-153.

(15) Epstein, S. G.: Human exposure to aluminum. *Environmental Geochemistry and Health* **1990**, *12*, 65-70.

(16) Schlesinger, A.; Eisenstadt, D.; Bar-Gil, A.; Carmely, H.; Einbinder, S.; Gressel, J.: Inexpensive non-toxic flocculation of microalgae contradicts theories; overcoming a major hurdle to bulk algal production. *Biotechnology Advances* **2012**, *30*, 1023-1030.

(17) Clasen, T.; McLaughlin, C.; Nayaar, N.; Boisson, S.; Gupta, R.; Desai, D.; Shah, N.: Microbiological effectiveness and cost of disinfecting water by boiling in semi-urban India. *The American Journal of Tropical Medicine and Hygiene* **2008**, *79*, 407-413.

(18) Rosa, G.; Miller, L.; Clasen, T.: Microbiological effectiveness of disinfecting water by boiling in rural Guatemala. *The American Journal of Tropical Medicine and Hygiene* **2010**, *82*, 473-477.

(19) http://www.dwaf.gov.za/Documents/Other/DWQM/DisinfectionPamphletJul05.pdf; Vol. 2012. Date accessed: 27 November 2012.

(20) Boorman, G. A., Dellarco, V., Dunnick, J. K., Chapin, R. E., Hunter, S., Hauchman, F., Gardner, H., Cox, M., Sills, R. C.,: Drinking water disinfection by-products: Review and approach to toxicity evaluation. *Environmental Health Perspectives* **1999**, *107*, 207-217.

(21) http://www.doh.wa.gov/Portals/1/Documents/Pubs/331-253.pdf; Vol. 2012. Date accessed: 27 November 2012.

(22) http://www.who.int/water_sanitation_health/publications/2011/tn11_chlorine_levels_en.pdf; Vol. 2013. Date accessed: 27 November 2012.

(23) Restaino, L., Frampton, E. W., Hemphill, J. B., Palnikar, P.,: Efficacy of ozonated water against various food-related microorganisms. *Applied Environmental Microbiology* **1995**, *61*, 3471-3475.

(24) Lee, J.; Deininger, R. A.: Survival of bacteria after ozonation. *Ozone: Science & Engineering* **2000**, *22*, 65-75.

(25) Hijnen, W. A. M.; Beerendonk, E. F.; Medema, G. J.: Inactivation credit of UV radiation for viruses, bacteria and protozoan (oo)cysts in water: A review. *Water Research* **2006**, *40*, 3-22.

(26) Hassen, A.; Mahrouk, M.; Ouzari, H.; Cherif, M.; Boudabous, A.; Damelincourt, J. J.: UV disinfection of treated wastewater in a large-scale pilot plant and inactivation of selected bacteria in a laboratory UV device. *Bioresource Technology* **2000**, *74*, 141-150.

(27) Khadre, M. A.; Yousef, A. E.; Kim, J. G.: Microbiological aspects of ozone applications in food: A review. *Journal of Food Science* **2001**, *66*, 1242-1252.

(28) http://www.kochmembrane.com/sep_uf.html. Date accessed: 23 December 2012.

(29) Gitis, V.: Rapid sand filtration of Cryptosporidium parvum: effects of media depth and coagulation. *Water Science & Technology: Water Supply* **2008**, *8*, 129-134.

(30) Arndt, R. E.; Wagner, E. J.: Rapid and slow sand filtration techniques and their efficacy at filtering triactinomyxons of *Myxobolus cerebralis* from contaminated water. *North American Journal of Aquaculture* **2004**, *66*, 261-270.

(31) Šostar-Turk, S.; Petrinić, I.; Simonič, M.: Laundry wastewater treatment using coagulation and membrane filtration. *Resources, Conservation and Recycling* **2005**, *44*, 185-196.

(32) Zhou, H.; Smith, D. W.: Advanced technologies in water and wastewater treatment. *Canadian Journal of Civil Engineering* **2001**, *28*, 49-66.

(33) Maartens, A.; Swart, P.; Jacobs, E. P.: Feed-water pretreatment: methods to reduce membrane fouling by natural organic matter. *Journal of Membrane Science* **1999**, *163*, 51-62.

(34) Hilal, N.; Ogunbiyi, O. O.; Miles, N. J.; Nigmatullin, R.: Methods employed for control of fouling in MF and UF membranes: A comprehensive review. *Separation Science and Technology* **2005**, *40*, 1957-2005.

(35) Ramakrishna, S.; Jose, R.; Archana, P. S.; Nair, A. S.; Balamurugan, R.; Venugopal, J.; Teo, W. E.: Science and engineering of electrospun nanofibers for advances in clean energy, water filtration, and regenerative medicine. *Journal of Materials Science* **2010**, *45*, 6283-6312.

(36) Gopal, R.; Kaur, S.; Ma, Z.; Chan, C.; Ramakrishna, S.; Matsuura, T.: Electrospun nanofibrous filtration membrane. *Journal of Membrane Science* **2006**, *281*, 581-586.

(37) Au, H.; Pham, L.; Vu, T.; Park, J.: Fabrication of an antibacterial non-woven mat of a poly(lactic acid)/chitosan blend by electrospinning. *Macromolecular Research* **2012**, *20*, 51-58.

(38) Desai, K.; Kit, K.; Li, J.; Michael Davidson, P.; Zivanovic, S.; Meyer, H.: Nanofibrous chitosan non-wovens for filtration applications. *Polymer* **2009**, *50*, 3661-3669.

(39) Yoon, K.; Kim, K.; Wang, X.; Fang, D.; Hsiao, B. S.; Chu, B.: High flux ultrafiltration membranes based on electrospun nanofibrous PAN scaffolds and chitosan coating. *Polymer* **2006**, *47*, 2434-2441.

(40) Ma, H.; Burger, C.; Hsiao, B. S.; Chu, B.: Ultra-fine cellulose nanofibers: new nano-scale materials for water purification. *Journal of Materials Chemistry* **2011**, *21*, 7507-7510.

(41) Ma, H.; Burger, C.; Hsiao, B. S.; Chu, B.: Ultrafine polysaccharide nanofibrous membranes for water purification. *Biomacromolecules* **2011**, *12*, 970-976.

(42) Das, S., Hollister, S. J., Flanagan, C., Adewunmi, A., Bark, K., Chen, C., Ramaswamy, K.,; Rose, D., Widjaja, E.,: Freeform fabrication of nylon 6 tissue engineering scaffolds. *Rapid Prototyping Journal* **2003**, *9*, 43-49.

(43) Ryu, Y. J.; Kim, H. Y.; Lee, K. H.; Park, H. C.; Lee, D. R.: Transport properties of electrospun nylon 6 nonwoven mats. *European Polymer Journal* **2003**, *39*, 1883-1889.

(44) Ma, Y.; Zhou, T.; Zhao, C.: Preparation of chitosan–nylon 6 blended membranes containing silver ions as antibacterial materials. *Carbohydrate Research* **2008**, *343*, 230-237.

(45) Shalaby, S. E.; Al-Balakocy, N. G.; Abdel-Fatah, O. M.; Elshafei, A. M.: Antimicrobial finishing of regular and modified nylon 6 fabrics. *Journal of Applied Polymer Science* **2008**, *110*, 738-746.

(46) Shalaby, S. E.; Al-Balakocy, N. G.; Abo El-Ola, S. M.: Surface modification of nylon 6 fibers for medical applications. *Journal of Applied Polymer Science* **2007**, *104*, 3788-3796.

(47) Sherrill, J.; Michielsen, S.; Stojiljkovic, I.: Grafting of light-activated antimicrobial materials to nylon films. *Journal of Polymer Science, Part A: Polymer Chemistry* **2002**, *41*, 41-47.

(48) Park, S. W.; Bae, H. S.; Xing, Z. C.; Kwon, O. H.; Huh, M. W.; Kang, I. K.: Preparation and properties of silver-containing nylon 6 nanofibers formed by electrospinning. *Journal of Applied Polymer Science* **2009**, *112*, 2320-2326.

(49) El-Newehy, M. H.; Al-Deyab, S. S.; Kenawy, E. R.; Abdel-Megeed, A.: Nanospider technology for the production of nylon 6 nanofibers for biomedical applications. *Journal of Nanomaterials* **2011**, *2011*.

(50) Shi, Q.; Vitchuli, N.; Nowak, J.; Noar, J.; Caldwell, J. M.; Breidt, F.; Bourham, M.; McCord, M.; Zhang, X.: One-step synthesis of silver nanoparticle-filled nylon 6 nanofibers and their antibacterial properties. *Journal of Materials Chemistry* **2011**, *21*, 10330-10335.

(51) de Vrieze, S.; Daels, N.; Lambert, K.; Decostere, B.; Hens, Z.; van Hulle, S.; de Clerck, K.: Filtration performance of electrospun polyamide nanofibres loaded with bactericides. *Textile Research Journal* **2012**, *82*, 37-44.

(52) Montazer, M.; Malekzadeh, S. B.: Electrospun antibacterial nylon nanofibers through *in situ* synthesis of nanosilver: Preparation and characteristics. *Journal of Polymer Research* **2012**, *19*, 9980.

(53) Pant, B.; Pant, H. R.; Pandeya, D. R.; Panthi, G.; Nam, K. T.; Hong, S. T.; Kim, C. S.; Kim, H. Y.: Characterization and antibacterial properties of AgNPs loaded nylon 6 nanocomposite prepared by one-step electrospinning process. *Colloids and Surfaces A: Physicochemical and Engineering Aspects* **2012**, *395*, 94-99.

(54) Vitchuli, N.; Shi, Q.; Nowak, J.; Kay, K.; Caldwell, J. M.; Breidt, F.; Bourham, M.; McCord, M.; Zhang, X.: Multifunctional ZnO/Nylon6 nanofiber mats by an electrospinning- electrospraying hybrid process for use in protective applications. *Science and Technology of Advanced Materials* **2011**, *12*, 055005.

(55) Pant, H. R.; Bajgai, M. P.; Nam, K. T.; Chu, K. H.; Park, S.-J.; Kim, H. Y.: Formation of electrospun nylon 6/methoxy poly(ethylene glycol) oligomer spider-wave nanofibers. *Materials Letters* **2010**, *64*, 2087-2090.

(56) Heikkilä, P.; Harlin, A.: Parameter study of electrospinning of polyamide 6. *European Polymer Journal* **2008**, *44*, 3067-3079.

(57) *Textbook of Polymer science*: 3rd ed.; Billmayer, F. W., Ed.; Wiley & Sons: New York, 1984.

(58) Jeong, E. H.; Yang, J.; Youk, J. H.: Preparation of polyurethane cationomer nanofiber mats for use in antimicrobial nanofilter applications. *Materials Letters* **2007**, *61*, 3991-3994.

(59) Franklin, N. M.; Rogers, N. J.; Apte, S. C.; Batley, G. E.; Gadd, G. E.; Casey, P. S.: Comparative toxicity of nanoparticulate ZnO, Bulk ZnO, and $ZnCl_2$ to a freshwater microalga (*Pseudokirchneriella subcapitata*): The importance of particle solubility. *Environmental Science & Technology* **2007**, *41*, 8484-8490.

(60) Alrousan, D. M. A.; Dunlop, P. S. M.; McMurray, T. A.; Byrne, J. A.: Photocatalytic inactivation of *E. coli* in surface water using immobilised nanoparticle TiO_2 films. *Water Research* **2009**, *43*, 47-54.

(61) Lala, N. L., Ramaseshan, R., Bojun, L., Sundarrajan, Barhate, R. S., Liu, Y.-J., Ramakrishna, S.: Fabrication of nanofibers with antimicrobial functionality used as

filters: Protection against bacterial contaminants. *Biotechnology and Bioengineering* **2007**, *97*, 1357-1365.

(62) Dasari, A.; Quirós, J.; Herrero, B.; Boltes, K.; García-Calvo, E.; Rosal, R.: Antifouling membranes prepared by electrospinning poly(lactic acid) containing biocidal nanoparticles. *Journal of Membrane Science* **2012**, *405–406*, 134-140.

(63) Gule, N. P.; Bshena, O.; De Kwaadsteniet, M.; Cloete, T. E.; Klumperman, B.: Immobilized furanone derivatives as inhibitors for adhesion of bacteria on modified poly(styrene- co -maleic anhydride). *Biomacromolecules* **2012**, *13*, 3138-3150.

(64) Gule, N. P.; De Kwaadsteniet, M.; Cloete, T. E.; Klumperman, B.: Electrospun poly(vinyl alcohol) nanofibres with biocidal additives for application in filter media, 2-antimicrobial activity, regeneration, leaching and water stability. *Macromolecular Materials and Engineering* **2012**, *297*, 618-626.

(65) Gule, N. P.; De Kwaadsteniet, M.; Cloete, T. E.; Klumperman, B.: Electrospun poly(vinyl alcohol) nanofibres with biocidal additives for application in filter media, 1-properties affecting fibre morphology and characterisation. *Macromolecular Materials and Engineering* **2012**, *297*, 609-617.

(66) Congiu, C.; Cocco, M. T.; Onnis, V.: Design, synthesis, and *in vitro* antitumor activity of new 1,4-diarylimidazole-2-ones and their 2-thione analogues. *Bioorganic & Medicinal Chemistry Letters* **2008**, *18*, 989-993.

(67) Khabnadideh, S.; Rezaei, Z.; Khalafi-Nezhad, A.; Bahrinajafi, R.; Mohamadi, R.; Farrokhroz, A. A.: Synthesis of *N*-Alkylated derivatives of imidazole as antibacterial agents. *Bioorganic & Medicinal Chemistry Letters* **2003**, *13*, 2863-2865.

(68) Goker, H.; Ertan, R.; Akgun, H.; Yulug, N.: Synthesis and antifungal activity of some new benzimidazole derivatives. *Archiv der Pharmazie* **1991**, *324*, 283-286.

(69) Samant, B. S.; Sukhthankar, M. G.: Compounds containing 2-substituted imidazole ring for treatment against human African *trypanosomiasis*. *Bioorganic & Medicinal Chemistry Letters* **2011**, *21*, 1015-1018.

(70) Crane, L.; Anastassiadou, M.; Hage, S. E.; Stigliani, J. L.; Baziard-Mouysset, G.; Payard, M.; Leger, J. M.; Bizot-Espiard, J.-G.; Ktorza, A.; Caignard, D.-H.; Renard, P.: Design and synthesis of novel imidazoline derivatives with potent antihyperglycemic activity in a rat model of type 2 diabetes. *Bioorganic & Medicinal Chemistry* **2006**, *14*, 7419-7433.

(71) Woolley, D. W.: Some biological effects produced by benzimidazole and their reversal by purines. *Journal of Biological Chemistry* **1944**, *152*, 225-232.

(72) Antolini, M.; Bozzoli, A.; Ghiron, C.; Kennedy, G.; Rossi, T.; Ursini, A.: Analogues of 4,5-*bis*(3,5-dichlorophenyl)-2-trifluoromethyl-1H-imidazole as potential antibacterial agents. *Bioorganic & Medicinal Chemistry Letters* **1999**, *9*, 1023-1028.

(73) Khan, N.; Soni, L.; Gupta, A.; Wakode, S.; Wagh, R.; Kaskhedikar, S.: QSAR analysis of *N*-alkyl imidazole analogues as antibacterial agents. *Indian Journal of Pharmaceutical Sciences* **2006**, *68*, 341-346.

(74) Sheehan, D. J.; Hitchcock, C. A.; Sibley, C. M.: Current and emerging azole antifungal agents. *Clinical Microbiology Reviews* **1999**, *12*, 40-79.

(75) White, T. C.; Marr, K. A.; Bowden, R. A.: Clinical, cellular, and molecular factors that contribute to antifungal drug resistance. *Clinical Microbiology Reviews* **1998**, *11*, 382-402.

(76) Rostom, S. A. F.; Ashour, H. M. A.; Razik, H. A. A. E.; Fattah, A. E. F. H. A. E.; El-Din, N. N.: Azole antimicrobial pharmacophore-based tetrazoles: Synthesis and biological evaluation as potential antimicrobial and anticonvulsant agents. *Bioorganic & Medicinal Chemistry* **2009**, *17*, 2410-2422.

(77) Sharma, S.; Gangal, S.; Rauf, A.: Convenient one-pot synthesis of novel 2-substituted benzimidazoles, tetrahydrobenzimidazoles and imidazoles and evaluation of their *in vitro* antibacterial and antifungal activities. *European Journal of Medicinal Chemistry* **2009**, *44*, 1751-1757.

(78) Klasen, H. J.: Historical review of the use of silver in the treatment of burns. I. Early uses. *Burns* **2000**, *26*, 117-130.

(79) Lansdown, A. B.: Silver. I: Its antibacterial properties and mechanism of action. *Journal of wound care* **2002**, *11*, 125-130.

(80) Li, W. R.; Xie, X. B.; Shi, Q. S.; Zeng, H. Y.; Ou-Yang, Y. S.; Chen, Y. B.: Antibacterial activity and mechanism of silver nanoparticles on *Escherichia coli*. *Applied Microbiology and Biotechnology* **2010**, *85*, 1115-1122.

(81) Radheshkumar, C.; Münstedt, H.: Antimicrobial polymers from polypropylene/silver composites—Ag+ release measured by anode stripping voltammetry. *Reactive and Functional Polymers* **2006**, *66*, 780-788.

(82) http://www.silversinus.com/historical-current-antimicrobial-uses-silver.html.; Vol. 2012. Date accessed: 29 December 2012.

(83) Silvestry-Rodriguez, N.; Sicairos-Ruelas, E. E.; Gerba, C. P.; Bright, K. R.: Silver as a disinfectant. 2007; Vol. 191; pp 23-45.

(84) Klueh, U.; Wagner, V.; Kelly, S.; Johnson, A.; Bryers, J. D.: Efficacy of silver-coated fabric to prevent bacterial colonization and subsequent device-based biofilm formation. *Journal of Biomedical Materials Research* **2000**, *53*, 621-631.

(85) Lok, C. N.; Ho, C. M.; Chen, R.; He, Q. Y.; Yu, W. Y.; Sun, H.; Tam, P. K. H.; Chiu, J. F.; Che, C. M.: Silver nanoparticles: Partial oxidation and antibacterial activities. *Journal of Biological Inorganic Chemistry* **2007**, *12*, 527-534.

(86) Guggenbichler, J. P.; Böswald, M.; Lugauer, S.; Krall, T.: A new technology of microdispersed silver in polyurethane induces antimicrobial activity in central venous catheters. *Infection* **1999**, *27*, S16-S23.

(87) Davies, R. L.; Etris, S. F.: The development and functions of silver in water purification and disease control. *Catalysis Today* **1997**, *36*, 107-114.

(88) Carr, H. S.; Wlodkowski, T. J.; Rosenkranz, H. S.: Silver sulfadiazine: *in vitro* antibacterial activity. *Antimicrobial Agents and Chemotherapy* **1973**, *4*, 585-587.

(89) Rai, M.; Yadav, A.; Gade, A.: Silver nanoparticles as a new generation of antimicrobials. *Biotechnology Advances* **2009**, *27*, 76-83.

(90) Kazachenko, A. S.; Legler, A. V.; Per'yanova, O. V.; Vstavskaya, Y. A.: Synthesis and antimicrobial activity of silver complexes with histidine and tryptophan. *Pharmaceutical Chemistry Journal* **2000**, *34*, 257-258.

(91) Abu-Youssef, M. A. M.; Dey, R.; Gohar, Y.; Massoud, A. a. A.; Öhrström, L.; Langer, V.: Synthesis and structure of silver complexes with nicotinate-type ligands having antibacterial activities against clinically isolated antibiotic resistant pathogens. *Inorganic Chemistry* **2007**, *46*, 5893-5903.

(92) Ruan, B.; Tian, Y.; Zhou, H.; Wu, J.; Liu, Z.; Zhu, C.; Yang, J.; Zhu, H.: Synthesis, crystal structure and *in vitro* antibacterial activity of two novel silver(I) complexes. *Journal of Organometallic Chemistry* **2009**, *694*, 2883-2887.

(93) Li, Y.; Dong, X.; Gou, Y.; Jiang, Z.; Zhu, H.-L.: Synthesis, characterization, and antibacterial activity of two silver(I) compounds with 4-dimethylaminopyridine. *Journal of Coordination Chemistry* **2011**, *64*, 1663-1672.

(94) Pandurangan, K.; Gallagher, S.; Morgan, G. G.; Muller-Bunz, H.; Paradisi, F.: Structure and antibacterial activity of the silver(I) complex of 2-aminophenoxazine-3-one. *Metallomics* **2010**, *2*, 530-534.

(95) Nemati Kharat, A.; Bakhoda, A.; Foroutannejad, S.; Foroutannejad, C.: Molecular structure and antimicrobial activity of a luminescent dinuclear silver(I) complex of

phenyl-bis(2-pyridyl)phosphine. *Zeitschrift fur Anorganische und Allgemeine Chemie* **2011**, *637*, 2260-2264.

(96) Nomiya, K.; Tsuda, K.; Sudoh, T.; Oda, M.: Ag(I)-N bond-containing compound showing wide spectra in effective antimicrobial activities: Polymeric silver(I) imidazolate. *Journal of Inorganic Biochemistry* **1997**, *68*, 39-44.

(97) Rowan, R.; Tallon, T.; Sheahan, A. M.; Curran, R.; McCann, M.; Kavanagh, K.; Devereux, M.; McKee, V.: 'Silver bullets' in antimicrobial chemotherapy: Synthesis, characterisation and biological screening of some new Ag(I)-containing imidazole complexes. *Polyhedron* **2006**, *25*, 1771-1778.

(98) Melaiye, A.; Sun, Z.; Hindi, K.; Milsted, A.; Ely, D.; Reneker, D. H.; Tessier, C. A.; Youngs, W. J.: Silver(I)−imidazole cyclophane *gem*-diol complexes encapsulated by electrospun tecophilic nanofibers: Formation of nanosilver particles and antimicrobial activity. *Journal of the American Chemical Society* **2005**, *127*, 2285-2291.

(99) Melaiye, A.; Simons, R. S.; Milsted, A.; Pingitore, F.; Wesdemiotis, C.; Tessier, C. A.; Youngs, W. J.: Formation of water-soluble pincer silver(I)−carbene complexes: A novel antimicrobial agent. *Journal of Medicinal Chemistry* **2004**, *47*, 973-977.

(100) Özdemir, İ.; Özcan, E. Ö.; Günal, S.; Gürbüz, N.: Synthesis and antimicrobial activity of novel Ag-N-heterocyclic carbene complexes. *Molecules* **2010**, *15*, 2499-2508.

(101) Patil, S.; Dietrich, K.; Deally, A.; Gleeson, B.; Müller-Bunz, H.; Paradisi, F.; Tacke, M.: Synthesis, cytotoxicity and antibacterial studies of novel symmetrically and nonsymmetrically 4-(methoxycarbonyl)benzyl-substituted *N*-heterocyclic carbene-silver acetate complexes. *Helvetica Chimica Acta* **2010**, *93*, 2347-2364.

(102) Abuskhuna, S.; Briody, J.; McCann, M.; Devereux, M.; Kavanagh, K.; Fontecha, J. B.; McKee, V.: Synthesis, structure and anti-fungal activity of dimeric Ag(I) complexes containing *bis*-imidazole ligands. *Polyhedron* **2004**, *23*, 1249-1255.

(103) Tan, K.; Obendorf, S. K.: Fabrication and evaluation of electrospun nanofibrous antimicrobial nylon 6 membranes. *Journal of Membrane Science* **2007**, *305*, 287-298.

(104) Sun, X., Zhang, L., Cao, Z., Deng, Y., Liu, L., Fong, H., Sun, Y.: Electrospun composite nanofiber fabrics containing uniformly dispersed antimicrobial agents as an innovative type of polymeric materials with superior antimicrobial efficacy. *Applied Materials & Interfaces* **2010**, *2*, 952-956.

(105) Kim, S. J.; Nam, Y. S.; Rhee, D. M.; Park, H.-S.; Park, W. H.: Preparation and characterization of antimicrobial polycarbonate nanofibrous membrane. *European Polymer Journal* **2007**, *43*, 3146-3152.

(106) Mei, Y.; Yao, C.; Fan, K.; Li, X.: Surface modification of polyacrylonitrile nanofibrous membranes with superior antibacterial and easy-cleaning properties through hydrophilic flexible spacers. *Journal of Membrane Science* **2012**, *417–418*, 20-27.

(107) Hilal, N.; Al-Khatib, L.; Atkin, B. P.; Kochkodan, V.; Potapchenko, N.: Photochemical modification of membrane surfaces for (bio)fouling reduction: a nano-scale study using AFM. *Desalination* **2003**, *158*, 65-72.

(108) Bhattacharya, A.; Misra, B. N.: Grafting: a versatile means to modify polymers: Techniques, factors and applications. *Progress in Polymer Science* **2004**, *29*, 767-814.

(109) *Polymer grafting and crosslinking*; Bhattacharya, A., Rawlins, J. W., Ray, P, Ed.; John Wiley & Sons, Inc. Publication: Hoboken, New Jersey, 2009.

(110) Mostafa, T. B.: Chemical modification of polypropylene fibers grafted vinyl imidazole/acrylonitrile copolymer prepared by gamma radiation and its possible use for the removal of some heavy metal ions. *Journal of Applied Polymer Science* **2009**, *111*, 11-18.

(111) Na, C. K.; Park, H. J.: Photoinduced cografting of vinyl benzyl trimethylammonium chloride and 2-hydroxyethyl methacrylate onto nylon nonwoven fabric for preparing an anion-exchange sorbent: Optimum cografting conditions and characterization. *Journal of Applied Polymer Science* **2010**, *116*, 2723-2733.

(112) Datta, P.; Chatterjee, J.; Dhara, S.: Electrospun nanofibers of a phosphorylated polymer—A bioinspired approach for bone graft applications. *Colloids and Surfaces B: Biointerfaces* **2012**, *94*, 177-183.

(113) Anjum, N.; Gulrez, S. K. H.; Singh, H.; Gupta, B.: Development of antimicrobial polypropylene sutures by graft polymerization. I. influence of grafting conditions and characterization. *Journal of Applied Polymer Science* **2006**, *101*, 3895-3901.

(114) Gupta, B.; Anjum, N.; Gulrez, S. K. H.; Singh, H.: Development of antimicrobial polypropylene sutures by graft copolymerization. II. Evaluation of physical properties, drug release, and antimicrobial activity. *Journal of Applied Polymer Science* **2007**, *103*, 3534-3538.

(115) Mokhtar, S. M.; Mostafa, T. B.; Hewedy, M. A.: Chemical induced grafting of indole onto chitin & chitosan - and their antimicrobial activity. *Australian Journal of Basic and Applied Sciences* **2010**, *4*, 3268-3279.

(116) Saad, G. R.; Elsawy, M. A.; Elsabee, M. Z.: Preparation, characterization and antimicrobial activity of poly(3-hydroxybutyrate-co-3-hydroxyvalerate)-g-poly(*N*-

vinylpyrrolidone) copolymers. *Polymer - Plastics Technology and Engineering* **2012**, *51*, 1113-1121.

(117) Torres-Giner, S.; Ocio, M. J.; Lagaron, J. M.: Novel antimicrobial ultrathin structures of zein/chitosan blends obtained by electrospinning. *Carbohydrate Polymers* **2009**, *77*, 261-266.

(118) Caner, H.; Yilmaz, E.; Yilmaz, O.: Synthesis, characterization and antibacterial activity of poly(*N*-vinylimidazole) grafted chitosan. *Carbohydrate Polymers* **2007**, *69*, 318-325.

(119) Sabaa, M. W.; Mohamed, N. A.; Mohamed, R. R.; Khalil, N. M.; Abd El Latif, S. M.: Synthesis, characterization and antimicrobial activity of poly (*N*-vinyl imidazole) grafted carboxymethyl chitosan. *Carbohydrate Polymers* **2010**, *79*, 998-1005.

(120) Chung, M. G.; Kim, H. W.; Kim, B. R.; Kim, Y. B.; Rhee, Y. H.: Biocompatibility and antimicrobial activity of poly(3-hydroxyoctanoate) grafted with vinylimidazole. *International Journal of Biological Macromolecules* **2012**, *50*, 310-316.

(121) Stoimenov, P. K.; Klinger, R. L.; Marchin, G. L.; Klabunde, K. J.: Metal Oxide Nanoparticles as Bactericidal Agents. *Langmuir* **2002**, *18*, 6679-6686.

(122) Jones, N.; Ray, B.; Ranjit, K. T.; Manna, A. C.: Antibacterial activity of ZnO nanoparticle suspensions on a broad spectrum of microorganisms. *FEMS Microbiology Letters* **2008**, *279*, 71-76.

(123) Yang, Y.; Zhang, C.; Hu, Z.: Impact of metallic and metal oxide nanoparticles on wastewater treatment and anaerobic digestion. *Environmental Science: Processes & Impacts* **2013**, *15*, 39-48.

(124) Wei, C.; Lin, W. Y.; Zainal, Z.; Williams, N. E.; Zhu, K.; Kruzic, A. P.; Smith, R. L.; Rajeshwar, K.: Bactericidal activity of TiO_2 photocatalyst in aqueous media: Toward a solar-assisted water disinfection system. *Environmental Science & Technology* **1994**, *28*, 934-938.

(125) Watts, R. J.; Kong, S.; Orr, M. P.; Miller, G. C.; Henry, B. E.: Photocatalytic inactivation of coliform bacteria and viruses in secondary wastewater effluent. *Water Research* **1995**, *29*, 95-100.

(126) Chong, M. N.; Jin, B.: Photocatalytic treatment of high concentration carbamazepine in synthetic hospital wastewater. *Journal of Hazardous Materials* **2012**, *199–200*, 135-142.

(127) Garg, K.; Bowlin, G. L.: Electrospinning jets and nanofibrous structures. *Biomicrofluidics* **2011**, *5*, 013403.

(128) Tucker, N.; Stanger, J. J.; Staiger, M. P.; Razzaq, H.; Hofman, K.: The history of the science and technology of electrospinning from 1600 to 1995. *Journal of Engineered Fibers and Fabrics* **2012**, *7*, 63-73.

(129) Bhardwaj, N.; Kundu, S. C.: Electrospinning: A fascinating fiber fabrication technique. *Biotechnology Advances* **2010**, *28*, 325-347.

(130) Hohman, M. M.; Shin, M.; Rutledge, G.; Brenner, M. P.: Electrospinning and electrically forced jets. I. Stability theory. *Physics of Fluids* **2001**, *13*, 2201-2220.

(131) Shin, Y. M.; Hohman, M. M.; Brenner, M. P.; Rutledge, G. C.: Electrospinning: A whipping fluid jet generates submicron polymer fibers. *Applied Physics Letters* **2001**, *78*, 1149-1151.

(132) Yarin, A. L.; Koombhongse, S.; Reneker, D. H.: Taylor cone and jetting from liquid droplets in electrospinning of nanofibers. *Journal of Applied Physics* **2001**, *90*, 4836-4846.

(133) Feng, J. J.: The stretching of an electrified non-Newtonian jet: A model for electrospinning. *Physics of Fluids* **2002**, *14*, 3912-3926.

(134) Feng, J. J.: Stretching of a straight electrically charged viscoelastic jet. *Journal of Non-Newtonian Fluid Mechanics* **2003**, *116*, 55-70.

(135) Ramakrishna, S.; Fujihara, K.; Teo, W.-E.; Lim, T.-C.; Ma, Z.: An Introduction to electrospinning and nanofibers. *World Scientific Publishing Co. Pte Ltd* **2005**.

(136) Kowalewski, T. A.; BŁoński, S.; Barral, S.: Experiments and modelling of electrospinning process. *Bulletin of the Polish Academy of Sciences: Technical Sciences* **2005**, *53*, 385-394.

(137) Teo, W. E.; Inai, R.; Ramakrishna, S.: Technological advances in electrospinning of nanofibers. *Science and Technology of Advanced Materials* **2011**, *12*, 013002.

(138) Koski, A.; Yim, K.; Shivkumar, S.: Effect of molecular weight on fibrous PVA produced by electrospinning. *Materials Letters* **2004**, *58*, 493-497.

(139) Gupta, P.; Elkins, C.; Long, T. E.; Wilkes, G. L.: Electrospinning of linear homopolymers of poly(methyl methacrylate): exploring relationships between fiber formation, viscosity, molecular weight and concentration in a good solvent. *Polymer* **2005**, *46*, 4799-4810.

(140) Shenoy, S. L.; Bates, W. D.; Frisch, H. L.; Wnek, G. E.: Role of chain entanglements on fiber formation during electrospinning of polymer solutions: good solvent, non-specific polymer–polymer interaction limit. *Polymer* **2005**, *46*, 3372-3384.

(141) Regev, O.; Vandebril, S.; Zussman, E.; Clasen, C.: The role of interfacial viscoelasticity in the stabilization of an electrospun jet. *Polymer* **2010**, *51*, 2611-2620.

(142) Mit-Uppatham, C.; Nithitanakul, M.; Supaphol, P.: Ultrafine electrospun polyamide 6 fibers: Effect of solution conditions on morphology and average fiber diameter. *Macromolecular Chemistry and Physics* **2004**, *205*, 2327-2338.

(143) Fong, H.; Chun, I.; Reneker, D. H.: Beaded nanofibers formed during electrospinning. *Polymer* **1999**, *40*, 4585-4592.

(144) Kriegel, C.; Kit, K. M.; McClements, D. J.; Weiss, J.: Influence of surfactant type and concentration on electrospinning of chitosan–poly(ethylene oxide) blend nanofibers. *Food Biophysics* **2009**, *4*, 213-228.

(145) Jia, L.; Qin, X.-h.: The effect of different surfactants on the electrospinning poly(vinyl alcohol) (PVA) nanofibers. *Journal of Thermal Analysis and Calorimetry* **2012**, 1-11.

(146) Uyar, T.; Besenbacher, F.: Electrospinning of uniform polystyrene fibers: The effect of solvent conductivity. *Polymer* **2008**, *49*, 5336-5343.

(147) Arayanarakul, K.; Choktaweesap, N.; Aht-ong, D.; Meechaisue, C.; Supaphol, P.: Effects of poly(ethylene glycol), inorganic salt, sodium dodecyl sulfate, and solvent system on electrospinning of poly(ethylene oxide). *Macromolecular Materials and Engineering* **2006**, *291*, 581-591.

(148) Keun Son, W.; Ho Youk, J.; Seung Lee, T.; Park, W. H.: Effect of pH on electrospinning of poly(vinyl alcohol). *Materials Letters* **2005**, *59*, 1571-1575.

(149) Vega-Lugo, A.-C.; Lim, L.-T.: Effects of poly(ethylene oxide) and pH on the electrospinning of whey protein isolate. *Journal of Polymer Science Part B: Polymer Physics* **2012**, *50*, 1188-1197.

(150) Jarusuwannapoom, T.; Hongrojjanawiwat, W.; Jitjaicham, S.; Wannatong, L.; Nithitanakul, M.; Pattamaprom, C.; Koombhongse, P.; Rangkupan, R.; Supaphol, P.: Effect of solvents on electrospinnability of polystyrene solutions and morphological appearance of resulting electrospun polystyrene fibers. *European Polymer Journal* **2005**, *41*, 409-421.

(151) Tan, S. H.; Inai, R.; Kotaki, M.; Ramakrishna, S.: Systematic parameter study for ultra-fine fiber fabrication via electrospinning process. *Polymer* **2005**, *46*, 6128-6134.

(152) Zong, X.; Kim, K.; Fang, D.; Ran, S.; Hsiao, B. S.; Chu, B.: Structure and process relationship of electrospun bioabsorbable nanofiber membranes. *Polymer* **2002**, *43*, 4403-4412.

(153) Buchko, C. J.; Chen, L. C.; Shen, Y.; Martin, D. C.: Processing and microstructural characterization of porous biocompatible protein polymer thin films. *Polymer* **1999**, *40*, 7397-7407.

(154) Li, Y.; Huang, Z.; Lǔ, Y.: Electrospinning of nylon 6,66,1010 terpolymer. *European Polymer Journal* **2006**, *42*, 1696-1704.

(155) Gu, S. Y.; Ren, J.; Vancso, G. J.: Process optimization and empirical modeling for electrospun polyacrylonitrile (PAN) nanofiber precursor of carbon nanofibers. *European Polymer Journal* **2005**, *41*, 2559-2568.

(156) Li, L.; Hsieh, Y.-L.: Ultra-fine polyelectrolyte fibers from electrospinning of poly(acrylic acid). *Polymer* **2005**, *46*, 5133-5139.

(157) Zhang, C.; Yuan, X.; Wu, L.; Han, Y.; Sheng, J.: Study on morphology of electrospun poly(vinyl alcohol) mats. *European Polymer Journal* **2005**, *41*, 423-432.

(158) Deitzel, J. M.; Kleinmeyer, J.; Harris, D.; Beck Tan, N. C.: The effect of processing variables on the morphology of electrospun nanofibers and textiles. *Polymer* **2001**, *42*, 261-272.

(159) Bölgen, N.; Menceloğlu, Y. Z.; Acatay, K.; Vargel, İ.; Pişkin, E.: In vitro and *in vivo* degradation of non-woven materials made of poly(ε-caprolactone) nanofibers prepared by electrospinning under different conditions. *Journal of Biomaterials Science, Polymer Edition* **2005**, *16*, 1537-1555.

(160) Zuo, W.; Zhu, M.; Yang, W.; Yu, H.; Chen, Y.; Zhang, Y.: Experimental study on relationship between jet instability and formation of beaded fibers during electrospinning. *Polymer Engineering & Science* **2005**, *45*, 704-709.

(161) Li, D.; Ouyang, G.; McCann, J. T.; Xia, Y.: Collecting electrospun nanofibers with patterned electrodes. *Nano Letters* **2005**, *5*, 913-916.

(162) Li, D.; Wang, Y.; Xia, Y.: Electrospinning nanofibers as uniaxially aligned arrays and layer-by-layer stacked films. *Advanced Materials* **2004**, *16*, 361-366.

(163) Matthews, J. A.; Wnek, G. E.; Simpson, D. G.; Bowlin, G. L.: Electrospinning of collagen nanofibers. *Biomacromolecules* **2002**, *3*, 232-238.

(164) Theron, A.; Zussman, E.; Yarin, A. L.: Electrostatic field-assisted alignment of electrospun nanofibres. *Nanotechnology* **2001**, *12*, 384-390.

(165) Teo, W. E.; Kotaki, M.; Mo, X. M.; Ramakrishna, S.: Porous tubular structures with controlled fibre orientation using a modified electrospinning method. *Nanotechnology* **2005**, *16*, 918-924.

(166) Baji, A.; Mai, Y.-W.; Wong, S.-C.; Abtahi, M.; Chen, P.: Electrospinning of polymer nanofibers: Effects on oriented morphology, structures and tensile properties. *Composites Science and Technology* **2010**, *70*, 703-718.

(167) Huang, Z.-M.; Zhang, Y. Z.; Kotaki, M.; Ramakrishna, S.: A review on polymer nanofibers by electrospinning and their applications in nanocomposites. *Composites Science and Technology* **2003**, *63*, 2223-2253.

(168) Megelski, S.; Stephens, J. S.; Chase, D. B.; Rabolt, J. F.: Micro- and nanostructured surface morphology on electrospun polymer fibers. *Macromolecules* **2002**, *35*, 8456-8466.

(169) Park, J. Y.; Lee, I. H.; Bea, G. N.: Optimization of the electrospinning conditions for preparation of nanofibers from polyvinylacetate (PVAc) in ethanol solvent. *Journal of Industrial and Engineering Chemistry* **2008**, *14*, 707-713.

(170) Thompson, C. J.; Chase, G. G.; Yarin, A. L.; Reneker, D. H.: Effects of parameters on nanofiber diameter determined from electrospinning model. *Polymer* **2007**, *48*, 6913-6922.

(171) Macossay, J.; Marruffo, A.; Rincon, R.; Eubanks, T.; Kuang, A.: Effect of needle diameter on nanofiber diameter and thermal properties of electrospun poly(methyl methacrylate). *Polymers for Advanced Technologies* **2007**, *18*, 180-183.

(172) Chowdhury, M. M.; Stylios, G. K.: Effect of processing parameters on nylon 6,6 nanofibres and their morphology. *International Journal of Basic & Applied Sciences* **2008**, *10*, 161-172.

(173) De Vrieze, S.; Van Camp, T.; Nelvig, A.; Hagström, B.; Westbroek, P.; De Clerck, K.: The effect of temperature and humidity on electrospinning. *Journal of Materials Science* **2009**, *44*, 1357-1362.

(174) He, J. H.: Effect of temperature on surface tension of a bubble and hierarchical ruptured bubbles for nanofiber fabrication. *Thermal Science* **2012**, *16*, 327-330.

(175) Fashandi, H.; Karimi, M.: Pore formation in polystyrene fiber by superimposing temperature and relative humidity of electrospinning atmosphere. *Polymer* **2012**, *53*, 5832-5849.

(176) Casper, C. L.; Stephens, J. S.; Tassi, N. G.; Chase, D. B.; Rabolt, J. F.: Controlling surface morphology of electrospun polystyrene fibers: Effect of humidity and molecular weight in the electrospinning process. *Macromolecules* **2003**, *37*, 573-578.

(177) Andrady, A. L., Ensor, D. S., : Electrospinning in a controlled gaseous environment. *US Patent 2008/0063741 A1* **2008**.

(178) Ramakrishna, S.; Fujihara, K.; Teo, W.-E.; Yong, T.; Ma, Z.; Ramaseshan, R.: Electrospun nanofibers: solving global issues. *Materials Today* **2006**, *9*, 40-50.

(179) Yoo, H. S.; Kim, T. G.; Park, T. G.: Surface-functionalized electrospun nanofibers for tissue engineering and drug delivery. *Advanced Drug Delivery Reviews* **2009**, *61*, 1033-1042.

(180) Lu, J.-W.; Zhu, Y.-L.; Guo, Z.-X.; Hu, P.; Yu, J.: Electrospinning of sodium alginate with poly(ethylene oxide). *Polymer* **2006**, *47*, 8026-8031.

(181) Gravano, S. M.; Borden, M.; von Werne, T.; Doerffler, E. M.; Salazar, G.; Chen, A.; Kisak, E.; Zasadzinski, J. A.; Patten, T. E.; Longo, M. L.: Poly(4-(aminomethyl)styrene)-b-polystyrene: Synthesis and Unilamellar Vesicle Formation. *Langmuir* **2002**, *18*, 1938-1941.

(182) Özden, Ş.; Çelik, S. Ü.; Bozkurt, A.: Synthesis and proton conductivity studies of polystyrene-based triazole functional polymer membranes. *Journal of Polymer Science, Part A: Polymer Chemistry* **2010**, *48*, 4974-4980.

(183) Kriegel, C.; Arrechi, A.; Kit, K.; McClements, D. J.; Weiss, J.: Fabrication, functionalization, and application of electrospun biopolymer nanofibers. *Critical Reviews in Food Science and Nutrition* **2008**, *48*, 775-797.

(184) Li, J.; Vergne, M. J.; Mowles, E. D.; Zhong, W.-H.; Hercules, D. M.; Lukehart, C. M.: Surface functionalization and characterization of graphitic carbon nanofibers (GCNFs). *Carbon* **2005**, *43*, 2883-2893.

(185) Sargeant, T. D.; Rao, M. S.; Koh, C.-Y.; Stupp, S. I.: Covalent functionalization of NiTi surfaces with bioactive peptide amphiphile nanofibers. *Biomaterials* **2008**, *29*, 1085-1098.

(186) Luo, Y.; Nartker, S.; Miller, H.; Hochhalter, D.; Wiederoder, M.; Wiederoder, S.; Setterington, E.; Drzal, L. T.; Alocilja, E. C.: Surface functionalization of electrospun nanofibers for detecting *E. coli* O157:H7 and BVDV cells in a direct-charge transfer biosensor. *Biosensors and Bioelectronics* **2010**, *26*, 1612-1617.

(187) Schneiderman, S.; Zhang, L.; Fong, H.; Menkhaus, T. J.: Surface-functionalized electrospun carbon nanofiber mats as an innovative type of protein adsorption/purification medium with high capacity and high throughput. *Journal of Chromatography A* **2011**, *1218*, 8989-8995.

(188) Koh, H. S.; Yong, T.; Chan, C. K.; Ramakrishna, S.: Enhancement of neurite outgrowth using nano-structured scaffolds coupled with laminin. *Biomaterials* **2008**, *29*, 3574-3582.

(189) Formo, E.; Lee, E.; Campbell, D.; Xia, Y.: Functionalization of electrospun TiO_2 nanofibers with Pt nanoparticles and nanowires for catalytic applications. *Nano Letters* **2008**, *8*, 668-672.

(190) Li, D.; McCann, J. T.; Gratt, M.; Xia, Y.: Photocatalytic deposition of gold nanoparticles on electrospun nanofibers of titania. *Chemical Physics Letters* **2004**, *394*, 387-391.

(191) Jones, A. C., Hitchman, M. L.: Overview of chemical vapour deposition. In *Chemical Vapour Deposition: Precursors, Processes and Applications*; Jones, A. C., Hitchman, M. L., Ed.; Royal Society of Chemistry, **2009**; 1-36.

(192) Ma, M.; Mao, Y.; Gupta, M.; Gleason, K. K.; Rutledge, G. C.: Superhydrophobic fabrics produced by electrospinning and chemical vapor deposition. *Macromolecules* **2005**, *38*, 9742-9748.

(193) Zander, N. E.; Orlicki, J. A.; Rawlett, A. M.; Beebe, T. P.: Quantification of protein incorporated into electrospun polycaprolactone tissue engineering scaffolds. *Applied Materials & Interfaces* **2012**, *4*, 2074-2081.

(194) Mohy Eldin, M. S.; Schroën, C. G. P. H.; Janssen, A. E. M.; Mita, D. G.; Tramper, J.: Immobilization of penicillin G acylase onto chemically grafted nylon particles. *Journal of Molecular Catalysis B: Enzymatic* **2000**, *10*, 445-451.

(195) Kaur, S.; Ma, Z.; Gopal, R.; Singh, G.; Ramakrishna, S.; Matsuura, T.: Plasma-induced graft copolymerization of poly(methacrylic acid) on electrospun poly(vinylidene fluoride) nanofiber membrane. *Langmuir* **2007**, *23*, 13085-13092.

(196) Hiroki Iwase, S.-i. S., Tetsuya Yamaki, Yasunari Maekawa,; Koizumi, S.: Preirradiation graft polymerization of styrene in a poly(tetrafluoroethylene) film investigated by time-resolved small-angle neutron scattering. *International Journal of Polymer Science* **2011**, 1-7.

(197) El-Masry, M. M.; De Maio, A.; Martelli, P. L.; Casadio, R.; Moustafa, A. B.; Rossi, S.; Mita, D. G.: Influence of the immobilization process on the activity of β-galactosidase bound to nylon membranes grafted with glycidyl methacrylate: Part 1. Isothermal behavior. *Journal of Molecular Catalysis B: Enzymatic* **2001**, *16*, 175-189.

(198) Ünal, H. I.; Inegöllü, C.; Şanli, O.: Graft copolymerization of *N*-vinylimidazole on poly(ethylene terephthalate) fibers in a swelling solvent using azobisisobutyronitrile as initiator. *Turkish Journal of Chemistry* **2003**, *27*, 403-415.

(199) Ongun, N.; Karakişla, M.; Aksu, L.; Saçak, M.: Graft polymerization of methacrylamide onto poly(ethylene terephthalate) fibers with benzoyl peroxide as

initiator and their characterization. *Macromolecular Chemistry and Physics* **2004**, *205*, 1995-2001.

(200) Chirowodza, H.; Sanderson, R. D.: Surface modification of poly(vinyl alcohol) fibers. *Macromolecular Materials and Engineering* **2010**, *295*, 1009-1016.

(201) Jackeray, R.; Jain, S.; Chattopadhyay, S.; Yadav, M.; Shrivastav, T. G.; Singh, H.: Surface modification of nylon membrane by glycidyl methacrylate graft copolymerization for antibody immobilization. *Journal of Applied Polymer Science* **2010**, *116*, 1700-1709.

(202) Liu, Y. H.; Li, S. X.; Zhou, W. Q.; Zhang, J. P.; Zhang, R. Y.; Deng, K. L.: Graft copolymerization of methyl acrylate onto nylon 6 initiated by potassium ditelluratocuprate (III). *Gaofenzi Cailiao Kexue Yu Gongcheng/Polymeric Materials Science and Engineering* **2006**, *22*, 39-42.

(203) Percec, V.; Barboiu, B.: "Living" radical polymerization of styrene initiated by arenesulfonyl chlorides and CuI(bpy)nCl. *Macromolecules* **1995**, *28*, 7970-7972.

(204) Shirai, Y.; Shirai, K.; Tsubokawa, N.: Effective grafting of polymers onto ultrafine silica surface: Photopolymerization of vinyl monomers initiated by the system consisting of trichloroacetyl groups on the surface and Mn2(CO)10. *Journal of Polymer Science Part A: Polymer Chemistry* **2001**, *39*, 2157-2163.

(205) Liu, Y.; Liu, Z.; Zhang, Y.; Deng, K.: Graft copolymerization of methylacrylate onto chitosan initiated by potassium diperiodatonickelate (IV). *Journal of Macromolecular Science, Part A* **2002**, *39*, 129-143.

(206) Wang, H.; Dong, X.; Yang, M.: Development of separation materials using controlled/living radical polymerization. *Trends in Analytical Chemistry* **2012**, *31*, 96-108.

(207) Mishra, V.; Kumar, R.: Grafting of 4-aminoantipyrine from guar gum substrates using graft atom transfer radical polymerization (ATRP) process. *Carbohydrate Polymers* **2011**, *86*, 296-303.

(208) Szwarc, M.: Living polymers. Their discovery, characterization, and properties. *Journal of Polymer Science Part A: Polymer Chemistry* **1998**, *36*, IX-XV.

(209) Bulbul Sonmez, H.; Senkal, B. F.; Sherrington, D. C.; Bicak, N.: Atom transfer radical graft polymerization of acrylamide from *N*-chlorosulfonamidated polystyrene resin, and use of the resin in selective mercury removal. *Reactive and Functional Polymers* **2003**, *55*, 1-8.

(210) Singh, N.; Wang, J.; Ulbricht, M.; Wickramasinghe, S. R.; Husson, S. M.: Surface-initiated atom transfer radical polymerization: A new method for preparation of polymeric membrane adsorbers. *Journal of Membrane Science* **2008**, *309*, 64-72.

(211) Tizpar, S.; Abbasian, M.; Taromi, F. A.; Entezami, A. A.: Grafting of poly(methyl methacrylate) or polyacrylonitrile onto polystyrene using ATRP technique. *Journal of Applied Polymer Science* **2006**, *100*, 2619-2627.

(212) Xia, J.; Matyjaszewski, K.: Controlled/"Living" radical polymerization. Atom transfer radical polymerization using multidentate amine ligands. *Macromolecules* **1997**, *30*, 7697-7700.

(213) Xia, J.; Gaynor, S. G.; Matyjaszewski, K.: Controlled/"Living" radical polymerization. Atom transfer radical polymerization of acrylates at ambient temperature. *Macromolecules* **1998**, *31*, 5958-5959.

(214) Geuskens, G.; Etoc, A.; Di Michele, P.: Surface modification of polymers VII.: Photochemical grafting of acrylamide and *N*-isopropylacrylamide onto polyethylene initiated by anthraquinone-2-sulfonate adsorbed at the surface of the polymer. *European Polymer Journal* **2000**, *36*, 265-271.

(215) Calgari, S.; Selli, E.; Bellobono, I. R.: Photochemical grafting of acrylated azo dyes onto polymeric surfaces. V. Grafting of some acryloxy-substituted aromatic diazenes as model molecules onto polypropylene, polycaprolactam, and poly(ethylene terephthalate) films. *Journal of Applied Polymer Science* **1982**, *27*, 527-533.

(216) Ang, C. H.; Garnett, J. L.; Levot, R.; Long, M. A.; Yen, N. T.: Photosensitized grafting of styrene 4-vinylpyridine and methyl methacrylate to polypropylene. *Journal of Polymer Science: Polymer Letters Edition* **1980**, *18*, 471-475.

(217) Davis, N. P.; Garnett, J. L.; Urquhart, R. G.: Photosensitized and γ-ray-induced graft copolymerizations of monomers to cellulose. *Journal of Polymer Science: Polymer Symposia* **1976**, *55*, 287-301.

(218) Edge, S.; Walker, S.; Feast, W. J.; Pacynko, W. F.: Surface modification of polyethylene by photochemical grafting with 2-hydroxyethylmethacrylate. *Journal of Applied Polymer Science* **1993**, *47*, 1075-1082.

(219) Moura, E.; Somessari, E. S. R.; Silveira, C. G.; Paes, H. A.; Souza, C. A.; Fernandes, W.; Manzoli, J. E.; Geraldo, A. B. C.: Influence of physical parameters on mutual polymer grafting by electron beam irradiation. *Radiation Physics and Chemistry* **2011**, *80*, 175-181.

(220) Yamagishi, H.; Saito, K.; Furusaki, S.; Sugo, T.; Ishigaki, I.: Comparison of simultaneous and preirradiation grafting of methyl methacrylate onto a porous membrane. *Chemistry of Materials* **1991**, *3*, 987-989.

(221) Brack, H.-P.; Buhrer, H. G.; Bonorand, L.; Scherer, G. G.: Grafting of pre-irradiated poly(ethylene--tetrafluoroethylene) films with styrene: influence of base polymer film properties and processing parameters. *Journal of Materials Chemistry* **2000**, *10*, 1795-1803.

(222) Rager, T.: Pre-irradiation grafting of styrene/divinylbenzene onto poly(tetrafluoroethylene-co-hexafluoropropylene) from non-solvents. *Helvetica Chimica Acta* **2003**, *86*, 1966-1981.

(223) Daneault, C.; Kokta, B.; Maldas, D.: Grafting of vinyl monomers onto wood fibers initiated by peroxidation. *Polymer Bulletin* **1988**, *20*, 137-141.

(224) Knaus, S.; Spoljaric-Lukacic, L.; Liska, R.; Saf, R.: Peroxide-initiated grafting of maleimides onto hydrocarbon substrates. *European Polymer Journal* **2005**, *41*, 2240-2254.

(225) Weaver, J. D.; Chowdhury, A. K.; Mowery, D. M.; Esseghir, M.; Cogen, J. M.; Chaudhary, B. I.: Structural comparison of products from peroxide-initiated grafting of vinylsilane and silane-functionalized nitroxyl to hydrocarbon and polyolefin substrates. *Journal of Polymer Science, Part A: Polymer Chemistry* **2008**, *46*, 4542-4555.

(226) Rattan, S.; Sehgal, T.: Stimuli-responsive membranes through peroxidation radiation-induced grafting of 2-hydroxyethyl methacrylate (2-HEMA) onto isotactic polypropylene film (IPP). *Journal of Radioanalytical and Nuclear Chemistry* **2012**, *293*, 107-118.

(227) Nisbet, D. R.; Rodda, A. E.; Finkelstein, D. I.; Horne, M. K.; Forsythe, J. S.; Shen, W.: Surface and bulk characterisation of electrospun membranes: Problems and improvements. *Colloids and Surfaces B: Biointerfaces* **2009**, *71*, 1-12.

(228) Deitzel, J. M.; Kosik, W.; McKnight, S. H.; Beck Tan, N. C.; DeSimone, J. M.; Crette, S.: Electrospinning of polymer nanofibers with specific surface chemistry. *Polymer* **2002**, *43*, 1025-1029.

(229) Giesche, H.: Mercury porosimetry: A general (practical) overview. *Particle and Particle Systems Characterization* **2006**, *23*, 9-19.

(230) Jena, A.; Gupta, K.: An innovative technique for pore structure analysis of fuel cell and battery components using flow porometry. *Journal of Power Sources* **2001**, *96*, 214-219.

(231) Li, D.; Frey, M. W.; Joo, Y. L.: Characterization of nanofibrous membranes with capillary flow porometry. *Journal of Membrane Science* **2006**, *286*, 104-114.

(232) Sirc, J.; Hobzova, R.; Kostina, N.; Munzarova, M.; Juklickova, M.; Lhotka, M.; Kubinova, S.; Zajicova, A.; Michalek, J.: Morphological characterization of nanofibers: Methods and application in practice. *Journal of Nanomaterials* **2012**, *2012*, 327369.

(233) Klein, K. L.; Melechko, A. V.; McKnight, T. E.; Retterer, S. T.; Rack, P. D.; Fowlkes, J. D.; Joy, D. C.; Simpson, M. L.: Surface characterization and functionalization of carbon nanofibers. *Journal of Applied Physics* **2008**, *103*, 061301.

(234) Muscariello, L.; Rosso, F.; Marino, G.; Giordano, A.; Barbarisi, M.; Cafiero, G.; Barbarisi, A.: A critical overview of ESEM applications in the biological field. *Journal of Cellular Physiology* **2005**, *205*, 328-334.

(235) Williams, D. B., Carter, C. B.: Transmission Electron Microscopy: A textbook for Material Science. **2009**, *1-4*.

(236) Reimer, L., Kohl, H.: Transmission Electron Microscopy: Physics of Image Formation. **2008**.

(237) Hou, H.; Ge, J. J.; Zeng, J.; Li, Q.; Reneker, D. H.; Greiner, A.; Cheng, S. Z. D.: Electrospun polyacrylonitrile nanofibers containing a high concentration of well-aligned multiwall carbon nanotubes. *Chemistry of Materials* **2005**, *17*, 967-973.

(238) Binnig, G.; Quate, C. F.; Gerber, C.: Atomic Force Microscope. *Physical Review Letters* **1986**, *56*, 930-933.

(239) Butt, H.-J.; Cappella, B.; Kappl, M.: Force measurements with the atomic force microscope: Technique, interpretation and applications. *Surface Science Reports* **2005**, *59*, 1-152.

(240) Lübben, J.; Hufenus, R.; Heuberger, M.: Fiber analytics using the AFM. *EMPA Activities* **2007**, 47.

(241) Lübben, J. F.; Fortunato, G.; Halbeisen, M.; Houis, S.; Keller, M.; Körner, E.: Characterization of synthetic fibers using the atomic force microscope. *Journal of Physics: Conference Series* **2007**, *61*, 735-739.

(242) Wu, N.; Shao, D.; Wei, Q.; Cai, Y.; Gao, W.: Characterization of PVAc/TiO2 hybrid nanofibers: From fibrous morphologies to molecular structures. *Journal of Applied Polymer Science* **2009**, *112*, 1481-1485.

(243) Hammiche, A.; Pollock, H. M.; Reading, M.; Claybourn, M.; Turner, P. H.; Jewkes, K.: Photothermal FT-IR Spectroscopy: A step towards FT-IR microscopy at a resolution better than the diffraction limit. *Applied Spectroscopy* **1999**, *53*, 810-815.

(244) Koprinarov, I.; Hitchcock, A. P.; Li, W. H.; Heng, Y. M.; Stöver, H. D. H.: Quantitative compositional mapping of core−shell polymer microspheres by soft x-ray spectromicroscopy. *Macromolecules* **2001**, *34*, 4424-4429.

(245) Liu, H.; Webster, T. J.: Nanomedicine for implants: A review of studies and necessary experimental tools. *Biomaterials* **2007**, *28*, 354-369.

(246) Merret, K., Cornelius, R. M., McClung, W. G., Unsworth, L. D., Sheardown, H.: Surface analysis methods for characterizing polymeric biomaterials. *Journal of Biomaterials Science, Polymer Edition* **2002**, *13*, 593-621.

(247) Ma, Z.; He, W.; Yong, T.; Ramakrishna, S.: Grafting of gelatin on electrospun poly(caprolactone) nanofibers to improve endothelial cell spreading and proliferation and to control cell orientation. *Tissue Engineering* **2005**, *11*, 1149-1158.

(248) Uyar, T.; Balan, A.; Toppare, L.; Besenbacher, F.: Electrospinning of cyclodextrin functionalized poly(methyl methacrylate) (PMMA) nanofibers. *Polymer* **2009**, *50*, 475-480.

(249) Ji, L.; Medford, A. J.; Zhang, X.: Electrospun polyacrylonitrile/zinc chloride composite nanofibers and their response to hydrogen sulfide. *Polymer* **2009**, *50*, 605-612.

(250) Chen, R.; Huang, C.; Ke, Q.; He, C.; Wang, H.; Mo, X.: Preparation and characterization of coaxial electrospun thermoplastic polyurethane/collagen compound nanofibers for tissue engineering applications. *Colloids and Surfaces B: Biointerfaces* **2010**, *79*, 315-325.

(251) Bai, J.; Li, Y.; Zhang, C.; Liang, X.; Yang, Q.: Preparing AgBr nanoparticles in poly(vinyl pyrrolidone) (PVP) nanofibers. *Colloids and Surfaces A: Physicochemical and Engineering Aspects* **2008**, *329*, 165-168.

(252) Zhang, K.; Zhang, L. L.; Zhao, X. S.; Wu, J.: Graphene/polyaniline nanofiber composites as supercapacitor electrodes. *Chemistry of Materials* **2010**, *22*, 1392-1401.

(253) Uyar, T.; Havelund, R.; Hacaloglu, J.; Besenbacher, F.; Kingshott, P.: Functional electrospun polystyrene nanofibers incorporating α-, β-, and γ-cyclodextrins: Comparison of molecular filter performance. *ACS Nano* **2010**, *4*, 5121-5130.

(254) http://www.ece2010.uni.goettingen.de/people/vthiel/images/tof_sims1.gif. Date accessed: 23 December 2012.

(255) Passarelli, M. K.; Winograd, N.: Lipid imaging with time-of-flight secondary ion mass spectrometry (ToF-SIMS). *Biochimica et Biophysica Acta (BBA) - Molecular and Cell Biology of Lipids* **2011**, *1811*, 976-990.

(256) Senoner, M.; Unger, W. E. S.: SIMS imaging of the nanoworld: applications in science and technology. *Journal of Analytical Atomic Spectrometry* **2012**, *27*, 1050-1068.

(257) Cui, W.; Chang, J.; Dalton, P. D.: Electrospun fibers for drug delivery. In *Comprehensive Biomaterials*; Editor-in-Chief: Paul, D., Ed.; Elsevier: Oxford, 2011; 445-462.

(258) Chigome, S.; Darko, G.; Buttner, U.; Torto, N.: Semi-micro solid phase extraction with electrospun polystyrene fiber disks. *Analytical Methods* **2010**, *2*, 623-626.

(259) Chigome, S.; Darko, G.; Torto, N.: Electrospun nanofibers as sorbent material for solid phase extraction. *Analyst* **2011**, *136*, 2879-2889.

(260) Chigome, S.; Torto, N.: Electrospun nanofiber-based solid-phase extraction. *Trends in Analytical Chemistry* **2012**, *38*, 21-31.

(261) Darko, G.; Chigome, S.; Tshentu, Z.; Torto, N.: Enrichment of Cu(II), Ni(II), and Pb(II) in aqueous solutions using electrospun polysulfone nanofibers functionalized with 1-[*bis*[3-(dimethylamino)-propyl]amino]-2-propanol. *Analytical Letters* **2011**, *44*, 1855-1867.

(262) Lee, S.; Obendorf, S. K.: Use of electrospun nanofiber web for protective textile materials as barriers to liquid penetration. *Textile Research Journal* **2007**, *77*, 696-702.

(263) Gorji, M.; Jeddi, A. A. A.; Gharehaghaji, A. A.: Fabrication and characterization of polyurethane electrospun nanofiber membranes for protective clothing applications. *Journal of Applied Polymer Science* **2012**, *125*, 4135-4141.

(264) Gallo, E.; Fan, Z.; Schartel, B.; Greiner, A.: Electrospun nanofiber mats coating—new route to flame retardancy. *Polymers for Advanced Technologies* **2011**, *22*, 1205-1210.

(265) Yoon, B.; Lee, S.: Designing waterproof breathable materials based on electrospun nanofibers and assessing the performance characteristics. *Fibers and Polymers* **2011**, *12*, 57-64.

(266) Ding, B.; Wang, M.; Yu, J.; Sun, G.: Gas sensors based on electrospun nanofibers. *Sensors* **2009**, *9*, 1609-1624.

(267) Balamurugan, R.; Sundarrajan, S.; Ramakrishna, S.: Recent trends in nanofibrous membranes and their suitability for air and water filtrations. *Membranes* **2011**, *1*, 232-248.

(268) Thavasi, V.; Singh, G.; Ramakrishna, S.: Electrospun nanofibers in energy and environmental applications. *Energy & Environmental Science* **2008**, *1*, 205-221.

(269) Gouma, P. I.: Nanostructured polymorphic oxides for advanced chemosensors. *Reviews on Advanced Materials Science* **2003**, *5*, 147-154.

(270) Sawicka, K. M.; Prasad, A. K.; Gouma, P. I.: Metal oxide nanowires for use in chemical sensing applications. *Sensor Letters* **2005**, *3*, 31-35.

(271) Merdrignac-Conanec, O.; Moseley, P. T.: Gas sensing properties of the mixed molybdenum tungsten oxide, $W_{0.9}Mo_{0.1}O_3$. *Journal of Materials Chemistry* **2002**, *12*, 1779-1781.

(272) Ding, B.; Yamazaki, M.; Shiratori, S.: Electrospun fibrous polyacrylic acid membrane-based gas sensors. *Sensors and Actuators, B: Chemical* **2005**, *106*, 477-483.

(273) Ding, D., Kikuchi, M., Li, C., Shiratori, S., Electrospun nanofibrous pelyelectrolyte membranes as high coatings for QCM-based gas sensors. In "Nanotechnology at the leading edge"; Dirote, E. V., Nova Science Publishers: New York, USA (2006) 1-28.

(274) Kang, X.-J.; Chen, L.-Q.; Zhang, Y.-Y.; Liu, Y.-W.; Gu, Z.-Z.: Performance of electrospun nanofibers for SPE of drugs from aqueous solutions. *Journal of Separation Science* **2008**, *31*, 3272-3278.

(275) Xu, Q.; Wu, S.-Y.; Wang, M.; Yin, X.-Y.; Wen, Z.-Y.; Ge, W.-N.; Gu, Z.-Z.: Electrospun nylon 6 nanofibrous membrane as SPE adsorbent for the enrichment and determination of three estrogens in environmental water samples. *Chroma* **2010**, *71*, 487-492.

(276) Yoshimatsu, K.; Ye, L.; Lindberg, J.; Chronakis, I. S.: Selective molecular adsorption using electrospun nanofiber affinity membranes. *Biosensors and Bioelectronics* **2008**, *23*, 1208-1215.

(277) Liu, Y.; Ding, Y.; Zhang, L.; Gao, P.-X.; Lei, Y.: CeO_2 nanofibers for in situ O_2 and CO sensing in harsh environments. *RSC Advances* **2012**, *2*, 5193-5198.

(278) Yang, Y.; Fan, X.; Long, Y.; Su, K.; Zou, D.; Li, N.; Zhou, J.; Li, K.; Liu, F.: A simple fabrication of electrospun nanofiber sensing materials based on fluorophore-doped polymer. *Journal of Materials Chemistry* **2009**, *19*, 7290-7295.

(279) Han, X.-J.; Huang, Z.-M.; He, C.-L.; Liu, L.; Wu, Q.-S.: Coaxial electrospinning of PC(shell)/PU(core) composite nanofibers for textile application. *Polymer Composites* **2008**, *29*, 579-584.

(280) Qin, X.-H.; Wang, S.-Y.: Filtration properties of electrospinning nanofibers. *Journal of Applied Polymer Science* **2006**, *102*, 1285-1290.

(281) Tan, S.; Huang, X.; Wu, B.: Some fascinating phenomena in electrospinning processes and applications of electrospun nanofibers. *Polymer International* **2007**, *56*, 1330-1339.

(282) Patanaik, A.; Jacobs, V.; Anandjiwala, R. D.: Performance evaluation of electrospun nanofibrous membrane. *Journal of Membrane Science* **2010**, *352*, 136-142.

(283) Dong, Z.; Kennedy, S. J.; Wu, Y.: Electrospinning materials for energy-related applications and devices. *Journal of Power Sources* **2011**, *196*, 4886-4904.

(284) Ballengee, J. B.; Pintauro, P. N.: Composite fuel cell membranes from dual-nanofiber electrospun mats. *Macromolecules* **2011**, *44*, 7307-7314.

(285) Tamura, T.; Kawakami, H.: Aligned electrospun nanofiber composite membranes for fuel cell electrolytes. *Nano Letters* **2010**, *10*, 1324-1328.

(286) Bonino, C. A.; Ji, L.; Lin, Z.; Toprakci, O.; Zhang, X.; Khan, S. A.: Electrospun carbon-tin oxide composite nanofibers for use as lithium ion battery anodes. *Applied Materials & Interfaces* **2011**, *3*, 2534-2542.

(287) Zhang, X.; Ji, L.; Toprakci, O.; Liang, Y.; Alcoutlabi, M.: Electrospun nanofiber-based anodes, cathodes, and separators for advanced lithium-ion batteries. *Polymer Reviews* **2011**, *51*, 239-264.

(288) Chuangchote, S.; Sagawa, T.; Yoshikawa, S.: Efficient dye-sensitized solar cells using electrospun TiO_2 nanofibers as a light harvesting layer. *Applied Physics Letters* **2008**, *93*, 033310.

(289) Joshi, P.; Zhang, L.; Chen, Q.; Galipeau, D.; Fong, H.; Qiao, Q.: Electrospun carbon nanofibers as low-cost counter electrode for dye-sensitized solar cells. *Applied Materials & Interfaces* **2010**, *2*, 3572-3577.

(290) Chen, X.; Xu, S.; Yao, N.; Shi, Y.: 1.6 V Nanogenerator for mechanical energy harvesting using PZT nanofibers. *Nano Letters* **2010**, *10*, 2133-2137.

(291) Chang, J.; Dommer, M.; Chang, C.; Lin, L.: Piezoelectric nanofibers for energy scavenging applications. *Nano Energy* **2012**, *1*, 356-371.

(292) Maensiri, S.; Nuansing, W.: Thermoelectric oxide $NaCo_2O_4$ nanofibers fabricated by electrospinning. *Materials Chemistry and Physics* **2006**, *99*, 104-108.

(293) Yin, T.; Liu, D.; Ou, Y.; Ma, F.; Xie, S.; Li, J.-F.; Li, J.: Nanocrystalline thermoelectric $Ca_3Co_4O_9$ ceramics by sol−gel based electrospinning and spark plasma sintering. *The Journal of Physical Chemistry C* **2010**, *114*, 10061-10065.

(294) Wee, G.; Soh, H. Z.; Cheah, Y. L.; Mhaisalkar, S. G.; Srinivasan, M.: Synthesis and electrochemical properties of electrospun V_2O_5 nanofibers as supercapacitor electrodes. *Journal of Materials Chemistry* **2010**, *20*, 6720-6725.

(295) Laforgue, A.: All-textile flexible supercapacitors using electrospun poly(3,4-ethylenedioxythiophene) nanofibers. *Journal of Power Sources* **2011**, *196*, 559-564.

(296) Bouten, C. V. C.; Dankers, P. Y. W.; Driessen-Mol, A.; Pedron, S.; Brizard, A. M. A.; Baaijens, F. P. T.: Substrates for cardiovascular tissue engineering. *Advanced Drug Delivery Reviews* **2011**, *63*, 221-241.

(297) Choi, J. S.; Leong, K. W.; Yoo, H. S.: In vivo wound healing of diabetic ulcers using electrospun nanofibers immobilized with human epidermal growth factor (EGF). *Biomaterials* **2008**, *29*, 587-596.

(298) Jia, H.; Zhu, G.; Vugrinovich, B.; Kataphinan, W.; Reneker, D. H.; Wang, P.: Enzyme-carrying polymeric nanofibers prepared via electrospinning for use as unique biocatalysts. *Biotechnology Progress* **2002**, *18*, 1027-1032.

(299) Song, J.; Kahveci, D.; Chen, M.; Guo, Z.; Xie, E.; Xu, X.; Besenbacher, F.; Dong, M.: Enhanced catalytic activity of lipase encapsulated in PCL nanofibers. *Langmuir* **2012**, *28*, 6157-6162.

(300) Kim, J. H.; Hwang, E. T.; Kang, K.-k.; Tatavarty, R.; Gu, M. B.: Aptamers-on-nanofiber as a novel hybrid capturing moiety. *Journal of Materials Chemistry* **2011**, *21*, 19203-19206.

(301) Ramakrishna, S.; Lala, N.; Garudadhwaj, H.; Ramaseshan, R.; Ganesh, V. K.: Polymer nanofibers for biosensor applications. In *Molecular Building Blocks for Nanotechnology*; Mansoori, G. A., George, T., Assoufid, L., Zhang, G., Eds.; Springer New York, 2007; Vol. 109; pp 377-392.

(302) Davis, B. W.; Niamnont, N.; Dillon, R.; Bardeen, C. J.; Sukwattanasinitt, M.; Cheng, Q.: FRET detection of proteins using fluorescently doped electrospun nanofibers and pattern recognition. *Langmuir* **2011**, *27*, 6401-6408.

(303) He, X.; Tan, L.; Wu, X.; Yan, C.; Chen, D.; Meng, X.; Tang, F.: Electrospun quantum dots/polymer composite porous fibers for turn-on fluorescent detection of lactate dehydrogenase. *Journal of Materials Chemistry* **2012**, *22*, 18471-18478.

(304) Khil, M.-S.; Cha, D.-I.; Kim, H.-Y.; Kim, I.-S.; Bhattarai, N.: Electrospun nanofibrous polyurethane membrane as wound dressing. *Journal of Biomedical Materials Research Part B: Applied Biomaterials* **2003**, *67B*, 675-679.

(305) Venugopal, J.; Ramakrishna, S.: Applications of polymer nanofibers in biomedicine and biotechnology. *Appl Biochem Biotechnol* **2005**, *125*, 147-157.

(306) He, W.; Ma, Z.; Teo, W. E.; Dong, Y. X.; Robless, P. A.; Lim, T. C.; Ramakrishna, S.: Tubular nanofiber scaffolds for tissue engineered small-diameter vascular grafts. *Journal of Biomedical Materials Research Part A* **2009**, *90A*, 205-216.

(307) Zhang, Y.; Venugopal, J. R.; El-Turki, A.; Ramakrishna, S.; Su, B.; Lim, C. T.: Electrospun biomimetic nanocomposite nanofibers of hydroxyapatite/chitosan for bone tissue engineering. *Biomaterials* **2008**, *29*, 4314-4322.

(308) Prabhakaran, M. P.; Venugopal, J. R.; Ramakrishna, S.: Mesenchymal stem cell differentiation to neuronal cells on electrospun nanofibrous substrates for nerve tissue engineering. *Biomaterials* **2009**, *30*, 4996-5003.

(309) Zamani, M.; Morshed, M.; Varshosaz, J.; Jannesari, M.: Controlled release of metronidazole benzoate from poly ε-caprolactone electrospun nanofibers for periodontal diseases. *European Journal of Pharmaceutics and Biopharmaceutics* **2010**, *75*, 179-185.

(310) Maretschek, S.; Greiner, A.; Kissel, T.: Electrospun biodegradable nanofiber nonwovens for controlled release of proteins. *Journal of Controlled Release* **2008**, *127*, 180-187.

(311) Oberhausen, K. J.; Richardson, J. F.; Buchanan, R. M.; Pierce, W.: Synthesis, structure and properties of a N_3 tridentate *bis*-imidazolyl ligand with copper(II). *Polyhedron* **1989**, *8*, 659-668.

(312) Kruse, L. I.; Kaiser, C.; DeWolf, W. E.; Finkelstein, J. A.; Frazee, J. S.; Hilbert, E. L.; Ross, S. T.; Flaim, K. E.; Sawyer, J. L.: Some benzyl-substituted imidazoles, triazoles, tetrazoles, pyridinethiones, and structural relatives as multisubstrate

inhibitors of dopamine β-hydroxylase. 4. Structure-activity relationships at the copper binding site. *Journal of Medicinal Chemistry* **1990**, *33*, 781-789.

(313) Roe, A. M.: The thermal condensation of imidazoles with carbonyl compounds. *Journal of the Chemical Society (Resumed)* **1963**, 2189-2194.

(314) Gran, G.: Determination of the equivalence point in potentiometric titrations. Part II. *Analyst* **1952**, *77*, 661-671.

(315) Gans, P.; O'Sullivan, B.: GLEE, a new computer program for glass electrode calibration. *Talanta* **2000**, *51*, 33-37.

(316) Bazzicalupi, C.; Bencini, A.; Bianchi, A.; Danesi, A.; Giorgi, C.; Valtancoli, B.: Anion binding by protonated forms of the tripodal ligand tren. *Inorganic Chemistry* **2009**, *48*, 2391-2398.

(317) Gans, P.; Sabatini, A.; Vacca, A.: Investigation of equilibria in solution. Determination of equilibrium constants with the HYPERQUAD suite of programs. *Talanta* **1996**, *43*, 1739-1753.

(318) Ayepola, O. O.: Evaluation of the antimicrobial activity of root and leaf extracts of Terminalia Glaucescens. *Advances in Natural and Applied Sciences* **2009**, *3*, 188-191.

(319) Tiwari, P., Rai, H., Upreti, D. K., Shukla, P., : Assessment of antifungal activity of some Himalayan *Foliose Lichens* against plant pathogenic fungi. *American Journal of Plant Sciences* **2011**, *2*, 841-846.

(320) Assessment of antibacterial finishes on textile materials: AATCC Test Method 100-2004. **2006**.

(321) Bruker (2005a). APEX2 Version 2009.1-0. Bruker AXS Inc., M., Winconsin, USA.

(322) Bruker (2005b). SAINT+. Version 7.60A (includes XPREP and SADAB) Bruker AXS Inc., M., Winconsin, USA.

(323) Bruker (1999). SHELXTL. Version 5.1 (includes XS, X., XP, XSHELL) Bruker AXS Inc., Madison, Winconsin, USA.

(324) Farrugia, L. J.: *Applied Crystallography* **1997**, *30*, 565.

(325) Standard test method for determining the antimicrobial activity of immobilized antimicrobial agents under dynamic contact conditions: ASTM E2149-10. 2010.

(326) Pan, J.: Poly[4(5)-vinylimidazole]/polyvinylidene fluoride composites as proton exchange membranes. Full, Rochester Institute of Technology, **2009**.

(327) Mosmann, T.: Rapid colorimetric assay for cellular growth and survival: Application to proliferation and cytotoxicity assays. *Journal of Immunological Methods* **1983**, *65*, 55-63.

(328) Sheng, C.; Che, X.; Wang, W.; Wang, S.; Cao, Y.; Miao, Z.; Yao, J.; Zhang, W.: Design and synthesis of novel triazole antifungal derivatives by structure-based bioisosterism. *European Journal of Medicinal Chemistry* **2011**, *46*, 5276-5282.

(329) Meloun, M.; Bordovská, S.: Benchmarking and validating algorithms that estimate pK a values of drugs based on their molecular structures. *Anal Bioanal Chem* **2007**, *389*, 1267-1281.

(330) Franz, R. G.: Comparisons of pK_a and log P values of some carboxylic and phosphonic acids: Synthesis and measurement. *AAPS Pharmsci* **2001**, *3*, 1-13.

(331) Reller, L. B.; Weinstein, M.; Jorgensen, J. H.; Ferraro, M. J.: Antimicrobial susceptibility testing: A review of general principles and contemporary practices. *Clinical Infectious Diseases* **2009**, *49*, 1749-1755.

(332) Denyer, S. P.: Mechanisms of action of antibacterial biocides. *International Biodeterioration & Biodegradation* **1995**, *36*, 227-245.

(333) Freeman, C. D.; Klutman, N. E.; Lamp, K. C.: Metronidazole: A therapeutic review and update. *Drugs* **1997**, *54*, 679-708.

(334) Jung, F.; Delvare, C.; Boucherot, D.; Hamon, A.; Ackerley, N.; Betts, M. J.: Synthesis and structure-activity relationship of new cephalosporins with amino heterocycles at C-7. Dependence of the antibacterial spectrum and .*beta*-lactamase stability on the pK_a of the C-7 heterocycle. *Journal of Medicinal Chemistry* **1991**, *34*, 1110-1116.

(335) Dalhoff, A.; Schubert, S.; Ullmann, U.: Effect of pH on the *in vitro* activity of and propensity for emergence of resistance to fluoroquinolones, macrolides, and a ketolide. *Infection, Supplement* **2005**, *33*, 36-43.

(336) Stiff, C. M.; Zhong, M.; Sarver, R. W.; Gao, H.; Ho, A. M.; Sweeney, M. T.; Zurenko, G. E.; Romero, D. L.: Correlation of carboxylic acid pK_a to protein binding and antibacterial activity of a novel class of bacterial translation inhibitors. *Bioorganic & Medicinal Chemistry Letters* **2007**, *17*, 5479-5482.

(337) Agarwal, S.; Wendorff, J. H.; Greiner, A.: Use of electrospinning technique for biomedical applications. *Polymer* **2008**, *49*, 5603-5621.

(338) Natu, M. V.; de Sousa, H. C.; Gil, M. H.: Effects of drug solubility, state and loading on controlled release in bicomponent electrospun fibers. *International Journal of Pharmaceutics* **2010**, *397*, 50-58.

(339) Lane, T. J.; Nakagawa, I.; Walter, J. L.; Kandathil, A. J.: Infrared investigation of certain imidazole derivatives and their metal chelates. *Inorganic Chemistry* **1962**, *1*, 267-276.

(340) McCann, M.; Coyle, B.; Briody, J.; Bass, F.; O'Gorman, N.; Devereux, M.; Kavanagh, K.; McKee, V.: Synthesis and antimicrobial activity of (Z)-3-(1H-imidazol-1-yl)-2-phenylpropenenitrile and its metal complexes: X-ray crystal structures of the Zn(II) and Ag(I) complexes. *Polyhedron* **2003**, *22*, 1595-1601.

(341) Quintal, S.; Concepción Gimeno, M.; Laguna, A.; Calhorda, M. J.: Silver(I) and copper(I) complexes with ferrocenyl ligands bearing imidazole or pyridyl substituents. *Journal of Organometallic Chemistry* **2010**, *695*, 558-566.

(342) Wiley, B. J.; Im, S. H.; Li, Z.-Y.; McLellan, J.; Siekkinen, A.; Xia, Y.: Maneuvering the surface plasmon resonance of silver nanostructures through shape-controlled synthesis. *The Journal of Physical Chemistry B* **2006**, *110*, 15666-15675.

(343) Siedenbiedel, F.; Tiller, J. C.: Antimicrobial polymers in solution and on surfaces: Overview and functional principles. *Polymers* **2012**, *4*, 46-71.

(344) Samaha, S. H.; Essa, D. M.; Tera, F. M.: Acrylonitrile grafting onto nylon-6 fabric. I. Synthesis and characterization. *Polymer - Plastics Technology and Engineering* **2004**, *43*, 503-517.

(345) Norrish, R. G. W., Bamford, C. H.: Photo-decomposition of aldehydes and ketones. *Nature* **1937**, *140*, 195-195.

(346) Anbarasan, R.; Jayaseharan, J.; Sudha, M.; Gopalan, A.: Free-radical grafting of 4-vinyl pyridine onto nylon 6 fiber. *Journal of Applied Polymer Science* **2002**, *86*, 3108-3113.

(347) Athawale, V. D.; Rathi, S. C.: Role and relevance of polarity and solubility of vinyl monomers in graft polymerization onto starch. *Reactive and Functional Polymers* **1997**, *34*, 11-17.

(348) Park, H. J.; Na, C. K.: Adsorption characteristics of anionic nutrients onto the PP-g-AA-Am non-woven fabric prepared by photoinduced graft and subsequent chemical modification. *Journal of Hazardous Materials* **2009**, *166*, 1201-1209.

(349) Na, C. K.; Park, H. J.: Preparation of acrylic acid grafted polypropylene nonwoven fabric by photoinduced graft polymerization with preabsorption of monomer solution. *Journal of Applied Polymer Science* **2009**, *114*, 387-397.

(350) Orozco, G.; Pérez, M. C.; Rincón, A.; Gutiérrez, C.: Electrooxidation of methanol on silver in alkaline medium. *Journal of Electroanalytical Chemistry* **2000**, *495*, 71-78.

(351) Sharma, V. K.; Yngard, R. A.; Lin, Y.: Silver nanoparticles: Green synthesis and their antimicrobial activities. *Advances in Colloid and Interface Science* **2009**, *145*, 83-96.

(352) Kim, J. S.: Reduction of silver nitrate in ethanol by poly(*N*-vinylpyrrolidone). *Journal of Industrial and Engineering Chemistry* **2007**, *13*, 566-570.

(353) Silvert, P.-Y.; Herrera-Urbina, R.; Duvauchelle, N.; Vijayakrishnan, V.; Elhsissen, K. T.: Preparation of colloidal silver dispersions by the polyol process. Part 1-Synthesis and characterization. *Journal of Materials Chemistry* **1996**, *6*, 573-577.

(354) http://www.chemistrymag.org/cji/2005/071001pe.htm; Vol. 2013. Date accessed: 05 February 2013.

(355) Thomas, G.: Medicinal Chemistry: An introduction. *John Wiley & Sons, Ltd* **2007**.

(356) Ranganatha, S. R.; Kavitha, C. V.; Vinaya, K.; Prasanna, D. S.; Chandrappa, S.; Raghavan, S.; Rangappa, K.: Synthesis and cytotoxic evaluation of novel 2-(4-(2,2,2-trifluoroethoxy)-3-methylpyridin-2-ylthio)-1H-benzo[d]imidazole derivatives. *Archives of Pharmacal Research* **2009**, *32*, 1335-1343.

(357) Sharma, D.; Narasimhan, B.; Kumar, P.; Judge, V.; Narang, R.; De Clercq, E.; Balzarini, J.: Synthesis, antimicrobial and antiviral evaluation of substituted imidazole derivatives. *European Journal of Medicinal Chemistry* **2009**, *44*, 2347-2353.

(358) Bhandari, K.; Srinivas, N.; Marrapu, V. K.; Verma, A.; Srivastava, S.; Gupta, S.: Synthesis of substituted aryloxy alkyl and aryloxy aryl alkyl imidazoles as antileishmanial agents. *Bioorganic & Medicinal Chemistry Letters* **2010**, *20*, 291-293.

(359) Abdel-Wahab, B. F.; Awad, G. E. A.; Badria, F. A.: Synthesis, antimicrobial, antioxidant, anti-hemolytic and cytotoxic evaluation of new imidazole-based heterocycles. *European Journal of Medicinal Chemistry* **2011**, *46*, 1505-1511.

(360) Assadieskandar, A.; Amini, M.; Ostad, S. N.; Riazi, G. H.; Cheraghi-Shavi, T.; Shafiei, B.; Shafiee, A.: Design, synthesis, cytotoxic evaluation and tubulin inhibitory activity of 4-aryl-5-(3,4,5-trimethoxyphenyl)-2-alkylthio-1H-imidazole derivatives. *Bioorganic & Medicinal Chemistry* **2013**, *21*, 2703-2709.